

The role of SRSF3 in nuclear splicing surveillance

Dissertation
zur Erlangung des Doktorgrades
der Naturwissenschaften



vorgelegt beim Fachbereich Biowissenschaften (FB15)
der Johann Wolfgang Goethe-Universität
in Frankfurt am Main

von Marius Wegener
aus Mainz

Frankfurt (2020)
(D30)

vom Fachbereich der Biowissenschaften (FB15)
der Johann Wolfgang Goethe Universität als Dissertation angenommen

Dekan:

Prof. Dr. Sven Klimpel

Gutachter:

JunProf. Michaela Müller-McNicoll, Ph.D.

Dr. Kathi Zarnack

Datum der Disputation:

Table of content

Abbreviations.....	VI
List of tables.....	VIII
List of figures.....	IX
1. Zusammenfassung	1
2. Introduction	5
2.1. The nuclear mRNA lifecycle.....	5
2.2. Regulation by RNA binding proteins.....	8
2.3. Pre-mRNA splicing.....	9
2.3.1. Spliceosome assembly.....	10
2.3.2. Splicing inhibition by small molecule inhibitors	13
2.4. SR proteins	16
2.4.1. SR protein functions in constitutive and alternative splicing	18
2.4.2. Regulation of SR protein localization and activity	19
2.4.3. Nuclear speckles	20
2.4.4. SR protein activation and de-phosphorylation during splicing.....	22
2.4.5. SR protein shuttling	24
2.4.6. SRSF3 domain structure and mRNA export activity.....	25
2.4.7. SRSF3 regulation in cellular proliferation	27
2.5. mRNA export and nuclear surveillance	28
2.5.1. Nxf1-mediated mRNA export	30
2.5.2. The interplay between nuclear splicing and mRNA export	35
2.5.3. Nuclear RNA retention.....	37
2.5.4. Nuclear surveillance in yeast and higher eukaryotes	41
2.5.5. The surveillance factor Nab2 in yeast.....	43
2.6. The zinc finger binding protein Zc3h14	48
2.6.1. Zc3h14 structure and functions.....	49
2.6.2. Impact of Zc3h14 in neurological disorders.....	49
2.6.3. Pluripotent mouse P19 cells as a model organism	50
3. Objectives.....	53
4. Material and methods.....	54
4.1. Equipment and chemicals	54
4.2. Software and online tools	59
4.3. Cell Culture	60
4.3.1. Freezing cells	60
4.3.2. Thawing cells	60
4.3.3. Cell harvesting	61
4.4. Generation of BAC cell lines	61
4.4.1. Bacterial artificial chromosome (BAC) isolation	61
4.4.2. BAC transfection	62
4.4.3. Selection of clones for overexpression studies	62
4.5. Isoginkgetin treatment.....	63

4.6.	siRNA and esiRNA knock downs	63
4.6.1.	esiRNA preparation.....	63
4.7.	Transfection.....	65
4.8.	Subcellular Fractionation.....	65
4.8.1.	Validation of fractionation.....	66
4.9.	Heterokaryon assay.....	66
4.10.	RNA work.....	67
4.10.1.	RNA extraction.....	67
4.10.2.	RNA binding assay	68
4.10.3.	UV Cross-linking and Immunoprecipitation (iCLIP).....	69
4.10.4.	Analysis of RNA-Seq and iCLIP data	70
4.10.5.	Reverse Transcription	71
4.10.6.	Splicing analysis	71
4.10.7.	Real time PCR.....	72
4.10.8.	RNA Fluorescence in situ Hybridization (FISH)	74
4.11.	Protein work.....	74
4.11.1.	Protein Extraction	74
4.11.2.	Shrimp alkaline phosphatase (SAP) treatment.....	75
4.11.3.	Co-immunoprecipitation (Co-IP).....	75
4.11.4.	Western Blot.....	76
4.11.5.	Phostag® Gels	77
4.11.6.	Mass spectrometry	78
4.11.7.	Fluorescence and Immunofluorescence microscopy.....	79
4.12.	Confocal microscopy	80
4.12.1.	Image processing.....	80
4.12.2.	Fluorescence quantification	81
4.12.3.	Line scans.....	81
4.13.	Statistical analysis.....	82
5.	Results.....	83
5.1.	Splicing inhibition by Isoginkgetin treatment causes global intron retention.....	83
5.2.	Polyadenylated RNA with retained introns are sequestered in nuclear foci.....	85
5.3.	Nuclear pA ⁺ foci are enlarged nuclear speckles that contain SRSF3.....	89
5.4.	SRSF3 interactome upon splicing inhibition reveals a decrease in export adaptors and surveillance factors.....	92
5.5.	Zc3h14 is a novel Nxf1 export adaptor.....	95
5.6.	Global identification of Zc3h14 targets reveals its involvement in cell cycle regulation.....	102
5.7.	Zc3h14 regulates the nuclear export of its targets	106
5.8.	Zc3h14 binds preferentially to polyA stretches and polyA tails	112
5.9.	Zc3h14 binding to its regulated target RNAs is sensitive to splicing inhibition.....	115
5.10.	Zc3h14 recruitment to mRNPs requires SRSF3 and is inhibited by SRSF3-hyperphosphorylation.....	117
6.	Discussion.....	123
6.1.	Isoginkgetin as a tool to investigate splicing surveillance in P19 cells	124
6.2.	The involvement of SRSF3 in nuclear splicing surveillance	129
6.2.1.	SRSF3: Its role between exosomal decay and nuclear export	132
6.3.	Zc3h14: A novel export adaptor in higher eukaryotes	134
6.3.1.	Zc3h14 facilitates the export of cell cycle regulators	139
6.3.2.	Zc3h14 export activity is splicing and SRSF3 dependent	141

6.4. The role of Zc3h14 and SRSF3 export function in neurological diseases	144
7. Conclusion and outlook.....	146
8. References	150
9. Supplementary tables	189
I. Eidesstattliche Versicherung.....	204
II. Curriculum Vitae	205
III. Acknowledgements.....	207

Abbreviations

A

AD	Alzheimer's disease
ALS	Amyotrophic lateral sclerosis
APA	Alternative polyadenylation
ARID	Autosomal recessive intellectual disability

B

BAC	Bacterial artificial chromosome
BP	Base pairs
BSA	Bovine serum albumin

C

CBP	Cap binding protein
cDNA	Copy DNA
CHX	Cycloheximide
CLIP	Cross-linking immunoprecipitation
Co-IP	Co-immunoprecipitation
CPSF	Cleavage and polyadenylation specificity factor
Cq	Quantification cycles
CSTF	Cleavage stimulation factor
CTD	C-terminal domain
CTE	Constitutive transport element
CTE BP	Constitutive transport element binding protein
Ctrl	Control

D

DM1	Myotonic dystrophy
DMSO	Dimethyl sulfoxide
DNA	Deoxyribonucleic acid
DSE	Downstream sequence element
dsRNA	Double stranded RNA
dT	Deoxythymidin homooligonucleotides

E

EGRF	Endothelial growth factor
EJC	Exon junction complex
ESCs	Embryonic stem cells
ESE	Exonic splicing enhancer
esiRNA	Endoribonuclease-prepared siRNA

E

ESS	Exonic splicing silencer
-----	--------------------------

F

FISH	Fluorescence <i>in situ</i> hybridization
FTLD	Frontotemporal lobar degeneration
FXS	Fragile X syndrome

G

GFP	Green fluorescent protein
GO	Gene ontology

H

HD	Huntington's disease
HKA	Heterokaryon assay
hnRNP	Heterogeneous ribonucleoprotein particle
HRP	Horseradish peroxidase

I

I3	Intron 3
iCLIP	Individual-nucleotide resolution UV cross-linking and immunoprecipitation
ID	Intellectual disability
IF	Immunofluorescence
IGC	Interchromatin granule cluster
igG	Immunoglobulin G
IP	Immunoprecipitation
IPSC	Induced pluripotent stem cell
ISE	Intronic splicing enhancer
IsoG	Isoginkgetin
ISS	Intronic splicing silencer
IVT	<i>In vitro</i> transcription

K

KD	Knock down
KH	K-homology domain

L

LAAHD	Lethal arthrogryposis with anterior horn cell disease
LB	Lysogeny broth
LCCS	Lethal congenital contracture syndrome
log2FC	log2 fold change
LRR	Leucine-rich repeat
Luc	Luciferase

M

MEF	Mouse embryonic fibroblast
miRNA	Micro RNA
mRNA	Messenger RNA
mRNP	Messenger ribonucleoprotein particle
MS	Mass spectrometry

N

NES	Nuclear export signal
NPC	Nuclear pore complex
NPSLE	Neuropsychiatric systemic lupus erythematosus
NS	Nuclear speckles
nt	Nucleotides
NTF2	Nuclear transport factor 2
Nup	Nucleoporin

O

o.n.	Over night
Oex	Overexpression
OI	Osteogenesis imperfecta
OPMD	Oculopharyngeal muscular dystrophy

P

pA+RNA	Polyadenylated RNA
PABP	PolyA binding protein
PAP	PolyA polymerase
PAS	Polyadenylation signal
PCR	Polymerase chain reaction
PF	Perichromatin fibrils
PIR	Percent intron retention
Pol	Polymerase

P

PPT	Polypyrimidine tract
pre-mRNA	Premature RNA
PTC	Premature termination codon

Q

qPCR	Quantitative PCR
------	------------------

R

r.t.	Room temperature
RA	Retinoic acid
RBD	RNA binding domain
RBP	RNA binding protein
RNA	Ribonucleic acid
RRM	RNA recognition motif
rRNA	Ribosomal RNA
RT	Reverse transcription

S

SAP	Shrimp alkaline phosphatase
SELEX	Systematic evolution of ligands by exponential enrichment
siRNA	Small interfering RNA
SMI	Small molecule inhibitors
snRNA	Small nuclear ribonucleic acid
snRNP	Small nuclear ribonucleoprotein
ss	Splice site
SSA	Spliceostatin A
SUMO	Small ubiquitin-like modifier
SV40	Simian vacuolating virus 40

T

TREX	Transcription-export complex
tRNA	Transfer RNA

U

UTR	Untranslated region
UV	Ultraviolet

Z

ZnF	Zincfinger domain
-----	-------------------

List of tables

Table 1: List of equipment.....	54
Table 2: Chemicals and reagents.....	55
Table 3: List of buffers and solution recipes.	57
Table 4: Biochemical kits.....	58
Table 5: List of software and online tools.	59
Table 6: Oligonucleotides used for stable cell line validation.	62
Table 7: siRNA sequence and esiRNA sequence regions.	63
Table 8: Taq PCR and IVT protocol and program.	64
Table 9: Oligonucleotides used for cellular fractionation validation.	66
Table 10: Phusion PCR protocol and program.	71
Table 11: Oligonucleotides used for splicing assays.....	71
Table 12: Oligonucleotides used for qPCR assays.	73
Table 13: qPCR protocol and program.	73
Table 14: FISH probe information.	74
Table 15: SAP treatment reaction protocol.....	75
Table 16: SDS-PAGE gel recipes.....	76
Table 17: Primary antibodies used in western blot assays.	77
Table 18: Secondary antibodies used in western blot assays.	77
Table 19: SDS-PAGE – Phostag [®] gel recipes.	77
Table 20: Primary antibodies used for immunofluorescence assays.	80
Table 21: Secondary antibodies used for immunofluorescence assays.	80
Table 22: The SRSF3 interactome.....	189
Table 23: The SRSF3 interactome upon IsoG treatment.	192
Table 24: Top 240 DEG upon Zc3h14 depletion.	200
Table 25: <i>Histone H3</i> abundance in fractions upon Zc3h14 depletion.	203
Table 26: <i>Histone H3</i> abundance in fractions upon Zc3h14 overexpression.	203

List of figures

Figure 1: The nuclear mRNA lifecycle. DNA is transcribed into pre-mRNA <i>via</i> RNA polymerase II (PolII). ..	7
Figure 2: RBPs regulatory interplay mode.....	9
Figure 3: snRNP composition and snRNA secondary structures.	11
Figure 4: Spliceosome assembly and splicing catalysis.	12
Figure 5: Splicing inhibitors and their mode of action.	15
Figure 6: Overview of SR proteins and their functional domains.....	17
Figure 7: Splicing activities of SR proteins.....	19
Figure 8: SR protein phosphorylation cycle.....	20
Figure 9: Phosphorylation and activation of SRSF1.....	23
Figure 10: SRSF3 domain organization.....	26
Figure 11: Molecular architecture and functions of the nuclear pore complex.....	29
Figure 12: Nxf1 domain organization.....	30
Figure 13: Nxf1 mediated nuclear mRNA export.	33
Figure 14: Mechanisms of nuclear mRNA retention.	39
Figure 15: Nab2 and Zc3h14 domain organization.	44
Figure 16: Nab2 nuclear surveillance function.....	47
Figure 17: IsoG treatment causes global intron retention in pluripotent P19 cells.	84
Figure 18: IsoG treatment causes an export block and the formation of pA+RNA foci.	86
Figure 19: Formation of pA+ foci upon IsoG is reversible.	88
Figure 20 Nxf1 accumulates inside enlarged nuclear speckles.	89
Figure 21: pA+RNA foci co-localize with SRSF3 in enlarged nuclear speckles.....	92
Figure 22: SRSF3 interaction with export factors is IsoG sensitive.....	94
Figure 23: Characterization of stable cell lines expressing GFP-tagged proteins.....	96
Figure 24: Zc3h14 depletion leads to nuclear accumulation of pA+RNA.	98
Figure 25: Zc3h14 shuttles between the nucleus and the cytoplasm.....	100
Figure 26: Zc3h14 shuttling capacity is highly splicing sensitive.	101
Figure 27 Global identification of Zc3h14 targets suggests an involvement in cell cycle regulation.	104
Figure 28: Zc3h14 levels affect the growth rate of pluripotent P19 cells.	105
Figure 29: Subcellular fractionation upon Zc3h14 depletion.	107
Figure 30: Zc3h14 levels modulate nuclear export of its targets.	109
Figure 31: Zc3h14 KD impairs nuclear export of <i>Smc4</i> mRNA leading to decreased protein expression.....	111
Figure 32: Global identification of the <i>in vivo</i> Zc3h14 binding landscape.....	114
Figure 33: Zc3h14 RNA binding specificity is modulated upon IsoG treatment.....	116
Figure 34: Zc3h14 binding to RNA requires SRSF3 and is decreased upon splicing inhibition.....	118
Figure 35: Splicing inhibition leads to hyper-phosphorylation of SRSF3 and impairs its interaction with Zc3h14 and Nxf1.	121
Figure 36: The role of SRSF3 in splicing surveillance.....	122

1. Zusammenfassung

Die Proteinbiosynthese ist ein zweistufiger Prozess bei dem die DNA während der sogenannten Transkription zunächst in eine messenger RNA (mRNA) umgeschrieben und anschließend in eine Aminosäure Sequenz übersetzt (translatiert) wird. In Eukaryoten findet die Transkription im Zellkern statt, der durch eine Doppelmembran vom Zytoplasma abgegrenzt ist. Diese Kompartimentierung von Zellen ist ein charakteristisches Merkmal von Eukaryoten und ermöglicht die räumliche und zeitliche Entkopplung von Transkription und Translation, wodurch die Zelle über multiple Ebenen der Proteinbiosyntheseregulation verfügt. Bevor die „reife“ mRNA den Zellkern verlässt, durchläuft ihre Vorläuferform (prä-mRNA) eine Reihe von Prozessierungsschritten. Ein essentieller Teilschritt dieser prä-mRNA Prozessierung ist das sogenannte prä-mRNA Spleißen. Während dieses Reifeprozesses werden nicht-kodierende Sequenzen (Introns) entfernt und kodierende Bereiche, sogenannte Exons, zu einem kontinuierlichen RNA Transkript legiert. Prä-mRNA Spleißen wird durch das Spleißosom katalysiert und über ein komplexes Zusammenspiel einer Vielzahl von Spleiß-Faktoren reguliert. Eine essentielle Familie von Spleiß-Faktoren sind Serin/Arginin-reiche Proteine (SR Proteine), die vorzugsweise an exonische Bereiche der prä-mRNA binden und dabei die Exon- bzw. Intron-Erkennung über die Rekrutierung des Spleißosoms an den jeweiligen Spleißstellen kontrollieren. Neben der Regulierung des Spleißens sind SR-Proteine an zahlreichen weiteren mRNA Prozessen beteiligt. So wurde SRSF3, das kleinste Mitglied der konservierten SR-Protein Familie, mit dem Export von mRNAs in Verbindung gebracht. In höheren Eukaryoten wird der mRNA Export über den Export-Faktor Nxf1 vermittelt. Nxf1 weist eine geringe Affinität zu mRNAs auf und ist daher funktional abhängig von Export-Adaptoren. Export-Adaptoren binden an mRNAs, bilden große ribonukleäre Protein-Komplexe (mRNP) und rekrutieren Nxf1, wodurch die Translokalisierung des mRNPs durch den Kernporenkomplex ins Zytoplasma vermittelt wird. Frühere Studien zeigten, dass SRSF3 als Export-Adaptor fungiert, Nxf1 rekrutiert, und dadurch den Export von zahlreichen Transkripten kontrolliert.

Diese Multifunktionalität von SRSF3 wirft die Frage auf, ob prä-mRNA Spleißen und mRNA Export über SRSF3 gekoppelt sind um sicherzustellen, dass nur gespleißte und reife mRNAs den Zellkern verlassen, während nicht-gespleißte, intron-haltige Transkripte im Zellkern zurückgehalten werden. Diese sogenannte Spleiß-Überwachung (*splicing surveillance*), ist essentiell für den zellulären Proteinhaushalt, da der Export und die Translation intron-haltiger Transkripte zur Synthese von nicht-funktionalen Proteinen führt, welches für die Zelle toxisch sein kann. Zur Untersuchung eines möglichen SRSF3-

vermittelten Spleiß-Überwachungsmechanismus, wurde das prä-mRNA-Spleißen mit Hilfe des Spleiß-Inhibitors Isoginkgetin gehemmt. Die hemmende Wirkung von Isoginkgetin in pluripotenten Maus-P19-Zellen wurde transkriptom-weit mittels RNAseq validiert und mehr als 14.532 Introns identifiziert, die infolge der Isoginkgetin-Behandlung ungespleißt bleiben. Mittels Fluoreszenz-in-situ-Hybridisierung (FISH) und Immunfluoreszenz (IF) wurden diese Introns visualisiert und wir konnten zeigen, dass polyadenylierte intron-haltige RNAs nicht exportiert werden und stattdessen in großen, runden nukleären Körperchen akkumulieren. Diese nukleären Körperchen erwiesen sich als erweiterte 'Nuclear Speckles' in denen Introns mit inaktiven SR-Proteinen, u.a. SRSF3 co-lokalisieren. Des Weiteren konnten wir zeigen, dass die Exportblockade reversibel ist, was auf einen Spleiß-Überwachungsmechanismus hindeutet, bei dem intron-haltige Transkripte nur vorübergehend in 'Nuclear Speckles' zurückgehalten werden. Um herauszufinden, ob die Exportblockade durch SRSF3 vermittelt wird, wurde das Interaktom von SRSF3 nach Spleiß-Inhibierung mittels quantitativer Massenspektrometrie (MS) untersucht. In Abwesenheit des Spleiß-inhibitors, wurde der Export-Faktor Nxf1, sowie zahlreiche Export-Adaptoren und Spleiß-Faktoren zusammen mit SRSF3 co-purifiziert. Diese SRSF3-Interaktionen waren jedoch deutlich reduziert nach Isoginkgetin-Behandlung. Eine verringerte Rekrutierung von Export-Faktoren und Adaptoren durch SRSF3 könnte die Zurückhaltung intron-haltiger Transkripte erklären und lässt eine Export-gekoppelte Spleiß-Qualitätskontrolle von SRSF3 vermuten.

Neben bekannten Export-Adaptoren identifizierten wir Zc3h14 als spleiß-sensitiven SRSF3 Interaktor. Obwohl über die Funktion von Zc3h14 sehr wenig bekannt ist, gilt das Zc3h14 Ortholog in *Saccharomyces cerevisiae* Nab2 als zentraler Vermittler zwischen mRNA Export und nukleärem Abbau. Zur Charakterisierung der Funktion von Zc3h14 in höheren Eukaryoten wurde Zc3h14 in P19-Zellen depletiert und überraschenderweise 7750 regulierte Transkripte mittels RNAseq identifiziert. Trotz dieser hohen Zahl an regulierten Transkripten, sind solche die an der Regulation des Zellzyklus beteiligt sind noch angereichert. Über Wachstumsversuche konnten wir zeigen, dass die Verdopplungsrate von P19-Zellen von der Menge an Zc3h14 Protein abhängig ist. Dabei wiesen Zellen mit geringen Zc3h14 Konzentrationen eine verringerte, und mit Zc3h14 Überexpression eine erhöhte Verdopplungsrate auf. Reduzierte RNA Level könnten auf eine mRNA Exportblockade zurückzuführen sein. Daher führten wir eine systematische Charakterisierung hinsichtlich einer möglichen Exportfunktion von Zc3h14 durch. RNA-Lokalisierungs-Experimente zeigten, dass Zc3h14 Depletion zur Akkumulation polyadenylierter RNAs im Zellkern führt, was auf eine Export Blockade hinweist. Fraktionierung von P19-Zellen in Zellkern und Zytoplasma bestätigte, dass eine Zc3h14 Depletion für fünf repräsentative mRNAs zu einem signifikanten Exportdefizit führt. Überexpression von Zc3h14 zeigte den entgegengesetzten Effekt und hatte eine Zunahme

zytoplasmatischer mRNAs zur Folge. Die Akkumulation von *Smc4* wurde zudem durch FISH-Experimente validiert und wir konnten zeigen, dass der verminderte mRNA-Export zu einer Verringerung der Protein-Expression führt. Da *Smc4* auch nach Nxf1- und SRSF3-Depletion im Zellkern akkumuliert, wäre eine Möglichkeit, dass Zc3h14, Nxf1 und SRSF3 den zytoplasmatischen Transport von Zellzyklus-Transkripten gemeinschaftlich regulieren. Co-Präzipitations-Experimente hatten bestätigt, dass die Zc3h14-SRSF3-Interaktion IsoG-sensitiv ist. Daher untersuchten wir als nächstes, ob SRSF3 die Rekrutierung von Zc3h14 an das mRNP vermittelt. Vergleichende RNA-Binde-assays von SRSF3, Nxf1 und Zc3h14 vor und nach Isoginkgetin-Behandlung ergaben, dass sowohl Nxf1 als auch Zc3h14 nach Spleiß-Hemmung wesentlich weniger RNA banden, während die RNA-Bindung von SRSF3 unverändert blieb. Darüber hinaus konnten wir zeigen, dass die RNA-Bindung von Zc3h14 von SRSF3 abhängig ist und bei SRSF3-Depletion signifikant reduziert ist. Daher zeigen diese Ergebnisse, dass Zc3h14 über SRSF3 spleißabhängig zum mRNP rekrutiert wird und dadurch eine Kopplung von prä-mRNA Spleißen und mRNA-Export ermöglicht wird. Um die RNA-Bindepräferenz von Zc3h14 genauer zu untersuchen, führten wir UV Cross-linking und Immunoprecipitation Experimente (iCLIP) durch und verglichen das Zc3h14-RNA-Bindemuster in P19-Zellen mit und ohne IsoG-Behandlung. Die iCLIP Analyse ergab, dass Zc3h14 eine hohe Präferenz zu Homoadenosin-Sequenzen aufweist. Neben der Bindung an *polyA tails* bindet Zc3h14 vorzugsweise an Transkript 3'Enden. Nach Spleiß-Inhibierung weist das Zc3h14-RNA-Bindemuster eine deutliche Reduzierung dieser 3'UTR Bindestellen auf. Das könnte darauf hindeuten, dass die spezifische Bindung von Zc3h14 an Transkript 3'Enden spleißsensitiv ist und über die Rekrutierung von SRSF3 erfolgt.

Die Aktivität von SR Proteinen ist abhängig von deren Menge und Phosphorylierungszustand. SR Proteine binden im hyper-phosphorylierten Zustand an die prä-mRNA und rekrutieren das Spleißosom und werden im Verlauf der Spleiß-Reaktion dephosphoryliert. Daher untersuchten wir, ob der Phosphorylierungsgrad von SRSF3 durch die Inhibierung des Spleißens verändert wird. Phosphorylierungs-sensitive Antikörper und Phostag®-Gele ergaben, dass die Phosphorylierung von SRSF3 im Verlauf der Spleiß-Hemmung deutlich zunimmt. Co-Immunopräzipitations-Experimente von Zc3h14 und Nxf1 zeigten weiterhin, dass Zc3h14 und Nxf1 nur mit hypo-phosphoryliertem SRSF3 interagieren, während hyper-phosphorylierte SRSF3 Proteine keine Interaktion aufweisen. Somit könnte hyper-phosphoryliertes SRSF3 nach Spleiß-Inhibierung eine Reduzierung der Interaktion mit Export-Faktoren wie Zc3h14 und Nxf1 zu Folge haben. Darüber hinaus zeigen unsere Interaktions-Studien, dass Zc3h14 und Nxf1 RNA-unabhängig miteinander interagieren und dass diese Interaktion nach Spleiß-Inhibierung verloren geht. Dies deutet darauf hin, dass Zc3h14 und Nxf1 über eine spleiß- und phosphorylierungsabhängige Interaktion mit SRSF3 zum mRNP rekrutiert werden.

Basierend auf diesen Ergebnissen schlagen wir ein Spleiß-Überwachungs-Modell vor, bei dem intronhaltige Transkripte durch eine fehlende SRSF3-dephosphorylierung nicht ausreichend mit Export-Adaptoren und Nxf1 ausgestattet werden, und dadurch als „export-inkompetent“ markiert werden und im Zellkern akkumulieren. Dagegen werden reife und gespleißte mRNAs über hypo-phosphoryliertes SRSF3 als “export-kompetent” markiert und deren nukleärer Export durch die Rekrutierung von Nxf1 und Zc3h14 stimuliert. Durch diesen Mechanismus wird prä-mRNA-Spleißen mit dem mRNA-Export gekoppelt und dadurch eine zelluläre Qualitätskontrolle des mRNA Reife-Prozesses ermöglicht. Darüber hinaus kann der Export von spezifischen Transkripten über die differentielle Rekrutierung von Export-Adaptoren wie Zc3h14 kontrolliert, und der zelluläre Proteinhaushalt reguliert werden.

Im Rahmen dieser Arbeit konnten wir zeigen, dass das polyA-Binde-Protein Zc3h14 am nukleären Export von Transkripten die an der Zellzyklus-Regulation beteiligt sind beteiligt ist, und stellen ein Exportmodell vor, welches bei der Ursachenforschung zahlreicher neuronaler Krankheiten von Bedeutung sein könnte. Funktionsverlustmutanten von Zc3h14 oder verminderte Zc3h14 Protein-Expression wurden mit mehreren neurologischen Störungen wie nicht-syndromischer autosomal rezessiver intellektueller Behinderung oder der Alzheimer-Krankheit in Verbindung gebracht. Zc3h14-assoziierte Krankheiten scheinen sich bevorzugt auf neuronale Entwicklungsstörungen auszuwirken, was mit der hohen gewebespezifischen Expression von Zc3h14 im Hippocampus korreliert ist. Neuronen sind durch einen Zellzyklus-Arrest in der S-Phase gekennzeichnet. Da unsere Daten zeigen, dass die Expression zahlreicher Zellzyklus-Regulatoren durch die Exportaktivität von Zc3h14 gesteuert wird, könnte eine Funktionsverlustmutante von Zc3h14 die Zellzyklus-Regulation beeinträchtigen und das neuronale Expressionsprofil stören. Patienten, die an dem Fragilen-X-Syndrom oder einer Septin 7 assoziierten Alzheimer-Erkrankung leiden, weisen die gleichen Krankheitssymptome auf wie Patienten, die eine mutierte Zc3h14-Isoform exprimieren. Unsere Ergebnisse zeigen, dass der Export von *Fmr1* und *Sept7* über Zc3h14 vermittelt wird. Daher könnte das Krankheitsbild, das durch den Verlust der physiologischen synaptischen Plastizität charakterisiert ist, auf eine Beeinträchtigung des Exports von *Fmr1* und *Sept7* zurückzuführen sein. Obwohl wir aktuell nicht wissen, ob diese Krankheiten mit unserem vorgeschlagenen Exportmodell in Verbindung stehen, könnten zukünftige Versuche und experimentelle Ansätze in differenzierten P19-Zellen Einblicke in das neuronale Exportsystem und in die Pathogenese multipler neuronaler Entwicklungsstörungen gewähren.

2. Introduction

2.1. The nuclear mRNA lifecycle

The main characteristic of eukaryotic cells is the existence of a membrane-bound nucleus, which is surrounded by the cytoplasm. This compartmentalization enables the cell to spatially and temporally separate gene expression in the two major processes of transcription and translation, and allows multiple layers of gene expression regulation.

Transcription refers to the first step of gene expression where a messenger RNA polymer (mRNA) is created from a DNA template in the nucleus. Prior to the nuclear export of mRNAs for cytoplasmic translation, transcripts are extensively processed. 5'capping, splicing and 3'end processing represent the two major maturation processes, before an mRNA is packed into an export-competent messenger ribonucleoprotein particle (mRNP) together with RNA binding proteins (RBPs). These mRNPs leave the nucleus through the nuclear pore complex (NPC) to complete the nuclear phase of the mRNA lifecycle (see Figure 1). Every nuclear processing step underlies a precise regulation and control, and enables the cell to fine-tune protein levels at very early steps of protein gene expression.

RNAs are transcribed by three RNA polymerases (Pol). While PolI is responsible for transcription of ribosomal RNAs (rRNA) and PolIII generates mainly tRNAs, the only polymerase that transcribes mRNA is PolII. PolII transcription is a three-phased process namely initiation, elongation and termination. While the initiation phase includes promoter recognition, DNA helix opening and the polymerization of a few nucleotides, PolII speeds up during the elongation phase to up to 50-100 kb/min (Cannon & Chubb, 2011) and transcribes the DNA into precursor mRNA (pre-mRNA). The elongation phase is followed by the termination phase, leading to the dissociation of the DNA–RNA hybrid and the release of the nascent transcript.

After PolII has transcribed 20-30 nucleotides (nt), the first processing step of the pre-mRNA -5'-capping-takes place co-transcriptionally. Synthesis of the 5'cap is supported by Ser₅ phosphorylation of the PolII C-terminal domain (CTD) (Ghosh et al., 2011; Suh et al., 2010) and involves the enzymatic addition of a 7-methylguanylate cap *via* a triphosphate linker to the mRNA (see Figure 1). This cap structure is co-transcriptionally and cooperatively bound by the cap-binding protein complex (CBC), consisting of the cap-

binding proteins (CBP) CBP20 and CBP80, which enhances RNA stability (Grudzien et al., 2006), stimulates subsequent pre-mRNA processing steps (Michlewski et al., 2008; Izaurralde et al., 1994; Wong et al., 2007), and serves several downstream cytoplasmic functions (Schwartz & Parker, 2000).

Most eukaryotic protein coding genes contain long intervening non-coding sequences called introns, which are flanked by exons. During the second step of pre-mRNA maturation, introns are excised from the pre-mRNA and the two flanking exons are joined to generate a functional coding sequence, a process coined pre-mRNA splicing. The excision of introns is catalyzed by the spliceosome, a megadalton ribonucleoprotein complex, which together with a multitude of splicing factors recognizes splice sites (ss) with single-nucleotide precision within tens of thousands of intronic nucleotides (see Figure 1).

PolIII transcription does not terminate at the 3' end of mRNAs but continues polymerizing the RNA beyond the transcript end. Thus, a crucial pre-mRNA processing step is the dissociation of the nascent pre-mRNA from the transcriptional apparatus called 3' end processing. This maturation phase is a two-step mechanism that involves the co-transcriptional cleavage of the pre-mRNA, followed by the addition of a homo-polyadenosine tail at the 3' end of the transcript.

Key players in the 3'-end processing reaction are the cleavage and polyadenylation specificity factor (CPSF) and the cleavage stimulating factor (CSTF), two multi-polypeptide complexes (Mandel et al., 2008). Both protein complexes feature several protein subunits and are required for the cleavage site recognition (Takagaki & Manley, 1997). While CPSF binds directly to the polyadenylation signal (PAS) AAUAAA (Schönemann, 2014), a hexanucleotide located 10-30 nt upstream of the actual cleavage site, the downstream sequence element (DSE) located in proximity to the PAS (roughly 40 nt downstream of the cleavage site) is recognized by the CSTF complex (Beyer et al., 1997; Bienroth et al., 1993). After both complexes have anchored to their sequences in a coordinated fashion, the endonucleolytic cleavage reaction occurs between the PAS and the DSE, followed by the addition of non-templated poly-adenosines (50-100 nt) (Chang et al., 2014) at the 3'OH end of the cleaved transcript catalysed by the PolyA-polymerase (PAP) (Wahle, 1991) (see Figure 1).

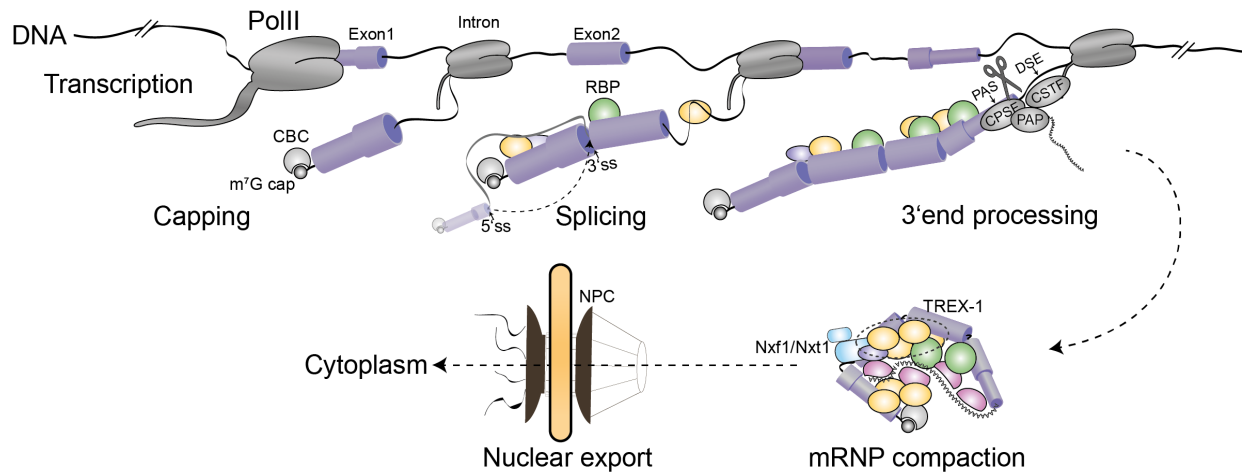


Figure 1: The nuclear mRNA lifecycle. DNA is transcribed into pre-mRNA *via* RNA polymerase II (PolII). Pre-mRNA is capped by the addition of a 7-methylguanylate cap (m⁷G) leading to the association of the cap-binding complex (CBC). During splicing, introns are removed and exons joined at the 5' and 3' splice site (ss). Splicing is regulated by multiple RNA-binding proteins (RBPs). Cleavage of the nascent pre-mRNA is regulated by the cleavage and polyadenylation specificity factor (CPSF) and the cleavage stimulating factor (CSTF), and takes place between the conserved polyadenylation signal (PAS) and the downstream element (DSE). The associated polyA-polymerase (PAP) adds a non-templated polyA tail to the cleaved transcript. After final compaction processes, the messenger ribonucleoproteins (mRNPs) are translocated through the nuclear pore complex (NPC) into the cytoplasm. Export-competent mRNPs contain numerous RBPs, export adaptors, such as TRanscription-EXport TREX-1, and the nuclear export factor.

While being processed, a multitude of RBPs associates co-transcriptionally with the nascent transcript to form the mRNP. Among these RBPs, the mRNA export complex TREX-1 associates with the transcript and recruits the export factor heterodimer Nxf1/Nxt1 (section 4 contains a detailed description of this export pathway). Upon release from the DNA, the export-competent mRNP enters the interchromatin space and is directed towards the nuclear pore complex (NPC). After reaching the nuclear periphery, the mRNP docks to the NPC basket *via* Nxf1/Nxt1 interactions and promotes the translocation of the mRNP towards the cytoplasmic site completing the nuclear mRNA lifecycle.

Although each of these reactions are biochemically distinct processes, they are interlinked and form a complex integral network in which different molecular processing machines influence each other's activities. This functional interdependency of transcription, 5' capping, splicing, 3' end processing and mRNP export generates superior layers of gene expression regulation and creates a potential of quality control mechanisms within the nuclear mRNA life cycle.

2.2. Regulation by RNA binding proteins

RBPs are the drivers of post-transcriptional gene expression and fine-tune protein synthesis by controlling maturation, localization, translation, and degradation of cellular RNAs. The human genome encodes 1,542 RBPs, which relates to 7.5% of the 20,500 known protein-coding genes (Gerstberger et al., 2014). This number mirrors the abundance of transcription factors and highlights the impact of RBP activity in gene expression regulation. Furthermore, RBPs exhibit higher expression levels compared to other protein-coding genes. Recent studies showed that 20% of the protein-coding transcriptome corresponds to RBPs (Gerstberger et al., 2014).

Most RBPs are ubiquitously expressed, deeply evolutionary conserved and display low tissue specificity (~2%) (Gerstberger et al., 2014). Despite their diversity, RBPs have a modular structure and contain one or multiple RNA-binding domains (RBDs) to recognize their targets (Lunde et al., 2007). The most prevalent domains include the RNA recognition motif (RRM), K-homology domain (KH), and the zinc-finger (ZnF) domain (Gerstberger et al., 2014). While each of these domains provide RBPs with different RNA binding capacities, RNA binding specificity is achieved through combinations of different domains, repeats and structural accessibility (Lunde et al., 2007).

Recent developments combining quantitative transcriptomics and proteomics led to the identification of numerous RBPs, its co-factors and RNA targets and unveiled a vast amount of interactions and regulatory networks that are connected with every process of the mRNA lifecycle. Studies combining *in vivo* UV RNA–protein crosslinking followed by polyA-RNA pulldown and protein mass spectrometry (RNA Interactome Capture) revealed that nearly 50% of these networks affected RBPs that act in RNA metabolic pathways, such as splicing, 3' end processing, polyadenylation, and mRNA transport (Gerstberger et al., 2014).

RBPs can act synergistically and enhance each other's RNA binding affinity and specificity (see Figure 2 on the left). In contrast to this cooperative interplay, other RBPs act antagonistically and compete for RNA binding sites to exert their functions (Dassi, 2017). In addition, multiple RBPs regulate each other's expression in a mutual interplay and fine-tune their abundance and action by controlling their protein expression (Dassi, 2017). Since the RBP network is interlinked between mRNA processes, the composition and balance of competing and cooperating RBPs on the target RNA species defines the regulatory outcome and makes RBPs the major players in post-transcriptional regulation.

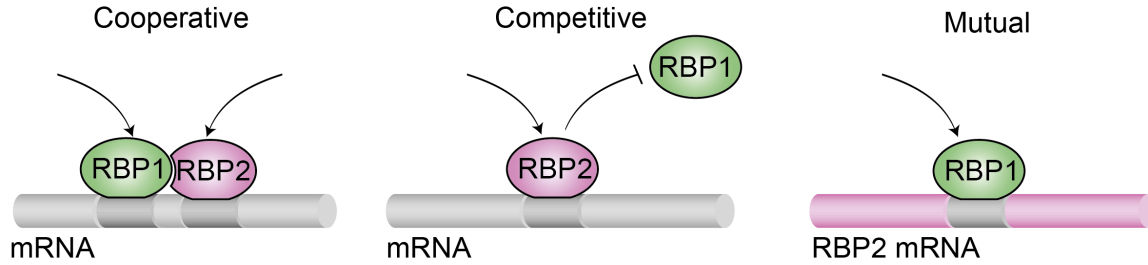


Figure 2: RBPs regulatory interplay mode. Left: RNA binding proteins (RBPs) bind cooperatively to their targets and physically interact to stimulate their association. Middle: The binding site of two RBPs overlap. These RBPs compete for the binding site and most likely act antagonistically. Right: Two RBPs control each other's expression levels and fine-tune the regulatory outcome by modulating their protein abundance (mod. (Dassi, 2017).

2.3. Pre-mRNA splicing

In the 1960s there was a major challenge in the understanding of gene expression in higher eukaryotes: when total RNA was radiolabeled, only a small fraction of nuclear RNA was exported to the cytoplasm while the vast majority was eliminated (Scherrer et al., 1963; HARRIS & Watts, 1962). This long-standing mystery was finally solved in two independent studies by Philip A. Sharp and Richard J. Roberts, who proposed the concept of “split genes” stating that primary transcripts contain multiple non-coding intervening sequences (introns) in between the coding sequences (exons), which are not present in cytoplasmic mature RNA (Chow et al., 1977; Berget et al., 1977). The discovery of pre-mRNA splicing fundamentally revolutionized the understanding of eukaryotic gene expression and was awarded the Nobel Prize for Physiology or Medicine in 1993. One year after the description of pre-mRNA splicing, the concept was extended by the model of alternative splicing (AS), in which the differential inclusion of alternative exons generates multiple mRNA isoforms (Gilbert, 1978). This idea formed another milestone for the understanding of pre-mRNA processing and explained the discrepancy between the number of human protein-coding genes (~20,500) and the approximately 90,000 different proteins that are actually being made.

Most of the splicing catalysis occurs co-transcriptionally. Taken into account average intron half-lives, which lie between 0.4 and 7.0 min (Schmidt et al., 2011; Audibert et al., 2002; Singh & Padgett, 2009), the average intron size of 5419 nt (Sakharkar et al., 2004) and the PolII transcription rate (1.8–4.0 kb per min) (Singh & Padgett, 2009; Danko et al., 2013; Darzacq et al., 2007), co-transcriptional splicing of one intron

should be completed when PolII has moved on average 5.9 kbp downstream of the 3' splice site (3'ss). However, recent studies in *Schizosaccharomyces pombe* suggest that splicing occurs much faster and is completed when PolII is transcribing a region only 45 nt downstream of the 3'ss (Herzel et al., 2018). In addition to this approximation, the existence of co-transcriptional splicing could be observed by several microscopic localization studies (Baurén & Wieslander, 1994; Beyer et al., 1981; Beyer & Osheim, 1988).

Post-transcriptionally spliced introns also exist, but they appear to mostly flank alternatively spliced exons (Pandya-Jones & Black, 2009; Vargas et al., 2011), are prevalently located at the 3' end (Pandya-Jones & Black, 2009; Baurén & Wieslander, 1994) and can be spliced in a signal transduction-dependent manner (Hirschfeld et al., 2009; Xu et al., 2008; Boutz et al., 2015). Post-transcriptional splicing occurs either in proximity to the transcription site or at distant sites in nuclear bodies called nuclear speckles (NS) (Vargas et al., 2011; Girard et al., 2012). Immunofluorescence studies in HeLa cells using an antibody against catalytically active spliceosomes led to the approximation that around 80% of pre-mRNA splicing occurs co-transcriptionally, while 15-25% of active spliceosomes localize to NS (Girard et al., 2012). Although it has been shown that pre-mRNAs are actively retained in NS until splicing is completed (Girard et al., 2012), it yet remains unclear how intron-containing mRNAs are sequestered in those nuclear bodies.

Most studies investigating splicing dynamics and nuclear retention are based on fluorescence *in situ* hybridization (FISH) techniques of a limited number of individual endogenous transcripts, non-physiological reporter constructs (Lacadie et al., 2006; Listerman et al., 2006; Pandya-Jones & Black, 2009; Singh & Padgett, 2009; Wada et al., 2009) or experiments being carried out in yeast, where splicing is much less prevalent (Neugebauer & Roth, 1997; Pandya-Jones & Black, 2009; Wada et al., 2009; Singh & Padgett, 2009).

2.3.1. Spliceosome assembly

The spliceosome consists of five small nuclear ribonucleoprotein particles (snRNPs) designated U1, U2, U4, U5 and U6, and a large number of protein components (Graveley, 2000; Will & Lührmann, 2011) (see Figure 3). A fully assembled and splicing active spliceosome contains more than 300 proteins, which makes it to one of the most complex cellular machineries described so far (Rappsilber et al., 2002; Zhou et al., 2002).

Four characteristic RNA elements are essential for spliceosome assembly: while the 5'ss (AG/GURAGU) and 3'ss define the intron- and exon-junctions, the polypyrimidine tract (PPT; YAG/N) at the 3'ss supports the splice site recognition and the branchpoint sequence (BP; YNYURAC) located at 20-40 nucleotides upstream of the 3'ss initiates a nucleophilic attack on the 5' donor ss (Wahl et al., 2009; Graveley, 2000) (Figure 4A).

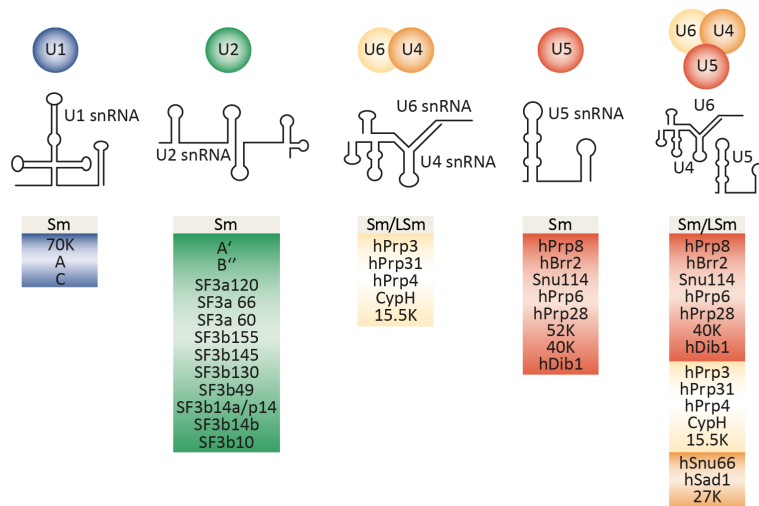


Figure 3: snRNP composition and snRNA secondary structures. The human major spliceosome is composed of small nuclear ribonucleoprotein particles (snRNPs), which consist of five snRNAs (U1 – U6) bound by various RBPs such as Sm and LSm proteins, and are associated with the snRNA at defined structural elements. Apart from SM proteins, each snRNP has a defined RBP composition. U4-U6, as well as U4-U6-U5, are associated with the nascent transcript as a tri-snRNP (mod. (Will & Lührmann, 2011)).

The recognition of these sequences is accomplished by a vast subset of splicing regulators, which specifically bind to these RNA elements and orchestrate a complex interaction network across introns and exons in order to precisely direct the spliceosome to its targets (Black, 2003). The spliceosome assembly is a multi-step process and undergoes several structural rearrangements, followed by a two-step catalytic splicing reaction. The assembly occurs *de novo* on each intron, in a sequential and coordinated fashion (Stevens et al., 2002) (Figure 3 Figure 4B). It is initiated by the binding of U1-snRNP, including its essential component U1-70K to the 5'ss. Concomitantly Splicing factor 1 (SF1) recognizes the conserved BP and the heterodimeric splicing factor U2 auxiliary factor (U2AF) recognizes the 3'ss and associates with the PPT and forms the early E complex (Graveley, 2000). After specific rearrangements, U2AF recruits the U2-snRNP by interacting with the SF3b sub-complex in an ATP-dependent manner and forms complex A. Subsequently U4–U6·U5 snRNPs are recruited as a preassembled tri-snRNP, to form the pre-catalytic spliceosomal complex B (Nguyen et al., 2015). The complex B assembly is stabilized by the activity of the ATP-dependent helicase Prp28, which is stimulated by its phosphorylation *via* the kinase SRPK2 (Price et al., 2014).

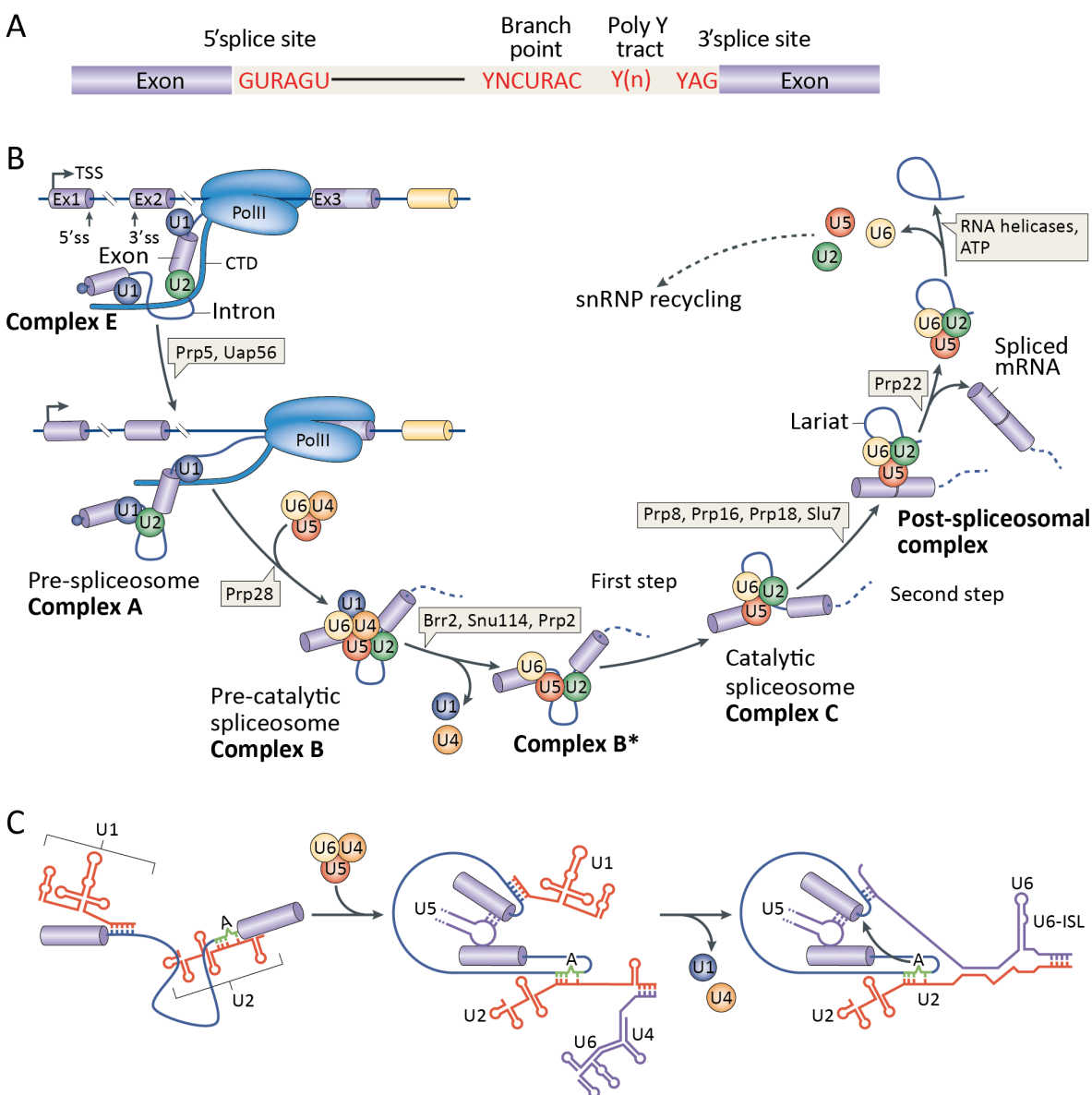


Figure 4: Spliceosome assembly and splicing catalysis. A) Conserved intronic sequence motifs for splice site recognition include the GURAGU motif at the 5' splice sites and branch point, the polypyrimidine tract (Poly Y tract) and the YAG motif at the 3' splice site. B) U1 and U2-snRNPs assemble at the 5' and 3' splice site co-transcriptionally and are stimulated by the PolIII CTD (complex E). The spliceosome is rearranged *via* the helicases Prp5 and Uap56 to form complex A. Prp28 catalyses subsequent conformational changes and stimulate the recruitment of the tri-snRNP U4-U6.U5 forming complex B. Additional structural rearrangement steps are catalyzed by a series of helical activities, leading to the release of U4 and U1 snRNPs, and the transition of the catalytically active complex B*. Complex B* promotes the first catalytical splicing reaction and generates complex C, which contains a free exon and the intron-exon lariat intermediate. After several rearrangements, the second catalytic step occurs, resulting in a post-spliceosome complex that contains the lariat intron and spliced exons. U2, U5 and U6 are finally released from the post-splicing mRNPs and recycled. C) U1 and U2 bind to the 5'ss and the branch point at the 3'ss respectively to form complex E. Complex A formation involves the association of U4-U6, leading to the base pairing of U6 with U2, and U5 with exonic sequences near the 5'ss. An extensive network of base-pairing interactions is formed between U6 and U2, juxtaposing the 5'ss and branch-point adenosine for the first catalytic step of splicing (mod. (Matera & Wang, 2014)).

The catalytically active complex B* is formed after a series of compositional and conformational rearrangements, in which U2-U6 assemble while U4 and U1 leave the complex (Nguyen et al., 2015). This complex catalyses the first splicing reaction, whereby U5 stabilizes the intron lariat and an intron-exon intermediate, as well as a free exon forming complex C. After additional ATP-dependent rearrangements, the second splicing reaction takes place, in which the two exons are brought in close proximity and are ligated *via* a transesterification reaction catalysed by U6 snRNA (Yean et al., 2000; Fica et al., 2013) (see Figure 4C). The resulting post-spliceosomal complex is subsequently recycled, and U2, U5 and U6 are released (Matera & Wang, 2014).

2.3.2. Splicing inhibition by small molecule inhibitors

Small molecule inhibitors (SMI) can influence the spliceosome assembly or reduce its catalytic activity at distinct stages. SMIs targeting the U2-snRNP component Sf3b1 stall the spliceosome assembly at a very early stage of complex E transition. Spliceostatin A (SSA), a well-studied natural product extracted from *Pseudomonas* species, was reported to inhibit pre-mRNA splicing in submicromolar concentration ranges (Kaida et al., 2007). SSA interacts with the U2-snRNP component SF3b155 and thereby interferes with the stable association of the U2-snRNP with the BP, and prevents the transition from complex E to complex A (Kaida et al., 2007; Corriero et al., 2011; Roybal & Jurica, 2010) (see Figure 5). Pladienolide (Koguchi et al., 1997; Miller-Wideman et al., 1992) and Herboxidiene isolated from *Streptomyces* species share the same target molecule and show the same mode of action as SSA (Effenberger et al., 2014; Kotake et al., 2007; Yokoi et al., 2011; Koguchi et al., 1997). A series of SSA derivatives coined Sudemycin and Meayamycin were synthesized to increase stability and optimize target accessibility (Fan et al., 2011; Convertini et al., 2014; Albert et al., 2009; Hasegawa et al., 2011). Due to the disruption of BP recognition, this class of complex E splicing inhibitors have been shown to retain numerous introns and alter the AS pattern of multiple genes (Convertini et al., 2014).

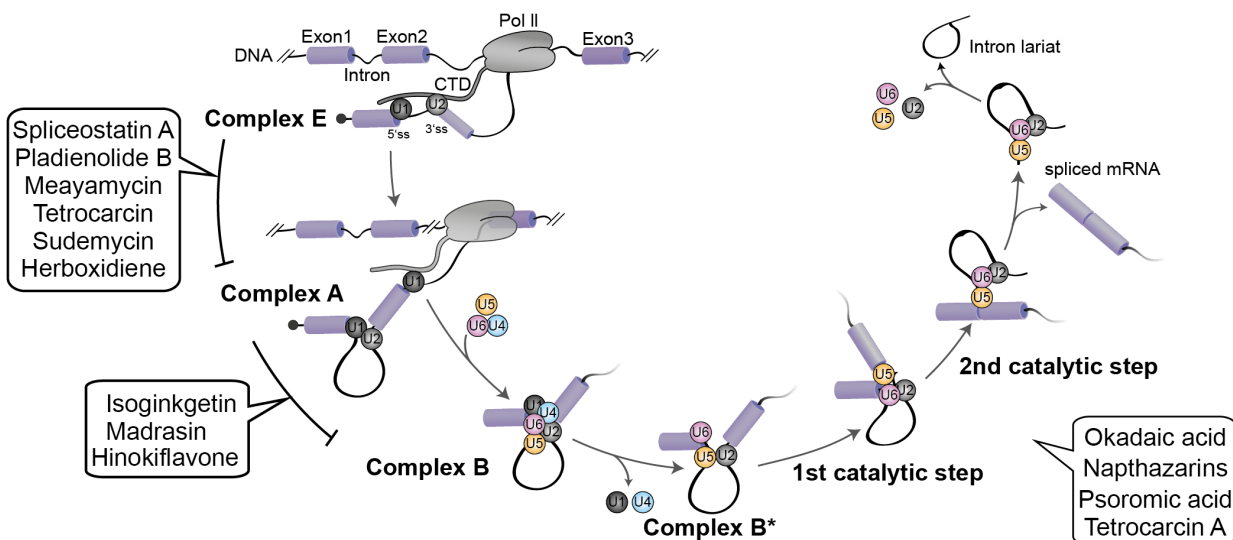
Another class of SMIs prevents the stable recruitment of the U4-U6-U5 tri-snRNPs during the transition from complex A to B. Isoginkgetin (IsoG), a natural biflavonoid extracted from the leaves of *Ginkgo biloba*, was identified using a luciferase splicing reporter in HEK293 cells (O'Brien et al., 2008). Semiquantitative RT-PCRs described the inhibitory properties of IsoG as dose- and time-dependent with IC₅₀ values (half

maximal inhibitory concentration) between 30 μ M and 50 μ M for HeLa cells (Effenberger et al., 2014; O'Brien et al., 2008).

Although very little is known about the targets of complex B SMIs, another plant flavonoid named Hinokiflavone was recently used in multiple human cell lines and was shown to increase the sumoylation of U2 snRNP components, by inhibiting SENP1 protease activity and modulation of the SUMO ligase (Pawellek et al., 2017). Sumoylation is a post-translational modification that covalently conjugates a small protein of 100 aa, called Small Ubiquitin-like Modifier (SUMO) to lysines (Meredith et al., 2016; Mahajan et al., 1997). It is thought that the sumoylation of essential splicing factors such as PRPF3 or SRSF1 interferes with the spliceosome assembly by preventing the interaction of the U4–U6–U5 tri-snRNP with the pre-mRNA directly or indirectly (Pawellek et al., 2017). Although it is not known whether the mode of action of other complex B SMIs such as IsoG or Madrasin is also based on sumoylation, other reports linked complex B SMIs properties with other post-translational modifications such as phosphorylation (Yoon et al., 2006).

SMIs can also inhibit the two splicing reactions. Although the targets of most of this SMI class are not known yet, okadaic acid has been shown to target the phosphatase PP1 and PP2A (Shi et al., 2006). Since these phosphatases de-phosphorylate splicing factors during splicing, it is thought that splicing inhibition occurs due to phosphorylation modulations of essential splicing factors such as SR proteins (Mermoud et al., 1992; Samatov et al., 2012; Berg et al., 2012).

Even before IsoG was described as a pre-mRNA splicing inhibitor, it was shown to regulate the activity of the phosphatidylinositol 3-kinase in the nuclear factor-kappaB pathway (O'Brien et al., 2008; Zhou et al., 2011; Kwak et al., 2002): Since IsoG influences the expression of genes involved in tumor invasion and metastasis such as Metalloproteinase-9, Cyclooxygenase 2 and Prostaglandin E2, this SMI has been assigned anti-cancer and anti-inflammation properties. These properties are in line with the effects of multiple SMIs, which have been shown to reduce metastasis formation (Hsu et al., 2015), increase cell viability in triple negative breast cancers, induce apoptosis, and inhibit tumor growth by changing the splicing pattern of oncogene transcription factors such as MYC or p27.



Splicing inhibition	Inhibitor	Target	Source
pre-spliceosome stalling Complex E	Spliceostatin A	SF3B1	(Kaida, et al. 2007)
	Pladienolide B	SF3B1	(Kotake, et al. 2007)
	Meayamycin	SF3B1	(Albert, et al. 2009)
	Tetrocarcin	n.A.	(Effenberger, et al. 2013)
	Sudemycin	SF3B1	(Fan et al. 2011; Lagisetti et al., 2013)
	Herboxidiene	SF3B1	(Hasegawa, et al. 2011)
pre-spliceosome stalling Complex A	Isoginkgetin	n.A.	(O'Brien et al., 2008)
	Madrasin	n.A.	(Pawellek, et al. 2014)
	Hinokiflavone	Sumoylation of U2	(Pawellek, et al. 2017)
Splicing catalysis	Okadaic acid	PP1, PP2A	(Mermoud, et al. 1992)
	Naphthazarins	(PRP6)	(Berg, et al. 2012)
	Psoromic acid	n.A.	(Samatov et al. 2012)
	Tetrocarcin A	n.A.	(Effenberger, et al. 2013)

Figure 5: Splicing inhibitors and their mode of action. Sub-categorization of small molecule inhibitors (SMIs) for complex E and complex A formation and for splicing catalysis. Complex E SMIs target the SF3B1 complex and block the association of the U2snRNP. The mode of action and the target molecule of most other splicing inhibitors are not known yet (n.A.).

The sensitivity of cancer-specific splice isoforms to SMIs is higher compared to most transcripts. Therefore SMIs represent a potential therapeutic target (Salton & Misteli, 2016). Treatment with SF3B1 inhibitors has already been tested in xenograft models and led to prolonged life of mice carrying murine ascites







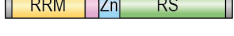





tumors by 40% (Hsu et al., 2015). In addition, treatment with Sudemycin reduced tumor size by 50%, Herboxidiene by 80% and Pladienolide by 60%, respectively, within nanomolar potency (Lagisetti et al., 2013; Sakai et al., 2002). Beyond that, a synthetic analog of Pladienolide B is currently being tested in a phase 1 clinical trial with patients harboring diverse types of solid tumors (Dehm, 2013; Eskens et al., 2013; Hong et al., 2014).

2.4. SR proteins

Among the large number of essential factors regulating the splicing process are the family of serine-arginine-rich proteins (SR proteins). SR proteins were first discovered in the early 90's by three independent research groups. Purified spliceosome complexes including associated factors were used to generate monoclonal antibodies against individual splicing factors. This led to the identification of a "splicing component" with a relative molecular mass of 35 kDa, coined SC35 (SRSF2), which is essential for complex A formation (Fu & Maniatis, 1992a; Fu & Maniatis, 1990). Shortly before, the alternative splicing factor (ASF), alias splicing factor 2 (SF2/SRSF1) was purified from human nuclear extracts (Ge & Manley, 1990; Krainer et al., 1990a). ASF/SF2 was described as a splicing factor that can complement S100 splicing-deficient HeLa cell extracts (Krainer et al., 1990a), influences the selection of 5'ss (Ge & Manley, 1990) and is essential for the splicing reaction (Krainer & Maniatis, 1985; Krainer et al., 1990a). SRSF1 was also the first SR protein shown to have roles in both constitutive and alternative splicing (Ge et al., 1991; Ge & Manley, 1990; Krainer et al., 1990b; Krainer et al., 1991). One year later, another group selectively purified a nuclear body component using high MgCl₂ concentrations, and identified an entire protein family using the monoclonal antibody mAb104. Due to their high serine and arginine content, these proteins were termed SR proteins (Roth et al., 1991; Zahler et al., 1992). Subsequently, additional SR protein members were identified, and the SR protein family was extended to currently 12 members. re-named with the prefix SRSF and numbered according to their discovery (Jeong, 2017) (see Figure 6). Per definition, SR proteins contain one or two N-terminal RNA recognition motifs (RRM), as well as a C-terminal RS domain with an RS content higher than 40% (Manley & Krainer, 2010) (see Figure 6). Beyond these structural criteria, a "classical" SR protein is defined by its dual function in constitutive and alternative splicing, as well as the recognition of its phospho-epitope by mAb104 (Long & Caceres, 2009). They are distinct from other RS-containing splicing factors such as U2AF or U1-70K, collectively referred

to as “SR-like” or “SR-related proteins”, which do not fulfill all criteria described above (Blencowe et al., 1999; Fu, 1995; Query et al., 1989; Zamore et al., 1992; Zhang et al., 1992).

Despite the identification of structural or functional orthologues in plants, flies or nematodes, SR protein counterparts are absent in yeast. SR proteins are structurally related and organized in a modular fashion: while the RNA binding specificity of individual SR proteins is achieved *via* the N-terminal RRM (Chandler et al., 1997; Tacke et al., 1997; Mayeda & Krainer, 1992; Schaal & Maniatis, 1999a), the C-terminal RS domain serves as a protein interaction platform (Kohtz et al., 1994; Wu & Maniatis, 1993).

SR protein	Alias	aa	RS	R/S content
SRSF1 	SF2, ASF, SRp30a	249	198–248	75%
SRSF2 	SC35, PR264	222	116–208	79%
SRSF3 	SRp20	164	107–164	69%
SRSF4 	SRp75	494	179–494	59%
SRSF5 	SRp40; HRS	272	180–267	90%
SRSF6 	SRp55, B52	345	188–344	66%
SRSF7 	9G8	238	121–238	76%
SRSF8 	SRp46	282	98–274	65%
SRSF9 	SRp30c	221	171–221	44%
SRSF10 	SRp38	262	106–260	53%
SRSF11 	SRp54, p54	484	245–373	66%
SRSF12 	SRp35	261	105–254	52%

50 aa





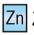
 RRM RNA recognition motif  ΨRRM pseudo-RRM  RS Arginine-Serine rich domain  L Linker region  Zn Zinc finger domain

Figure 6: Overview of SR proteins and their functional domains. Domain organization of all twelve SR proteins, their alias and total length of their amino acid chain (aa). SR proteins can contain a (pseudo) RNA recognition motif, a linker and zinc knuckle domain, and an RS domain characterized by multiple arginine-serine di-repeats. The relative R/S content within the RS domain is shown in the last column (Wegener & Müller-McNicoll, 2020).

Various *in vitro* and *in vivo* approaches such as (functional) SELEX (Liu et al., 1998; Long & Caceres, 2009) and different CLIP techniques have been used to identify the global RNA binding landscape, and revealed distinct consensus RNA motifs for each SR protein (Müller-McNicoll et al., 2016; Pandit et al., 2013;

Bradley et al., 2015). While some of the classical SR proteins exhibit divergent RNA binding preferences (Änkö et al., 2010; Änkö et al., 2012; Müller-McNicoll et al., 2016), structurally related family members such as SRSF1 and SRSF2 display an extensive overlap of RNA binding sites, which indicates that RNA interactions can occur in an antagonistically or compensatory fashion (Pandit et al., 2013; Müller-McNicoll et al., 2016).

2.4.1. SR protein functions in constitutive and alternative splicing

Both, the RRM and RS domains have been shown to be essential for constitutive splicing (Zuo & Manley, 1993; Cáceres & Krainer, 1993). Nevertheless, splicing assays using diverse RRM and RS mutants demonstrate that i) substrate specificity is determined by the RRMs and is independent from the presence of the RS domain, and ii) the RS domain is interchangeable between different SR proteins or can even be fused to a heterologous RNA binding domains without losing its activity (Chandler et al., 1997; Graveley & Maniatis, 1998; Wang et al., 1998), indicating the functional redundancy of the RS domain among distinct SR proteins family members for constitutive splicing.

Transcriptome-wide approaches, such as RNA-Seq and CLIP-Seq enabled the integration of global SR protein-RNA interactomes with their splicing targets. These studies demonstrated that SR proteins have thousands of RNA targets and can be considered master regulators of constitutive and alternative splicing (Ajiro et al., 2015; Anczuków et al., 2015; Pandit et al., 2013). SR proteins bind mainly to exonic splicing enhancers (ESEs), which acts as a barrier, prevents exon skipping and coordinates a sequential splicing order along the pre-mRNA (Ibrahim et al., 2005). SR protein-ESE-binding stabilizes the association of U1-70K to the 5'ss (Jamison et al., 1995; Zahler & Roth, 1995; Zhou & Fu, 2013; Kohtz et al., 1994) and U2AF35 to the 3'ss, respectively (Wang et al., 1995; Li & Blencowe, 1999; Zuo & Maniatis, 1996; Shepard et al., 2002), thereby stimulating the interplay of both splice sites to promote exon definition (Cavaloc et al., 1999; Liu et al., 2000; Schaal & Maniatis, 1999b; Tacke & Manley, 1995; Shepard & Hertel, 2009; Sanford et al., 2005; Blencowe et al., 1998; Blencowe et al., 2000; Stark et al., 1998; Fu & Maniatis, 1992b; Boukis et al., 2004; Hertel & Maniatis, 1999; Wu & Maniatis, 1993; Robberson et al., 1990). In addition, SR proteins regulate subsequent spliceosome assembly steps by triggering the incorporation of the tri-snRNP U4/U6•U5 into the spliceosome (Shepard & Hertel, 2009). This recruitment model is thought to have important roles in alternative splicing, since alternative exons comprise generally weak ss, and their recognition is regulated by SR protein binding and recruitment of the splicing machinery (Fu & Ares, 2014).

In addition to this recruitment model, SR proteins can promote spliceosome assembly by inhibiting the activity of splicing suppressors such as hnRNPs. These splicing suppressors bind to exonic splicing silencers (ESSs) and block ss selection (Wang et al., 2006). SR proteins antagonize these negative splicing activities. Both models, the recruitment and the suppressor pathway likely operate in a synergistic fashion and control spliceosome assembly (Sanford et al. 2005; Zhu et al. 2001; Rooke et al. 2003; Kan und Green 1999). In contrast, SR protein binding to intronic sequences, so called intronic splicing silencers (ISS) can have opposing effects in exon inclusion by suppressing the recruitment of spliceosome components through steric hindrance or non-productive spliceosome assembly leading to exon skipping (Zuo & Manley, 1994; Shen & Mattox, 2011; Long & Caceres, 2009; Huang & Steitz, 2005; Erkelenz et al., 2013; Dembowski et al., 2012; Shepard & Hertel, 2009).

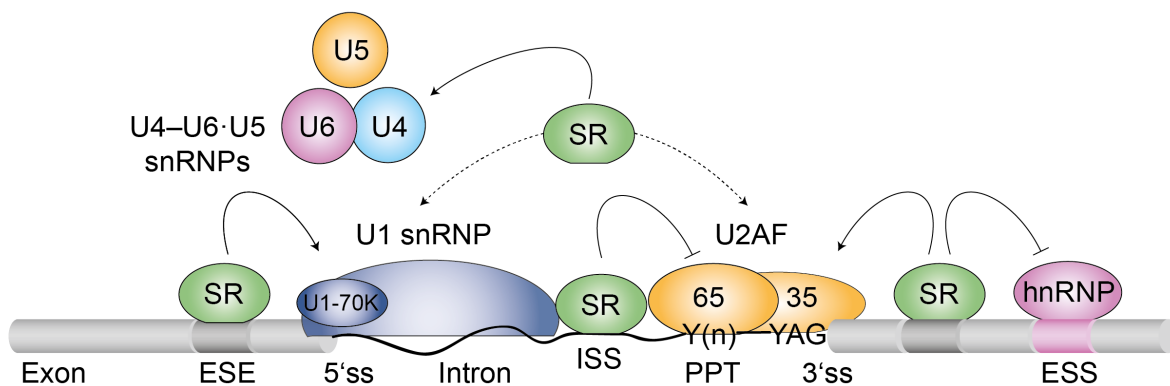


Figure 7: Splicing activities of SR proteins. SR proteins bind to exonic splicing enhancer sequences (ESE) and assist in spliceosome assembly by recruiting the U1-snRNP component U1-70K to the 5' splice site (5'ss), the U2snRNP auxiliary factor U2AF35 to the pyrimidine track (Y(n)) or the 3' splice site (3'ss), or the tri-snRNP U4/U6•U5. SR proteins inhibit the activity of splicing suppressors such as hnRNPs, which bind to exonic splicing silencers (ESS). SR proteins can also bind to silencer regions, for instance in introns (Intronic splicing silencers, ISS) and can inhibit the splicing reaction.

2.4.2. Regulation of SR protein localization and activity

The RS domain of SR proteins can be phosphorylated at all serine residues. The status of its phosphorylation state determines SR protein activities and subcellular localization. RS domains engage in protein-protein interactions with diverse processing factors thus participating in multiple nuclear

processing steps. They mediate the recruitment of snRNPs to its target sequences (Kohtz et al., 1994; Keshwani et al., 2015; Xiao & Manley, 1997; Roscigno & Garcia-Blanco, 1995), regulate the splicing catalysis (Mermoud et al., 1994; Stojdl & Bell, 1999; Mermoud et al., 1992) and determine the subcellular localization, nucleo-cytoplasmic shuttling sites (Duncan et al., 1998; Misteli et al., 1997; Aubol et al., 2018a; Müller-McNicoll et al., 2016) and nuclear re-import of SR proteins (Lai et al., 2001). Figure 8 illustrates the phosphorylation cycle of SR proteins and is mostly based on studies of SRSF1. In the following sections, SR protein dynamics will be introduced in detail.

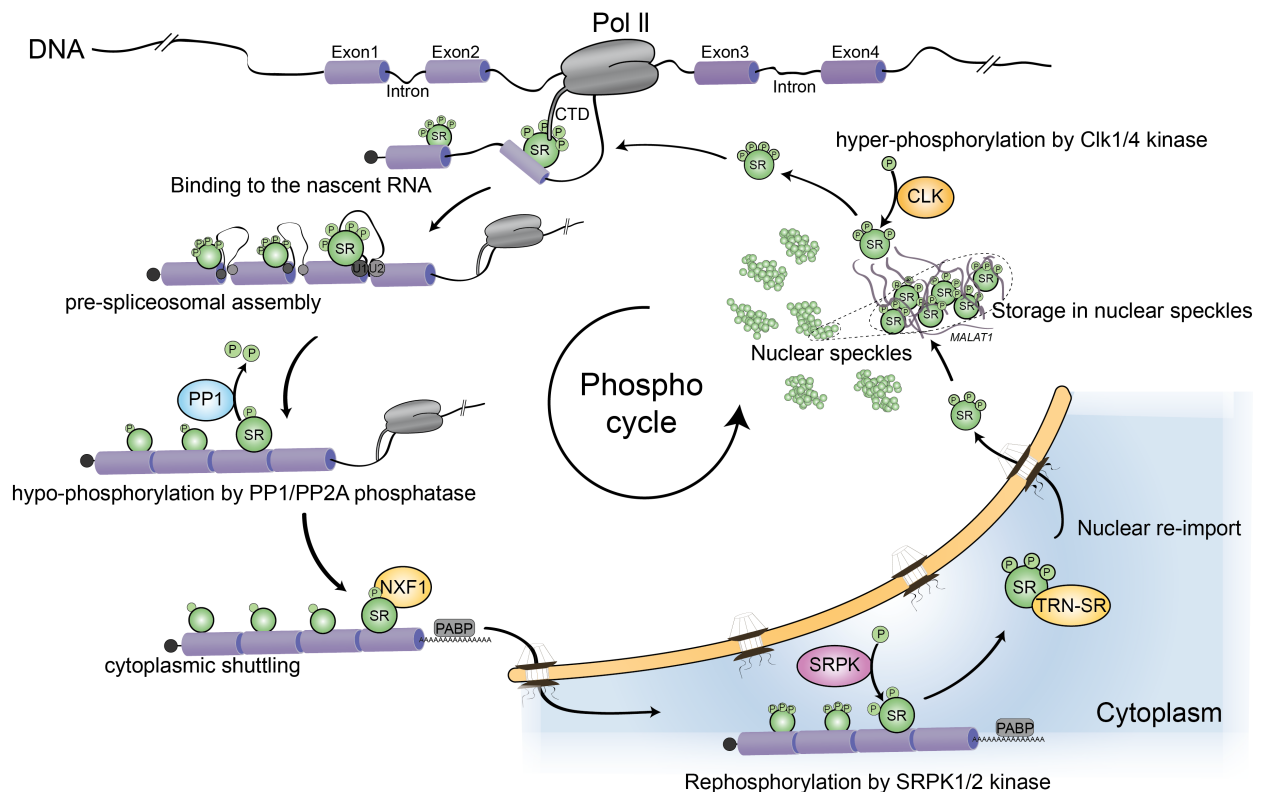


Figure 8: SR protein phosphorylation cycle. SR proteins are activated by Clk-mediated hyper-phosphorylation and bind to nascent transcripts. Hyper-phosphorylated SR proteins recruit the spliceosome and are de-phosphorylated by PP1/PP2A during splicing. Hypo-phosphorylated SR proteins interact with the export factor Nxf1 and shuttle to the cytoplasm as part of the mRNP. SRPK kinases re-phosphorylate SR proteins following their dissociation from the mRNP by moving ribosomes. This intermediate phosphorylation state stimulates their nuclear re-import *via* transportin-SR (TRN-SR) and their targeting to nuclear speckles (Wegener & Müller-McNicoll, 2020).

2.4.3. Nuclear speckles

All canonical SR proteins are concentrated and stored in nuclear speckles (NS) in a transition state. These self-associating membrane-less structures form due to high RNA and Protein concentrations, which favors phase separation by forming a boundary in aqueous solutions, also known as liquid-liquid droplets (Misteli, 2000; Li et al., 2012; Mintz et al., 1999; Saitoh et al., 2004). NS are being enriched in pA+RNA,

the non-coding RNA (ncRNA) *Malat1*, as well as approximately 200 proteins, involved in transcription, pre-mRNA processing and mRNA export (Spector & Lamond, 2011; Hall et al., 2006).

Like other nuclear bodies, NS are structured and sub-compartmentalized into a shell and a core (Kim et al., 2018; Fei et al., 2017). Super-resolution immunofluorescence studies using an antibody specific for the NS marker SC35, which recognizes SR proteins in their intermediate phosphorylation state, revealed that SR proteins (Kim et al., 2018; Fei et al., 2017) and SR like-proteins (Carter et al., 1993; Hall et al., 2006) localize to the NS core (Fu & Maniatis, 1990). They form a scaffold structure that is decorated by pA+RNA surrounding these splicing factors (Kim et al., 2018; Fei et al., 2017). This multilayer structure is promoted by the multivalent nature of *Malat1*, which is massively bound by all SR proteins (Änkö et al., 2012; Miyagawa et al., 2012; Sanford et al., 2009; Tripathi et al., 2010) and basepairs with several other RNAs (Engreitz et al., 2014; Lu et al., 2016; Nguyen et al., 2016). Mammalian nuclei contain 20-50 NS, with sizes ranging between 0.5 and 4.0 μm (Spector & Lamond, 2011; Fu & Maniatis, 1990). Based on electron microscopic and fluorescence imaging, NS are categorized into two morphologically and functionally distinct types: the electron dense interchromatin granule clusters (IGCs) and the perichromatin fibrils (PFs) located at the NS periphery. IGCs are large and irregular shaped RNP granules that measure around 20 nm and are sites of processing factor and pA+RNA storage (Mintz et al., 1999; Carter et al., 1991). Beside this storage function, IGCs have been shown to serve as a platform for post-transcriptional processing events, such as splicing, mRNP compaction or final maturation processes to gain mRNA export competency (Ando et al., 2016; Dias et al., 2010; Girard et al., 2012; Hall et al., 2006; Han et al., 2011; Mor et al., 2016). IGCs that are mostly found at the NS core, are connected with thin PFs, which are highly structured with a preferentially round shape and a diameter between 3 to 5 nm (Spector, 1993, 1996; Thiry, 1995a, 1995b). Studies using incorporation of [^3H] uridine into nascent transcripts demonstrated that PFs are sites of active transcription and splicing (Spector, 1993). This was further supported by findings showing that chromatin regions containing highly transcribed genes tend to co-localize at the NS periphery (Hall et al., 2006; Hu et al., 2010; Khanna et al., 2014; Yang et al., 2011), which is in contrast to low PolIII activity and the lack of DNA in the NS core (Fakan & van Driel, 2007; Spector & Lamond, 2011).

Several lines of evidence demonstrated that intron-containing pA+RNA cluster around or inside IGCs. Therefore it is thought that NS serve as an active quality hub, nuclear RNAs transit for final maturation steps prior to their cytoplasmic export (Hall et al., 2006; Han et al., 2011; Hu et al., 2010; Khanna et al., 2014; Moen et al., 2004; Shopland et al., 2002; Smith et al., 1999; Yang et al., 2011). This is in agreement

with the findings that transcription (Zhang et al., 2016b) or splicing inhibition (Kaida et al., 2007) results in the formation of enlarged NS due to pA+RNA sequestration. NS are highly dynamic and can perform directed motions towards other speckles with velocities between 0.2-1.5 $\mu\text{m}/\text{min}$ (Kim et al., 2018). These dynamics are due to constant flux of its constituent molecules. Fluorescence recovery after photobleaching (FRAP) revealed that SR proteins/SR-like proteins and other splicing factors bound to RNA can be turned over within seconds (Kota et al., 2008; Kruhlak et al., 2000; Wagner et al., 2004).

2.4.4. SR protein activation and de-phosphorylation during splicing

SR proteins are sequestered in NS in their intermediate phosphorylation state, which is balanced by a precise control of the phosphatase (PP1) and kinase activities (Clk1/SRPK1) within these bodies (Aubol et al., 2017). In addition, SRSF1 phosphorylation is fine-tuned by an interplay between PP1 repressive activity at the N-terminus and PP1 processive stimulation at the RS domain (see Figure 9) (Aubol et al., 2017; Aubol et al., 2018b; Novoyatleva et al., 2008).

SR proteins are activated by a highly regulated phosphorylation process, which is catalyzed by the Cdc2-like kinase Clk1 (Aubol et al., 2018a). Clk1 phosphorylation stimulates the translocation of SR proteins from IGCs to the nucleoplasm and/or PFs. This favors binding of hyper-phosphorylated SR proteins to nascent pre-mRNAs at active transcription and splice sites (Duncan et al., 1998; Ngo et al., 2005; Misteli et al., 1997; Aubol et al., 2018a; Keshwani et al., 2015; Ghosh & Adams, 2011; Zhou & Fu, 2013). The hyper-phosphorylation state is essential for splicing activity since overexpression or inhibition of SR specific kinases has been shown to drastically modify the splicing outcome (Cardinali et al., 1994; Sarkissian et al., 1996; Duncan et al., 1997; Hartmann et al., 2001; Muraki et al., 2004; Cho et al., 2011). Importantly, only hyper-phosphorylated SR proteins bound to nascent transcripts support spliceosome assembly. Hyper-phosphorylated SR proteins recruit U1-70K proteins during complex A formation (Kohtz et al., 1994; Keshwani et al., 2015; Xiao & Manley, 1997) and promote the integration of tri-snRNPs during complex B formation (Rosigno & Garcia-Blanco, 1995) (see Figure 9).

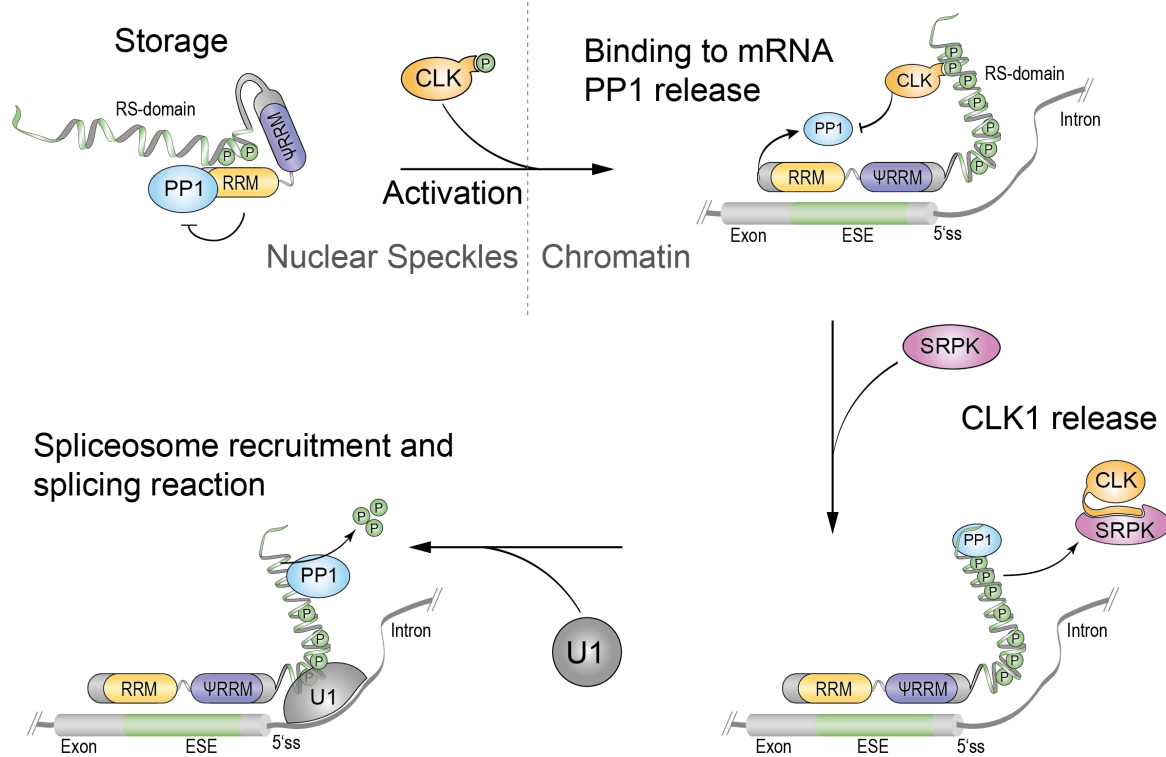


Figure 9: Phosphorylation and activation of SRSF1. The two RNA recognition motifs of SRSF1 interact with the RS domain and keep SRSF1 splicing-inactive within nuclear speckles. The phosphatase PP1 is bound at an N-terminal inactivation domain. Hyper-phosphorylation of the RS domain by the kinase Clk1 changes the RS domain structure into a more ordered form. This leads to a disruption of the RRM-RS interaction, release from nuclear speckles and binding of the SR protein to the nascent transcript at the chromatin. Clk1 release is stimulated by the SR specific kinase SRPK and leads to the association of PP1 at the RS domain. The U1-snRNP1 is recruited to the 5'ss. During the splicing process, SRSF1 is de-phosphorylated by (Wegener & Müller-McNicoll, 2020).

Once the spliceosome is fully assembled, splicing activity is dependent on SR protein de-phosphorylation by phosphatases. Early *in vitro* studies demonstrated that inhibition of Ser/Thr-specific phosphatases such as PP1 and PP2A result in the blockage of both catalytic splicing steps (Mermoud et al., 1992). By using various phosphatase inhibitors such as okadaic acid, tautomycin, or microcystin-LR, it was shown that the first splicing step is dependent on PP1 and the second step relies on PP2A without affecting spliceosome assembly (Mermoud et al., 1994; Stojdl & Bell, 1999). *In vitro* studies further revealed that both phosphatases activate splicing (Mermoud et al., 1992; Mermoud et al., 1994), co-purify with several spliceosome co-factors (Tran et al., 2004), and reduce the phosphorylation state of several SR proteins (Kanopka et al., 1998; Misteli & Spector, 1996). These observations were in agreement with studies using thio-phosphorylated splicing factors including SR proteins (Cao et al., 1997; Tazi et al., 1993); Thio-phosphates were immobilized and could not be de-phosphorylated. They had no effect on spliceosome assembly, but displayed similar defects as phosphatase inhibitors in subsequent steps of the

splicing reactions (Cao et al., 1997; Tazi et al., 1993). Conversely, *in vitro* experiments using purified PP1 blocked the formation and the maturation of the spliceosome, but did not have any effects on the splicing reaction itself (Mermoud et al., 1994; Stojdl & Bell, 1999). This blockage of spliceosome assembly could be alleviated by the addition of excess SR proteins (Mermoud et al., 1994). This demonstrates the great importance of the highly regulated phosphorylation dynamics of SR proteins, where hyper-phosphorylated RS-domains recruit the spliceosome to the splice sites, and its hypo-phosphorylated state is critical for spliceosome catalysis.

In contrast to SR protein-specific kinases that phosphorylate their substrates sequentially in C- to N-terminal direction by means of a binding channel, de-phosphorylation by PP1 and PPA2 rely on SR protein conformation. Depending on the accessibility of the RS domain, it originates at the N-terminus (Ma et al., 2010; Corkery et al., 2015) and de-phosphorylates the RS-domain towards the C-terminus (Corkery et al., 2015). PP1 can bind to an inhibitory interacting motif (RVxF), which is highly conserved in various splicing factors (Novoyatleva et al., 2008) and located within the RRM of several SR proteins (Aubol et al., 2017). In contrast to other PP1-interactors, this allosteric platform has low affinity for PP1, which enables a dynamic activity control and fine tunes de-phosphorylation of SR proteins, which is highly relevant for downstream functions such as mRNA export (Sanford et al., 2004; Huang et al., 2004), RNA stability (Popp & Maquat, 2014), cytoplasmic translation (Sanford et al., 2004) and cell *viability* (Lin et al., 2005; Cazalla et al., 2002).

Despite the importance of SR protein phosphorylation in multiple molecular mechanisms, most studies describing phosphorylation dynamics of SR proteins were performed with SRSF1 (see Figure 9). However, recent studies point to distinct phosphorylation mechanisms for other members of the SR protein family (Long et al., 2019).

2.4.5. SR protein shuttling

Numerous RBPs and export factors have been shown to remain bound to mRNAs during their translocation from the nucleus to the cytoplasm and are subsequently re-imported into the nucleus, thus exhibiting nucleo-cytoplasmic shuttling. SR protein re-import was suggested in several studies and confirmed by quantitative heterokaryon assays (Twyffels et al., 2011; Hammarskjöld & Rekosh, 2017; Botti et al., 2017). SR protein shuttling capacities vary among the SR protein family: While SR proteins such as SRSF2, exhibit low shuttling capacities and remain in the nucleus (Cazalla et al., 2002; Lin et al., 2005),

“high-shuttlers” such as SRSF1, SRSF3 or SRSF7 are nuclear exported and subsequently re-imported in a phosphorylation-dependent fashion (Twyffels et al., 2011; Hammarskjold & Rekosh, 2017; Botti et al., 2017). Re-phosphorylation is catalyzed by the SR protein specific kinase SRPK1 (Kataoka et al., 1999; Lai et al., 2000; Lai et al., 2001; Yun & Fu, 2000). Unlike most kinases, which randomly add phosphates to protein domains, SRPK1 contacts SR proteins *via* a conserved docking motif (RVKVDGPR) (Lukasiewicz et al., 2007; Ngo et al., 2005) and accommodates the RS domain in an internal channel to phosphorylates its substrates in a sequential C- to N-terminal direction (Ma et al., 2010).

SRPK1 kinase activity has been only characterized for SRSF1 and exhibits two phases. In the productive phase, SRPK1 rapidly phosphorylates 6-8 peptides at the N-terminus of the RS-domain (Lai et al., 2000; Aubol et al., 2003). This phase is then followed by a slower phase where the remaining 4-6 serines are phosphorylated by a dual-track mechanism incorporating both processive and distributive activity steps (Aubol & Adams, 2011; Ma et al., 2009; Lai et al., 2000). After cytoplasmic re-phosphorylation, the RS-domain interacts with transportin-SR (TRN-SR) (Lai et al., 2000), a member of the importin- β /transportin family, which facilitates the nuclear re-import and re-localization of SR proteins to NS for the next round of splicing (Ding et al., 2006).

2.4.6. SRSF3 domain structure and mRNA export activity

SRSF3 alias SRp20 is the smallest member of the SR protein family. The 164 amino acid (aa) long protein contains a single canonical RRM at its N-terminus and a short RS domain of 78 aa (69% RS content) at its C-terminus (see Figure 10). Although phosphorylation plays a major role in its capacity to regulate alternative splicing, the mechanism by which SRSF3 is phosphorylated has only recently been discovered (Long et al., 2019). In contrast to SRSF1, which is phosphorylated by SRPK1, SRSF3 is phosphorylated by SRPK2. SRPK2 phosphorylation sites are distributed over the RS domain of SRSF3. SRPK2 binds the RS domain *via* a docking groove and phosphorylates SRSF3 in a C- to N-terminal direction (Long et al., 2019). SRPK2 interaction is crucial for SRSF3 activity and localization, since SRPK2 knock out experiments lead to the translocation of SRSF3 from nuclear speckles to the nucleoplasm (Long et al., 2019).

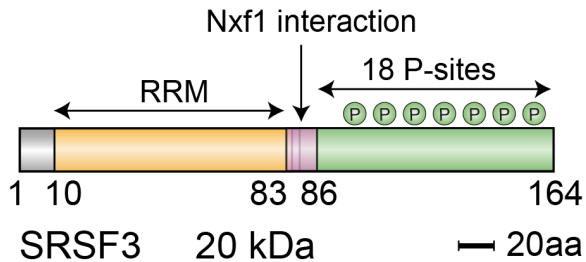


Figure 10: SRSF3 domain organization. SRSF3 alias SRp20 consists of an N-terminal RNA recognition motif (RRM), a linker domain which interacts with Nxf1 (pink), and a 78 amino acid (aa) long RS-domain containing 18 serines, which can be potentially phosphorylated.

SRSF3 regulates the alternative splicing of many transcripts including its own mRNA. It binds to exon 4 within its pre-mRNA and promotes its inclusion. This generates a highly unstable isoform with an in-frame stop codon, enabling SRSF3 to autoregulate its own expression (Galiana-Arnoux et al., 2003; Gonçalves et al., 2008; Jumaa et al., 1997; Jumaa & Nielsen, 1997, 2000; Yu et al., 2004).

Besides its essential role in constitutive and alternative splicing, SRSF3 regulates the mRNA life cycle regulation at multiple levels, such as transcription termination (Cui et al., 2008), alternative polyadenylation (APA) (Lou et al., 1998; Müller-McNicoll et al., 2016), as well as mRNA export (Müller-McNicoll et al., 2016). The SRSF3 mRNA export function was recently shown to be essential for pluripotency and reprogramming, e.g. by mediating the mRNA export of pluripotency factor *Nanog* (Ratnadiwakara et al., 2018; Ohta et al., 2013). SRSF3 controls mRNA export at multiple levels. First, it regulates *Nxf1* alternative splicing and promotes retention of intron 10 to generate a truncated *Nxf1* isoform which is incapable of interacting with the NPC, thus reducing the levels of a functional export machinery (Ratnadiwakara et al., 2018; Li et al., 2016b). Second, SRSF3 acts as an export adaptor by directly interacting with Nxf1. This adaptor function was demonstrated by SRSF3 overexpression experiments leading to increased Nxf1 mRNA binding capacities (Müller-McNicoll et al., 2016). In addition, the RNA-binding profiles of SRSF3 and Nxf1 determined by iCLIP revealed that Nxf1 and SRSF3 co-bind at transcript 3' ends and have similar binding motifs, indicating that SRSF3 recruits Nxf1 to 3'untranslated regions (UTR) (Müller-McNicoll et al., 2016). Two regions in the linker domain, which are located between the RRM and the RS domain are important for the SRSF3-Nxf1 interaction: a region between 81-90 aa, has been shown in pull down experiment to be sufficient for Nxf1 interaction (Hargous et al., 2006). In addition an arginine di-repeat at position 98-99 aa mutation reduces Nxf1 interaction (Botti et al., 2017).

Although other SR protein family members, such as SRSF1 and SRSF7 also act as Nxf1 export adaptors, a systematic quantitative comparison of SR protein shuttling capacities, Nxf1 interaction profiles and global RNA-binding patterns revealed that SRSF3 is the most potent export adaptor among the SR protein family (Botti et al., 2017; Müller-McNicoll et al., 2016). A transcriptome-wide analysis of seven SR proteins

identified 1189 export targets; more than one third belonged to SRSF3 (Müller-McNicoll et al., 2016). Quantitative heterokaryon assays to measure the nucleo-cytoplasmic shuttling capacities of canonical members of the SR protein family categorized SRSF1, SRSF7 and SRSF3 as high shuttlers (Botti et al., 2017). SRSF3 exhibited the highest shuttling dynamics comparable with Nxf1, suggesting that both proteins co-shuttle within the same mRNPs (Botti et al., 2017). Co-immunoprecipitation experiments revealed further that the interaction of SR proteins with Nxf1 is highly phosphorylation dependent. Only hypo-phosphorylated SRSF1, SRSF3 and SRSF7 co-purify with Nxf1 (Huang et al., 2004; Müller-McNicoll et al., 2016). Since SR proteins become partially de-phosphorylated during the splicing reaction, these findings suggest that the phosphorylation state of SR proteins regulates mRNA export in a splicing dependent manner. But this has not been directly demonstrated so far.

2.4.7. SRSF3 regulation in cellular proliferation

At physiological conditions, SRSF3 expression levels and functions are tightly regulated during cell cycle progression (Jia et al., 2010). SRSF3 associates with chromatin in a cell cycle dependent manner, suggesting its involvement in cell cycle control *via* chromatin organisation (Shirahata-Adachi et al., 2017). Cellular growth rates are proportional to SRSF3 protein concentrations and correlate with reciprocal apoptotic tendencies. Cells with reduced SRSF3 levels have decreased growth rates due to cell cycle arrest, but show an activation of the apoptosis pathway (He et al., 2011). In agreement with these findings, different cancer types exhibit high SRSF3 levels suggesting that SRSF3 dysregulation is involved in tumor initiation and progression. Interestingly, SRSF3 dysregulation has been shown to modify the alternative splicing pattern of p53, a tumor suppressor, which is mutated in most cancer types, indicating that SRSF3 controls the cell cycle in multiple ways (Ibrahim et al., 2014).

Pluripotent stem cells are characterized by their high proliferative rates. Recent studies highlighted the impact of SRSF3 during induced pluripotent stem cell (iPSC) generation. The upregulation of SRSF3 during iPSC generation is characterized by a biphasic expression profile that reflects the two transcriptional waves of pluripotent cell reprogramming (Ratnadiwakara et al., 2018). SRSF3 expression is synchronized with increased expression of the OSKM factors (*Oct4*, *Klf4*, *Sox2* and *Myc*), the four key transcription factors that drive and maintain cellular pluripotency and thereby coordinate the pluripotency gene expression program (Ratnadiwakara et al., 2018). SRSF3-dependent transcriptome modulations are also essential during embryonic fibroblast development (MEFs), as well as blastocyst formation (Ohta et al.,

2013; Los Angeles et al., 2015). However, how SRSF3 coordinates the differential expression of distinct transcripts is only poorly understood.

2.5. mRNA export and nuclear surveillance

The compartmentalization of eukaryotic cells created additional mechanisms to regulate gene expression and to control the quality of RNA maturation. Multiple nuclear export pathways exist for the different RNA species. Although they are mechanistically distinct, all export pathways adhere to the same five principles: i) RNA export is selective and affects only export-competent RNA species; ii) RNA export is directed and *per se* irreversible; iii) RNA export is energy consuming and requires ATP; iv) RNAs are exported *via* the NPC; and v) export is facilitated through export factors, which interact with the NPC. With around 125 mDa, the NPC is one of the largest protein complexes in eukaryotes and traverses the outer and inner nuclear membrane (Bodoor et al., 1999). It forms an octagonal structure, which is highly conserved among eukaryotes and is composed of a nuclear basket, a central cylindrical transport channel and eight cytoplasmic fibrils (see Figure 11). The NPC scaffold contains distinct copies (8, 16, 32) of 30-50 different proteins, collectively named nucleoporins (Nups) (Li et al., 2016a). Some Nups are characterized by multiple repeats of phenylalanines (F) and glycines (G) separated by spacer sequences. These so-called FG-Nups are thought to facilitate the interaction with export factors in domains that are distinct from their respective cargo (Li et al., 2016a).

While molecules smaller than 40 kDa can freely pass the NPC *via* diffusion (Aramburu & Lemke, 2017), the NPC acts as a selective barrier for larger complexes such as mRNPs. Active translocation of mRNPs involves multiple rearrangements within the NPC and expands the central transport channel from 9 nm to 25 nm in diameter (Wente & Rout, 2010). Despite this, the active transport of RNPs and the translocation capacity of NPCs is enormous. Studies using high temporal resolution SPEED (single-point edge-excitation subdiffraction) microscopy estimated that mRNAs are exported within a timeframe of 20-180 ms (Kelić & Yang, 2014; Grünwald & Singer, 2010), where docking and release are the time limiting processes, each taking around 40% of the entire export process (Grünwald & Singer, 2010). This time frame corresponds with flow rates in the order of 10^3 translocation events per second. Since one eukaryotic cell contains around 3,000-5,000 NPCs, millions of macromolecules are actively being transported in every cell each second (Ribbeck & Görlich, 2001).

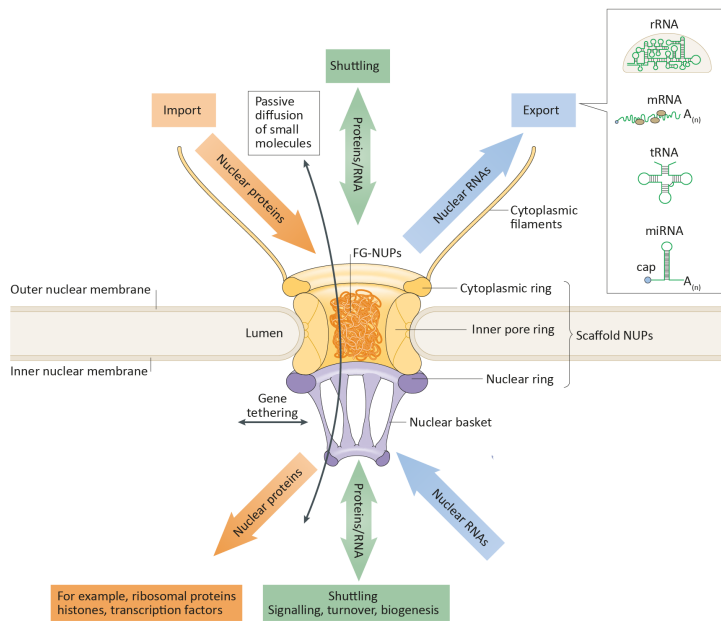


Figure 11: Molecular architecture and functions of the nuclear pore complex. The nuclear pore complex (NPC) is embedded within the nuclear envelope and anchored by scaffold nucleoporins (Nups). It is composed of the cytoplasmic/inner/nuclear ring and peripheral elements such as cytoplasmic filaments, which supports the disassembly of the mRNP and the nuclear basket, which functions as a mRNP tethering platform. The central NPC channel contains multiple repeats of phenylalanine (F) and glycine (G) rich Nups (FG-Nups), which control the nuclear RNA export. The NPC controls the transport of macromolecules in both directions. While small molecules diffuse freely through the NPC, nuclear export and import of macromolecules are active processes (mod. Beck & Hurt, 2017).

Nuclear export is not restricted to protein-coding mRNAs but also includes transfer RNAs (tRNAs), micro RNAs (miRNAs), ribosomal RNAs (rRNAs) and small nuclear RNAs (snRNAs). Since rRNAs and snRNAs are not translated into proteins, the nuclear export of these RNA species is part of a cytoplasmic maturation process that prevents the aberrant association of nuclear pre-cursors with its respective ribozyme (Hyjek et al., 2015; Zemp & Kutay, 2007).

Most RNA species such as rRNAs, snRNAs, replication-dependent histone RNAs, and tRNAs share a highly similar organization, structure and *cis*-acting elements. Thus, maturation and export follow a defined mechanism, which is distinct for each RNA species. This contrasts with mRNAs, which are highly heterogeneous since the length of transcripts, UTRs or introns, as well as the composition of *cis*-acting elements can vary extremely. Hence, mRNA export is distinct from the export of most other RNA species and includes additional steps, e.g. the recruitment of export factors *via* numerous RBPs collectively named export adaptors. Usually export adaptors bind RNA with high affinity and specificity and anchor export factors *via* protein interaction platforms. Most of them have additional functions in mRNA processing and thereby couple mRNA export to each nuclear mRNA maturation step. This interconnected network raises the question whether processing factors that exhibit export adaptor capabilities act in quality control or surveillance mechanisms and prevent mis-processed mRNA species from their export.

2.5.1. Nxf1-mediated mRNA export

Similar to many other molecular pathways in mammalian cells, the Nxf1-mediated mRNA export pathway was initially discovered by studies of host-virus interactions. In the early 1990s, a novel *cis*-acting RNA element was identified in the Mason Pfizer monkey virus. This so-called constitutive transport element (CTE) was shown to be essential for the export of viral RNAs, since point mutations in its stem-loop led to a complete export block (Cullen, 1998; Gruter et al., 1998; Li et al., 2006; Segref et al., 1997).

Microinjection experiments in *Xenopus* oocytes and mammalian cells demonstrated that the CTE element also triggers the export of other RNA species (Pasquinelli et al., 1997; Saavedra et al., 1997b). These results strongly suggested an interaction of the viral RNA with a host cell protein that is directly involved in mRNA export. A proteome-wide screen of CTE-binding proteins (CTE BP) led to the identification of Nxf1 (alias TAP) (Gruter et al., 1998). The role of Nxf1 as a *bona fide* mRNA export factor for cellular mRNAs was supported by experiments which showed that: i) excess CTE RNA inhibited the export of cellular mRNAs, but did not interfere with other export pathways (Pasquinelli et al., 1997; Saavedra et al., 1997b); ii) injection of recombinant TAP protein overcame this mRNA export block (Gruter et al., 1998), and iii) bulk pA+RNA export was dependent on the Nxf1 yeast orthologue Mex67 in *Saccharomyces cerevisiae* (Segref et al., 1997). Moreover, Nxf1 depletion led to the export block of bulk pA+RNA in other cell types and organisms, establishing Nxf1 as the major export factor in metazoans (Aibara et al., 2015).

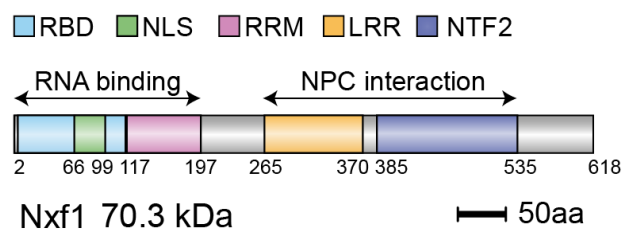


Figure 12: Nxf1 domain organization. Nxf1 contains an N-terminal RNA binding domain (RBD), including a classical nuclear localization signal (NLS) and a pseudo RNA recognition motif (RRM), which serves as an interaction domain with export adaptors and mRNA targets. The C-terminal domain consists of a leucine rich repeat (LRR) and a nuclear transport factor 2-like domain (NTF2) to contact the Nxf1 co-factor Nxt1 and the nuclear pore complex.

Nxf1 is evolutionary conserved and shows high sequence similarities in worms, flies, fishes and mammals (Herold et al., 2000b). The N-terminus of Nxf1 is generally arginine-rich and serves as an RNA binding region. It harbors an RNA binding domain (RBD), a nuclear localization signal (NLS) as well as a pseudo RNA recognition motif (ψ RRM) (Bachi et al., 2000; Bear et al., 1999; Truant et al., 1999) (see Figure 12). The C-terminus of Nxf1 is composed of a leucine rich repeat (LRR) domain and a nuclear transport factor 2-like domain

(NTF2). These domains directly contact FG-Nups of the NPC and interact with the Nxf1 co-factor Nxt1 (p15), which has been shown to be essential for the NPC interaction (Izaurralde, 2002). Hence, the

heterodimeric export factor complex Nxf1/Nxt1 synergistically permits the translocation of mRNAs through the central channel of the NPC.

RBD and LRR have been shown to be both necessary and sufficient to bind the CTE element (Ho et al., 2002). However, most cellular mRNAs do not contain CTEs and their association with Nxf1/Nxt1 heterodimers is dependent on its recruitment through trans-acting export adaptors. Since the N-terminal RBD of Nxf1 binds to RNA non-specifically and with low affinity (Viphakone et al., 2012; Walsh et al., 2010), the interplay of Nxf1/Nxt1 with export adaptors bridges the interaction between mRNAs and the export factor.

Interestingly, Nxf1 exports unspliced RNAs when being tethered to it (Li et al., 2006; Hargous et al., 2006). This indicates that mRNA export is unselective and specificity is solely achieved *via* selective RNA-binding, assigning export adaptors an essential role in controlling the mRNA export process. Several export adaptors such as SR proteins, Uap56, and Alyref, as well as several co-adaptors (Chtop, Thoc5, Cpsf6, Rbm7) associate co-transcriptionally with the nascent transcript (Bentley, 2005; Viphakone et al., 2019). Some of them are recruited by the phosphorylated CTD of PolII (see Figure 13). They recruit the export factor by interacting with its N-terminal domain (TREX-1) or the linker domain (SR proteins). Their binding generally increases the RNA binding capacity of Nxf1, which is a hallmark of an Nxf1 export adaptor.

The TREX-1 complex is the most important export adaptor in metazoans and recruits the Nxf1/Nxt1 heterodimer. It consists of the helicase Uap56, the Tho complex with Thoc1 (THO1/Hpr1/p84), Thoc2 (THO2), Thoc3 (THO3/Tex1), Thoc5 (THO5/fSAP79), Thoc6 (THO6/fSAP35), and Thoc7 (THO7/fSAP24) Alyref and Cip29 (pDIP3/ZC11A) (Strasser et al., 2002). The association of its constituents occurs co-transcriptionally and in a sequential order. The ATP-bound form of Uap56 stimulates the recruitment of Alyref, which is dependent on the association of the cap-binding complex to the nascent transcript. In turn, Alyref triggers the helicase activity of Uap56 to unwind the RNA, change the mRNP composition and handover Alyref to the exon junction complex (EJC) (Bentley, 2014; Taniguchi & Ohno, 2008; Viphakone et al., 2019).

The EJC, which is composed of Eif4a3, Rbm8a and Magoh is deposited 20-24 nt (Hauer et al., 2016; Le Hir et al., 2000) upstream of exon-exon junctions and hence binds post-splicing (Viphakone et al., 2019). Thoc5 and Alyref binding induce a conformational change in Nxf1 from a closed form with low RNA binding

capacities, to an open form with increased RNA binding affinity (Viphakone et al., 2012). The Uap56-interacting factor Uif subsequently interacts with Nxf1 and directs the mRNP complex through the interchromatin space to the NPC.

The mature and export-competent mRNP allows docking to the nuclear basket in an Uif-dependent manner. A series of interactions between Nxf1/Nxt1, Tpr and multiple FG-Nups, namely Nup153, Nup98 and Rae1, finally translocate the mRNP through the central channel to the cytoplasmic site where cytoplasmic fibrils release RBP cargoes and export factors/adaptors are recycled and shuttle back to the nucleus for the next mRNA export round (Coyle et al., 2011; Ernst et al., 1997; Wang et al., 2015).

This shuttling process is highly regulated and dependent on NPC-associated fibrils. Overexpression of the oncogene eIF4E led to major alterations in the composition of the cytoplasmic face of the NPC and resulted in the loss of fibrils, which enhanced mRNA export due to an elevated release and recycling of export factors/adaptors (Culjkovic-Kraljacic et al., 2012). The export factor heterodimer Nxf1/Nxt1 is not restricted to the adaptor TREX-1 but can also associate with an alternative mRNA export complex coined AREX (Yamazaki et al., 2010). Although AREX exhibits high similarities to TREX-1 and includes the common constituent Cip29, as well as Urh49 a protein that shares more than 96% sequence homology with Uap56, a transcriptome-wide analysis of subcellular fractionated cells revealed that TREX-1 and AREX regulate the export of distinct sets of mRNAs.

While TREX-1 targets the majority of mRNAs, AREX regulates the export of a small subset of transcripts involved in cell cycle regulation and mitosis (Yamazaki et al., 2010). Depletion of the AREX component Urh49 resulted in the down-regulation of mitotic mRNAs and led to mitotic defects, chromosome arm resolution disorders and failure of cytokinesis due to an impaired export of *Survivin* and *PRC1* mRNAs (Yamazaki et al., 2010). Thus, it is conceivable that multiple export adaptors control specific RNA regulons *via* bridging specific RNA binding and recruitment of export factors to these RNA subsets.

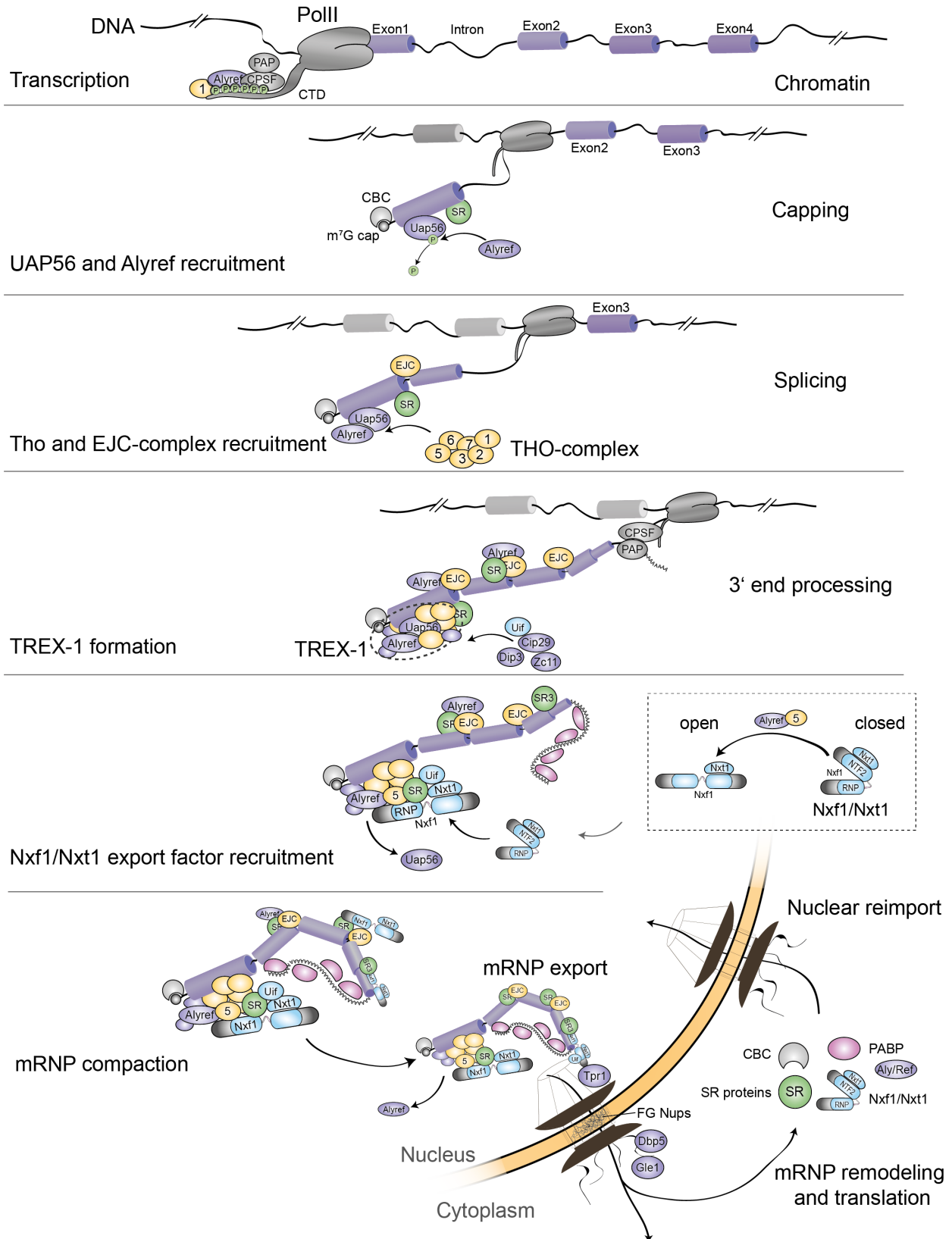


Figure 13: Nxf1 mediated nuclear mRNA export. TREX-1 complex constituents (Thoc1, Alyref) associate to the phosphorylated CTD of PolII. Co-transcriptionally, these factors as well as SR proteins and phosphorylated Uap56 are

recruited to the nascent transcript in a cap-binding complex-dependent manner. De-phosphorylation of Uap56 leads to re-arrangements of the RBP composition and recruitment of Alyref, THO-complex and Cip29, Dip3, Zc11 and forms TREX-1. After the splicing reaction, the exon junction complex (EJC) associates to the nascent transcript. SR proteins, TREX-1 and EJC each can recruit Nxf1/Nxt1 hetero-dimers, whereas Thoc5 and Alyref stimulate the conformational change of Nxf1 from the closed form to an open form with increased RNA binding affinity. The Uap56-interacting factor associates with the transcript and leads the export competent and compacted mRNP to the NPC. Uap56 and Alyref dissociate from the mRNP prior to cytoplasmic translocation. The C-terminal domain of Nxf1 and Nxt1 docks at the NPC including its “gate keeper” Tpr1 and promotes the export by interacting with FG-Nups. On the cytoplasmic face, export factors and adaptors dissociate from the mRNP *via* the helicase activity of Dbp5, which is associated with the cytoplasmic fibrils. Nxf1 switches back to its low binding conformation. SR proteins, the CBC complex, Nxf1 and nuclear polyA binding proteins (PABPs) shuttle back to the nucleus and are recycled (mod. (Viphakone et al., 2019)).

Single export adaptor or export adaptor configurations can stimulate the export of defined mRNAs. One example is the Tho-complex component Thoc5, which is not essential for nuclear export of bulk pA+RNA, but triggers the export of the heat shock protein *HSP70* under certain cellular stresses (Tran et al., 2014; Katahira et al., 2009). However, in combination with Thoc2, the Thoc5 mRNA export target pool is extended to the pluripotency factors *Nanog*, *Sox2*, *Klf4* and *Esrrb*, thereby controlling and maintaining pluripotency (Wang et al., 2013). Another export adaptor, which selectively stimulates the nuclear export of a subset of transcripts is the TREX-2 constituent Ganp. Transcriptome wide identification of Ganp targets revealed that mRNA export kinetics of Ganp-dependent transcripts are more rapid than non-targets, although the export pathway is mediated *via* Nxf1. The authors suggested that the Ganp-facilitated export provides the cell with a “fast track” to quickly stock up protein levels, which are crucial for cellular homeostasis (Wickramasinghe et al., 2014).

Export adaptor activities seem to be interchangeable and can compensate and replace each other. Depletion experiments, in combination with pA+RNA FISH retention assays, revealed that the export adaptor activity of Alyref and Uif is functionally redundant and they can be replaced by other export adaptors such as Luzp4, which is up-regulated in a range of tumors, and increases tumor progression by stimulating the export of bulk pA+RNA (Viphakone et al., 2015). In addition, the recruitment of export adaptors to mRNAs can be modulated by other factors that stimulate their RNA binding affinity and this way trigger the export of a specific subset of transcripts. One example was described where the Alyref RNA binding capacity and specificity to transcripts that encode for proteins involved in genome duplication and repair is controlled by the inositol polyphosphate multikinase (IPMK) (Wickramasinghe et al., 2013).

The constantly growing number of studies reporting the selective export of specific transcripts *via* specific export adaptor compositions suggests that higher eukaryotes may even use additional export adaptors to regulate specific cellular processes that have not been identified so far. Moreover, several studies demonstrated that the SR protein export adaptor function is crucial for the nuclear export of numerous transcripts, however, their interplay with other export adaptor complexes is not yet understood.

2.5.2. The interplay between nuclear splicing and mRNA export

Although the inter-dependency of nuclear splicing and cytoplasmic export was under debate, first observations were already published in the 90's, where mutations of the β -globin transcript at either the 5' or the 3' ss resulted in the accumulation of mutant reporter RNAs in the nucleus (Chang & Sharp, 1989). These results were in agreement with a study using subcellular fractionated monkey cells. Here, the authors co-transfected plasmids containing the full length Simian-Virus 40 (SV40) DNA as well as a SV40 construct that lacked introns, and found that the full-length SV40 transcript was efficiently transported, while its cDNA counterpart was largely retained in the nucleus (Ryu & Mertz, 1989). Nineteen years later, a very similar study confirmed the splicing-dependent nucleo-cytoplasmic distribution of SV40 mRNA by FISH experiments in human HeLa cells (Valencia et al., 2008). Meanwhile, there are multiple lines of evidence that splicing and export are coupled. Several studies reported that inhibition of splicing by small molecule inhibitors (Effenberger et al., 2014; Kaida et al., 2007; Hett & West, 2014; Yoshimoto et al., 2017; Brody et al., 2011; Pawellek et al., 2017), depletion of essential splicing factors (Kaida et al., 2007), or direct targeting of the spliceosomal snRNAs (O'Keefe, 1994; Hett & West, 2014) caused the nuclear retention of polyadenylated mRNAs.

The tight interconnection between splicing and mRNA export enables the cell to control the quality of the maturation process of pre-mRNAs and retain potentially immature transcripts in the nucleus. This superior quality control mechanism can be termed as an export-dependent splicing surveillance pathway and follows two different mechanistic principles. Firstly, export adaptors associate with the mRNP in a splicing-dependent manner and export of immature RNA species is impaired due to a lack of export factor recruitment. Secondly, retention factors actively anchor improperly spliced RNA in the nucleus and override the activities of export factors that are associated with the mRNP.

The selective association of export factors with fully spliced mRNAs has been reported in several studies and mostly affect components of the TREX-1 complex. Most of the TREX-1 complex components have been shown to interact with splicing factors and co-localize with the splicing machinery in nuclear speckles (Rodrigues et al., 2001; Zhou et al., 2000; Masuda et al., 2005). When these components are depleted, polyadenylated mRNAs accumulate in nuclear speckles as exemplified for Alyref and Uap56 (Dias et al., 2010; Girard et al., 2012). Splicing activity and the TREX-1 recruitment are tightly connected: splicing promotes the TREX-1 complex recruitment to its RNA targets *via* an interaction between the cap-binding protein CBP80, Alyref and the Tho complex (Cheng et al., 2006). The TREX-1 complex additionally interacts with the EJC, which is a marker of completed splicing. Reversely, TREX-1 binding stimulates the release of spliced mRNAs from nuclear speckles (Cheng et al., 2006; Zhou et al., 2000).

Heterogeneous nuclear RNP (hnRNP) proteins can act antagonistically to both processes: nuclear splicing and export. They function as antagonists of SR proteins and repress splice site recognition. Their export/retention function has been sub-categorized into nuclear export signal (NES) containing export mediators, which are characterized by a high nucleo-cytoplasmic shuttling capacity, and a non-shuttling group of hnRNP proteins bearing a nuclear retention sequence (NRS) which overrides the NES (Nakielny & Dreyfuss, 1996).

Post-translational protein modifications (PTMs) represent an additional layer in the splicing-export interplay. Since most SR proteins get hypo-phosphorylated during the splicing process and have been reported to promote mRNA export (Huang et al., 2004; Huang & Steitz, 2005), SR proteins are prime candidates to act in nuclear splicing surveillance at the interface between RNA binding, monitoring of the splice status, and the decision between nuclear retention and cytoplasmic transport. Their potential function as nuclear surveillance factors has been suggested, because insertion of strong SR protein binding sites into a reporter transcript lacking introns caused the nuclear retention of the intron-less RNA. Conversely, insertion of an intron and thus active splicing rescued this retention phenotype and led to cytoplasmic mRNA accumulation, most likely promoted by hypo-phosphorylated SR proteins (Taniguchi et al., 2007). This suggests that the SR protein phosphorylation state determines whether they function as export adaptors or retention factors. Hypo-phosphorylated , SRSF1 and SRSF7 marked complete splicing events and recruited the export factor Nxf1, unlike the hyper-phosphorylated states of these two SR proteins (Huang et al., 2004; Huang & Steitz, 2005; Hargous et al., 2006). Conversely, hyper-phosphorylated SRSF1, mimicking an incomplete splicing event, has been shown to increase its affinity to

the retention factor U1-70K and thereby retain immature transcripts in nuclear speckles (Cho et al., 2011). In addition, SRSF5 arginine-methylation and SRSF3 sumoylation has been shown to modulate Nxf1 interaction and splicing efficiency respectively (Botti et al., 2017; Pawellek et al., 2017; Pozzi et al., 2017). However, most studies that suggested an involvement of SR proteins in splicing surveillance were performed *in vitro* or with non-physiological reporter constructs, and they are limited to the SR proteins SRSF1 and 7. An involvement of the most potent export factor SRSF3 in nuclear splicing surveillance was so far not demonstrated.

The cross-regulation of splicing and export is not limited to preventing mis-spliced mRNAs from being exported and translated in the cytoplasm, but also provides eukaryotic cells with an additional layer of gene expression regulation. Transcriptome-wide studies in mouse embryonic stem cells revealed that polyadenylated RNA contains a significant fraction of retained introns, which are conserved among mammalian cells (Jacob & Smith, 2017). These introns were distinct from constitutively spliced introns, highly stable and regulated by post-transcriptional splicing events (Boutz et al., 2015). Splicing can occur upon several cellular stimuli such as DNA damage or neuronal activity and enable the cell with a rapid gene expression response (Boutz et al., 2015; Mauger et al., 2016; Yap et al., 2012; Naro et al., 2017). How these post-transcriptional splicing events are controlled and how mRNAs with specific cellular functions are sequestered and prevented from nuclear exit is not yet understood.

2.5.3. Nuclear RNA retention

Live-cell measurements of labeled RNAs gave first insights into nucleo-cytoplasmic mRNA export dynamics. The nuclear life span of mRNAs was found to be unexpectedly high on a range of 45 min before labeled mRNAs were exported. In the early 80's, Breathnach and colleagues fractionated chicken oviducts using sucrose gradients and detected a significant amount of pre-cursor ovalbumin mRNAs accumulating in the nuclear matrix (Breathnach et al., 1977). Since then, different molecular mechanisms have been proposed how RNAs are retained in the nucleus, which are mostly related to alterations in RNA processing (see below). Nowadays, it is increasingly recognized that nuclear retention constitutes a novel layer of gene expression regulation that fine-tunes protein production by making use of RNA stockpiles and their controlled nuclear release to rapidly respond to changes in cellular conditions (Wegener & Müller-McNicoll, 2018; Fuke & Ohno, 2007).

Some features and *cis*-acting elements have been described in nuclear-retained transcripts, such as long coding regions or 3'UTRs, as well as a reduced GC content (Mauger et al., 2016; Solnestam et al., 2012; Braunschweig et al., 2014). A recent study using a novel massively parallel RNA assay (MPRNA) identified a cytosine-rich (C-rich) motif, that is overrepresented in nuclear versus cytoplasmic sub-cellular fractions (Shukla et al., 2018). In agreement with this study, a similar C-rich motif was enriched in a reporter construct, when a library of DNA-fragments of nuclear RNAs was cloned to its 3' or 5'UTR (Lubelsky & Ulitsky, 2018). This motif was further shown to be bound by the RBP Heterogeneous nuclear Ribonucleoprotein K (HNRNPK) (Lubelsky & Ulitsky, 2018).

In addition, several studies have demonstrated that the polyA tail length can influence the export potential of mRNAs. While short polyA tails of around 50 nt stimulated mRNA export, hyper-adenylated transcripts containing poly-A tails of more than 400 nt in length are nuclear-retained (Gudde et al., 2017). Polyadenylation processivity and activity is tightly controlled by polyA-binding proteins (PABPs) and can be regulated in response to various stimuli and thereby balance the export of transcripts. However, the impact of polyA tail length control on mRNA nuclear export is only poorly understood at this point.

Nuclear-retained RNAs seem to be located at distinct nuclear sites depending on the cause of retention: studies using β -globin reporter transcripts with a mutated splice site lead to an impaired assembly of the spliceosome, and caused its retention at the chromatin together with a stalled transcription machinery (Almeida et al., 2010; Martins et al., 2011). Interestingly, when splicing was inhibited by the small molecule inhibitor SSA, the same reporter with an intact splice site was efficiently cleaved at the 3' end and released from the chromatin but accumulated in NS (Carvalho et al., 2017; Martins et al., 2011). However, sequestration in NS is not limited to reporter genes. Several studies demonstrated that splicing inhibition by different small molecule inhibitors lead to enlarged NS due to the retention of bulk pA+RNA (Carvalho et al., 2017; Kaida et al., 2007; Pawellek et al., 2017). Within this nuclear body, immature mRNAs are stabilized and are protected from exosomal decay. This enables unspliced polyadenylated RNA species, which enter NS associated with stalled spliceosomes, to proceed with splicing later on upon inhibitor withdrawal (Girard et al., 2012).

Immature RNAs are thought to be anchored in NS by RS-domain containing splicing factors, such as U1-70K or U2AF65 (see Figure 14). Their interplay with hyper-phosphorylated SR proteins such as SRSF1 has been suggested to shield the mRNP from interacting with Nxf1 (Cho et al., 2011). Depletion experiments

of Alyref and Uap56 also led to mRNA accumulation in NS, which suggest that release of mRNAs from NS is dependent on the association with the TREX-1 complex (Dias et al., 2010; Girard et al., 2012). However, it remains unclear how the different causes of splicing inhibition are communicated to the retention machinery leading to distinct retention sites.

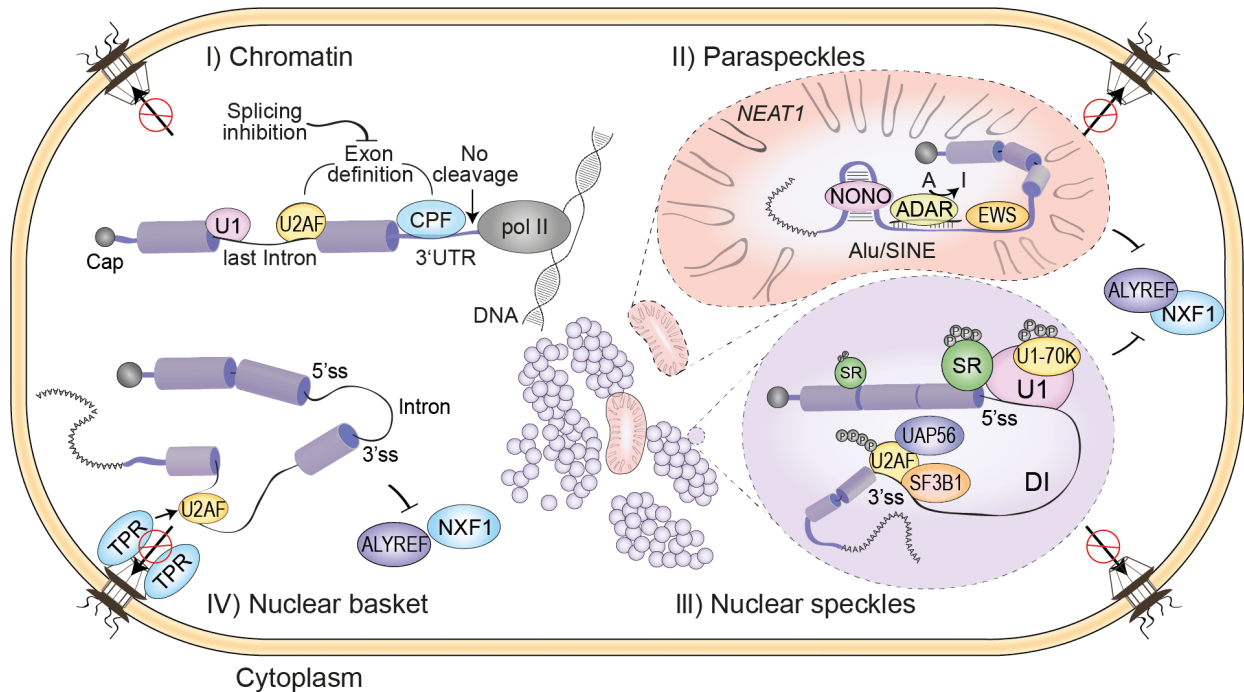


Figure 14: Mechanisms of nuclear mRNA retention. I) Transcripts are retained at the chromatin due to an impaired 3' end processing by the cleavage and polyadenylation factors (CPF), stalled polymerase II (pol II) or inefficient splicing of the last exons. II) Transcripts with dsRNA regions are edited by adenosine deaminase acting on RNA (ADAR) catalyzing adenosine to inosine conversions, which are recognized by NONO and EWS and actively retain edited mRNAs in para-speckles. III) Transcripts with retained introns are bound by pre-spliceosome complexes or RS domain containing RBPs and sequester introns containing transcripts in nuclear speckles. IV) Transcripts lacking the export factor Nxf1, hence being export-incompetent, are recognized by the gate-keeper Tpr, rejected, and return to the nucleoplasm (Wegener & Müller-McNicol, 2018).

Another nuclear RNA retention mechanism is based on editing events within the mRNA sequence. This post-transcriptional modification is catalyzed by adenosine deaminases that act on RNAs (ADARs), which recognize double-stranded RNA (dsRNA) and convert adenosines to inosines (A-to-I RNA editing). Inosines are recognized by specific protein complexes containing PSPC1, NONO and MATR3 and actively retain inosine-containing RNAs in paraspeckles, which are nuclear bodies located in close proximity to NS (Prasanth et al., 2005; Chen & Carmichael, 2009) (see Figure 14).

Successful docking at the NPC does not consequently result in efficient mRNP export. A recent study estimating the translocation efficiency using high-resolution microscopy found that only 25-35% of all mRNPs that dock at the NPC are actually translocated into the NPC central channel, while the remaining 75-65% are rejected and return to the nucleoplasm (Kelich & Yang, 2014). Most of these inefficient NPC translocations are based on the last nuclear quality control checkpoint, which is located at the nuclear basket. The translocated promoter region nuclear basket protein Tpr1 (Mlp1 in yeast) is required for nuclear retention of intron-containing mRNAs or improperly assembled mRNPs (Green et al., 2003; Vinciguerra et al., 2005). Although the underlying mechanism is not completely understood especially in higher eukaryotes, depletion of Tpr1 has been shown to reduce the residence time of mRNPs at the nuclear periphery and causes cytoplasmic leakage of intron containing transcripts (Saroufim et al., 2015). However, computational modeling identifying the minimal system required by nuclear retention mechanisms revealed that the low affinity of RBPs to mis-processed transcripts impairs their interaction with export factors and leads to a decreased interplay with Tpr1, which hinders the export of aberrant mRNAs (Soheilypour & Mofrad) (see Figure 14).

Similar to other physiological processes, the cellular export system responds to a variety of cellular stresses including UV, heat, oxidative and osmotic stress (Datta et al., 2014; Furuta et al., 2004; Kelley & Paschal, 2007; Kodiha et al., 2008; Miyamoto et al., 2004; Yoshimura et al., 2013). Accompanying general inhibition of RNA transcription and processing, most mRNAs are blocked from export (Yost & Lindquist, 1986, 1991). This paves the way for the selective production of proteins that are essential for the stress response. For instance, heat shock leads to the induction of heat shock protein mRNA transcription by distinct transcription factors in mammalian cells, while bulk pA+RNA transcription decreases (Imamoto, 2018). Since most heat shock mRNAs do not contain introns, they are not affected by the inhibition of splicing. In addition, heat shock mRNAs are exported from the nucleus *via* a distinct transport system. *Cis*-acting sequence elements, such as AU-rich elements (AREs) within the mRNAs of heat shock proteins, are recognized by specific transport proteins and guide them to the NPC *via* the chromosomal maintenance 1 (Crm1) export pathway (Gallouzi et al., 2001). Since the mRNA lifecycle of transcripts coding for proteins involved in the heat stress response seem to be distinct from most other mRNAs, a general shut down of mRNA processing and nuclear export can be bypassed. The preferential expression of specific genes enables the cell to respond to multiple stress conditions, and adjust the protein synthesis with high efficiency and efficacy.

Although several studies have shown that nuclear retention occurs due to non-productive or aberrant RNA processing, the underlying molecular retention mechanisms are barely understood. However, the importance of functional export control has been linked to different diseases. For instance, a point mutation in the export factor Gle1, which normally interacts with NPC-associated Nups, renders it defective. Gle1 deficiency results in impaired mRNA export, and has been linked to several motoneuronal diseases, such as lethal congenital contracture syndrome LCCS1 and LCCS2, as well as lethal arthrogryposis with anterior horn cell disease (LAAHD) (Folkmann et al., 2014; Narkis et al., 2007; Nousiainen et al., 2008).

Repeat expansion diseases are also characterized by a dysregulated mRNA export. They are caused by an abnormal number of RNA repeats in different genes and can lead to the formation of nuclear aggregates that sequester multiple essential RBPs, such as splicing factors, thereby impairing RNA processing and mRNA export globally. Patients with repeat expansion mutations can suffer from neuromuscular disorders, such as oculopharyngeal muscular dystrophy (OPMD) (Raz & Raz, 2014; Klein et al., 2016; Bengoechea et al., 2012; Bastide et al., 2016), myotonic dystrophy type 1 (DM1) (Pettersson et al., 2015), Huntington's disease (HD) (Mezer et al., 2011) or neurodegenerative diseases, such as amyotrophic lateral sclerosis (ALS) (Freibaum et al., 2015), and frontotemporal lobar degeneration (FTLD) (Buratti, 2015). Numerous disorders and diseases are caused by splice site mutations and mis-regulated splicing. Transcripts with splicing defects are most likely also impaired in the mRNA export. In fact, patients suffering from Osteogenesis imperfecta (OI) (Johnson et al., 2000) or Alzheimer's disease (Xu et al., 2008) have been shown to generate abnormal transcript isoforms that are sequestered in NS. Thus, it is conceivable that deregulation of mRNA export contributes to numerous genetic disorders. Although many studies have shown that nuclear-retained RNAs are sequestered in NS, the molecular retention mechanism and the role of SR proteins in this process is not yet fully understood.

2.5.4. Nuclear surveillance in yeast and higher eukaryotes

Nuclear surveillance mechanisms differ between yeast and higher eukaryotes (Wegener & Müller-McNicoll, 2018). The reason for this is the fact, that in higher eukaryotes RNA processing events such as splicing occur more frequent, have more sophisticated regulons and correspondingly have multiple levels of quality control. Over 95% of the human genes constitute introns (Lander et al., 2001), which is in stark contrast to the genome of *Saccharomyces cerevisiae*, which contains only around 250 introns in 6,000 genes, which corresponds to 4% of all yeast genes (Parenteau et al., 2008). Since pre-mRNA splicing are

rather rare events, splicing dependent surveillance mechanisms do not regulate the majority of mRNAs in yeast.

Nuclear surveillance mechanisms in yeast are dependent on the interplay between mRNA export, and decay by the nuclear exosome. The nuclear exosome is highly conserved among eukaryotes. It is composed of a central hexameric ring associated with three subunits Rrp40, Rrp4 and Csl4 layered on the upper surface (Makino et al., 2015). This 9-protein complex, named EXO9 forms the exosomal backbone, is catalytically inactive and is also found in the cytoplasmic counterpart of the exosome. The catalytic activity is supplied by the associated nucleases EXOSC10 (Rrp6) and EXOSC11 (Dis3) positioned at the opposite ends of EXO9 (Makino et al., 2015). EXOSC10 and 11 are 3' to 5' exonucleases while the latter has an additional endonucleolytic activity (Lebreton et al., 2008; Schaeffer et al., 2009; Schneider et al., 2009). Since EXOSC10 associate to a co-factor C1D (Rrp47) the nuclear exosome is also coined EXOSC12 according to the total subunits (Makino et al., 2015). In higher eukaryotes EXOSC10 is restricted to the nucleolus (Allmang et al., 1999; Kilchert et al., 2016; Tomecki et al., 2010), while the yeast counterpart Rrp6 is equally distributed in both nucleoplasm and nucleolus (Allmang et al., 1999; Staals et al., 2010; Shiomi et al., 1998).

Several studies in the last decade describe, that exosomal targeting is achieved by co-factors that recognize RNA substrates and lead the degradation machinery to its targets (Meola & Jensen, 2017). In *Saccharomyces cerevisiae* a well-studied co-factor Trf4/5-Air1/2-Mtr4 polyadenylation named TRAMP complex recognizes a variety of RNA species such as tRNAs (Kadaba et al., 2004; Vanáčová et al., 2005), rRNAs (Dez et al., 2006; Wlotzka et al., 2011), sn/snoRNAs (Wlotzka et al., 2011; Losh et al., 2015), telomeric RNAs (Houseley et al., 2007), cryptic unstable transcripts (CUTs) (Wlotzka et al., 2011; Wyers et al., 2005), and pre-mRNAs (Wlotzka et al., 2011; Bresson et al., 2017; Roth et al., 2009). It consists of the poly(A) polymerase (PAP) (Trf4/Trf5), an RNA binding protein (Air1/Air2) and the RNA helicase Mtr4 (Han & van Hoof, 2016; Wang et al., 2007; Xu et al., 2009). While the Trf4 adds a short homopolymeric adenosine-tail to its targets, the helicase activity of Mtr4 unwinds and threads the RNA into the central channel of the exosome (Bernstein et al., 2007; Patrick et al., 2017; Jia et al., 2012).

The involvement of exosomal decay in nuclear surveillance in higher eukaryotes is only poorly understood. Three exosomal co-factors have been identified yet in human nuclei (NEXT, PAXT and hTRAMP). While NEXT and PAXT are not present in yeast, the human counterpart of TRAMP, is confined to the nucleolus

and has been reported to predominantly participate in processing and degradation of rRNA (Lubas et al., 2011). The NEXT complex and the PAXT connection share common features and follow the same mechanism: While RNA-binding capability and specificity is provided by the bridging factors RBM7 (NEXT) and PABPN1 (PAXT), the helicase activity of hMTR4 is stimulated and controlled by ZcC8 (NEXT) and ZFC3H1 (PAXT) (Lubas et al., 2011; Meola et al., 2016). Both exosomal adaptor complexes NEXT and PAXT are activated by interacting with two additional factors ARS2 and Zc3H18 (Puno & Lima, 2018; Meola et al., 2016). ARS2 is associated to the cap-binding proteins CBP20 and CBP80 *via* the adapter protein Zc3H18 and forms the so-called CBCA complex (Lubas et al., 2011; Lubas et al., 2015). The CBCA complex associates with NEXT/PAXT and tether the nuclear exosome to its targets.

How cells discriminate between high and low quality processed transcripts and modulate mRNA half-life accordingly is not understood. In yeast, surveillance factors involved at the interphase between nuclear export and exosomal decay control nuclear surveillance and define the mRNA life-cycle. If these surveillance factors, their activity and the molecular mechanisms are conserved among eukaryotes is so far not known.

2.5.5. The surveillance factor Nab2 in yeast

Nab2 has been shown to act as the key surveillance factor in yeast that connects nuclear RNA export with nuclear retention and exosomal decay. It was first described in 1993, when Anderson and colleagues isolated UV-crosslinked hnRNPs and subsequently detected nuclear polyadenylated RNA-binding protein 2 (Nab2) using a polyclonal antiserum against yeast RNPs. Nab2 was one of the most abundant proteins associated with nuclear polyadenylated RNA. Further characterization using *in vitro* RNA-binding assays revealed a high affinity of Nab2 to RNA homopolymers, as well as to single stranded DNA sequences (Anderson et al., 1993). Studies using nitrocellulose filter-binding assays (Hector et al., 2002), microarray analysis (Kim Guisbert et al., 2005) and SELEX experiments (Riordan et al., 2010) reported a high affinity of Nab2 to poly-adenosines, which led to its classification as a polyA binding protein (PABP).

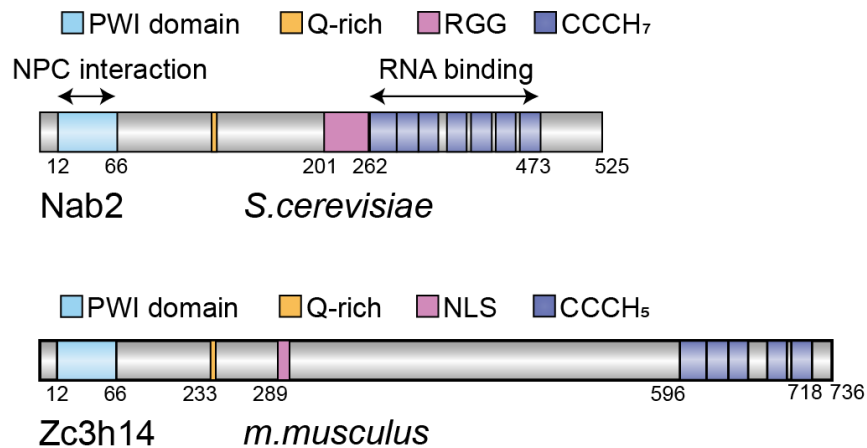


Figure 15: Nab2 and Zc3h14 domain organization. Nab2 contains an N-terminal PWI-like domain, which contacts the nuclear pore complex (NPC), a glutamine-rich (Q-rich) domain with unknown function, an RGG-rich domain, serving as nuclear import signal and seven C-terminal CCCH-type zinc finger domains (ZnFs) which contact mRNAs. Zc3h14 shares a similar organization but contains only five ZnFs and a classical nuclear localization signal (NLS).

In contrast to most PABPs, where binding affinity and specificity is achieved *via* an RRM, Nab2 is the founding member of a novel class of PABPs containing CCCH-type zinc finger domains (ZnFs) (Kelly et al., 2007; Leung et al., 2009). The protein architecture is highly conserved among eukaryotes and is characterized by two domains: the N-terminus contains a five alpha-helical bundle with a PWI-like fold (Grant et al., 2008; Marfatia et al., 2003; Leung et al., 2009) and functions as a protein-interaction platform (Grant et al., 2008; Marfatia et al., 2003; Suntharalingam et al., 2004; Fasken et al., 2008; Zheng et al., 2010). The C-terminal domain contains seven tandem ZnF domains, which provide Nab2 with its RNA-binding capacity and specificity (see Figure 15).

Nab2 exhibits multiple functions, which are essential for cellular RNA homeostasis in yeast: it regulates polyA tail length, controls nuclear mRNA export and stimulates the exosomal decay of transcripts (Soucek et al., 2012). These functions are highly interconnected since polyA tail length is a decisive feature for mRNA export or nuclear decay. The first observation involving Nab2 in polyA tail length control was published by Hector and colleagues in 2002. They performed *in vitro* polyadenylation assays with total RNA treated with an RNase T1/A cocktail that hydrolyzes RNAs at C, U and G residues, but not As. The length of the remaining radiolabeled polyA tail was determined by electrophoresis and led to the observation that its length increased nearly 2-fold when Nab2 was depleted (Hector et al., 2002).

The RNA-binding capacity of Nab2 is dependent on its C-terminal ZnF domains. Only the three highly conserved ZnFs 5-7 are functional and essential for pA+RNA binding (Marfatia et al., 2003; Anderson et al., 1993). Solution and crystal structures indicated that binding of the non-conserved ZnFs 1-5 is restricted to short 2-3 nt adenosine oligomers (Brockmann et al., 2012; Kuhlmann et al., 2014; Martínez-Lumbreras

et al., 2013), while the conserved ZnF domains form a highly geometric structure. Nab2 homodimerizes at this site and is surrounded by a polyadenosine track, which covers a length of approximately 60 nt (Aibara et al., 2017; Viphakone et al., 2008). In agreement with this observation, mutagenesis of ZnFs 5-7, but not the N-terminal region displayed a diminished polyA binding capacity, and correlated with an extension of polyA tails (Kelly et al., 2010; Hector et al., 2002). These Nab2 mutants also showed defects in the cytoplasmic export of pA+RNA (Hector et al., 2002; Marfatia et al., 2003) and were highly sensitive to nuclear decay by the nuclear exosomal subunit Rrp6 (Grenier St-Sauveur et al., 2013).

The best-studied nuclear regulator of polyA tail length in yeast is Pabp2 (Goss & Kleiman, 2013). Pabp2 targets are clearly overlapping with those of Nab2. However, the two PABPs are acting antagonistically and have opposing effects on diverse regulatory mechanisms: while Pabp2 has positive effects on polyA tail length by increasing the processivity of the polyA polymerase (PAP), Nab2 limits the length of polyA tails. Despite their different RNA-binding domains - a ZnF domain in Nab2 and a conventional RRM in Pabp2 - both proteins share the same RNA targets and can replace each other (Grenier St-Sauveur et al., 2013). The binding affinity to polyadenosine RNA of both proteins is similar with Nab2 (10.5 - 30 nM) (Hector et al., 2002; Kelly et al., 2007; Wahle, 1991; Wahle & Regsegger, 1999) and Pabp2 (10 nM) (Bienroth et al., 1993; Benoit et al., 1999). It has been suggested that Nab2 binds strongly to a certain polyA tail length and induces a RNP rearrangement, leading to the dissociation of Pabp2 from the RNA (Soucek et al., 2012). Indeed there is evidence that binding of Nab2 induces structural changes and compresses RNAs into defined and distinct particles which have been suggested to serve as a final maturation step of mRNPs prior to cytoplasmic release (Aibara et al., 2017).

Once the mRNP is rearranged and export-competent, Nab2 facilitates its nuclear export through the NPC (see Figure 15). Nab2 export activity depends on functional N- and C-termini (Marfatia et al., 2003; Grant et al., 2008; Fasken et al., 2008). Mutations in either domain cause nuclear accumulation of bulk pA+RNA and diminished nuclear export. The phenotype of the C-terminal depletion is rather weak and results in the accumulation of pA+RNA in the nucleolus, which is thought to be due to a diminished RNA binding affinity of Nab2. Deletion of 97 amino acids in the N-terminal PWI-like domain showed defects in RNA processing and retained bulk pA+RNA at the nuclear pore complex (Green et al., 2002; Chekanova et al., 2001). Several lines of evidence demonstrated that Nab2 facilitates the export of export-competent mRNPs *via* an interaction with the Yeast RNA Annealing protein Yra1 (Aly/Ref) (Iglesias et al., 2010) and the nuclear pore-associated export factor Mlp1 (Tpr1) (Green et al., 2003; Fasken et al., 2008). Nuclear

export is dependent on the essential export receptor Mex67 (Nxf1), which promotes the subsequent translocation of the mRNP to the cytoplasmic face of the NPC (see Figure 16).

At the NPC, the assembly and the mRNP composition undergo a quality control mechanism through the interaction of Nab2, Aly/Ref and the yeast Tpr1 orthologue Mlp1. Subsequently, Gfd1 binds to the Nab2 N-terminus, thereby tethering Nab2 and retaining the mRNP on the cytoplasmic face of the NPC (Suntharalingam et al., 2004; Zheng et al., 2010). Nuclear protein export assays using a temperature-sensitive nucleoporin allele that exhibits a defect in protein re-import revealed that Nab2 has high shuttling capacities and stays bound to the mRNP during the export process (Green et al., 2002; Duncan Kent et al., 2000). The mRNP is decorated with the inactive DEAD-box RNA helicase Dbp5. Once translocated to the cytoplasm, Dbp5 is activated by Gle1 and promotes the ATP-dependent mRNP remodelling leading to the dissociation of Nab2, Mex67, and other RBPs from the transcript (Tran et al., 2007; Lund & Guthrie, 2005).

The Nab2-facilitated export can be influenced by certain cellular stress conditions. Studies in yeast exposed to heat or salt stress - conditions which have been implicated to cause mRNA retention in the nucleus (Saavedra et al., 1997b; Saavedra et al., 1996) - resulted in the dissociation of Nab2 and the export factor Mex67 from the mRNP (Zander et al., 2016). Under these stress conditions Nab2 as well as Mex67 exhibited significantly reduced RNA-binding capacities, leading to a general export block of bulk pA+RNA (Zander et al., 2016). Interestingly, heat shock mRNAs were rapidly exported by a direct binding of Mex67 to the transcripts allowing a highly selective mRNA export.

The dissociation of Nab2 from the mRNP occurred due to post-translational modifications. Under heat stress, Nab2 becomes phosphorylated on threonine 178 and serine 180 by Slt2, a kinase which appears to be activated upon certain stress conditions (Carmody et al., 2010). Phosphorylated Nab2 then accumulates together with other export adaptors, such as Yra1 and Mlp1 in nuclear foci, and constitutes a general RNA export block (Carmody et al., 2010; Wallace et al., 2015). This export adaptor sequestration and spatial separation from its targets retains the majority of transcripts in the nucleus, while heat shock mRNAs are exported in a direct Mex67-dependent pathway.

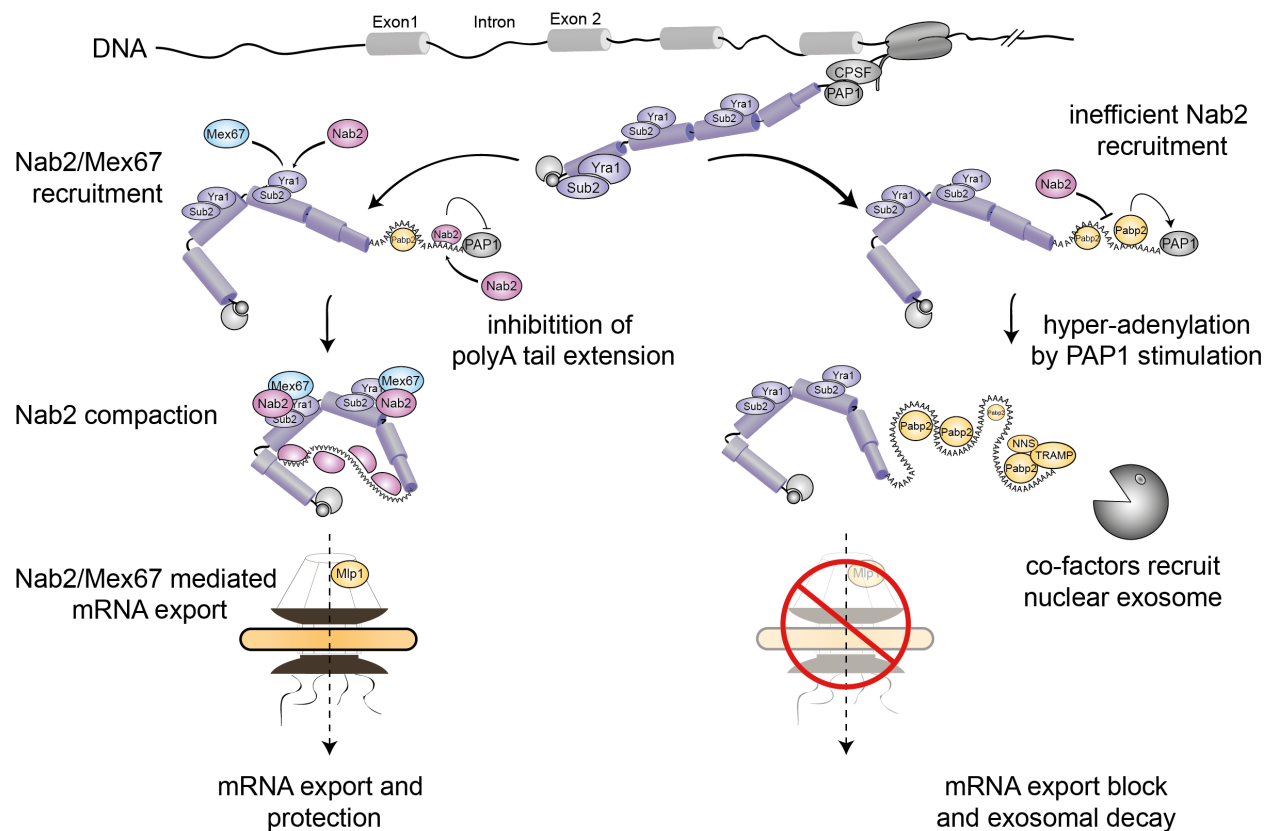


Figure 16: Nab2 nuclear surveillance function. Left: Nab2 stimulates the efficient mRNA export by restricting polyA tail length, export factor (Mex67) recruitment and mRNP compaction, and translocates the mRNP by interacting with NPC-associated factors. Right: Inefficient Nab2 recruitment leads to hyper-adenylation and exosomal co-factor recruitment, such as The Trf–Air–Mtr4 polyadenylation (TRAMP) and the Nrd1p/Nab3p/Sen1p (NNS) complex, which stimulates the decay by the nuclear exosome (mod. (Tudek et al., 2018)).

Nab2 export and polyadenylation is tightly linked to the exosomal degradation machinery and to its catalytic subunit Rrp6. Rrp6 can physically interact with Nab2 and even displace/block Nab2 from polyA tails and *vice versa*, suggesting that nuclear mRNP biogenesis is monitored by the interplay of the exosome and the PABPs (Schmid et al., 2012; Tudek et al., 2018). Nab2 binding to nascent polyA tails protects mRNAs from decay; Kinetic studies revealed that pA+RNA export and nuclear decay decisions are regulated by Nab2 in a concentration-dependent manner. Additional deletion of Rrp6 partially restores mRNA levels and rescues the lethality of Nab2-deficient cells (Schmid et al., 2015). For the export function of Nab2, a “timer-model” was recently proposed whereby cells overcome nuclear retention of pA+RNA through an efficient export activity of Nab2 (Tudek et al., 2018). When export is weak and inefficient, Nab2 is displaced from the mRNP through Rrp6. The activity of Rrp6 is further stimulated by the extended polyA tails occurring in the absence of Nab2. This kinetic timer model places Nab2 as the key player in

nuclear surveillance in yeast by acting at the interphase between mRNA processing, nuclear export and exosomal decay (Tudek et al., 2018).

2.6. The zinc finger binding protein Zc3h14

Despite the essential role of Nab2 in nuclear export and surveillance in *Saccharomyces cerevisiae*, not much is known about the functions and activity of its mammalian orthologue - Zc3h14. Although *in silico* predictions hint to an evolutionary preserved structure of Nab2, RNA FISH studies upon Zc3h14 depletion showed only weak nuclear accumulation of pA+RNA in *Schizosaccharomyces pombe* (Grenier St-Sauveur et al., 2013), *Drosophila melanogaster* (Pak et al., 2011) and mouse neuro2A (N2A) cells (Kelly et al., 2014), suggesting that the Zc3h14 export activities for bulk pA+RNA is poorly conserved across kingdoms. This contrasts with polyA tail length control: studies in neuronal cells including mouse neuroblastoma cell lines, cortex, hippocampus and liver tissue have suggested that Zc3h14 also affects polyA tail length (Rha et al., 2017; Pak et al., 2011).

Zc3h14 expression levels are tissue-specifically regulated and strongly enriched in testes and the brain (Leung et al., 2009; Rha et al., 2017; Kelly et al., 2012; Pak et al., 2011). In the brain, Zc3h14 showed the highest concentration in the hippocampus, cerebral cortex and cerebellum (Rha et al., 2017; Kelly et al., 2012; Pak et al., 2011). In agreement with a rather brain-specific expression of Zc3h14, only few targets (171) have been identified in a recent microarray screen in the breast cancer cell line MCF-7 upon Zc3h14 depletion (Wigington et al., 2016). These targets were mostly downregulated upon Zc3h14 knock down. RNA-Immunoprecipitation revealed that Zc3h14 binds to the pre-mRNAs of those targets and interacts with several processing factors such as the Tho- and EJC-complex components and Alyref (Morris & Corbett, 2018). These findings pointed to an involvement of Zc3h14 in nuclear RNA processing and the regulation of a small subset of transcripts in higher eukaryotes. However, whether Zc3h14 has a function in mRNA export and nuclear surveillance of specific mRNA targets is still not understood and requires a systematic functional characterization.

2.6.1. Zc3h14 structure and functions

The domain organization of Zc3h14 is modular and resembles the one of Nab2: Zc3h14 contains five repeats of a CCCH-type zinc finger domain (ZnF) at its C-terminal (see Figure 15). Although Nab2 contains two more ZnFs compared to Zc3h14, these two ZnFs have been shown to exhibit low RNA binding affinities and are unlikely to directly contact RNA (Brockmann et al., 2012; Kuhlmann et al., 2014; Martínez-Lumbreras et al., 2013). While the nuclear localization of Nab2 is determined by its arginine-glycine rich domain (RGG), Zc3h14 contains a putative classic nuclear localization signal (NLS) encoded in exon 7 (Leung et al., 2009). The N-terminal PWI-like domain is highly conserved across kingdoms and has been identified in *S. cerevisiae*, *S. pombe*, *C. thermotolerans*, *D. melongaster*, *C. elegans*, *M. musculus* and *H. sapiens* (Kelly et al., 2012). However, it is not known whether the C-terminal ZnF and the N-terminal PWI-like domain are functional in higher eukaryotes.

While Nab2 expresses only one isoform in *S. cerevisiae*, alternative splicing generates four splice variants of Zc3h14 in human cells (Leung et al., 2009). Three isoforms share the same array of tandem-ZnFs, suggesting that all splice variants are able to bind poly-adenosines. Zc3h14 isoforms 1, 2 and 3 contain the same translational start site and differ only in the inclusion of three internal exons (exons 10, 11, 12). A fourth shorter splice variant, which was identified in HEK293 cells contains an alternative 5'UTR starting in exon 7, and lacks the exons encoding a part of the PWI-domain and the NLS (Leung et al., 2009), so that consequently this protein isoform is localized in the cytoplasm. In contrast to the cytoplasmic localization of isoform 4, splice variants 1-3 localize to nuclear speckles (Leung et al., 2009).

2.6.2. Impact of Zc3h14 in neurological disorders

The impact of Zc3h14 in mammalian cells might be tissue-specific. In contrast to the strict requirement for its orthologs in yeast (Anderson et al., 1993) and flies (Pak et al., 2011), neurons appear to be particularly sensitive to changes in Zc3h14 levels in humans, which correlates with the high expression levels of isoform 1-3 in neurons (Leung et al., 2009). The importance of Zc3h14 was highlighted by the finding that a loss-of-function mutation causes an autosomal recessive form of intellectual disability (ID) (Pak et al., 2011). ID has been estimated to affect 1-3% of the population worldwide (Maulik et al., 2011; Leonard & Wen, 2002). This neurodevelopmental disorder is characterized by a limitation in learning or adaptive behavior (Ropers, 2008) and a reduced intellect with an IQ below 70 (Kaufman et al., 2010; Ellison et al., 2013).

Patients with non-syndromic autosomal recessive intellectual disability (ARID) express a truncated Zc3h14 isoform with a nonsense mutation at the arginine 154. The truncated protein lacks the NLS, leading to its mis-localization in the cytoplasm and a loss of function (Pak et al., 2011). The importance of a functional Zc3h14 in mammalian neurons was recently confirmed in a mouse model expressing a mutated version of Zc3h14. Deletion of exon 13 led to the translation of an isoform lacking the essential conserved ZnFs 1 and 2. The mice showed an increased size of lateral brain ventricles, modest deficits in behavioural paradigms, and an impaired working memory (Rha et al., 2017). In agreement with these studies, first insights from post-mortem human brain samples indicated the involvement of Zc3h14 in Alzheimer's disease (AD). Immunohistochemical studies demonstrated a remarkable decrease in Zc3h14 levels in the hippocampus of patients with AD (Guthrie et al., 2011), suggesting an ubiquitous function of Zc3h14 in neuronal development.

Studies in other model organisms such as flies and nematodes indicated that Zc3h14 functions are evolutionary conserved. In *Drosophila melanogaster* dNab2-null mutants have been shown to exhibit reduced *viability* and locomotor activity, impaired short-term memory, and defects in the neuronal patterning in the learning and memory center (Pak et al., 2011; Kelly et al., 2016). In addition, neuronal expression of human Zc3h14 Isoform 1 in dNab2 mutant flies rescues defects in the development and locomotion, which suggests a species-interdependent functional conservation of Zc3h14 (Kelly et al., 2014). The relevance of Zc3h14 in neurons has also been reported in nematodes. Here, loss-of-function mutations of SUT-2, the Zc3h14 orthologue in *Caenorhabditis elegans*, cause Tau aggregation, neurodegeneration, and uncoordinated movements (Guthrie et al., 2009). Although these neuronal disorders are apparently dependent on Zc3h14 expression, insights in the molecular and mechanistic cause of these diseases are yet lacking and will depend on the basic understanding of the cellular Zc3h14 function.

2.6.3. Pluripotent mouse P19 cells as a model organism

P19 cells are embryonic stem cells (ESCs) derived from pluripotent germ cell teratocarcinomas. In 1982, McBurney and Rogers crossed a C3H/He female with a feral male mouse. The 7.5-day male mouse embryo was implanted into the testis of a C3H/He 4 month old acceptor mouse, which resulted in the formation and proliferation of a teratocarcinoma (McBurney & Rogers, 1982; McBurney et al., 1982; Nau et al., 1991). In contrast to benign teratomas, malignant teratocarcinomas also contain populations of

undifferentiated stem cells. These undifferentiated stem cells were isolated from the tumour and cultured *in vitro* (McBurney & Rogers, 1982). The pluripotency of P19 cells was confirmed by injecting the cells into mouse blastocysts, which resulted in the generation of tissue from all three germ layers (McBurney & Rogers, 1982). Furthermore, P19 cells express multiple early embryonic markers, such as the embryonic antigen SSEA-1, confirming its pluripotent potential (Solter & Knowles, 1978; Knowles et al., 1978).

Like other ESCs, pluripotent P19 cells can be differentiated into all three primary germ layers: endoderm, mesoderm and ectoderm (Martin and Evans, 1975; van der Heyden and Defize, 2003). However, P19 cellular differentiation is highly efficient compared to other ES, since drugs identified to induce differentiation did not show any toxic effects in P19 cells. The pluripotent cell line was one of the first models described to differentiate in cardiomyocytes. Induction with 0.5%-1.0% (v/v) dimethyl sulfoxide (DMSO) lead to the development of multipotent muscle cells followed by the differentiation into cardiac muscle cells after five days, and skeletal muscle cells after eight days (McBurney et al., 1982).

P19 cell neuronal differentiation has been extensively studied and serves as a common *in vitro* model to study neuronal differentiation pathways (Levine & Flynn, 1986; Sharma & Notter, 1988). Since the treatment with a certain retinoic acid (RA) concentration induces P19 differentiation into neuronal cells (Kanungo, 2017; Jones-Villeneuve et al., 1982; Edwards & McBurney, 1983; Jones-Villeneuve et al., 1983), astroglia and fibroblasts, gene expression profiles of P19 mutants served as a model to understand neurogenesis and myogenesis (Edwards et al., 1983), as well as mitochondrial physiology (Vega-Naredo et al., 2014; Matsu-ura et al., 2016), and was used for drug screens.

Neurons that form upon the P19 differentiation exhibit high physiological potential: it was shown that transplantation of RA-treated neuronal P19 progenitors into an adult rat striatum lead to a final maturation of neuronal cells, as well as glia formation. These neurons displayed electrophysiological properties and survived for at least 13 weeks (Magnuson et al., 1995a; Magnuson et al., 1995b). P19 cells have a normal male euploid karyotype (40:XY) (McBurney & Rogers, 1982), grow rapidly in culture and - in contrast to most ES - are, independent from feeder cells or any additions such as leukemia inhibitory factors (LIFs) (van der Heyden, Marcel A G & Defize, 2003). Additionally, its pluripotency is maintained without any chemical additions. They are genetically accessible and can be immortal due to the expression of an inactivated p53 isoform (Schmidt-Kastner et al., 1998; Schmidt-Kastner et al., 1996). Since these features generate a reproducible cell system where slight differences in differentiation levels can be

detected, P19 cells serve as a potent model organism to study the effect of compounds or ectopic gene expression on the neuronal development, and furthers the understanding of neurodevelopmental or neurodegenerative disorders.

With regards to the impact of Zc3h14 in neuronal disorders, we characterized the function of Zc3h14 in P19 cells. These functions can further be investigated in differentiated P19 cells in a neuronal scenario, and potentially give insights into the pathogenesis of multiple neuronal disorders caused by Zc3h14 loss-of-functions.

3. Objectives

Nuclear splicing surveillance provides the cell with quality control mechanisms to prevent the protein synthesis of aberrantly spliced transcripts. Recent reports in higher eukaryotes point to surveillance pathways that are based on the interplay between splicing and nuclear export. Although the factors regulating this process are not known, SR proteins have been suggested to act at the interface between RNA recognition, splicing regulation and nuclear export.

In this study, we aimed to investigate the role of SRSF3 in nuclear splicing surveillance. To fulfill this aim we followed four strategies:

- Establishment of the splicing inhibitor Isoginkgetin as a tool to study the interplay between splicing and nuclear export.
- Characterization of the SRSF3 interaction network and splicing sensitive interactors.
- Identification of novel export and surveillance factors.
- Characterization of Zc3h14 with respect to its function in mRNA export.
- Elucidation of the molecular mechanism of SRSF3 and Zc3h14 mediating splicing surveillance.

4. Material and methods

4.1. Equipment and chemicals

Table 1: List of equipment.

Equipment	Model	Supplier
Balance PCB	PCB	KERN
Bioanalyzer	2100	Agilent
Cell counter	EVE	NanoEnter
Centrifuge	5439R	Eppendorf
Centrifuge	SU1550	sunLab
Centrifuge	Micro star 17R	VWR
Chemiluminescence detection system	ChemiDocTM MP I	BioRad
DNA gel electrophoresis system	VWR® Maxi 20	VWR
DNA gel electrophoresis system	VWR® mini Horizontal	VWR
Freezer -80°C	HFU series	Thermo Fisher Scientific
Gel documentation system	Gel doc GENi	Syngene
Heatblock	Digital heat block	VWR
Incubator	Heracell 150i CO2	Thermo Fisher Scientific
Microscope	AE31	Motic
Microscope (confocal spinning disc)	Cell observer SD	Zeiss
Microscope (confocal)	ChemiDocTM MP I	Zeiss
PCR Thermo cycler	Mastercycler Nexus gradient	Eppendorf
Photometer	NanoDrop 1000	Thermo Fisher Scientific
Power supply	PowerPac™ Basic	Biorad
Protein gel electrophoresis system	mini-PROTEAN Tetra Vertical Electrophoresis Cell	Biorad
Protein gel electrophoresis system	XCell SureLock® mini-Cell	Novex - Thermo Fisher Scientific
qPCR Thermocycler	PikoReal96	Thermo Fisher Scientific
Rocking platform	VWR 100 Rocking Platform Shaker	VWR
Rotator	SB2	Stuart
Safety cabinet	Herasafe KSP 1 biological	Thermo Fisher Scientific
Sonifier	Sonicator digital sonifier	Branson
Stackable shaker	MAXQ 4450	Thermo Fisher Scientific
Stiring platform D-6010	D-6010	neoLab
Thermo mixer	comfort	Eppendorf
UV crosslinker	CL-1000 UV crosslinker	Analytic Jena
Vortex mixer	44013	neoLab
Water bath	VWB12	VWR

Table 2: Chemicals and reagents.

Chemical/Reagent	Catalog #	Supplier
10XTBE	AM9865	Thermo Fisher Scientific
2-Mercaptoethanol	M6250-100 ML	Sigma-Aldrich
2-Propanol	A3928	Appllichem panreac
Agar	J637-1KG	Amresco
Agarose	A9539-500G	Sigma-Aldrich
Ampicillin	A9518-5G	Sigma-Aldrich
Antifade Diamond	P36970	Invitrogen
Bicine	B3876-250G	Sigma-Aldrich
BIS-TRIS	B9754-500G	Sigma-Aldrich
Bis-Tris protein gels	NP0321BOX	Life Technologies
Boric acid	B6768-1KG	Sigma-Aldrich
Bovine serum albu min (BSA)	A3059-100G	Sigma-Aldrich
Calciumchlorid	CN93.2	Carl Roth
Chloramphenicol	C0378-25G	Sigma-Aldrich
Cycloheximide	C7698-1G	Sigma-Aldrich
DNA ladder 1kb	SM0311	Thermo Fisher Scientific
DNA ladder 1kb plus	SM1331	Thermo Fisher Scientific
DNA ladder Low molecular weight	N3233S	New England Biolabs (NEB)
DNA ladder 50bp	10416014	Invitrogen
DNA polymerase AccuPrime Supermix	12342010	Life Technologies
DNA polymerase OneTaq Hot Start	M0481L	New England Biolabs (NEB)
DNA polymerase Platinum® Taq High Fidelity	11304-011	Thermo Fisher Scientific
DNA transfection reagent	PPLU117-15	VWR
DNase I	A3778,0100	AppliChem
DNase TURBO&trade	AM2239	Invitrogen
dNTP Mix	R0192	Thermo Fisher Scientific
Doxycycline hydrochloride	D3447-500MG	Sigma-Aldrich
Dynabeads® Protein G	10004D	Thermo Fisher Scientific
ECL	RPN2232	GE Healthcare
EDTA	E9884-100G	Sigma-Aldrich
EDTA (0.5M; pH 8.0)	AM9260G	Life Technologies
Effectene Transfection Reagent (1 ml)	301425	Qiagen
Ethanol (70%)	T913	Carl Roth
Ethanol (99.8%)	9065	Carl Roth
Fetal Bovine Serum (FBS)	10270106	Thermo Fisher Scientific
Formaldehyde (16% w/v)	28908	Thermo Fisher Scientific
Gelatin	G1393-100 ML	Sigma-Aldrich
Geneticin (50 mg/ml)	10131035	Thermo Fisher Scientific

Glycerin	6967.1	Carl Roth
GlycoBlue™ Coprecipitant (15 mg/ ml)	AM9516	Thermo Fisher Scientific
Hexanucleotide Mix	11277081001	Sigma-Aldrich
HiScribe T7 High Yield RNA Synthesis Kit	E2040S	New England Biolabs (NEB)
Hoechst 34580	63493-5MG	Sigma-Aldrich
IGEPAL®	CA-630	Sigma-Aldrich
IPTG	#R0392	Fermentas
Isoginkgetin	83513	PhytoLab
Kaliumchlorid	P017.1	Carl Roth
Kaliumhydroxid	P747.1	Carl Roth
Kanamycin	K4000-25G	Sigma-Aldrich
LB Broth,powder	L3022-1KG	Sigma-Aldrich
Magnesium chloride solution (1 M)	A3888	Appllichem Panreac
Magnesium chloride solution (1M)	M9530G	Life Technologies
Magnesiumchlorid	25108.295	VWR
Manganese(II)-chloride-Tetrahydrate	T881.1	Carl Roth
DNA ladder 1kb	SM0311	Thermo Fisher Scientific
Milk powder	A0830	Appllichem
MOPS	M3183-500G	Sigma-Aldrich
Natriumhydroxid	6771.1	Carl Roth
NuPAGE® MOPS SDS Running Buffer (20X)	NP0001	Life Technologies
Opti-MEM®	31985070	Thermo Fisher Scientific
Penicillin-Streptomycin (10,000 U/ ml)	15140122	Life Technologies
Phenol:Chloroform:Isoamyl alcohol	P3803-400 ML	Sigma-Aldrich
Phosphate buffered saline (10xPBS)	P5493-1L	Sigma-Aldrich
Phusion polymerase	M0530L	New England Biolabs (NEB)
Ponceau	K793-500 ML	Amresco
Potassium acetate	P5708-500G	Sigma-Aldrich
Protein inhibitor	11697498001	Roche Applied Science
Protein inhibitor EDTA-free	11873580001	Roche Applied Science
Protein Ladder (Prestained)	26616	Life Technologies
Protein Ladder (Prestained)	26616	Life Technologies
Reverse transcriptase SuperScript® III	18080-044	Life Technologies
RiboLock RNase Inhibitor	EO382	Thermo Fisher Scientific
RNA Gel Loading Dye (2X)	R0641	Thermo Fisher Scientific
RNA Ladder	SM1831	Thermo Fisher Scientific
RNase I (cloned) 100U/µL	AM2295	Invitrogen
Protein Ladder (Prestained)	26616	Life Technologies
SDS Solution	161-0416	Bio-Rad
Protein Ladder (Prestained)	26616	Life Technologies
Shrimp Alkaline Phosphatase (rSAP)	M0371L	New England Biolabs (NEB)

Sodium acetate 3M	AM9740	Life Technologies
Sodium chloride	S3014-1KG	Sigma-Aldrich
Sodium chloride solution (5M)	AM9760G	Life Technologies
Sodium citrate	71402-1KG	Sigma-Aldrich
Sodium deoxycholate	30970-100G	Sigma-Aldrich
SYBR® Gold	S-11494	Thermo Fisher Scientific
T4 Polynucleotide Kinase (PNK)	M0236 L	New England Biolabs (NEB)
T4 RNA Ligase 1	M0437 M	New England Biolabs (NEB)
TBE buffer	0478-40L	Amresco
TBE-Urea Gels (6%)	EC68652BOX	Life Technologies
TBE-UREA Sample Buffer	LC6876	Life Technologies
Tetracyclin	87128-25G	Sigma-Aldrich
TRI Reagent	T9424-200 ML	Sigma-Aldrich
Trichloroacetic acid	T9159-100G	Sigma-Aldrich
TRIS (1M, pH 7.0)	AM9850G	Life Technologies
TRIS (1M, pH 8.0)	AM9855G	Life Technologies
Triton X 100	3051	Carl Roth
Triz base	T1503-5KG	Sigma-Aldrich
TRIzol® Reagent	15596018	Thermo Fisher Scientific
Trypsin 0.05% EDTA	MDTH25-051-CI	VWR
TWEEN 20	M147-1L	Amresco

Table 3: List of buffers and solution recipes.

esiRNA preparation		
DsRNA digestion buffer pH 7.9	TE buffer, pH 7.9	Equilibration buffer pH 7.5
20 mM Tris-HCl 0.5 mM EDTA 5 mM MgCl ₂ 1 mM DTT 140 mM NaCl 2.7 mM KCl 5% (v/v) glycerol Dissolved in nuclease free H ₂ O	10 mM Tris-HCl 1 mM EDTA Dissolved in nuclease free H ₂ O	20 mM Tris-HCl 1 mM EDTA 300 mM NaCl Dissolved in nuclease free H ₂ O
Wash buffer pH 7.5	Elution buffer pH 7.5	
20 mM Tris-HCl 1 mM EDTA 400 mM NaCl Dissolved in nuclease free H ₂ O	20 mM Tris-HCl 1 mM EDTA 520 mM NaCl Dissolved in nuclease free H ₂ O	

iCLIP/RNA binding assay		
Lysis Buffer	High-salt wash buffer	PNK wash buffer
50 mM Tris-HCl, pH 7.5 100 mM NaCl 1% (v/v) IGEPAL 0.1% (m/v) SDS	50 mM Tris-HCl, pH 7.5 1 M NaCl 1 mM EDTA 0.1% (m/v) SDS	20 mM Tris-HCl pH 7.5 10 mM MgCl ₂ 0.2% (v/v) Tween-20 Dissolved in nuclease free H ₂ O

0.5% (m/v) Sodium deoxycholate Dissolved in nuclease free H ₂ O Freshly added 1XPI (-EDTA) Freshly added RNaseIn (1:500)	0.5% (m/v) Sodium deoxycholate 1% (v/v) IGEPAL Dissolved in nuclease free H ₂ O	
5X PNK buffer; pH 6.5	Proteinase K buffer	Proteinase K buffer/Urea
350 mM Tris-HCl pH 6.5 50 mM MgCl ₂ 5 mM DTT Dissolved in nuclease free H ₂ O	100 mM Tris-Cl pH 7.5 50 mM NaCl 10 mM EDTA Dissolved in nuclease free H ₂ O	7 M UREA 100 mM Tris-Cl pH 7.5 50 mM NaCl 10 mM EDTA Dissolved in nuclease free H ₂ O
TE buffer		
10 mM Tris-HCl pH 8.0 1 mM EDTA pH 8.0 Dissolved in nuclease free H ₂ O		
Protein extraction/ Western blot		
NET2 buffer	5X Laemmli buffer	10X SDS-running buffer
50 mM Tris-HCl 150 mM NaCl 0.05% (v/v) NP-40 10 mM β-Phosphoglycerate Freshly added 1XPI	10% (m/v) SDS 50% (v/v) Glycerol 300 mM Tris pH 6.8 0.05% (m/v) Bromophenol blue	250 mM Tris-Base 1.9 M Glycine 1.0% (m/v) SDS
5XSDS-transfer buffer	10XTBST	Blocking solution
125 mM Tris-Base 960 mM Glycine For 1X preparation: 20% (v/v) methanol	200 mM Tris-Base 1.5 M NaCl 0.5% (v/v) Tween 20	5% (m/v) milk powder in 1XTBST or 3% (m/v) BSA in 1X TBST
Phos-tag washing buffer		
1xSDS-transfer buffer 50 mM EDTA, pH 8.0 20% (v/v) Methanol		
DNA electrophoresis		
10XTBE	Immunofluorescence	
1M Tris-Base 1M Boric Acid 20mM EDTA	Fixation buffer	Blocking/Permeabilizing solution
	4% (m/v) PFA Dissolved in 1XPBS	5% (m/v) BSA 1XPBS 0.1% (v/v) Triton X100
Co-immunoprecipitation		
NET2 buffer	High-salt wash buffer	Stringent Washing buffer
50 mM Tris-HCl 150 mM NaCl 0.05% (v/v) NP-40 Freshly added 1XPI And 10 mM β-Phosphoglycerate	50 mM Tris-HCl, pH 7.5 1 M NaCl 1 mM EDTA 0.1% (m/v) SDS 0.5% (m/v) Sodium deoxycholate 1% (v/v) IGEPAL	50 mM Tris pH 7.5 150 mM NaCl 0.2% (v/v) NP-40 Freshly added 1XPI And 10 mM β-Phosphoglycerate

Table 4: Biochemical kits.

Kits	Company
Amersham ECL Prime Western Blotting Detection Reagent	GE Healthcare
Cell Fractionation Kit - Standard (ab109719)	Abcam
DNA, RNA and protein purification	Machery & Nagel
Effectene® Transfection Reagent	Qiagen

HiScribe T7 High Yield RNA Synthesis Kit	New England Biolabs (NEB)
ORA™ SEE qPCR Green ROX L Mix	highQu
Stellaris® RNA FISH	Biosearch Technologies
Q Sepharose Fast Flow	GE Healthcare

4.2. Software and online tools

Table 5: List of software and online tools.

Software	Version	Supplier	Purpose
Adobe Illustrator	22.1	Adobe	Illustrations and graphics
Bioanalyzer software	2100 Expert Software	Agilent	Processing and quantification of splicing gels
Biovoxxel imageJ plug in	https://imagej.net/BioVoxxel_Toolbox	(Schindelin et al., 2012)	Processing and fluorescence quantifications of images
Citavi	9.2	Swiss Academic Software	Reference management
DAVID	https://david.ncifcrf.gov/	Laboratory of Human Retrovirology and Immunoinformatics	Functional Annotation Bioinformatics Microarray Analysis
DEQOR	http://cluster-1.mpi-cbg.de/Deqor/deqor.html	(Henschel et al., 2004)	Identification of esiRNA regions
DESeq2	https://doi.org/10.1186/s13059-014-0550-8	(Love et al., 2014)	Differential gene expression analysis
FastQC	https://www.bioinformatics.babraham.ac.uk/projects/fastqc/	Babraham Institute	RNAseq quality check
Image Lab	6.0.1	BioRad	Processing and quantification of immunoblots
ImageJ	https://fiji.sc/	Fiji	Processing and analysis of images
Integrative Genomics Viewer (IGV)	2.5	Broad institute University of California	RNAseq browser shots
PikoReal	2.1	Thermo Fisher Scientific	Processing and analysis of qPCR data
Primer Blast	https://www.ncbi.nlm.nih.gov/tools/primer-blast/	National Center for Biotechnology Information	Primer design
Prism8	8.0.1	GraphPad	Statistical analysis and graphics
Pubmed NCBI	https://www.ncbi.nlm.nih.gov/pubmed/	National Center for Biotechnology Information	Bibliographic review
RStudio	3.5.3	R Foundation for Statistical Computing	GO-term analysis
Refseq NCBI	https://www.ncbi.nlm.nih.gov/refseq/	National Center for Biotechnology Information	Export of Annotated DNA/RNA sequences
Snapgene	4.2.4	GSL Biotech LLC	Experimental design
UCSC	https://genome.ucsc.edu/	University of Santa Cruz	iCLIP browser shots

4.3. Cell Culture

Pluripotent mouse P19 and HeLa cells were cultured with Dulbecco's Modified Eagle Medium (DMEM), and GlutaMAX™ (Thermo Fisher Scientific) supplemented with 10% (v/v) heat inactivated Fetal Bovine Serum (Thermo Fisher Scientific), 100 U/ml penicillin and 100 µg/ml streptomycin (Thermo Fisher Scientific). When cell cultures reached confluence, they were passaged to new 10 cm. For seeding, the DMEM culture medium was removed and cells were washed with 5 ml Dulbecco's Phosphate Buffered Saline (PBS) (Sigma-Aldrich). 1.5 ml of Trypsin-EDTA phenol red (Thermo Fisher Scientific) was added to the cells, and the plate was incubated for 3 min at room temperature (RT) until cells detached from the dish surface. Subsequently, the trypsin was inactivated with 3 ml of fresh culture medium and cells were split and separated by multiple up and down pipetting. Before transferring the cell suspension for P19 cells the new plate was pre-coated with 0.1% (v/v) gelatin diluted in PBS. After incubation for 10 min the gelatin was removed and replaced with 10 ml DMEM. 350 µl for P19 and 400µl of HeLa cell suspension were transferred to the new 10 cm. The fresh culture was subsequently swirled to achieve a homogenous cell density throughout the dish surface. The cells were incubated at 37°C and 5% CO₂.

4.3.1. Freezing cells

To freeze cells, confluent 10 cm plates were trypsinized, inactivated and separated as described above. Cell suspensions were transferred into 15 ml Falcon tubes and pelleted by centrifugation (1000xg for 5 min at 4°C). After centrifugation, the supernatant was removed, and cells were resuspended in 2 ml freezing medium containing 10% (v/v) DMSO (99.7% Dimethyl sulfoxide, Sigma-Aldrich) in DMEM and aliquoted into 4 cryovials each containing 500 µl of the cell suspension. Cryovials were placed in a freezing container (stored at RT; Thermo Fisher Scientific) containing Isopropanol (2-Propanol, VWR) and transferred to a -80°C freezer for a minimum of 24 h. For short-term storage the cells were kept in the freezer, for long-term storage transferred to a liquid nitrogen tank.

4.3.2. Thawing cells

To thaw cells cultures, a cryovial containing 500 µl of frozen cells was thawed in a water bath at 37°C until only a small ice block was visible in the cell suspension. After adding 1 ml of DMEM culture medium to the cell suspension, the cells were pelleted by centrifugation (1,000xg for 5 min at 4°C). The supernatant was removed, and the cell pellet was carefully resuspended in 1 ml DMEM and subsequently transferred to 10

cm or 6 cm culture dishes containing 10 ml or 3 ml of culture medium. For P19 cells, dishes were pre-coated with gelatin (0.1% (v/v) gelatin diluted in PBS) for 10 min prior the DMEM culture medium addition.

4.3.3. Cell harvesting

After experiment completion, cells were harvested for RNA and/or protein extraction. The culture medium was removed, and cells were washed twice with 1xPBS (Phosphate buffered saline, 10x; Sigma-Aldrich, diluted in distilled water). An appropriate volume of PBS (10 ml for 15 cm plates; 5 ml for 10 cm plates; 3 ml for 6 cm plates) was added to the plates, and cells were scraped and collected in a 15 ml or 1.5 ml tube. Tubes were centrifuged for 5 min at 1,000xg, 4°C and the supernatant was removed. For RNA work, cell pellets were resuspended in TRIzol (Thermo Fisher Scientific) for further RNA extraction techniques; for protein work cell pellets were snap-frozen in liquid nitrogen. Pellets and TRIzol suspension were stored at -80°C.

4.4. Generation of BAC cell lines

Glycerol stocks of *Escherichia coli* (*E. coli*) DH10 cells containing the BACs with the entire SRSF3, Nxf1 and Zc3h14 genomic locus, green fluorescent protein (GFP) sequence, kanamycin and chloramphenicol resistance genes sequences were stably inserted in P19 wild type cells as previously described (Poser et al., 2008). The next subsections provides a brief description of the method.

4.4.1. Bacterial artificial chromosome (BAC) isolation

To isolate BACs, *E. coli* DH10 cells were streaked on lysogeny broth (LB) on plates containing 50 µg/ml of kanamycin (Sigma-Aldrich) and chloramphenicol (Sigma-Aldrich) and were incubated at 37°C overnight (o.n.). Single colonies were picked and transferred to 2 ml tubes containing LB medium supplemented with kanamycin and chloramphenicol (50 µg/ml) and incubated at 37°C on a thermomixer for 6 h. From this culture, 20 µL were transferred to 100 ml Erlenmeyer flasks containing 20 ml LB medium supplemented with kanamycin and chloramphenicol (50 µg/ml). After o.n. incubation at 37°C, BACs were then isolated using the BAC prep kit (Macherey & Nagel) according to the manufacturer's instructions. After isolation, BAC DNA was resuspended in Tris-EDTA buffer and the concentration was spectrometrically determined using a NanoDrop (Thermo Fisher Scientific).

4.4.2. BAC transfection

For transfection, 30 μ l of a P19 wild type (WT) cells were seeded from a confluent 10 cm plate into 6 well plates. 24 h after seeding, cells were transfected with 1 μ g of the isolated BAC plasmid DNA using the effectene transfection kit (Qiagen) following the manufacturer's protocol. 24 h after transfection, the transfection reagent was removed and replaced with new medium supplemented with 4.5 mg/ml of geneticin (Thermo Fisher Scientific). Thereby geneticin serves as a selection marker of BAC transfected cells, since the Lab-tag contains a resistance cassette. WT cells were co-cultured and served as a screening negative control. After cells reached confluence, they were transferred to 10 cm plates and cultured as previously described. The genomic integration of the BAC and its expression was validated by i) immunoblotting using protein specific and GFP antibodies ii) amplification and sequencing of the exogenous cDNA using primer spanning the respective transcript and the GFP tag. The following primer sequences were used:

Table 6: Oligonucleotides used for stable cell line validation.

Name	Target	Sequence
qPCR_Nxf1_1_fw	<i>Nxf1</i>	CCACGCTTTCCCAGAACAGCA
Zc3h14_autor_for	<i>Zc3h14</i>	AAGCAGATTGTCCTTCA
Lap_reverse	Lap-Tag	GGTTCGTCGAGCCTGGAAGt

4.4.3. Selection of clones for overexpression studies

To select cell lines with high expression rates of the respective GFP-tagged proteins, we selected overexpression (Oex) clones for each cell line. Therefore, a confluent 10 cm plate of P19 cells were trypsinized as previously described and cell suspension was transferred to a 50 ml falcon tube and vortexed for 10 sec at intermediate speed. From this cell suspension, different cell amounts (1 μ l, 3 μ l, 5 μ l) were transferred to a new falcon tube containing 10 ml of culture medium. After vortexing (10 sec, intermediate speed), 1 ml of the diluted cell suspension was transferred to a new falcon tube containing 9 ml of culture medium, and thoroughly mixed by vortexing. The final diluted cell suspension was then transferred to a 10 cm dish and incubated o.n.. Single cells distributed over the petri dish were monitored until growth into colonies. Colonies were transferred to 24-well plates using cloning discs. Briefly, cell medium was removed, and cells were washed with PBS. Cloning discs were soaked in trypsin and placed on top of the colonies. After 5 min, each cloning disc containing a colony was transferred to one well of a

24 well plate. Clone colonies were cultured until confluence was reached and subsequently passaged to 6 cm and 10 cm dishes.

4.5. Isoginkgetin treatment

For Isoginkgetin (IsoG) treatment, P19 and HeLa cells were seeded on petri dishes and cultivated for at least 24 h prior to IsoG incubation. Due to the observed arrested growth of cells upon IsoG treatment, the number of cells for the IsoG plates was 1.7 times higher compared to the control. 33 mM IsoG (Phytolab) was dissolved in DMSO, aliquoted and stored at -20°C. After 24 h, IsoG aliquots were thawed and diluted for P19 to 33 µM (1/1000) and for HeLa to 100 µM (1/333) in DMEM cell medium. The cell culture medium was exchanged with either the IsoG solution or a DMSO solvent control with the respective concentration. P19 cells were treated for most experiments for 16 h with IsoG/DMSO and HeLa cells for 21 h.

4.6. siRNA and esiRNA knock downs

Knock downs (Kd) were performed using two different strategies: for *SRSF3* and *Nxf1* depletion, endoribonuclease-prepared small interference RNAs (esiRNAs) were prepared as described in the next section. For *Zc3h14*, commercial small interference RNAs (siRNAs) were acquired from Sigma. Sequences from esiRNAs and siRNAs are listed in Table 7.

Table 7: siRNA sequence and esiRNA sequence regions. Sequence interval indicates the region from the transcript where the esiRNA was designed. Incubation time indicates the total KD time.

Name	Target	Sequence/Region	Supplier	Incubation time
si_Zc3h14_tot	<i>Zc3h14</i>	UGUUUGUGCAUCCAAAUUGUA	Sigma aldrich	48h
si_Luciferase_Ctrl	<i>Luciferase</i>	CGUACGCGGAUACUUCGA	Selfmade	48h
Nxf1_esi_R1	<i>Nxf1</i>	NM_016813: 216-567 bp	Selfmade	24h
Nxf1_esi_R3	<i>Nxf1</i>	NM_016813: 581-938 bp	Selfmade	24h
Nxf1_esi_R5	<i>Nxf1</i>	NM_016813:1247-1536 bp	Selfmade	24h
SRSF3_esi_R1	<i>SRSF3</i>	NM_013663:557-1068 bp	Selfmade	32h

4.6.1. esiRNA preparation

esiRNA target regions of around 400 bp of *SRSF3*, *Nxf1* and *GFP* transcripts were identified using the DEQOR software online tool. To amplify the target regions, primers were designed which included the T7

promotor sequence at the 5' and 3' end respectively. To amplify the target sequence and provide the targets with the T7 promotor sequence, a PCR was performed using the Taq Polymerase to amplify the selected regions from P19 WT cDNA. Next, an *in vitro* transcription (IVT) was performed to synthesize the RNA using the T7 promotor sequence. PCR and IVT reaction protocol are described in Table 8.

Table 8: Taq PCR and IVT protocol and program.

Taq PCR protocol	Taq PCR program	
20.9 µl water	95°C	30 sec
2.5 µl 10x Taq buffer	95°C	30 sec
0.5 µl 10 mM dNTPs Mix	60°C	30 sec
0.125 µl Taq	68°C	1 min/kb
0.5 µl 10mM forward primer	68°C	5 min
0.5 µl 10mM reverse primer	4°C	infinite
1 µ cDNA		
20.9 µl water		

} **34 cycles**

IVT Protocol	IVT program	
1xtranscription buffer	Transcription:	37°C 12 h
7.5 mM ATP	Annealing:	90°C 3 min
7.5 mM GTP	Denaturation:	ramp to 20°C with 0.1°C/sec
7.5 mM CTP		
7.5 mM UTP		
10.0 mM DTT		
4 U/l T7 RNA polymerase		
0.5 ug PCR product		

After the *in vitro* transcription of the full-length esiRNA transcript, the +400 bp double stranded RNA (dsRNA) was digested into small fragments of 20-22 nt. For the digestion, 25-50 µg of transcribed RNA was diluted in 10 µl of RNase free water and added to 90 µl of digestion buffer (buffer recipe listed in Table 3) and incubated with 6 µg of RNaseIII for 2 h at 37°C while shaking.

The digestion efficiency and presence of 20-22 nt fragments was validated by a 4% agarose gel electrophoresis, using 2xloading dye premixed with the digested RNA product. After confirming the fragment size, digested esiRNAs were purified using Q Sepharose FastFlow kit (Amersham) as described by the manufacturer's instructions.

4.7. Transfection

Knock downs (KDds) were performed in P19 WT and GFP-tagged cell lines. Cells were cultivated in 6 cm-15 cm dishes and seeded 8 h prior the transfection. For 6 cm plates 120 μ l of cells from a confluent 10 cm dish were seeded into 6 cm plates. 3 μ g esiRNAs or 0.2 nmol siRNAs were transfected using jetPRIME[®] Transfection Reagent (Polyplus) as recommended by the manufacturer's instructions. The incubation time of the knock down was dependent on the esiRNA/siRNA efficiency and is described in Table 7. Depleted cells were subsequently harvested.

4.8. Subcellular Fractionation

Subcellular fractionation of P19 cells was performed using a Cell Fractionation kit (Abcam - ab109719) according to the manufacturer with minor modifications. Buffer A, B and C was supplemented with RNaseIn (1/500 diluted) for RNA work and 1xProtease Inhibitor Cocktail +EDTA (Roche) and 10 mM B-phosphoglycerate for protein work. Briefly, confluent 10 cm dishes of P19 cells were washed with 1xPBS and trypsinized as previously described. Cell suspension was transferred to 15 ml falcon tubes and centrifuged at 4°C, 300x g for 5 min. Supernatant was removed, and cells were washed with buffer A and centrifuged at 4°C, 300x g for 5 min. Supernatant was discarded and cells were resuspended in 1200 μ l of buffer A. Next, 200 μ l of cell suspension was transferred to two 1.5 ml tubes (100 μ l each) and saved as input for RNA and protein extraction. For RNA extraction, 900 μ l of TRIzol was added to the input sample. The remaining 1000 μ l of cell suspension were divided into two tubes each containing 500 μ l of the cell suspension for the subsequent subcellular fractionation. To break the cytoplasmic membranes, 500 μ l of buffer B was added to the 500 μ l suspension, mixed by inverting and incubated on a rotatory wheel for 7 min at RT. Cell suspension was centrifuged at 5,000xg for 1 min at 4°C and supernatant containing cytoplasmic fraction was transferred to a new tube. For RNA extraction, total cytoplasmic lysate was divided into three tubes (330 μ l each) and 900 μ l of TRIzol was added to each cytoplasmic fraction. After resuspending the nuclear pellet (50x up and down pipetting) buffer C, a high stringent detergent-containing buffer which disrupts the nuclear membrane, was added. The suspension was incubated in on the rotatory wheel for 10 min at RT and subsequently centrifuged at 5,000xg for 1 min at 4°C. Supernatant was removed and the nuclear pellet was resuspended in 500 μ l of buffer A for posterior protein extraction or 500 μ l TRIzol for RNA extraction. Samples were stored at -80°C for further processing (RNA or protein extraction).

4.8.1. Validation of fractionation

Subcellular fractionation was validated by immunoblotting as described in section 4.11.4 using the indicated antibodies. Additionally, fractionation was confirmed on the RNA level using two techniques: First, by RT-PCR as described in section 4.10.5 using random hexamers. cDNA was amplified as described in section 4.10.6 using the following primer combinations:

Table 9: Oligonucleotides used for cellular fractionation validation.

Primer name	Target	Sequence	Concentration
qPCR_primer_BA_2	<i>ActB</i>	GAGCACAGCTTCTTTGCAGCTC	Exon1
qPCR_primer_BA_6		CAACCGTGAAAAGATGACCCAG	Exon3
qPCR_primer_BA_5	<i>ActB</i>	AAGCCTGGGGTTTTCTTGGG	Intron2
qPCR_primer_BA_6		CAACCGTGAAAAGATGACCCAG	Exon3
qPCR_primer_Tubb_2	<i>Tubb</i>	CTATAAACCTTCCCTTCTGCCAG	Intron2
qPCR_primer_BA_6		CAGCAAGATCCGAGAAGAATACCCTG	Exon4

Denaturing UREA Polyacrylamide Gel Electrophoresis (UREA PAGE) was additionally performed to determine fractionation efficiency and RNA quality. Therefore, Novex™ TBE-UREA Gels (Thermo Fisher Scientific) were assembled and 1xTBE running buffer was added to the Novex running chamber. After flushing the wells, the UREA gel was pre-ran at 180 V for 15 min at 4°C. 2XRNA loading buffer was added to 1 µg of fractionated RNA. Together with a LR Riboruler marker samples were denatured in the heatblock and incubated for 3 min at 80°C. After cooling down on ice, samples were loaded on the UREA gel and ran at 150 V for 2.5 h at 4°C. Fractionated RNA was subsequently stained with SYBR® Gold (1/10 000 dilution in 1xTBE), incubated for 30 min at RT while shaking and imaged using a GelDoc station (Syngene).

4.9. Heterokaryon assay

To quantify shuttling capacities, heterokaryon assays were performed according to a previously described protocol (McNicoll & Müller-McNicoll, 2018). Briefly, 18 mm coverslips were pre-treated with gelatin 0.1% (v/v) for at least 24 h. Clonal P19 cell lines stably expressing the SRSF3, Nxf1, Zc3h14 and Prp8 GFP-tagged proteins were seeded onto 12 well plates containing coverslips together with HeLa cells stably expressing CAAX-mCherry marking the cell membranes, which served as a cell fusion control. P19 and HeLa cells were seeded in a 2:1 proportion and incubated for 8h until cells were attached. To inhibit the *de novo* protein

synthesis, cells were treated with the translational inhibitor cycloheximide (CHX) in two phases: First, the DMEM medium was removed and 50 µg/ml of CHX in DMEM was added to the cells and incubated for 2 h at 37°C and 5% CO₂. For the second incubation the CHX containing medium was removed and replaced by 100 µg/ml of CHX incubated for 30 min at 37°C and 5% CO₂. Next, the CHX was removed and the cells were fused for exactly 2 min with 250 µl of Polyethylene Glycol 1500 (PEG1500) diluted in PBS containing 100 µg/ml CHX. After fusion, cells were washed 3 times with PBS and new medium containing 100 µg/ml CHX was added to the cells. Cells were incubated for 3 h at 37°C with 5% CO₂ to allow protein shuttle. For shuttling assays in combination with IsoG, treatment with CHX was co-induced with either IsoG or DMSO resulting in a total 6 h induction. Next, cells were washed two times with 1 ml of ice-cold PBS containing 100 µg/ml CHX. Subsequently, cells were fixed with 4% Paraformaldehyde solution (PFA) (diluted from 16% Paraformaldehyde; Sigma-Aldrich) for 20 min. Subsequently, cells were washed twice with 1XPBS and then incubated with Hoechst nuclear staining solution diluted in TBST (1:4000) for 30 min. Coverslips were then washed two times with 1XPBS and dried on a paper towel for 10 min. After drying, coverslips were mounted on microscopic slides with ProLong® Diamond Antifade Mountant (Invitrogen). For optimal mounting medium hardening, the slides were dried overnight at RT and stored afterwards at 4°C until imaging.

4.10. RNA work

4.10.1. RNA extraction

Total RNA was extracted from cells using TRIzol. Harvested cell pellets were resuspended and lysed in TRIzol (Thermo Fisher Scientific) (500 µL/6 cm plate) and stored in the freezer (-80°C) for at least 2 h prior RNA extraction. After TRIzol lysates were thawed on ice, 100 µl chloroform (Carl Roth) per 500 µl of TRIzol was added. RNA/DNA were phase separated from proteins by centrifugation (17,000xg for 15 min at 4°C) and transferred to a new tube. RNA was precipitated with isopropanol (Sigma Aldrich) (1vol) for 30 min on ice. After precipitation, RNA was pelleted by centrifugation (17,000xg for 25 min at 4°C) and subsequently washed with 440 µl of 70% ethanol (100% ethanol - VWR - diluted in RNase free water – Sigma Aldrich) by centrifuging at 12,000xg for 5 min at 4°C. To avoid DNA contamination, a DNase treatment was performed using 4U of TurboDNase (Thermo Fisher Scientific) and incubated for 30 min at 37°C. To remove the DNase and phenol residues, the RNA was again precipitated with 550 µl 100% ethanol (VWR) and 20 µl 3M sodium acetate pH 5.5 (Life Technologies) overnight at -80°C. On the next day, RNA was pelleted (17,000xg for 25 min at 4°C) and washed with 70% ethanol (12,000xg for 5 min at 4°C). After

removing the ethanol, the RNA pellets were dried up-side down for 10 min. Any residual ethanol was removed on the microtube surface. Subsequently the RNA pellet was turned around and dried for another 10 min. Next, the clean RNA pellet was resuspended in RNase free water by pipetting up and down followed by a 5 min incubation at 37°C. RNA was then quantified using a Nanodrop and stored at -80°C.

4.10.2. RNA binding assay

To determine the RNA binding capacity, P19 cell lines expressing SRSF3-, Nxf1- and Zc3h14-GFP tagged proteins were co-cultured and treated with IsoG (33 μ M) or DMSO for 16h in two 15 cm plates. For SRSF3 depletion experiments the Zc3h14 BAC lines was incubated with 6 μ g of *SRSF3* esiRNAs or *Luciferase* siRNAs for 32 h. Before harvesting, cells were UV-irradiated one time with 150mJ/cm² at 254nm to cross-link RNA-protein complexes. After cell harvesting, the cell pellets of two 15 cm plates were combined and snap-frozen in liquid nitrogen and stored at -80°C. Cell pellets were subsequently thawed on ice and lysed in 1 ml lysis buffer. Lysates were sonicated for 30 sec at 20% amplitude and cleared by centrifugation for 10 min; 13,000 RPM at 4°C. Next, an RNase treatment was performed to digest the RNA to lengths of 80-200nt using RNaseI with 33 mU/ μ l combined with a DNase treatment (4U/ μ l) incubated for 3 min at 37°C while shaking at 1,200 rpm. GFP-tagged proteins were immunoprecipitated using Protein G Dynabeads® (ThermoFisher Scientific) coupled with an anti-GFP antibody (12 μ g, provided by D. Drechsel, MPI-CBG, Dresden) for 2 h at 4°C on a rotating wheel. Coupled beads were washed ones with high salt wash buffer and twice with lysis buffer and resuspended in lysis buffer containing RNaseIn (1:500 diluted). Lysates were then added to the Dynabeads magnetic beads and incubated for 2 h at 4°C on a rotating wheel. IPs were stringently washed and RNAs bound to the purified proteins were then de-phosphorylated using T4 polynucleotide kinase (PNK) and radioactively labeled with P32 at their 5'end. The radiolabeled RNA-protein complexes were subsequently separated by SDS gel-electrophoresis using the Novex pre-cast system with 4–12% NuPAGE gradient gels and transferred as described in section 4.11.4. After the western blot transfer, the radiolabeled RNA was visualized by a phosphor imager.

To normalize the co-purified RNA by the bait, the IP-efficiency of each sample was determined by immunoblotting the membrane with an anti-GFP antibody. Therefore, the membranes were blocked with 5% bovine serum albumin (BSA) and then probed with goat anti-GFP antibody overnight at 4°C. After two washes with TBST, a secondary goat antibody coupled with horseradish peroxidase (HRP) was added to

the membranes for 1 h at RT. Two more washes were performed and total GFP-tagged protein levels were visualized using enhanced chemiluminescence reagent (ECL). The amount of bait protein for SRSF3, Nxf1 and Zc3h14 was acquired with a ChemiDoc image system (Biorad) and posteriorly quantified using ImageLab software. All the buffers used in this experiment are listed in Table 3.

4.10.3. UV Cross-linking and Immunoprecipitation (iCLIP)

iCLIP sample preparation was performed by Francois McNicoll. P19 Zc3h14-GFP tagged cell lines were cultured and IsoG treatment was performed as previously described. Before harvesting, cells were UV-irradiated one time with 300 mJ/cm² at 254nm. Two 15 cm dishes were combined per sample, and one non-cross-linked sample was added as a negative control. Cells were harvested, and pellets were snap-frozen in liquid nitrogen. The iCLIP experiment and the library preparation was performed by Francois McNicoll according to (Huppertz et al., 2014). All buffers and reagents used for the iCLIP experiment are listed in Table 3. In brief, cells were lysed in 1 ml lysis buffer and RNA was partially digested to lengths of 80-200 nucleotides with RNase I (Invitrogen) for 5 min at 37°C. After digestion, Zc3h14-GFP protein was immunoprecipitated using Protein G Dynabeads® (ThermoFisher Scientific) coupled with an anti-GFP antibody (12 µg, provided by D. Drechsel, MPI-CBG, Dresden) for 2 hours at 4°C on a rotating wheel. Bound RNA fragments were dephosphorylated using T4 polynucleotide kinase (PNK) (New England Biolabs) and an L3 linker (IDT) was ligated to the 3' end of the RNAs overnight using T4 ssRNA ligase (New England Biolabs). Ligated RNA fragments were radioactively labeled with P32 at their 5' end and a Western Blot was performed to stringently purify and size select all RNA fragments that were cross-linked to Zc3h14. Cross-linked RNA was extracted from the membrane by degrading all proteins with Proteinase K (Thermo Fisher Scientific). Isolated RNA fragments were reverse transcribed with Superscript IV (ThermoFisher Scientific) and barcoded RT-primers that anneal to the L3 linker (sequences on Table 6). cDNA fragments were resolved on a 6% TBU acrylamide gel (Invitrogen) and fragments of 150 to 300 bp were cut from the gel. After purification, cDNA fragments were circularized using CirLigase™ (Epicentre) and re-linearized by BamHI (NEB). The final cDNA libraries now containing 5' and 3' adaptors were amplified using AccuPrime (Thermo Fisher Scientific) and sequenced on an Illumina HiSeq2000 machine (single-end 75 nucleotide reads, 20 million reads per replicate).

4.10.4. Analysis of RNA-Seq and iCLIP data

RNAseq data analysis was performed by Michaela Müller-McNicoll and You Zhou. RNAseq reads were quality controlled using FastQC. Reads with Phred score >20 and with more than 20 nucleotide length were filtered using Flexbar (version 2.5). Reads were mapped to the mouse genome (version MM10) based on GENCODE annotation. Reads were mapped with STAR (Dobin et al., 2013) and differential expression analysis was performed with DESeq2 (Love et al., 2014), and an adjusted P-value of .05 was considered for the differentially expressed genes (DEGs) using Deseq2 (version 1.24.0). Gene ontology (GO) analysis was performed with clusterprofiler (version 3.12.0) in R (Table 5).

Analysis of the iCLIP sequencing data was performed using the iCOUNT package (<http://icount.biolab.si>) with default options by Michaela Müller-McNicoll and Igor Ruiz de Los Mozos. Briefly, adaptors and barcodes were removed from all iCLIP reads before mapping to the mouse mm9 genome assembly (version Ensembl65) using Bowtie (version 0.12.7). After analysis of reproducibility, replicates were pooled to allow determination of statistically significant cross-link events (X-links). For this, all uniquely mapping reads were used, PCR duplicates were removed using the random barcodes within the 3' adaptor, and X-link sites were extracted (1st nucleotide of the read) and randomized within co-transcribed regions. Significant X-links (false discovery rate [FDR] <0.05) were calculated using normalized numbers of input X-links as previously described (König et al., 2010). The entire iCOUNT script for the analysis is available on github: <https://github.com/tomazc/iCount>. For quantification of significant X-links in genes and genic regions, significant X-links were counted into transcript regions using mm9 transcript coordinates (Ensembl59) using the iCount annotation and segment functions respectively.

For motif searching, a z-score analysis for enriched k-mers was performed as described previously (König et al., 2010). Sequences surrounding significant X-links were extended in both directions by 30 nucleotides (windows: -30 to -5 nt and 5-30 nt). All occurring k-mers within evaluated interval were counted and weighed. Then, a control dataset was generated by 100x randomly shuffling significant X-links within the same genes, and a Z-score was calculated relative to the randomized genomic positions. The top 20 k-mers were aligned to determine the *in vivo* binding consensus motif. Sequence logos were produced using WebLogo (<http://weblogo.berkeley.edu/logo.cgi>).

4.10.5. Reverse Transcription

To perform splicing analyses and quantitative PCRs (qPCR), cDNA was synthesized from total RNA by reverse transcription. For reverse transcription, 1 µg of total RNA was diluted in H₂O, in a final volume of 10 µl. Reverse transcription primers (random hexanucleotide mix and/or oligodT: indicated in the results; Sigma Aldrich) were mixed with dNTPs (Thermo Fisher Scientific) (1:1 ratio) and added to the RNA dilution. RNA was denatured at 65°C for 5 minutes and cooled down to 4°C. Subsequently, the master mix containing 1XFirst Strand buffer, 0.1 M DTT, 40 U of Ribolock RNase Inhibitor, and 200 U of SuperScript III (Thermo Fisher Scientific) was added to the samples (Thermo Fisher Scientific). As a DNase control, one of the samples was prepared with only the master mix lacking the reverse transcriptase superscript (RT-control). The reverse transcription was initiated by incubating the sample mastermix for 60 min at 50°C. Reaction was inactivated by incubation at 75°C for 15 min. After reverse transcription, cDNA was stored at -20°C until use.

4.10.6. Splicing analysis

To detect intron retention, splicing PCRs using primers spanning the respective intron were performed. Primers were designed using SnapGene in combination with the PrimerBlast tool of NCBI using the mouse Refseq database. PCRs were performed with Phusion-DNA polymerase (New England Biolabs). Protocol and concentrations are described in Table 10. Primers used for splicing analyses are listed in Table 11.

Table 10: Phusion PCR protocol and program.

Phusion PCR protocol	Phusion PCR program
1X Phusion HF buffer	98°C 2 min
0.3 mM dNTPs	98°C 30 sec
0.4 mM forward primer	63°C 30 sec
0.4 mM reverse primer	72°C 30 sec/kb
10 ng/µl cDNA	72°C 5 sec
0.08 U Phusion polymerase	4°C infinite

} **34 cycles**

Table 11: Oligonucleotides used for splicing assays.

Primer name	Target	Sequence	Region
DNAJB1_exon2_for	<i>DNAJB1</i>	AAGATAAGATCCTGACCATCGAAGT	Exon2
DNAJB1_exon3_rev		CTCATCCAGAACCATCCTGG	Exon3
mNip7_exon2_for	<i>Nip7</i>	TCCTAGTGGACAGACCCGAC	Exon2
mNip7_exon3_rev		CGTGCAAGCGGAACCTGT	Exon3

mHgh1_exon3_for	<i>Hgh1</i>	CCCAAGTCGACATTCTCCCC	Exon3
mHgh1_exon4_rev		GCTCCCGTTGCTTGCTGG	Exon4
18SrRNA-Ctrl_for	18SrRNA	GCGTATATTAAGTTGCTGCAGT	645-668
18SrRNA-Ctrl_rev		GTCATGGGAATAACGCCG	1106-1124

For visualization of the amplified PCR products, agarose gels and Bioanalyzer testing was used. For agarose gels, DNA loading dye (Orange DNA loading dye 6X - Thermo Fisher Scientific) was added to the PCR products and these were resolved on 2% agarose gels, dissolved in 0.7XTBE. A 50 bp DNA ladder (O' GeneRuler 50 bp DNA Ladder; Thermo Fisher Scientific) was used to estimate the PCR products size. Gels were stained with RedSafe staining solution (Hiss Diagnostics) and images were acquired with a GelDoc station (Syngene). For Bioanalyzer testing (Agilent), the PCR product was diluted 1:3 in H₂O. First the chip was set up and the gel-dye mix was injected into the chip according to manufacturer's instructions (Agilent DNA 1000 Kit Quick Start). The diluted PCR products were injected into the chip by reverse-pipetting and analyzed using the Agilent 2100 Expert software.

4.10.7. Real time PCR

RNAseq validation experiments were performed by quantitative real-time qPCR. Primers were designed using SnapGene and located at exon-exon junctions. The respective sequences were blasted to the mouse Refseq database using PrimerBlast to avoid unspecific amplification (primer sequences are listed in Table 6). To assure that the qPCR assays were quantitative, primer efficiency tests were performed for all primer pairs used in this work. For the primer efficiency test, at least two different primer concentrations were prepared (500 nM and 1000 nM) and a serial cDNA dilution was performed. cDNAs were diluted into 1:10, 1:20, 1:40 and 1:80 concentrations and a qPCR reaction was conducted for each primer concentration. In the qPCR reaction, a melting curve step was included to evaluate the specificity of the primer pairs. The presence of one single fluorescence peak was considered as specific amplification, while primer concentrations which presented more than one peak were excluded due to potential unspecific product amplification and/or primer dimer formation. The primer efficiency was calculated and primers that presented a sequential increase in the average cycle number and an exponential correlation between C_q value and cDNA dilution were considered as efficient. C_q values per dilution were plotted in Excel and a line trend was generated. The value of the slope was used to calculate the primer efficiency, and primer pairs with 95-105% efficiency were selected for the experiments. Validated primer sets used for cDNA quantification are listed in Table 12. Table 13 shows the qPCR protocol and program.

Table 12: Oligonucleotides used for qPCR assays.

Primer name	Target	Sequence	Concentration
Smc4_qPCR_val_for	<i>Smc4</i>	TGTTCAAGTGTTCGGCCACCT	500 nM
Smc4_qPCR_val_rev		AGGGGAGTGGGCTTGTAGTGA	
Fmr1_qPCR_val_for	<i>Fmr1</i>	ACATGTCAAAGGAGGTTAGCCGT	1000 nM
Fmr1_qPCR_val_rev		AGCAAGTTAGCGCCTTGCTGA	
Kif20B_qPCR_val_for	<i>Kif20B</i>	GCCACCAGCAAAGAAAGGGCTTA	500 nM
Kif20B_qPCR_val_rev		GCTGCTGCAAACCTACAACCT	
Cdc25A_qPCR_val_for	<i>Cdc25A</i>	AAACCTTGCCGATCGTTGCG	500 nM
Cdc25A_qPCR_val_rev		CATCCGCCTTCGCTTCACA	
Sept7_qPCR_val_for	<i>Sept7</i>	GGTTCCATTGCATGCAGCCT	500 nM
Sept7_qPCR_val_rev		AGGTTCTGGCTACAGGGGCA	
qPCR_primer_BA_2	<i>ActB</i>	GAGCACAGCTTCTTTGCAGCTC	1000 nM
qPCR_primer_BA_6		CAACCGTGAAAAGATGACCCAG	
Hist1h1e-6_for	<i>Hist1h1e</i>	CTTTC AATTGTGTTTCGAGC	1000 nM
Hist1h1e-6_rev		CCTCACTTGCTCCTGC	

The validated primer sets with the respective concentration were used for quantitative real time PCRs (qPCRs). Therefore, cDNA was first diluted 1:10 in nuclease free H₂O and added to the primer set mix and the ORA™ SEE qPCR Green ROX L kit (highQu). After centrifuging the mastermix, the MicroWell 96 well plate was inserted into the thermo cycler (Thermo scientific PikoReal). A melting curve step was added to confirm primer specificity in each experiment. The analysis of the Ct values was determined by using the Thermo Scientific PikoReal Software 2.1.

Table 13: qPCR protocol and program.

qPCR protocol (1 reaction)	qPCR program
2.5 µl ORA qPCR mastermix	95°C 2 min
1.5 µl primer set mix (0.5-2.0 µM)	95°C 20 sec
1 µl cDNA (1:10 diluted)	60°C 20 sec
	72°C 30 sec
	72°C 5 min
	60°C > 95°C Hold 1sec; temperature increase after hold 0.2°C
	25°C Infinite hold

} 30 cycles

4.10.8. RNA Fluorescence in situ Hybridization (FISH)

For FISH-experiments, 12mm diameter coverslips were pre-coated with 0.1% (v/v) gelatin in PBS for 24 h in 10 cm plates. After removing the gelatin, cells were seeded on the 10 cm plates and prepared for the respective experiment. Subsequently the culture medium was removed and the 10 cm plates, including the coverslips, were washed with 1X PBS. The coverslips were collected using tweezers and transferred to 24 well plates, while the cells on the 10 cm plate were harvested for RNA or protein work. FISH was performed using Stellaris probes and buffers (LG Bioserch Technologies) following the manufacturer's instructions with slight modifications. Briefly, cells were fixated with 4% Paraformaldehyde solution (diluted from 16% Paraformaldehyde; Sigma-Aldrich) for 20 min. After fixation, cells were washed twice with 1xPBS and permeabilized with 70% ethanol for 24 h at 4°C. Next, cells were washed with wash buffer A and coverslips were placed in a humidified chamber and were hybridized for 16 hours at 37°C in the dark. Polyadenylated RNA (pA+RNA), *Malat1*, *Smc4*, *Hist1H Nip7-intron3* Stellaris probes coupled with quasar fluorophores (probe sequences intervals are listed in Table 14) were diluted in its respective concentration in hybridization buffer (see Table 14). After hybridization, cells were incubated twice for 30 min at 37°C in wash buffer A solution. The second incubation was performed with the addition of Hoechst 34580 (Sigma-Aldrich) diluted 1:4000 in wash buffer A. Coverslips were washed for 2-5 min with wash buffer B and then dried for 15 min at RT in the dark and subsequently mounted in slides as described in section 4.11.7.

Table 14: FISH probe information. Sequence interval indicates the region from the transcript were the probes were designed.

FISH probe name	Target	FISH probe region	Dilution
pA+RNA	polyA RNA	Polyadenylated RNA	1/70,000
Nip7-I3	<i>Nip7</i> intron3	NM_025391: 536-1170 bp	4/70
Malat1	<i>Malat1</i>	NR_002847: 1-6983 bp	3/70
SMC4	<i>Smc4</i>	NM_133786: 1-4314 bp	4/70
Histone	<i>Histone</i>	Binds to repl. dep. histones: NM_013550.5: 1-479 bp	3/70

4.11. Protein work

4.11.1. Protein Extraction

Cell pellets were thawed on ice for 10 min and subsequently resuspended with NET2 buffer (NET2 buffer recipe in Table 3 and incubated for 10 min on ice. Lysates were sonicated three times for 10 sec at 20%

amplitude with 20 sec cool down phases in between, and afterwards cleared by centrifugation for 10 min, 13,000 rpm at 4°C. Supernatants were transferred to new tubes and protein concentration was quantified with Quick Start™ Bradford 1x Dye Reagent (Biorad) on a Nanodrop. Protein concentrations were adjusted according to the Bradford quantification and subsequently mixed with 5XLämmli buffer (recipe in Table 3). Protein denaturation was performed by incubating the samples at 95°C for 3 min, before samples were directly loaded for an SDS-PAGE or stored at -20°C.

4.11.2. Shrimp alkaline phosphatase (SAP) treatment

For protein de-phosphorylation assays, proteins were extracted as described above, using NET2 buffer supplemented with Protease inhibitors (-EDTA) and 10 mM MgCl₂, but without β-phosphoglycerate. SAP treatment was performed for 30 min at 37°C shaking at 300 rpm. SAP reaction was performed as described in Table 15 for +/- SAP samples. After the treatment, 5XLämmli buffer without glycerol was added to +SAP samples and with glycerol to -SAP samples. Lysates were boiled at 90°C for 3 min and loaded onto 12% SDS-PAGE gels with or without phostag®.

Table 15: SAP treatment reaction protocol.

+SAP	-SAP
10 µg protein	10 µg protein
1XSAP buffer	1XSAP buffer
0.25 U/µl SAP	-
Adjusted with NET-2+MgCl ₂ +PI(-EDTA)	Adjusted with NET-2+MgCl ₂ +PI(-EDTA)
After reaction 1XLämmli buffer w/o glycerin	After reaction 1XLämmli buffer with glycerin

4.11.3. Co-immunoprecipitation (Co-IP)

For Co-IPs, P19 GFP-tagged cell lines were cultivated in two 15 cm dishes. Cells were washed twice with PBS, harvested using 5 ml of PBS and combined in one 15 ml falcon tube. Cell suspension was pelleted by centrifugation at 1000xg for 5 min at 4°C. Supernatant was removed and cell pellets were snap frozen in liquid nitrogen and stored at -80°C. For the co-immunoprecipitation (Co-IP) cells were lysed in 1 ml NET2 buffer as described in section Table 3. Lysate was split into two 1.5 ml tubes (-/+ RNase) each containing 500 µl of cell lysate. 100 µg/ml RNase A was added to the +RNase. Both samples (-) and (+) RNase were incubated for 20 min at 24°C. 0.2% (v/v) of the lysate was transferred to a new tube and served as the input. GFP-tagged proteins were immunoprecipitated using Protein G Dynabeads® (Thermo Fisher Scientific) coupled with either an anti-GFP antibody (12 µg, provided by D. Drechsel, MPI-CBG, Dresden)

or 12 µg of a goat IgG (Sigma-Aldrich) (IgG control) for 2 h at 4°C on a rotating wheel. Coupled beads were washed once with high salt wash buffer and twice with lysis buffer and resuspended in 500 µl NET2 buffer (incl. 1X PI and 10 mM β-Phosphoglycerate) and then combined with the treated cell lysates for 1.5 h at 4°C on a rotatory wheel. Subsequently, beads were washed using stringent buffers (listed in Table 3) and co-precipitated proteins, as well as IgG and input samples were eluted by the addition of 25 µl of 1.3X Laemmli buffer and heating at 95°C for 3 min. Input and co-precipitated proteins were then loaded onto pre-cast 4–12% NuPAGE gradient gels and Western Blot was performed as described in section 4.11.4.

Table 16: SDS-PAGE gel recipes.

Solution	Separation gel (8%)	Stacking gel (4%)
H ₂ O	2.05 ml	1.22 ml
30% (v/v) Bis-Acrylamide	1.6 ml	260 µl
1 M Tris-HCl pH 8.8	2.25 ml	-
1 M Tris-HCl pH 6.8	-	500 µl
10% (m/v) SDS	60 µl	20 µl
10% (m/v) APS	30 µl	25 µl
TEMED	10 µl	2.5 µl

4.11.4. Western Blot

For immunoblotting, two different systems were used: a precast-system from Novex (Thermo Fisher Scientific) and a BioRad system consisting of self-made SDS-gels with the following gel composition. For immunoblot detection 20-30 µg of protein extracts dissolved in 1X Laemmli buffer were loaded into SDS gels (recipe in Table 11) or pre-cast gradient gels (NuPAGE™ 4-12% Bis-Tris Protein Gels; Thermo Fisher Scientific). Gels were run at 180 V for 1.1 h and transferred onto nitrocellulose membranes (0.1 µm pore size) according to the recommendations of the respective system (BioRad for self-made gels and NOVEX for pre-cast gels). After blotting, the membranes were blocked for with either 3% (m/v) BSA in TBST (2h at RT) or 5% (m/v) milk solution diluted in TBST (1 h at RT). A primary antibody solution with its respective dilution was added to the membranes and incubated overnight at 4°C or for 2 h at RT (see antibody dilutions in Table 17). After primary antibody incubation, membranes were washed twice with 1XTBST for 15 min and the respective secondary antibody was added (1:10,000 dilution) and incubated for 45-60 min at RT (see Table 18). Membranes were washed again twice with 1XTBST and developed on Chemiluminescent Imager (Biorad) using the ECL Prime detection reagent (GE Healthcare). Chemiluminescent signals were acquired with multiple exposure times. Images were subsequently processed, and protein quantification was performed with Imagelab software (Biorad).

Table 17: Primary antibodies used in western blot assays.

Primary antibody	Target	Clone	Company/catalogue #	Dilution	Blocking
α -Nxf1	unknown epitope	53H8	Santa Cruz Biotechnology, Inc. (sc-32319)	1:1000	3% BSA
α -Zc3h14	unknown epitope	Tier2	Provided by Katja Straesser	1:1000	5% Milk
α -GFP	-	-	D. Drechsel, MPI-CBG, Dresden, Germany	1:3000	3% BSA
α -SRSF3	aa: 1-85	2D2	Sigma Aldrich (WH0006428M8)	1:400	5% Milk
α -Ctnnb	aa: 750-781	Polyclonal	Abcam (ab2365)	1:1000	3% BSA
α -Histone H3	aa: 100-136	Polyclonal	Abcam (ab1791)	1:1000	3% BSA
α -Actin	C-terminal isoforms: SGPSIVHRKCF	AC-40	Sigma Aldrich (A4700)	1:1000	3% BSA
α -PABPN1	aa: 1-100	EP3000Y	Abcam (ab75855)	1:1000	3% BSA
α -GAPDH	unknown epitope	6C5	Santa Cruz Biotechnology, Inc. (sc-32233)	1:400	3% BSA
α -Phospho-Bcl-2	phosphorylated Thr56	Polyclonal	Cell Signalling Technology (2875)	1:500	3% BSA
α -mAb104	SR phospho-epitope	-	provided by Karla Neugebauer	1:3	3% BSA

Table 18: Secondary antibodies used in western blot assays.

Secondary antibody	Host	Type	Company/catalogue #	Dilution
α -mouse	Donkey	IgG	Sigma Aldrich (AP192P)	1:10,000
α -mouse	Donkey	IgM	Jackson ImmunoResearch (715-035-020)	1:10,000
α -rabbit	Donkey	IgG	Sigma Aldrich (AP182P)	1:10,000
α -goat	Donkey	IgG	Sigma Aldrich (AP182P)	1:10,000

4.11.5. Phostag® Gels

To discriminate distinct SRSF3 protein phosphorylation states, phostag® gels were performed with the following composition:

Table 19: SDS-PAGE – Phostag® gel recipes.

Solution	Separation gel (12%)	Stacking gel (4%)
H ₂ O	1.62 ml	2.32 ml

30% (v/v) Bis-Acrylamide	2.00 ml	600 μ l
1.5 M Tris-HCl pH 8.8	1.25 ml	-
1 M Tris-HCl pH 6.8	-	1000 μ l
10 mM MnCl ₂	40 μ l	-
10% (m/v) SDS	50 μ l	40 μ l
10% (m/v) APS	25 μ l	40 μ l
TEMED	5 μ l	4 μ l
Phostag [®]	10 μ l	-

To control the phostag[®] gel efficiency, a second gel without phostag was simultaneously prepared. Protein lysates were prepared as previously described (section 4.11.1), using NET2 buffer, but without protease inhibitors and β -phosphoglycerate. Both gels were loaded with 10 μ g of protein lysates including SAP treated lysates. Electrophoresis was performed for 2 h at 160 V at 4°C with SDS running buffer as previously described in section 4.11.4. Prior to transfer, phostag[®] gels were washed 3 times with transfer buffer +EDTA for 10 min, and one time with transfer buffer –EDTA for 10 min (buffer recipes are listed in Table 3). The gel transfer onto a nitrocellulose membrane, blocking, and incubation with the SRSF3 antibody was performed as previously described.

4.11.6. Mass spectrometry

For SRSF3 mass spectrometry experiments, P19 the SRSF3 GFP-tagged cell lines were cultivated in two 15 cm dishes in the presence or absence of the IsoG (33 μ M 16 h). In addition, an NLS-GFP line expressing a nuclear localization signal fused to GFP was cultivated and served as a control and mass spectrometry background signal. The cells were harvested after washing the 15 cm plates twice with 10 ml ice cold 1XPBS. SRSF3 -IsoG, SRSF3 +IsoG, and NLS-GFP samples were subsequently immunoprecipitated as previously described in section 4.11.3. Prior elution from the magnetic beads, 10% (v/v) of the bead solution was transferred to an additional microfuge tube and served as an IP-control. The IP-control was stored at 4°C until loading on a coomassie gel. The remaining 90% (v/v) were eluted with 50 μ l 6M Guanidin-Hydrochloride (ph 8.0 in Tris pH 8.0) while shaking at 400 rpm for 5 min at RT and repeated twice with a final elution volume of 150 μ l. Subsequently, the IP-control was prepared by re-suspending the beads in 1.3XLaemmli buffer and boiling them at 95°C for 5 min. After boiling, the samples were loaded on an SDS-PAGE (section 4.11.4) and subsequently coomassie stained with 0.1% coomassie blue R250 in 10% (v/v) glacial acid, 50% (v/v) methanol, and 40% (v/v) H₂O. The gel was stained for 30 min at RT for 2

h in 10% (v/v) acetic acid, 50% (v/v) methanol, and 40% (v/v) H₂O and subsequently imaged as previously described in section 4.10.2.

The mass spectrometric analysis was performed by Dr. Christian Muench (Institut für Biochemie II, Theodor-Stern-Kai 7, 60596 Frankfurt am Main). In short, peptides were resuspended in 0.1% (v/v) FA and separated on an easy nLC 1200 (Thermo Fisher Scientific) and a 22 cm long, 75 µm ID fused-silica column, which has been packed in-house with 1.9 µm C18 particles (ReproSil-Pur, Dr. Maisch), and kept at 45°C using an integrated column oven (Sonation).

Peptides were eluted by a non-linear gradient from 5-38% acetonitrile over 120 min and directly sprayed into a QExactive HF mass-spectrometer equipped with a nanoFlex ion source (Thermo Fisher Scientific) at a spray voltage of 2.3 kV. Full scan MS spectra (350-1400 m/z) were acquired at a resolution of 120,000 at m/z 200, a maximum injection time of 100 ms and an AGC target value of 3×10^6 . Up to 20 most intense peptides per full scan were isolated using a 1 Th window and fragmented using higher energy collisional dissociation (normalized collision energy of 35). MS/MS spectra were acquired with a resolution of 45,000 at m/z 200, a maximum injection time of 80 ms and an AGC target value of 1×10^5 . Ions with charge states of 1 and > 6, as well as ions with unassigned charge states were not considered for fragmentation. Dynamic exclusion was set to 20 s to minimize repeated sequencing of already acquired precursors.

4.11.7. Fluorescence and Immunofluorescence microscopy

To acquire fluorescent images of the GFP-tagged proteins in P19 and HeLa cell lines, coverslips were added to 10 cm dishes and pre-coated with 0.1% (v/v) gelatin for 24 h. Cells were seeded as previously described and incubated for 24 h to allow cell attachment. After the respective treatment, 10 cm plates were washed twice with 5 ml 1XPBS. Subsequently the coverslips were transferred to 24-well plates, while the 10 cm plates were harvested for protein or RNA validation experiments. Cells grown on the coverslips were fixated with 4% Paraformaldehyde solution (PFA; diluted from 16% Paraformaldehyde; Sigma-Aldrich) for 20 min. For visualization of GFP-tagged proteins (fluorescence assay), cells were washed twice with 1XPBS and then incubated with Hoechst nuclear staining solution (1:4000) for 30 min at RT. Coverslips were then washed twice with 1XPBS and dried on a paper towel for 15 min RT. After drying, coverslips were mounted on microscopy slides with ProLong® Diamond Antifade Mountant (Invitrogen). For optimal mounting medium hardening, the slides were dried overnight at RT and then stored at 4°C until imaging.

For immunofluorescence experiments, fixation and washing steps were followed by a permeabilizing procedure. Therefore, the cells were incubated with blocking/permeabilizing solution for 30 min (see recipe in Table 3). After blocking/permeabilization, cells were incubated with a primary antibody diluted in 3% BSA in 1XPBS for 2 h at RT. After primary antibody incubation, cells were washed twice with 1XPBS. Next, cells were incubated with a secondary antibody diluted in 3% (m/v) BSA in 1XPBS for 1 h at RT. Nuclear staining and slide preparation were performed as described above for the fluorescence assay. All antibodies used for immunofluorescence are listed in Table 20 and Table 21.

Table 20: Primary antibodies used for immunofluorescence assays.

Primary antibody	Target	Clone	Company/catalogue #	Dilution
α -SC35	SR protein phospho-epitope	SC-35	Abcam (ab11826)	1:200
α -Coilin	aa: 277-576	H-300	Santa Cruz Biotechnology, Inc. (sc-32860)	1:50
α -Fibrilarin	aa: 61-200	F-6	Santa Cruz Biotechnology, Inc. (sc-166000)	1:50
α -Sam68	C-ter minus	C-20	Santa Cruz Biotechnology, Inc. (sc-333)	1:50

Table 21: Secondary antibodies used for immunofluorescence assays.

Secondary antibody	Host	Dye	Company/catalogue #	Dilution
α -mouse	Donkey	Fluor 555	Abcam (ab150110)	1:200
α -rabbit	Donkey	Fluor 647	Abcam (ab150075)	1:50

4.12. Confocal microscopy

Cell images were acquired using a confocal laser-scanning microscope (LSM780; Zeiss) with a Plan-Apochromat 63x objective with a numerical aperture of 1.4, using immersion oil. The Zen 2012 software was used to acquire the images. Images from the same experiment were acquired on the same day with the same settings for all conditions (laser power, gain, pin hole size and offset). For HKA experiments, 12 slices of the respective heterokaryon were acquired compromising both entire cells.

4.12.1. Image processing

Fiji software was used to process and analyze the acquired images of fluorescence, FISH and immunofluorescence experiments. Contrasting was performed with the same intensity of control and treated images. Pictures were cropped with Image crop function and scale bars were added. Below, the strategies for quantification and image processing are detailed.

4.12.2. Fluorescence quantification

For fluorescence quantification, fields with comparable cell density were captured until at least 100 cells were obtained. Pictures were opened in Fiji (Schindelin et al., 2012) and the channels corresponding to Hoechst (nuclear staining), pA+RNA and *Smc4* were used to acquire threshold images (“Threshold Li” for nucleus and “Threshold Triangle” for total *Smc4* and pA+RNA signal). Next, regions of interest (ROIs) were acquired from nucleus and total cell threshold images and transferred to the *Smc4*/pA+RNA channel image. Fluorescence was quantified for each area using the ‘integrated density value’ (mean gray value per pixel x area). The cytoplasmic fluorescence signal was calculated by subtracting the nuclear from the total cell fluorescence signal. Fluorescence values were plotted in GraphPad Prism.

HKA shuttling quantification was performed using the imageJ software as described in (McNicoll & Müller-McNicoll, 2018). In short, GFP and Hoechst fluorescent stacks were hyperstacked using the projection type max intensity. Donor, recipient and background nuclear region of interest (ROI) were drawn manually with the pencil tool. Using the ROI GFP, fluorescent intensities were hyperstacked using the projection type sum slices. For each image, both the donor and recipient nuclei were subtracted from the background mean pixel intensity. Total pixel intensity of the recipient nucleus was divided by the donor nucleus and multiplied by 100 to obtain the value of the shuttling capacity in percent.

4.12.3. Line scans

To acquire the fluorescence intensity per pixel in a cell area, and visualize co-localization of *Nip7* intron3 and pA+RNA fluorescence, a straight line was drawn across the cell nucleus. To obtain the maximum speckle signal, this line was drawn from one extremity of the cell nucleus to another, crossing the nucleolus. The line scans were performed in one-cell zooms to increase resolution. A straight line was traced in one channel of interest and the profile was acquired from Fiji (Analyze – Plot profile). The same line was transferred to the other channels and the fluorescence of each channel was plotted in the line area. The values of each graphic were saved and a profile for all the channels was plotted in GraphPad Prism.

4.13. Statistical analysis

To compare nuclear export RNA capabilities upon splicing inhibition, or Zc3h14 depletion relative RNA levels and fluorescence intensity, values were analyzed using the GraphPad Prism software. One-way ANOVA followed by Dunnett's multiple comparisons test was performed using GraphPad Prism version 8.00 for Windows, GraphPad Software, La Jolla California USA, www.graphpad.com. Asterisks indicate significance. HKA statistical analysis is based on student's t-test and paired Wilcoxon rank-sum test.

5. Results

5.1. Splicing inhibition by Isoginkgetin treatment causes global intron retention

To study the role of SRSF3 in splicing surveillance, we first aimed to disturb splicing globally by using a splicing inhibitor. We decided to use the previously described naturally occurring biflavonoid Isoginkgetin (IsoG). O'Brien and collaborators had shown that IsoG (21 h; 33 μ M) treatment lead to splicing inhibition and caused intron retention of three endogenous transcripts (*Tubb*, *Actb*, *DNAJb1*) in HeLa cells due to stalling of pre-spliceosomal assembly (O'Brien et al., 2008). To determine the sensitivity of IsoG and find optimal splicing inhibitory conditions for P19 cells, we assayed intron retention in a time course experiment. We monitored accumulation of intron 2 in the previously described IsoG-sensitive transcript *DNAJb1* by RT-PCR over 20 h with primers within intron 2 (Figure 17A/B). Starting from 8 h after IsoG addition an additional band corresponding to retained intron 2 was detectable, while the solvent control (-IsoG; 1/1000 DMSO) was unaffected and solely the fully spliced *DNAJb1* isoform was amplified. To verify whether IsoG inhibited splicing globally we next performed RNA-seq. P19 cells were treated with 33 μ M IsoG or DMSO for 16 h, since intron 2 retention of *DNAJb1* was maximal at this condition (Figure 17B). To avoid the detection of pre-mRNAs, we isolated polyadenylated RNA (pA+RNA) from two replicates and sequenced the libraries on an Illumina NEXT-Seq 500 machine. Retained introns were identified and quantified using the IRFinder tool (Middleton et al., 2017) and differential expression was quantified using DESeq2 (Figure 17C). Interestingly, the majority of differentially expressed transcripts were protein-coding genes (83%) (Figure 17D), which is in agreement with IsoG acting as splicing inhibitor of mRNAs, which could lead to the differential expression of genes (O'Brien et al., 2008; Yoshimoto et al., 2017). IRFinder revealed that 18,511 introns were differentially retained upon IsoG treatment (Figure 17E). Surprisingly, although the majority of introns (79%) were increased upon IsoG (14,532 introns), a subset of introns decreased (3,979 introns; 21%).

To understand why some introns are more sensitive to IsoG than others, we divided them into regulated and constitutive introns using the most recent ENSEMBL annotation (NCBI m37). Regulated introns comprise introns, which are retained under certain conditions, while constitutive introns are constantly spliced. We found that IsoG treatment affected the retention of regulated and constitutive introns to a similar extent (Figure 17E), but many retained introns might not be annotated as regulated yet.

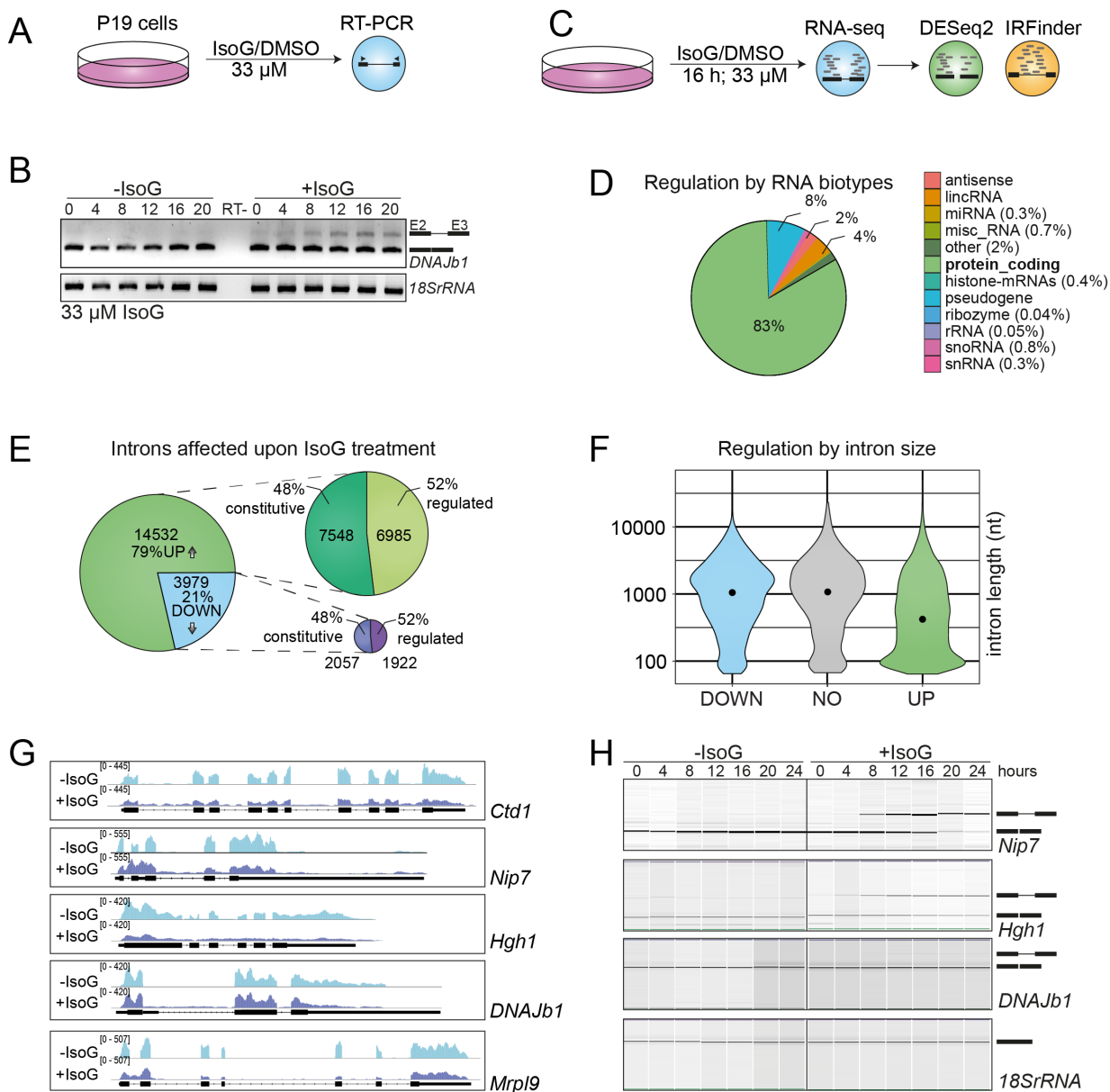


Figure 17: IsoG treatment causes global intron retention in pluripotent P19 cells. Experimental design for the identification of optimal IsoG treatment conditions for splicing inhibition in P19 cells. B) RT-PCR (1.5% agarose gels) of a time course of IsoG treatment to detect spliced and unspliced isoforms of the *DNAJb1* transcript. Amplified isoforms are depicted beside the gel. *18SrRNA* was used as control for cDNA levels. C) Pipeline used for the identification and quantification of transcripts and introns affected by IsoG treatment. D) Pie chart displaying RNA biotypes that are differentially expressed upon IsoG treatment. E) Pie charts displaying the total number of introns that are up/down-regulated upon IsoG treatment. Smaller pie charts on the right show the number of differentially retained introns that are annotated as constitutive or regulated introns. F) Violin plot showing the length distribution of up/down/non-regulated introns. G) Browser shots showing the RNA-seq read coverage on the *Ctd1*, *Nip7*, *Hgh1*, *Mrp19*, *DNAJb1* genes in IsoG- and IsoG+ samples using IGV. Constitutive exons of the main protein-coding isoform are shown as black boxes and introns as black lines. The scale represents the maximum number of reads per nucleotide position. H) Analyses of intron retention in the *Nip7*, *Hgh1* and *DNAJb1* transcripts using a Bioanalyzer. Amplified isoforms are depicted beside the gel. *18SrRNA* was used as control for levels.

Several studies have shown that splicing efficiency is dependent on intron length (Braunschweig et al., 2014). Therefore we next compared intron length of non-regulated, up-regulated and down-regulated introns. Interestingly, we found that up-regulated introns tend to be much shorter than down-regulated ones (Figure 17F). While the majority of up-regulated introns were approximately 100 nt long, down-regulated or non-regulated introns have a similar length distribution and vary between 1,000 and 10,000 nucleotides.

To validate our IRFinder analysis, we chose four transcripts, which showed significantly increased intron retention and visualized their RNA-seq read coverage using the IGV-software (Figure 17G). Browser shots of *Ctd1*, *Nip7*, *Hgh1*, *Mrpl9* and the positive control *DNAJb1* showed higher read coverage within the identified introns in the presence of the splicing inhibitor, while the control samples showed only negligible coverage. RT-PCR using random hexamers and primers within the flanking exons followed by bioanalyzer visualization confirmed the accumulation of *Nip7* intron 1, *Hgh1* intron 1 and *DNAJb1* intron 2 over the time of IsoG treatment. Already eight hours after IsoG addition, intron 1 of *Nip7* and *Hgh1* accumulated massively, while 18S rRNA was unaffected by IsoG (Figure 17H). Taken together, our results show that IsoG treatment leads to global intron retention validating the use of this inhibitor to globally block splicing in P19 cells. Pluripotent mouse P19 cells seem to be highly sensitive to IsoG since intron accumulation can be detected at very early time points, whereas previously described human cell models, such as HeLa cells seem to be more resistant (O'Brien et al., 2008).

5.2. Polyadenylated RNA with retained introns are sequestered in nuclear foci

Our data showed that IsoG treatment caused global splicing inhibition and intron retention in pA+RNAs in a time dependent manner. To monitor the cellular fate of these intron-retained pA+RNAs over time we visualized their subcellular localization using RNA fluorescence *in situ* hybridization (FISH). We designed oligodT probes (30Ts) and performed FISH in P19 cells in the presence and absence of IsoG. Figure 18A shows a 24 h time course experiment in which pA+RNA was visualized in intervals of four hours. pA+RNA FISH in the absence of IsoG (-IsoG) shows the expected pA+RNA pattern (Figure 18A): a predominant cytoplasmic localization, corresponding to exported mature mRNAs and a weaker signal within nuclear speckles. In the solvent control (-IsoG), each time point displayed a highly similar pA+RNA pattern. In

contrast, 4-8 h after IsoG addition, nuclear export of pA+RNA is blocked, indicated by a strong decrease in cytoplasmic pA+ fluorescence intensities. Concomitantly nuclear pA+RNA signal increased over time and ultimately lead to the formation of large polyA foci 12-16 h after IsoG addition. These foci were characterized by a round geometry and a donut-like pA+RNA intensity pattern (Figure 18A). Longer IsoG incubation times (20-24 h) finally lead to the formation of smaller pA+RNA bodies, which correspond to pA+ decay foci. Decay foci have been proposed to be nuclear sites of exosomal RNA degradation, suggesting that mis-processed pA+ mRNAs are stored for some time in larger storage foci, but ultimately undergo decay by the nuclear exosome (Silla et al., 2018; Fan et al., 2018).

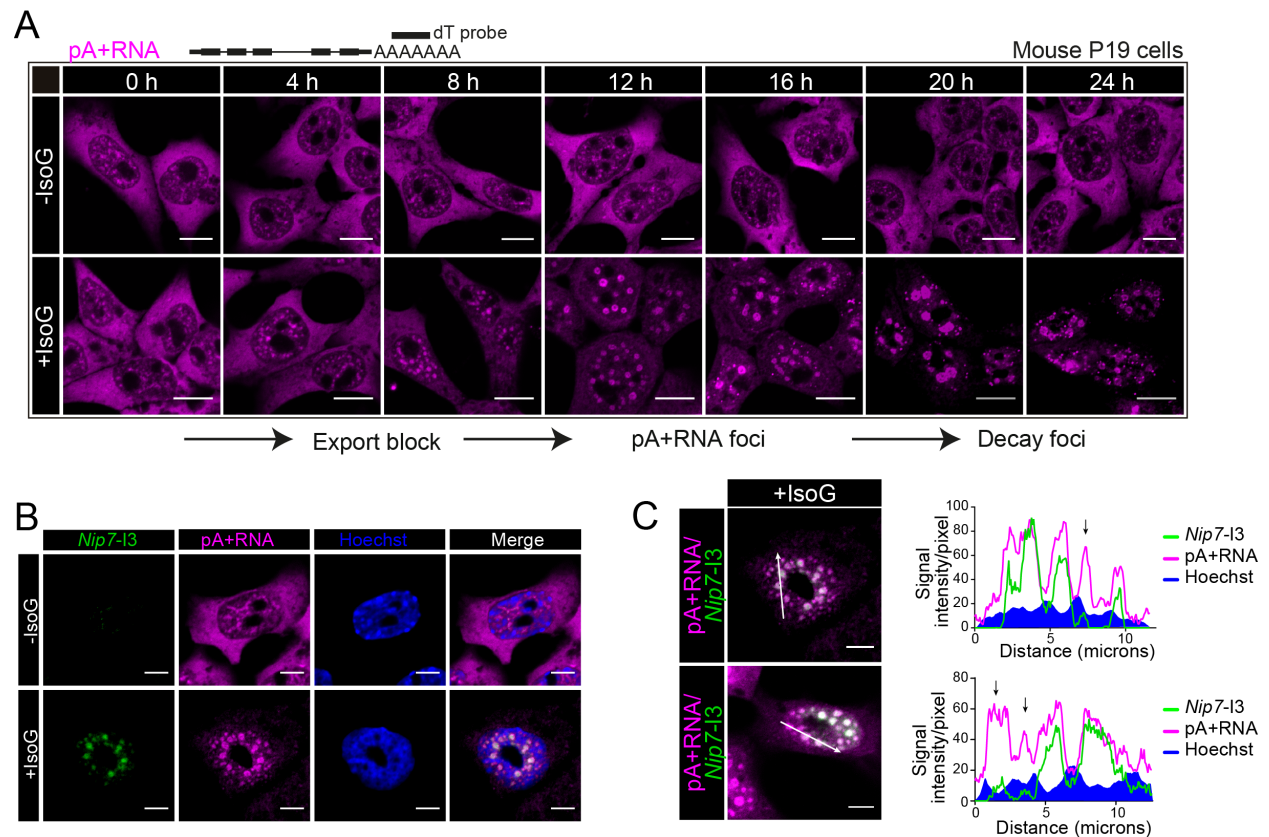


Figure 18: IsoG treatment causes an export block and the formation of pA+RNA foci. A) Time course of IsoG treatment for 24 h. Panel of representative pA+RNA FISH images of control (IsoG-) and IsoG treated P19 cells (IsoG+). Probe hybridization site and time points for which images were acquired are indicated above the cell images. B) FISH images of P19 cells using probes specific for *Nip7* intron 3 (green) and pA+RNA (magenta). Nuclear DNA was stained with Hoechst (blue). C) Representative images of IsoG treated P19 cells showing the merge of the *Nip7* intron 3 (green) and pA+ RNA (magenta) probes. A line (white) was traced through the cell nucleus across nuclear foci containing pA+ RNA signal. The signal intensity per pixel in the line area from *Nip7* intron 3 (green), pA+ RNA (magenta) and Hoechst (blue) was measured using Fiji and was plotted using GraphPad Prism. Black arrows indicate sites of nuclear pA+ RNA signal where *Nip7* intron 3 signal is absent. (Scale bars = 5 μ m).

To confirm that these large pA+RNA foci indeed contain IsoG-sensitive introns, we designed FISH probes hybridizing to intron 3 of the *Nip7* transcript, which was retained upon IsoG treatment (Figure 17G/H). We performed a FISH experiment where P19 cells were co-hybridized with *Nip7* intron three (*Nip7*-I3) probes and oligodT probes in the presence and absence of IsoG (16 h, 33 μ M). Indeed *Nip7*-I3 signal intensities increased massively upon IsoG treatment and overlapped completely with pA+RNA foci (Figure 18B). To confirm this co-localization, we used line scans (Figure 18C). We observed that *Nip7*-I3 fluorescence (green) co-localizes with pA+RNA signal (pink) in regions that are devoid of DNA as indicated by low Hoechst staining (blue). Conversely, pA+RNA signal does not always co-localize with *Nip7*-I3 signal (black arrows), indicating that some pA+RNA foci lack *Nip7* with retained intron 3.

Splicing inhibition is a cellular stress and might lead to the activation of the apoptosis pathway. This irreversible process commits a cell towards death, which can be monitored by Caspase 3 cleavage and Bcl2 phosphorylation (Ruvolo et al., 2001; Wolf et al., 1999). To investigate whether IsoG treatment causes apoptotic cell death, we performed a recovery experiment. P19 cells were treated with IsoG for 16 h (splicing inhibition) followed by a medium change for 8 h (recovery; Figure 19A). Intron retention and the formation of large pA+RNA foci upon IsoG treatment were monitored by FISH visualizing *Nip7*-I3 and pA+RNA fluorescent signal intensities in 4 hours (splicing inhibition) and 2 hours (recovery) intervals, respectively (Figure 19B).

Accumulation of *Nip7*-I3 and formation of nuclear pA+RNA bodies eight hours after splicing inhibition confirmed the efficiency of the IsoG treatment. Interestingly, already two hours after IsoG withdrawal *Nip7*-I3 intensities were strongly decreased with a concomitant disappearance of pA+RNA bodies and an increase of cytoplasmic pA+RNA signal intensities. Eight hours after medium exchange the recovery of the cells seem to be complete as *Nip7*-I3 fluorescence disappeared and the pA+RNA signal pattern was comparable to cells before IsoG treatment. These observations strongly suggest that IsoG treated cells are non-apoptotic and can return to homeostasis after the splicing stress is relieved. To further confirm this, we assayed the expression of the apoptotic markers, phosphorylated Bcl-2 and cleaved-Caspase-3, in P19 cells that have been treated with IsoG or DMSO for 16 h at 33 μ M (Figure 19C). As a positive control we UV-irradiated P19 cells under conditions (UV 60 mJ/cm², incubation 24 h), which have been shown to induce apoptosis (Kong et al., 2016; Martin & Ouchi, 2005). We detected a slight increase in the levels of both apoptotic markers in IsoG treated cells, when compared to the control treatment, indicating that IsoG induces some level of apoptosis, however, this was minor in comparison UV- treated cells, confirming that IsoG causes only modest apoptosis induction. Taken together, these results indicate that splicing

inhibition causes a reversible export block and the storage of intron containing pA+RNAs in nuclear bodies. They further suggest that upon inhibitor withdrawal, retained introns can be spliced post-transcriptionally and the transcripts are subsequently exported to the cytoplasm.

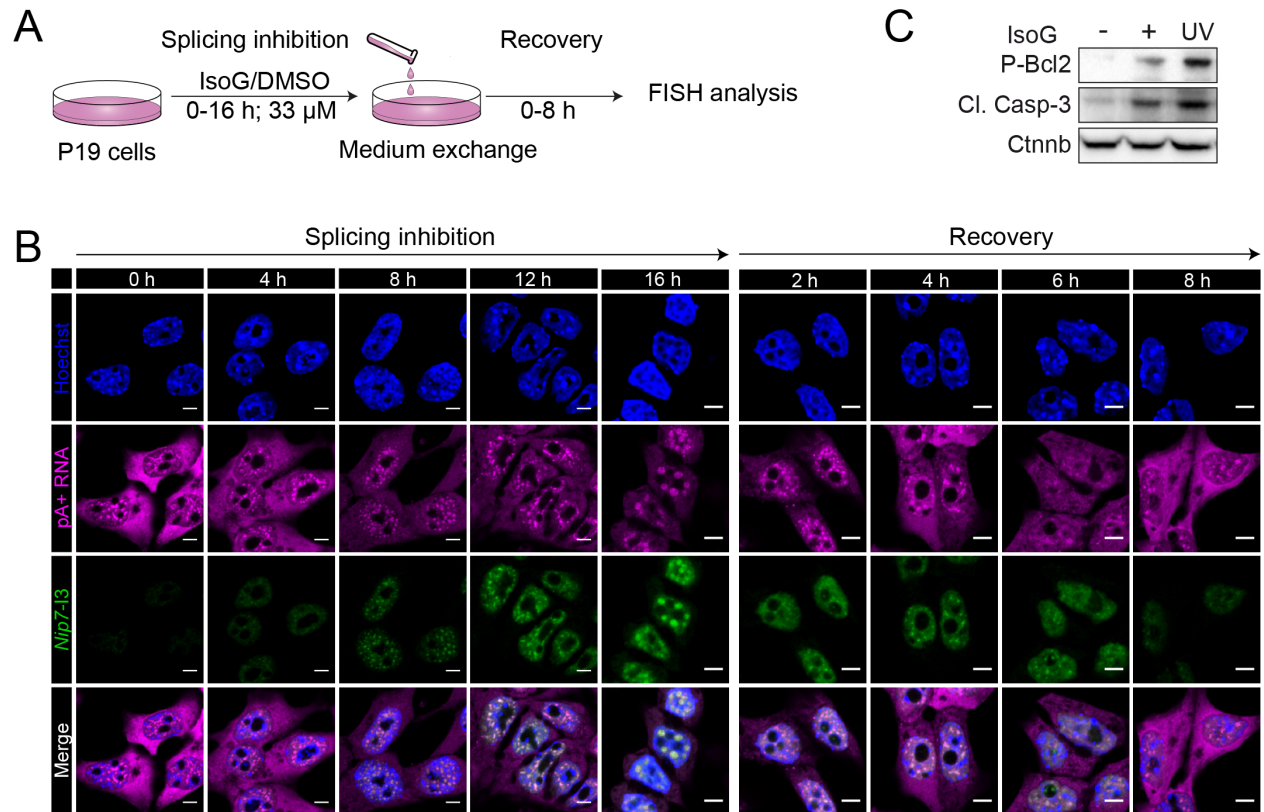


Figure 19: Formation of pA+ foci upon IsoG is reversible. A) Workflow of the splicing inhibition recovery experiment. B) FISH images of P19 cells showing *Nip7* intron 3 (green), pA+RNA (magenta), Hoechst staining (blue) and the merge of all channels. Cells were treated with IsoG (IsoG+) or DMSO (IsoG-) for 16 h and subsequently IsoG was removed to allow cell recovery for 8 h. Images were acquired at the indicated time points. (Scale bars = 5 μ m). C) Representative WB from IsoG+/- P19 cells (33 μ M; 16 h) and UV treated cells (60 mJ/cm² and subsequent incubation for 24h) probed with antibodies for the apoptosis markers: phosphorylated Bcl2 (P-Bcl2) and cleaved caspase 3 (Cl. Casp-3). Beta Catenin (Ctnnb) was used as loading control.

5.3. Nuclear pA+ foci are enlarged nuclear speckles that contain SRSF3

Previous studies have described that pA+RNAs are retained in enlarged nuclear speckles (ENS) after depletion of essential splicing factors or snRNAs (Dias et al., 2010; Tripathi et al., 2012; Hett & West, 2014; O'Keefe, 1994), or after addition of different splicing inhibitors (Kaida et al., 2007; Carvalho et al., 2017; Pawellek et al., 2017; Fan et al., 2018). Nuclear speckles (NS) are enriched in splicing factors and have been shown to serve as quality control hubs, where mRNAs transit prior to their nuclear export. Since we observed that intron-containing pA+RNAs are prevented from nuclear export upon IsoG addition and accumulate in large foci, we next investigated whether these foci correspond to ENS and whether export block occurs due to an impaired recruitment of the export factor Nxf1.

To test whether pA+ bodies correspond to ENS and contain Nxf1 we used a previously established P19 cell line that stably expresses Nxf1-GFP at physiological levels (Müller-McNicoll et al., 2016) and performed FISH (Figure 20) and immunofluorescence (IF) using an antibody for the nuclear speckle marker SC35 (Figure 20). Microscopic analysis revealed that the pA+RNA signal co-localize with the SC35 speckle pattern and Nxf1-GFP. However, Nxf1-GFP shows additional nucleoplasmic signal intensities. Upon splicing inhibition (IsoG+), SC35 and pA+RNA accumulate in polyA bodies and surround Nxf1. The presence of pA+RNA and SC35 in the pA+ bodies suggests that they have the same composition as NS and are therefore termed enlarged nuclear speckles (ENS).

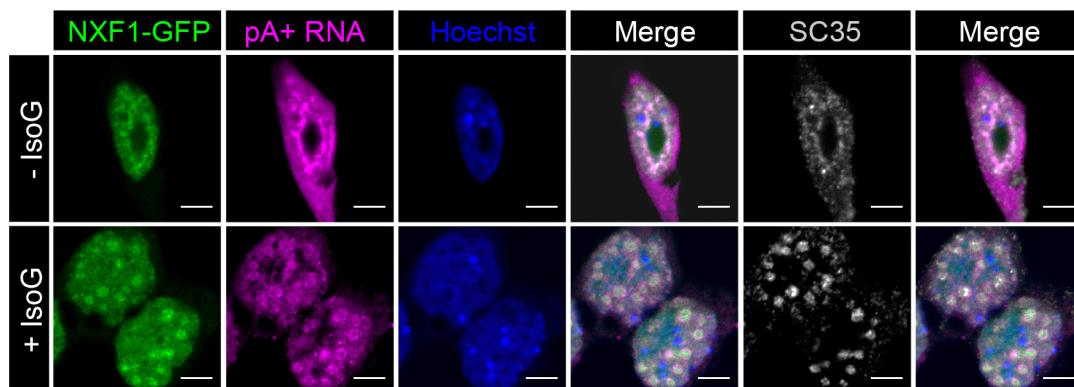


Figure 20 Nxf1 accumulates inside enlarged nuclear speckles. Representative FISH/IF images of P19 NXF1-GFP cells (green) hybridized/stained with the pA+ probes (magenta), SC35 speckle antibody (grey), Hoechst staining (blue) and the merge of all channels (white). Treatment with DMSO or IsoG (IsoG-, IsoG+) was performed using 33 μ M for 16 h. Scale bars = 5 μ m.

We next tested whether these ENS contain also SRSF3 using a P19 cell line that stably expresses SRSF3-GFP at endogenous levels (Müller-McNicoll et al., 2016). Similar to Nxf1, SRSF3 is surrounded by pA+RNA

bodies and SC35 signal upon IsoG treatment and display a donut-like shape with SRSF3 present in the core and pA+RNA/SC35 in the periphery (Figure 21A and B). Moreover, *Nip7-I3*, which is bound by SRSF3 under normal conditions (Figure 21E left panel), accumulates in the same pA+ core (Figure 21C). This ring spheroidal structure is characteristic for NS, wherein inactive splicing factors form a scaffold structure decorated by pA+RNA (Kim et al., 2018; Fei et al., 2017). Altogether, these data indicate that Nxf1 and SRSF3 accumulate in ENS together with polyadenylated intron-containing transcripts.

In addition to scaffolding proteins, NS are enriched in the long non-coding RNA (lncRNA) *Malat1*. *Malat1* is massively bound by splicing factors including SRSF3 (Figure 21E right panel), but under certain stress conditions it is excluded from NS to allow retention of mRNAs (Hochberg-Laufer et al., 2019). To test whether this is true for IsoG treatment we performed FISH experiments using *Malat1*-specific probes. We found that in the absence of the splicing inhibitor *Malat1* is localized in NS. However, upon splicing inhibition the characteristic *Malat1* speckle localization is lost and the lncRNA is excluded from ENS and shows a dispersed nucleoplasmic fluorescent signal pattern. This is in agreement with a recent study that reported the redistribution of *MALAT1* under replication stress where instead mRNAs accumulated in NS (Hochberg-Laufer et al., 2019). Our data suggest that upon IsoG treatment mRNAs are prevented from nuclear export and instead accumulate in ENS. Export block is not due to a spatial separation of export factors and export adapters from accumulating mRNAs. The change in *Malat1* distribution further suggests that mRNA sequestration in ENS requires the binding to splicing factor scaffolds, including SRSF3. Accumulating mRNA replaces *Malat1* from these scaffolds causing its release to the nucleoplasm.

To investigate whether ENS merged with other known nuclear bodies, we performed IF for the nuclear body markers Coilin (Cajal bodies), Fibrillarin (nucleolus), PSPC1 (paraspeckles) and SAM68 (heat stress bodies). Due to the lack of efficient mouse antibodies, IF experiments were performed in HeLa WT cells, in stable HeLa cell lines expressing PSPC1-GFP (paraspeckle marker) or SRSF2-GFP (NS marker) or in P19 SRSF3-GFP cells (Botti et al., 2017). HeLa cells were treated with the previously described IsoG conditions (100 μ M; 21 h) and ENS formation was monitored using the SC35 NS marker (O'Brien et al., 2008). Coilin-stained control cells show clearly the presence of 2-3 Cajal bodies per cell, while in IsoG treated cells Cajal bodies and Coilin signal disappeared (Figure 21F). This phenotype has been described in a previous study with the related splicing inhibitor hinokiflavone (Pawellek et al., 2017) and indicates that during splicing inhibition, Cajal bodies, which are the sites of snRNP assembly and maturation, are disassembled, most likely due to a high occupation of snRNAs on intron-containing pA+RNA.

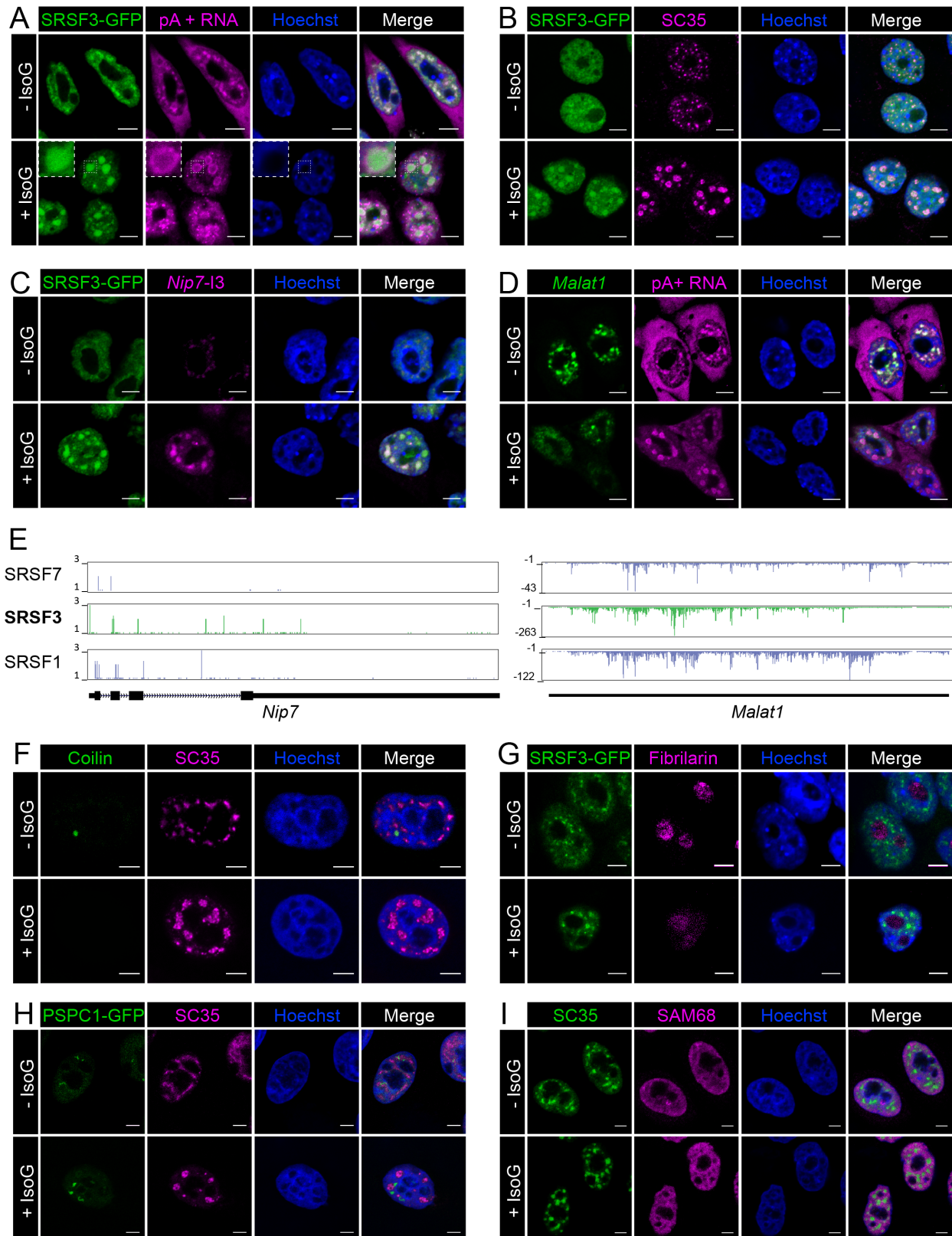


Figure 21: pA+RNA foci co-localize with SRSF3 in enlarged nuclear speckles. A-D; F-I) Representative FISH/IF images of P19 SRSF3-GFP cells (A, B, C and G), P19 WT cells (D), HeLa WT cells (F), HeLa PSCP1-GFP cells (H) and HeLa SRSF2-GFP cells (I), hybridized/stained with the indicated probes/antibodies. All panels show Hoechst nuclear staining (blue) and a merge of all channels. Treatment with DMSO or IsoG (IsoG-, IsoG+) was performed using 33 μ M for 16 h (P19 cells) or 100 μ M for 21 h (HeLa cells). Scale bars = 5 μ m. E) Browser shots showing the distribution of significant SRSF1,3 and7 X-links on *Nip7* and *MALAT1* genes. Browser shots acquired using previously published data from (Brugiolo et al., 2017).

Staining of Fibrillarin, a nucleolar marker, in P19 SRSF3-GFP cells showed that the formation of nucleoli is not affected by IsoG treatment and that ENS are not fused with nucleoli (Figure 21G). Paraspeckles localize in close proximity to NS under physiological conditions (-IsoG). Although the size and number of paraspeckles increases upon splicing inhibition, apparent from the fluorescence intensity of PSCP1-GFP, they surround ENS and are distinct from them (Figure 21H). Sam68 protein is a marker of nuclear stress bodies, but such bodies do not form upon IsoG treatment and SAM68 signal does not co-localize with ENS (Figure 21I). Taken together our results show that IsoG treatment stimulates the formation of enlarged nuclear speckles, which are distinct from other nuclear bodies, accumulate pA+RNA, intron-containing transcripts, SRSF3 and Nxf1, but exclude *Malat1*.

5.4. SRSF3 interactome upon splicing inhibition reveals a decrease in export adaptors and surveillance factors

Previous studies have shown that SRSF3 acts as a potent export adaptor: It interacts with the nuclear export factor Nxf1 and stimulates the nuclear export of multiple mRNAs (Huang & Steitz, 2005; Müller-McNicoll, 2016). Our data showed that during splicing inhibition by IsoG, SRSF3 and Nxf1 both accumulate in ENS together with intron-containing pA+RNAs that are prevented from nuclear export. We next asked whether the export block might be due to an impaired interaction of SRSF3 with nuclear export adaptors. To identify changes in the splicing-dependent SRSF3 interactome comprehensively, we used quantitative mass spectrometry (in collaboration with Christian Münch). We treated P19 cells expressing SRSF3-GFP for 16 h with 33 μ M IsoG or DMSO (control). SRSF3-GFP was purified by stringent immunoprecipitation using an anti-GFP antibody coupled to magnetic beads (Figure 22A). SRSF3-GFP co-bound interactors were subsequently identified by quantitative mass spectrometry, normalized to a control cell line expressing GFP fused to a nuclear localization signal (GFP-NLS) and compared between IsoG-treated and control cells.

To validate our mass spectrometry analysis, we compared the SRSF3 interactome (SRSF3/NLS; -IsoG) with previously described protein-protein interactors using the STRING database (<https://string-db.org/>) (Figure 22B). We identified every previously described interactor of SRSF3 including multiple hnRNPs, Uap56 and SR proteins (Figure 22C). In addition, we identified novel interactors, e.g. splicing factors of the U2af (U2af1, U2af2), Sf3b (Sf3b1, Sf3b3, Sf3b6) and EJC (Rbm8a, Eif4a3, Magoh) complexes as well as spliceosome core components (Snrpf, Rbm22) (Section 9 Table 22). Interestingly, IsoG treatment led to a drastic decrease in the interaction of SRSF3 with multiple export factors/adaptors. Among these export adaptors were subunits of the Thoc complex (Thoc1, 2, 3, 5, 7), the Uap56-interaction factor UIF, the selective mRNA export adaptors Bclaf1 and Thrap3 and the nuclear export factor Nxf1 (Figure 22C and section 9 Table 23). In agreement with this, gene ontology (GO) analysis of SRSF3 interactors that significantly decreased upon splicing inhibition confirmed an enrichment of the biological processes 'mRNA processing', 'mRNA transport' and 'nuclear mRNA export' (Figure 22F).

In addition, we identified proteins whose SRSF3 interaction increased upon splicing inhibition, such as the U2snRNP subunits Sf3b4 and U2af1, as well as the small ubiquitin-related modifier Sumo3 (Figure 22E and Table 23). Interestingly, recent studies showed that these post-translational modifiers are covalently attached to splicing factors including SR proteins (Pawellek, 2018), and prevent spliceosomal assembly (Pozzi et al 2017). Sumoylation was shown to be induced upon treatment with the splicing inhibitor Hinokiflavone and led to impaired spliceosome assembly and cell cycle deficiencies (Pawellek et al., 2017).

Among the SRSF3 interactors that decreased upon IsoG we also identified the Zinc finger protein 14 (Zc3h14) (Figure 22E). Its yeast orthologue, Nab2, has been extensively studied and is a key RNA surveillance factor in *Saccharomyces cerevisiae* (Tudek et al., 2018). It acts at the interface between Nxf1-facilitated mRNA export (*Mex68* in yeast) and nuclear decay by Rrp6 and thereby balances cellular transcript supply (Tudek et al., 2018). Despite these essential functions of Nab2 in *S. cerevisiae*, it is not known whether Zc3h14 fulfils surveillance and export functions in higher eukaryotes. Therefore, we focused on this protein and investigated its potential role in the control of nuclear splicing surveillance in conjunction with SRSF3. To validate its interaction with SRSF3, we performed co-immunoprecipitations (co-IPs) with P19 SRSF3-GFP cells lines treated with IsoG and DMSO (Figure 22G). In control cells we successfully co-purified Nxf1 and Zc3h14, however, in IsoG treated cells the interactions dropped by nearly 80% for Zc3h14 and by 30% for Nxf1 (Figure 22H). The interactions are RNA-independent since RNaseA treatment had only little effect on the interactions of SRSF3 with Nxf1 and Zc3h14, but efficiently impaired its interaction with the polyA binding protein Pabpn1 (Figure 22H).

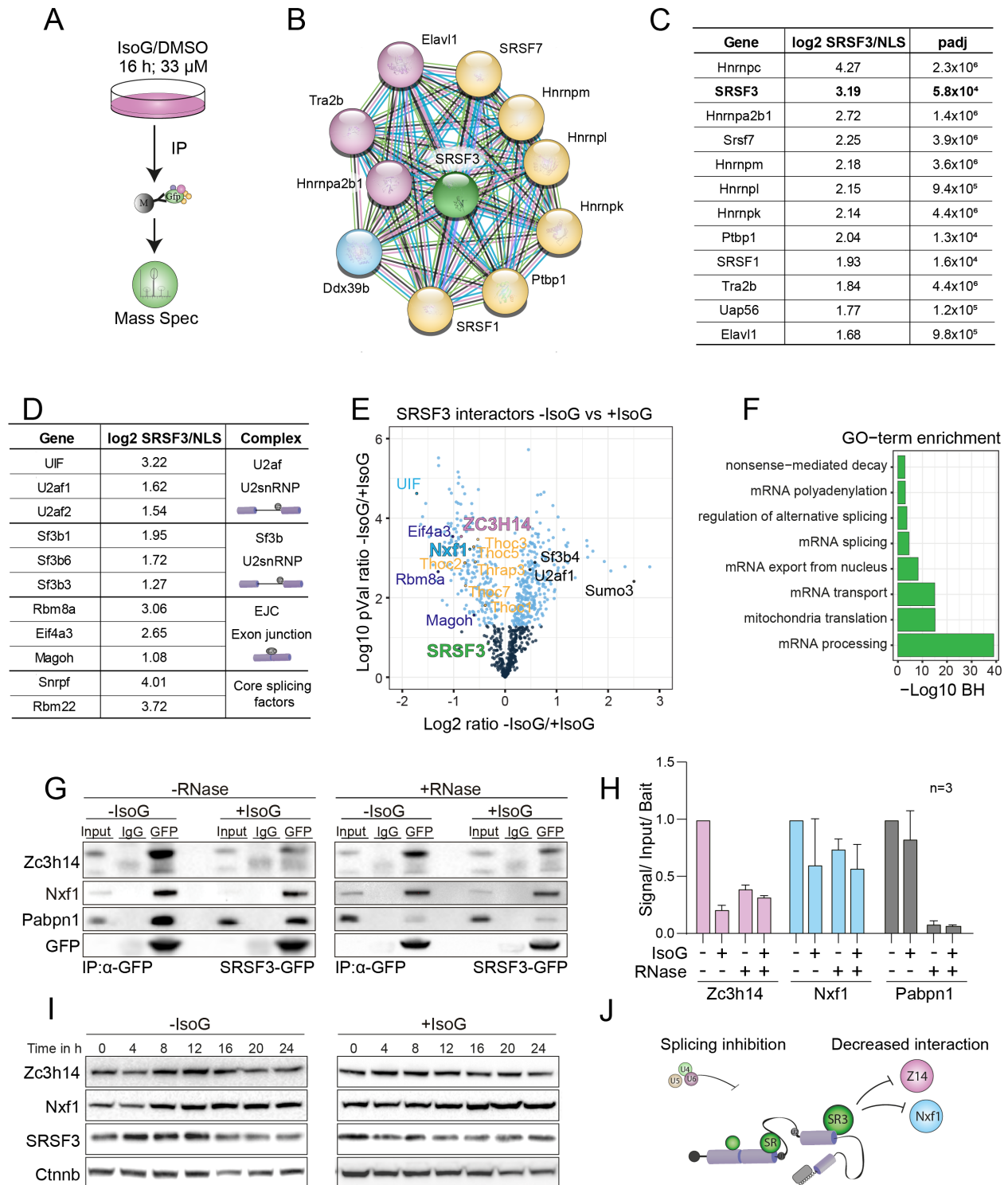


Figure 22: SRSF3 interaction with export factors is IsoG sensitive. A) Workflow of the SRSF3 purification assay for mass spectrometry analysis. B) Illustration of the SRSF3 interactome network, acquired using STRING. C) Table listing significantly co-purified SRSF3 protein interactors identified by mass spectrometry. D) The log₂ fold changes SRSF3/NLS show the enrichment of the co-purified proteins by SRSF3 pull down normalized to a control cell line expressing GFP fused to a nuclear localization signal (GFP NLS). E) Volcano plot showing changes in SRSF3 protein

interactors upon IsoG treatment relative to DMSO control cells (n = 3 replicates per condition). Proteins that significantly changed are shown in blue. Top interactors with highest gain/loss in SRSF3 interaction are indicated with the protein names. F) GO-term analysis of biological processes (BP) for proteins that significantly decreased in interaction with SRSF3 upon IsoG treatment (padj<0.05) using DAVID. BH = Benjamini-Hochberg corrected P-value. G) Co-IP of purified SRSF3-GFP with or without RNaseA treatment upon IsoG treatment (IsoG+) or DMSO control (IsoG-) (33 μ M for 16 h). WBs were probed with α -Nxf1, α -Zc3h14 and α -GFP to confirm SRSF3-GFP purification. Pabpn1 was used to control for successful RNase treatment. IgG = unspecific antibody control. H) Quantification of three Co-IP experiments with and without RNase A treatment, in the presence of IsoG or DMSO control (IsoG-). Protein signals were normalized to baits and inputs. I) Representative WB from a 24 h time course experiment with IsoG treated/untreated P19 WT cells probed with antibodies against Nxf1, Zc3h14 and SRSF3. Beta catenin (CtnnB) was used as loading control. J) Scheme of interaction loss of SRSF3 with Zc3h14 and Nxf1 upon splicing inhibition.

To exclude that the IsoG-dependent decrease in SRSF3 interactions is due to a decrease in protein levels of the interactors, we performed an IsoG time course experiment and monitored the expression levels of Zc3h14, Nxf1 and SRSF3 (Figure 22I). No major changes in their expression level during IsoG treatment were detected, excluding the possibility that the loss of interaction is due to lower protein levels. Taken together our results show that the SRSF3 interactome is highly sensitive to the splicing inhibitor IsoG. Especially SRSF3 interactors involved in nuclear mRNA export are decreased upon splicing inhibition. This suggests that SRSF3 may control the export competency of mRNPs *via* interaction with different export adaptors or surveillance factors. Upon splicing inhibition SRSF3-containing RNPs are prevented from export, e.g. through a decreased interaction with Zc3h14 and Nxf1 (Figure 22J).

5.5. Zc3h14 is a novel Nxf1 export adaptor

We next investigated whether Zc3h14 acts as an export adaptor or surveillance factor in P19 cells. For this, we generated P19 cell lines stably expressing Zc3h14 fused to a GFP-tag. We integrated the entire Zc3h14 gene including the N-terminal PWI-protein interaction platform and the C-terminal tandem Zinc-finger domain fused to a GFP at its C-terminus using bacterial artificial chromosomes (BACs) (Figure 23A/B). BACs contain not only coding sequences but also endogenous non-coding regulatory sequences, including promoters, UTRs and introns. Therefore, Zc3h14-GFP is expressed at physiological levels and three distinct isoforms are generated *via* alternative splicing (Figure 22A). Expression of Zc3h14-, Nxf1- and SRSF3-GFP was validated by WB for each cell line using antibodies that detected both, endogenous and GFP-tagged proteins (Figure 23C). Correct subcellular localization of SRSF3, Zc3h14 and Nxf1 was confirmed by confocal microscopy. We found that Zc3h14-GFP co-localizes with SC35 in NS, while Nxf1-

GFP was rather diffusely distributed in the nucleoplasm, in agreement with previous studies (Herold et al., 2000a; Irwin et al., 2005; Leung et al., 2009)(Figure 23D). To examine whether Zc3h14 affects nuclear export of mRNAs, we first tested the impact of Zc3h14 overexpression on the subcellular distribution of pA+RNA by RNA FISH. For this we selected a clone with high Zc3h14-GFP expression (Figure 24A). Interestingly, overexpression (Oex) of Zc3h14 led to a decrease of endogenous Zc3h14 levels. The presence of an additional band of lower molecular weight suggests that Zc3h14 might autoregulates its protein levels by expressing a potentially non-functional isoform, but this remain to be tested. Despite the reduction of endogenous protein, quantification of all Zc3h14 isoforms revealed a 2.1-fold overexpression for Zc3h14. Overexpressing clones for Nxf1 (1.7-fold) and SRSF3 (1.4-fold) were used as controls (Figure 24A).

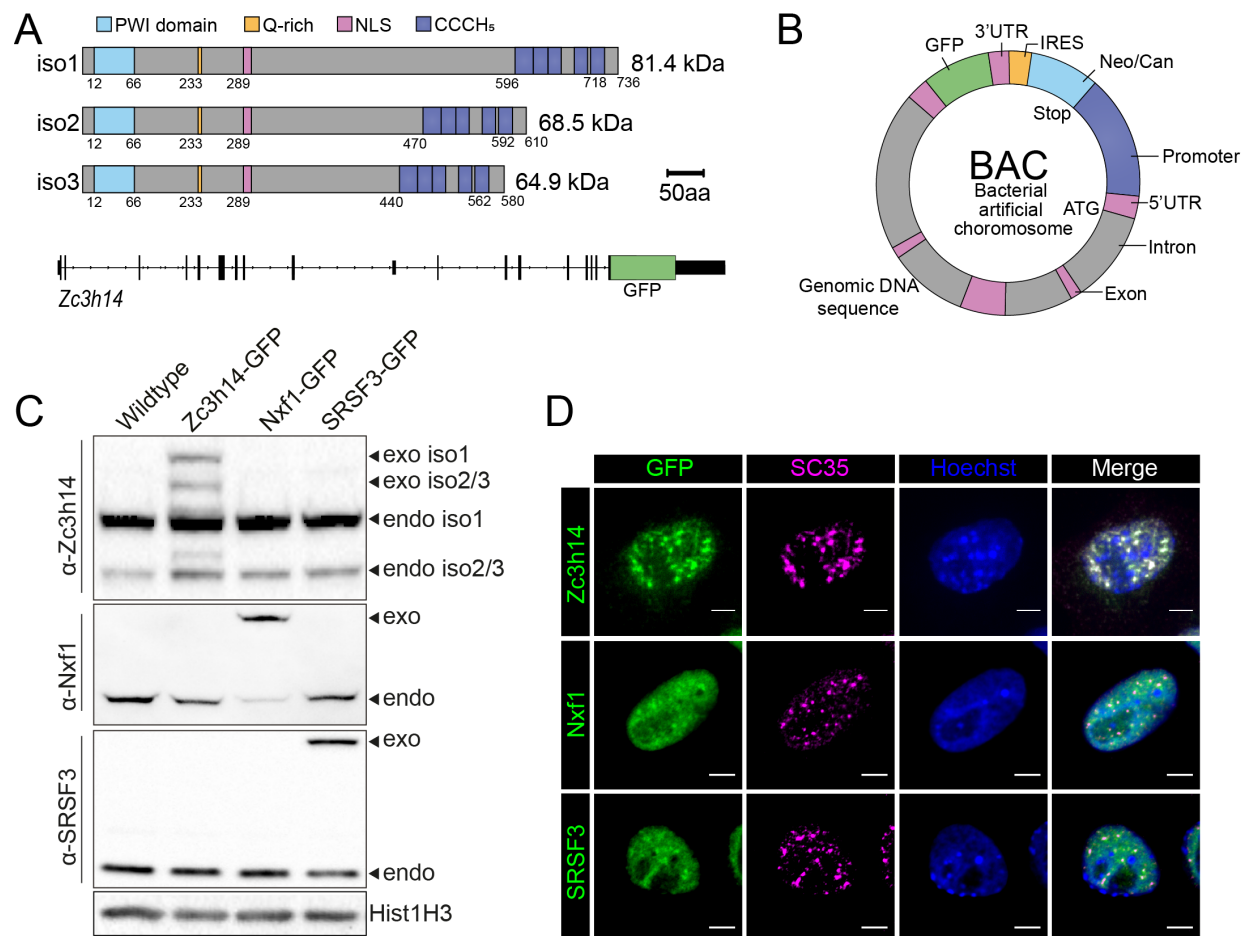


Figure 23: Characterization of stable cell lines expressing GFP-tagged proteins. A Representative scheme of Zc3h14 protein isoforms with the described protein domains. Square sizes represent the number of amino acids in the protein regions (scale = 50 amino acids). Below, the Zc3h14 gene with a C-terminal GFP-tag (green) is shown (exons are black boxes and introns are black lines). B) Scheme of the BAC that was stably integrated into P19 WT cells. The pink boxes represent exons and the grey boxes introns of the Zc3h14 gene. A GFP-tag is inserted before the STOP

codon (green). The BAC contains additionally an internal ribosome entry site (IRES), which allows translation of a Neomycin resistance gene used for selection. C) Validation of Zc3h14, Nxf1 and SRSF3-GFP tagged P19 cell lines. WBs were probed with specific antibodies against Zc3h14, Nxf1 and SRSF3 to visualize endogenous and exogenous protein levels. WT P19 cell line served as control. D) Panel of representative IF images of Zc3h14-, Nxf1- and SRSF3-GFP expressing P19 cell lines. The GFP channel is shown in green, the SC35 speckle marker in magenta and Hoechst DNA staining in blue. For each cell line all channels were merged. Scale bars = 5 μ m.

We performed FISH experiments using oligodT probes (Figure 24B) and quantified the pA+RNA fluorescence signal intensities of 100 nuclei (n=3) and determined the nuclear area using Hoechst staining (Figure 24C). We did not detect significant changes in the distribution of cytoplasmic and nuclear pA+RNA signal intensities in any of the cell lines compared to the WT control. This suggests that the extent of Oex was either not sufficient, or Oex of a single export adaptor is not sufficient to stimulate overall export activity since nuclear mRNA export involves the interplay of multiple factors. Unfortunately, we did not detect significant changes in nuclear pA+RNA signal intensities compared to the WT control in any of the cell lines. This suggests that the extent of overexpression was either not sufficient, or overexpression of a single export factor might not be sufficient to stimulate the overall export activity as nuclear mRNA export involves the interplay of multiple factors.

On the other hand, depletion of export adaptors should impair mRNA export, at least partially, leading to the nuclear retention of pA+RNAs. To test this, we performed RNA FISH experiments in P19 WT cells after knock down (KD) of Zc3h14 (70% KD), Nxf1 (80% KD) and SRSF3 (60% KD) (Figure 24D). Quantification of the nuclear pA+RNA signal of 100 nuclei (n=2) revealed a mild but significant increase of pA+RNA by 27% upon Zc3h14 depletion (Figure 24E). Interestingly, pA+RNA accumulates at the nuclear rim, an export deficiency phenotype that is also observed in Nxf1 depleted cells, albeit to a higher extent (Figure 24E). In contrast, SRSF3 depletion led to pA+RNA accumulation in NS, which is agreement with previous studies (Fei et al., 2017; Escudero-Paunetto et al., 2010). Taken together our data reveal that Zc3h14 depletion leads to an increase in the levels of pA+RNAs, which suggests that Zc3h14 either promotes the nuclear export or nuclear stability of a subset of transcripts in higher eukaryotes. One characteristic of export factors is their ability to shuttle between the nucleus and the cytoplasm. Many export and processing factors, such as SRSF3 and Nxf1 associate with mRNAs in the nucleus and remain bound to the mRNA during nuclear export and enter the cytoplasm together with the mRNP prior to its dissociation (Katahira et al., 1999; Katahira et al., 2009; Zhou et al., 2000; Rodrigues et al., 2001; Müller-McNicoll et al., 2016). To determine the shuttling capacity of Zc3h14, we used our previously developed quantitative shuttling assay, which is based on interspecies heterokaryons (McNicoll & Müller-McNicoll, 2018; Botti et al., 2017).

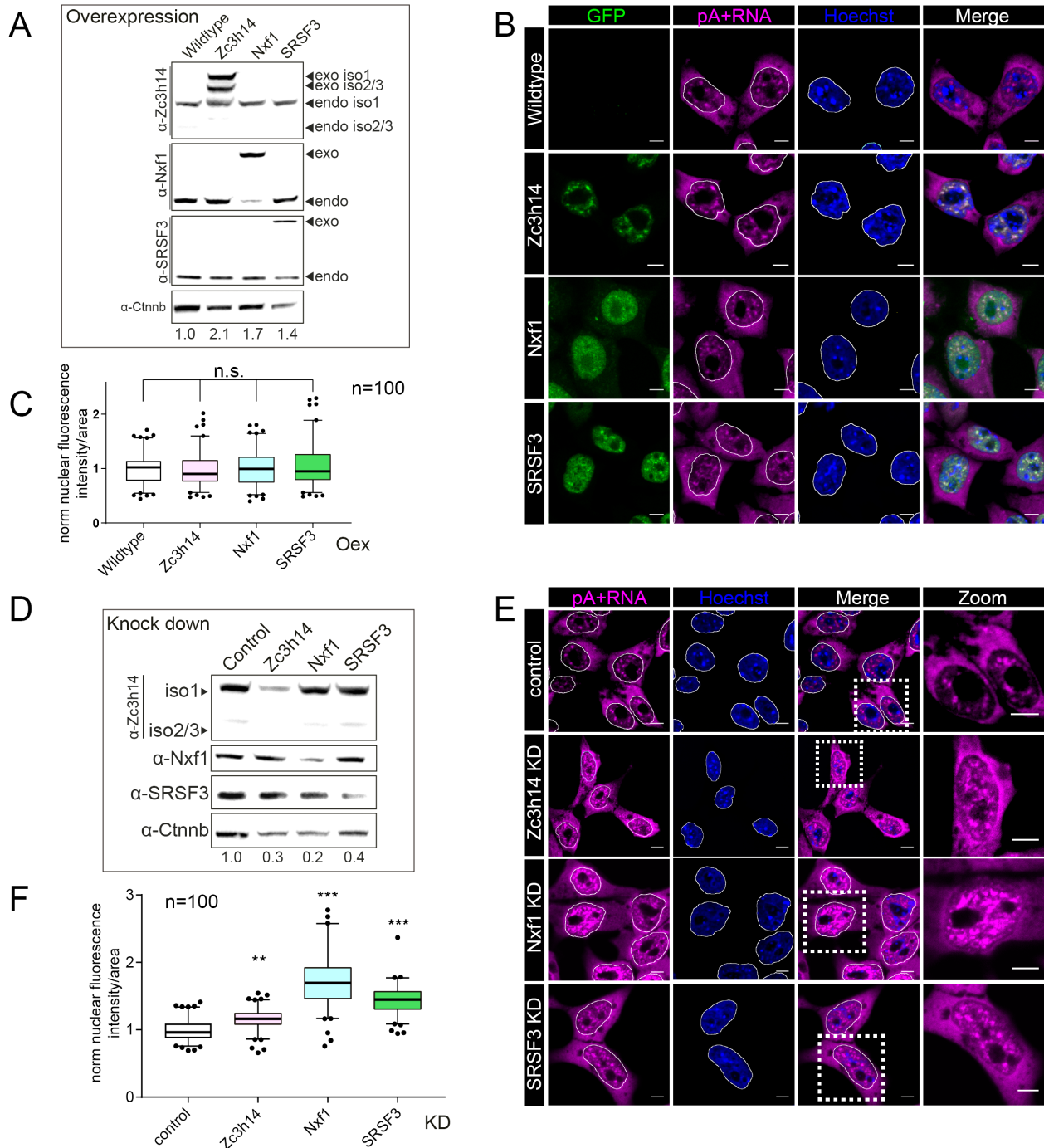


Figure 24: Zc3h14 depletion leads to nuclear accumulation of pA+RNA. A) Validation of Zc3h14-, Nxf1- and SRSF3-GFP overexpression in P19 cells. Antibodies against Zc3h14, Nxf1 and SRSF3 were used to visualize endogenous and exogenous protein levels (black arrow heads). Beta catenin was used as loading control (Ctnnb). Endogenous + exogenous protein level were quantified. Total overexpression (Oex) levels relative to WT cells are indicated below. B) Representative RNA-FISH images of WT, Zc3h14-GFP, Nxf1-GFP and SRSF3-GFP Oex cell lines hybridized with OligodT probes for pA+RNA visualization (pA+RNA, magenta). GFP signals are shown in green, Hoechst staining in blue. C) Mean nuclear pA+RNA fluorescence intensity values of WT, Zc3h14-GFP, Nxf1-GFP and SRSF3-GFP Oex cell lines (n = 100 cells). Differences in nuclear fluorescence intensities were calculated for every cell line relative to the WT and tested for significance using a 2-sided -Fisher's least significant difference- t-test (ns = non-significant). Scale

bars = 5 μm . D) Validation of Zc3h14, Nxf1 and SRSF3 KD efficiency in P19 cell lines using specific antibodies (indicated at the right side). E) Representative images of pA+RNA FISH in control and KD cells. Panel displays pA+RNA (magenta), Hoechst nuclei staining (blue), the merge of both channels and a representative cell zoom (indicated on the merge image by a white square). F) Mean nuclear pA+RNA fluorescence intensity values of Zc3H14, NXF1, SRSF3 KD and control cells ($n = 100$ cells). Differences of nuclei fluorescence intensities were calculated for KD relative to the control cells using a 2-sided -Fisher's least significant difference- t-test (** $p < 0.01$; *** $p < 0.001$). Scale bars = 5 μm .

In this assay a donor cell (P19) expressing a GFP-tagged protein and a recipient cell (HeLa), expressing a membrane marker labeled with an alternative fluorophore (CAAX-mCherry) is fused (McNicoll & Müller-McNicoll, 2018) (Figure 25A). While the membrane marker serves as an indicator for complete cell fusions, the shuttling capacities of the GFP-tagged protein are determined by GFP signal measurements in the recipient nucleus. Given that the recipient cell does not express any GFP, the quantified GFP signal directly correlates with the shuttling capacity of the protein (Figure 25A).

In addition to SRSF3 and Nxf1, which are high shuttling proteins (Botti et al., 2017), we included the pre-mRNA splicing factor 8 (Prp8) in our analysis as negative control, since it had been classified as a non-shuttling protein (Botti et al., 2017; Sapra et al., 2009). Performing quantitative shuttling assays with P19 cells expressing Zc3h14-GFP, we detected high GFP fluorescence intensities in the recipient HeLa nuclei (Figure 25B). This indicated that Zc3h14 shuttles between the nucleus and the cytoplasm. Quantification of 15 heterokaryons confirmed that Zc3h14 shuttling capacities were similar to those of the high shuttling Nxf1 and higher than SRSF3, while Prp8 shuttling was not detectable (Figure 25C). This indicates a high mobility across the nuclear membrane and supports a potential activity of Zc3h14 in nuclear mRNA export.

Since Zc3h14 dissociates from SRSF3-containing mRNPs upon IsoG treatment, we next tested whether the Zc3h14 shuttling capacity is also sensitive to IsoG. Our previous FISH analysis showed, that long incubation times of IsoG treatments (16 h; 33 μM) reduces general cellular dynamics. Thus, we first determined conditions which lead to the initiation of nuclear retention. Therefore, we performed a time course experiment with early timepoints (4 – 8 h) and determined the pA+RNA signal of the nuclear and cytoplasmic compartment, using the Hoechst staining to identify the nuclear region and discriminate both compartments (Figure 26A/B).

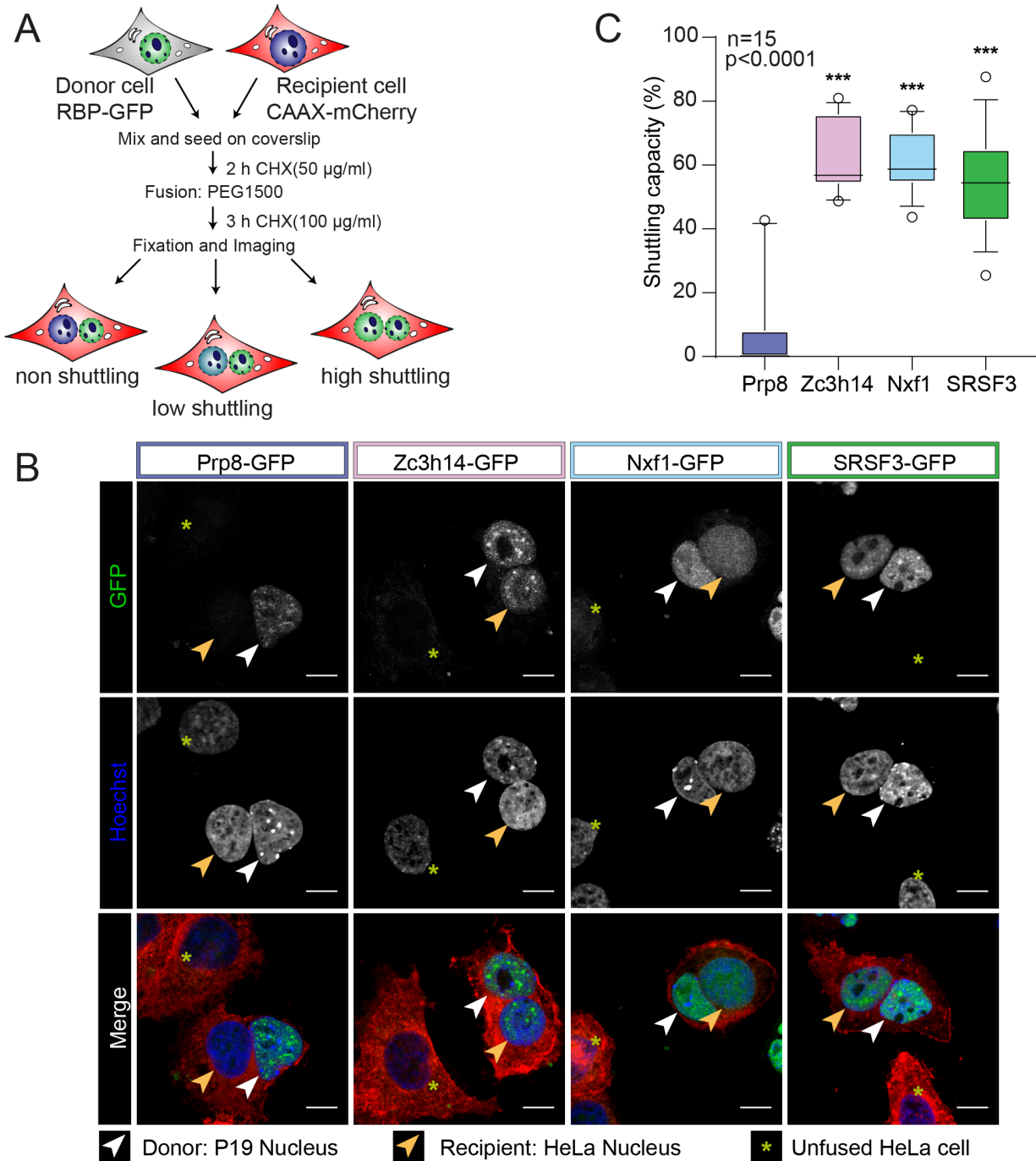


Figure 25: Zc3h14 shuttles between the nucleus and the cytoplasm. A) Workflow of the quantitative shuttling assays. Zc3h14-GFP, Nxf1-GFP and SRSF3-GFP P19 cells were used as donors, HeLa cells stably expressing CAAX-mCherry tethered to their cell membranes were used as recipient cells. A PRP8-GFP P19 cell line was used as non-shuttling control donor cells. B) Representative images of HeLa-P19 heterokaryons and unfused cells for each cell line. GFP and Hoechst staining are shown in gray. Merge of all channels display heterokaryons and unfused cells. CAAX is shown in red, GFP in green and Hoechst nuclear staining in blue. Scale bars = 5 µm. C) Mean shuttling capacity of each protein was calculated by dividing the GFP signal of the HeLa cell nuclei (receptor) after background subtraction by the total GFP signal (donor + recipient). Differences in shuttling capacities were calculated for each protein relative to the PRP8 non-shuttling control and tested for significance using Wilcoxon rank sum test (n = 15 cells per cell line, ***p<0.0001).

We detected decreased cytoplasmic and increased nuclear pA+ fluorescence signal intensities already at 4-6 h after IsoG addition, hence we used 6 hours IsoG treatment to determine changes in shuttling capacities upon splicing inhibition (Figure 26B). Using this splicing inhibitory conditions, IsoG treatment indeed reduced the shuttling capacities of Zc3h14 (Figure 26C). Quantification of 15 heterokaryons in both conditions confirmed that Zc3h14 shuttling capacity was significantly reduced by 28.5% (Figure 26D). Surprisingly, 6 hours IsoG treatment did not affect the shuttling capacities of Nxf1 and SRSF3 (Figure 26D). This suggests that either Zc3h14 targets are more sensitive to splicing inhibition by IsoG, or that Zc3h14 shuttling inhibition is one of the earliest events in export inhibition.

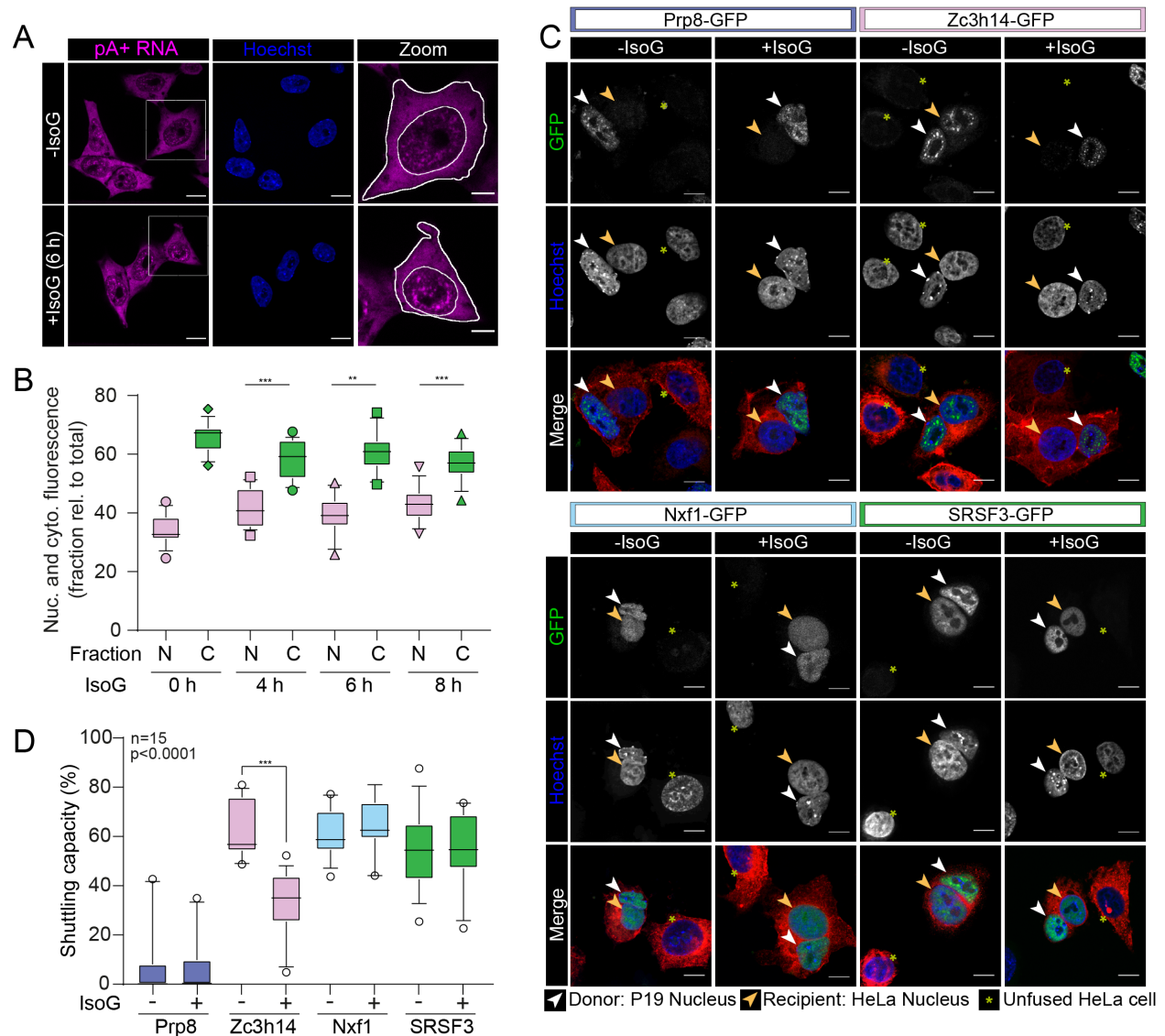


Figure 26: Zc3h14 shuttling capacity is highly splicing sensitive. A) Representative FISH images of P19 cells treated with IsoG/DMSO for 6 h with pA+RNA (magenta), Hoechst DNA staining (blue) and a representative cell zoom with measured cytoplasmic signal (total – nuclei signal). The representative cell is highlighted in the pA+RNA image with a white square. B) Average pA+RNA fluorescence signal in nuclear (nucleus/total) and cytoplasmic fraction (total –

nuclei/total) signal measurements. A t-test was performed to test for significant differences between nuclei fraction signal in DMSO control and IsoG treated cells ($n = 15$ cells, $**p < 0.01$) in different time points, indicated underneath the graph. C) Panel of representative HeLa-P19 heterokaryons and unfused HeLa cells. Shuttling assays were performed with Zc3h14-GFP, Nxf1-GFP and SRSF3-GFP P19 cells as donors and HeLa CAAX-mCherry cells as recipient. Cells were treated for 6 h with IsoG or DMSO as control before fusion. A PRP8-GFP expressing P19 cell line was used as a non-shuttling control donor cell. D) The mean shuttling capacity was determined for each GFP-tagged protein in both conditions ($n = 15$ cells per cell line per condition). Differences were calculated relative to the DMSO control and tested for significance by Wilcoxon rank sum test, $***p < 0.0001$).

Taken together we found that Zc3h14 shuttles robustly between the nucleus and the cytoplasm, which is a common characteristic of export adaptors such as SRSF3. Interestingly, Zc3h14 shuttling capacity is highly sensitive to splicing inhibition. This suggests that the nuclear retention of pA+RNA upon IsoG might be caused by the reduced shuttling capacity of Zc3h14. Both, Zc3h14 shuttling and its high sensitivity to cellular stresses are reminiscent of Nab2 activities in *S. cerevisiae*.

5.6. Global identification of Zc3h14 targets reveals its involvement in cell cycle regulation

Although Nab2-mediated export has been extensively studied (Green et al., 2002; Chekanova et al., 2001), it is unknown whether its ortholog Zc3h14 is involved in mRNA export in higher eukaryotes. Our data so far suggest that Zc3h14 might act as export adaptor, as it shuttles robustly between nucleus and cytoplasm and its depletion led to the partial nuclear accumulation of pA+RNAs. However, the effect of Zc3h14 depletion was lower compared to depletion of SRSF3 and Nxf1. This suggests that Zc3h14 promote nuclear export of only a subset of mRNAs.

To identify Zc3h14 targets, we depleted Zc3h14 in P19 cells for 48 h achieving KD efficiencies of 70% (Figure 27A). We performed RNA-seq of KD and control samples (Ctrl) in two biological replicates. To avoid a potential normalization bias in case that many transcripts were affected by Zc3h14 depletion, we used ERCC spike-ins as normalization controls (Lee et al., 2016; Lun et al., 2017). 20 ng ERCC spike-ins were added to 2 μ g of total RNA of each sample before RNA-seq library preparation. Both replicates were highly similar and were used for differential gene expression analyses using DESeq2 (Figure 27B). After ERCC normalization we found a huge number (7750; $FDR < 0.05$) of differentially expressed genes (DEGs) upon Zc3h14 depletion. Strikingly, almost all DEGs were down-regulated (Figure 27C and section 9 Table 24).

Among the most down-regulated genes was *Zc3h14* itself, with a log₂-fold change of -2.8, validating the KD efficiency and the bioinformatic analysis (Figure 27C). Interestingly, depletion of Nxf1 and Uap56 also led to a global decrease in transcript abundance. This was proposed to be due to the different half-lives and amounts of transcripts in the cytoplasm and nucleus (Herold et al., 2003).

We next investigated, whether *Zc3h14* targets and Nxf1 export targets overlap. Therefore, we used a fractionated RNA-seq data set upon Nxf1 depletion in P19 cells (unpublished data) and compared the sum of down-regulated genes in the cytoplasmic fraction with *Zc3h14* targets from total RNA. Interestingly, *Zc3h14* and Nxf1 targets overlap to 42% (4333) suggesting that *Zc3h14* and Nxf1 share a large number of export targets.

To further characterize *Zc3h14* regulated transcripts, we performed GO term analyses and found that down-regulated transcripts were highly enriched for the biological processes ‘cellular stress’ (DNA repair, proteasomal protein catalysis), ‘nuclear mRNA lifecycle’ (histone modification, mRNA processing, RNP biogenesis) and ‘cell cycle regulation’ (regulation of mitotic cycle, cell projection assembly, DNA, metabolic process regulation, negative regulation of cell cycle) (Figure 27E). Interrogation of the DESeq2 data confirmed that transcripts, coding for essential cell cycle regulators, such as the structural maintenance of chromosomes 4 (*Smc4*), centrosomal protein 192 (*Cep192*) and cyclins are among the most down-regulated genes (Figure 27F).

These results suggest that *Zc3h14* might regulate the expression/or nuclear export of factors involved in cell cycle regulation of P19 cells. To test the effect of *Zc3h14* of the cell cycle, we performed proliferation assays in P19 cells upon *Zc3h14* KD and Oex. *Zc3h14* was depleted for 36 h and subsequently the cells were counted, seeded and cultivated for another 60 h in the presence of *Zc3h14* siRNAs. KD efficiencies were determined at 48 h and 96 h, and they remained constant at 70% (Figure 28A). Cells were counted every 12 hours and the numbers plotted as a growth curve (Figure 28B). This revealed that *Zc3h14* depleted cells exhibited slower growth rates compared to control cells. Using the least square exponential growth fitting model (Mathusian), we determined the doubling time and found, that cells transfected with control siRNAs had a doubling time of 11.4 h, while *Zc3h14* KD cells had doubling times of 13 h (Figure 28B), suggesting that *Zc3h14* promotes growth or cell cycle progression

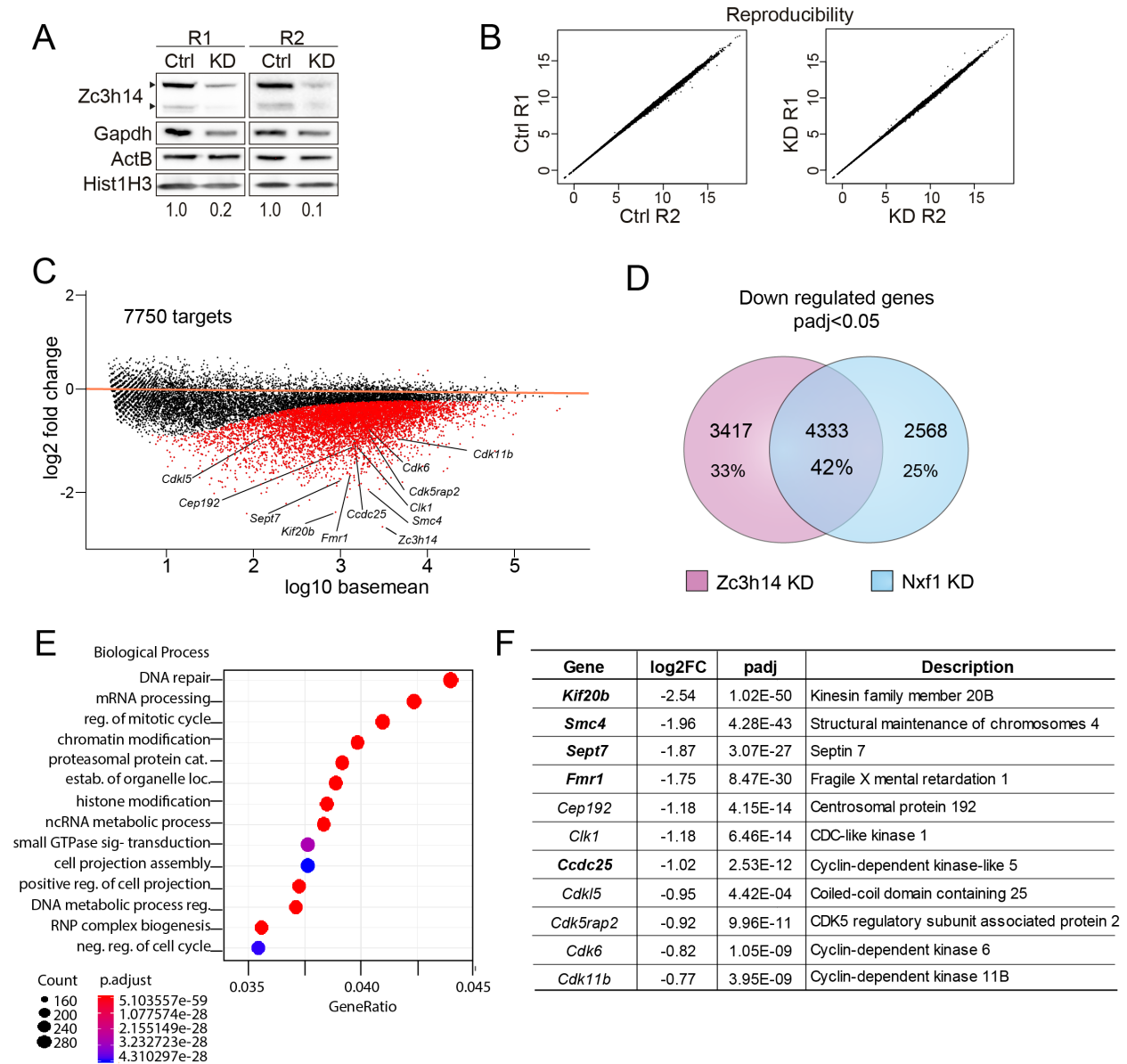


Figure 27 Global identification of Zc3h14 targets suggests an involvement in cell cycle regulation. A) Validation of Zc3h14 KD in P19 cells by WB. P19 cells were transfected with siRNAs against *Luciferase* (Ctrl) and *Zc3h14* (KD). WBs were probed with an antibody against Zc3h14 (two isoforms indicated by black arrows). Antibodies against Gapdh, Histone1H3 (H3) and Actin were used as loading controls. R1-2 = replicate 1 and 2. Total Zc3h14 protein levels were quantified for KD samples relative to the Ctrl (values are indicated below the blot). B) Scatter plot of RLog-transformed read counts demonstrate a high replicate correlation and reproducibility for control and KD samples. C) MA plot showing log₂-fold change differences for all annotated genes upon Zc3h14 KD. Genes, which were significantly up- or down-regulated are shown in red (adjusted p-value < 0.05). Genes of interest listed in F are highlighted in the plot. D) Venn diagram displaying the overlap of genes whose expression was down-regulated upon Zc3h14 KD and upon Nxf1 KD (unpublished data). E) GO-term analysis of biological processes (BP) performed on significantly down-regulated genes (P-value < 0.05) using GOEnrich. E) Table showing eleven significantly down-regulated genes quantified with DESeq2. Log₂-fold change relative to the control (log₂FC), adjusted P-value (padj) and gene name (description) are listed. Transcripts selected for validation are shown in bold.

To test whether Zc3h14 promotes cell cycle progression we performed the same proliferation assays with P19 WT and Zc3h14-GFP Oex cells. WB confirmed a 2-fold Oex of Zc3h14 relative to WT cells (Figure 28C). Growth curve analysis of WT cells revealed a doubling time of 10.4 h, which is comparable to previously reported doubling times of pluripotent P19 cells (Mummery et al., 1986). Strikingly, cells expressing 2-fold higher levels of Zc3h14 protein showed an increase in their proliferation rates and exhibited lower doubling times of 8.9 h (Figure 28D). This indicates that KD and Oex of Zc3h14, both affect cell growth or cell cycle length, but in opposite directions. In summary, Zc3h14 affects the expression of many cell cycle regulators at the mRNA level, and cellular growth rates correlate with Zc3h14 expression levels, suggesting a potential role of Zc3h14 in the cell cycle regulation in pluripotent P19 cells.

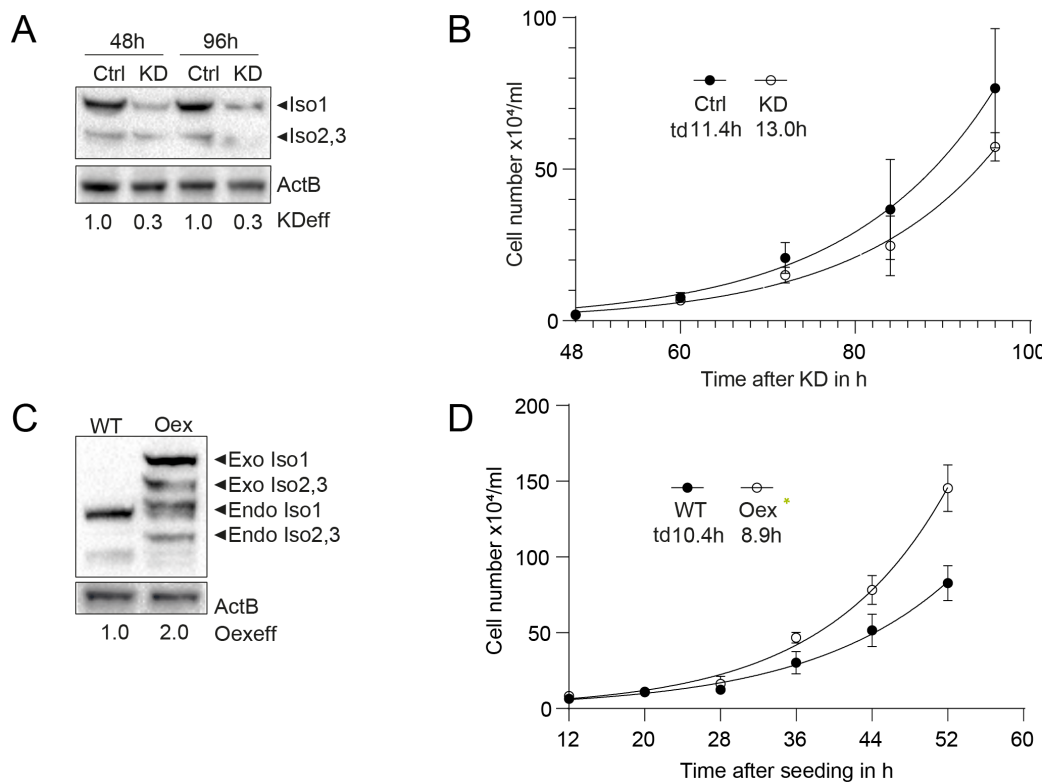


Figure 28: Zc3h14 levels affect the growth rate of pluripotent P19 cells. A) WB probed with an antibody against Zc3h14 (three isoforms indicated by black arrows) for validation of KD efficiencies (KDeff; values shown below the blot). Beta actin (ActinB) was used as loading control. B) Growth curve of P19 cells upon Zc3h14 KD and control (Ctrl). P19 cells were transfected with siRNAs against *Luciferase* (Ctrl) and *Zc3h14* (KD). Cells were seeded after 36 h KD and cell number was counted at each indicated time point. td = doubling time. C) WB validating Zc3h14-GFP Oex. Membranes were probed with anti-Zc3h14, (three isoforms indicated by black arrows). Oex efficiency was calculated relative to the WT protein level (Oexeff; values are shown below the blot). D) Growth curve of WT and Zc3h14-GFP overexpresser cells. P19 cells were seeded and cell numbers were counted at each indicated time point. td = doubling time.

5.7. Zc3h14 regulates the nuclear export of its targets

We have identified thousands of transcripts, which are differentially expressed upon Zc3h14 depletion and the vast majority of these targets were down-regulated. In line with our hypothesis that Zc3h14 acts as an export factor in P19 cells, previous studies had also shown that export factor depletions led to a decrease in total mRNA levels (Herold et al., 2003). If this were true, some of the down-regulated transcripts should be impaired in their nuclear export, i.e. exhibit decreased cytoplasmic and/or elevated nuclear mRNA levels upon Zc3h14 depletion. To test this, we performed subcellular fractionations of P19 cells after Zc3h14 KD (48 h) and analyzed transcript levels by RNA-seq and qPCR (Figure 29A). Zc3h14 KD efficiency was confirmed by WB and showed a 70% KD. Beta-actin (ActB) and Gapdh were used as loading controls, since their transcripts were not affected by Zc3h14 depletion (Figure 29B).

Most studies using subcellular fractionation validate subcellular fractionation efficiency solely by WB and lack proper control experiments. To monitor potential RNA leakage, we followed two strategies: we confirmed the purity of sub-cellular fractions at the RNA level on denaturing urea polyacrylamide gels as well as by RT-PCR, and at the protein level by WB.

Transfer RNAs (tRNAs) served as a cytoplasmic RNA marker, and small nuclear RNAs (snRNA) as nuclear markers to validate the purity of sub-cellular fractions on denaturing RNA gels (Jády et al., 2003). We observed an enrichment of snRNAs in the nuclear fraction, and an enrichment of tRNAs in the cytoplasmic fraction, confirming the efficiency of the fractionation (Figure 29C left panel). In addition we performed RT-PCRs using primers that anneal to exon 1 and exon 3 of the spliced *ActB* mRNA as well as to intron 2 of *Actb* and *Tubulin (Tubb)* pre-mRNAs. Amplicons corresponding to intron-containing pre-mRNAs were only detected in the input and nuclear fractions, while spliced *ActB* mRNAs were mostly detected in the cytoplasmic fractions (Figure 29C right panel). We also validated the subcellular fractionation efficiency at the protein level by WB (Figure 29D). The cytoplasmic marker protein Gapdh was enriched in the cytoplasm, while Histone (Hist1H3) and Polymerase II (polII), commonly used as nuclear markers, were mainly detected in the nucleus.

We further confirmed the subcellular fractionation efficiency by visualizing the RNA-seq read coverage of specific marker RNAs in each fraction (Figure 29E). As expected, read coverage of *Malat1*, a known nuclear speckle marker, was maximally enriched in the nuclear fractions of control and KD samples, with negligible reads in the cytoplasmic fractions.

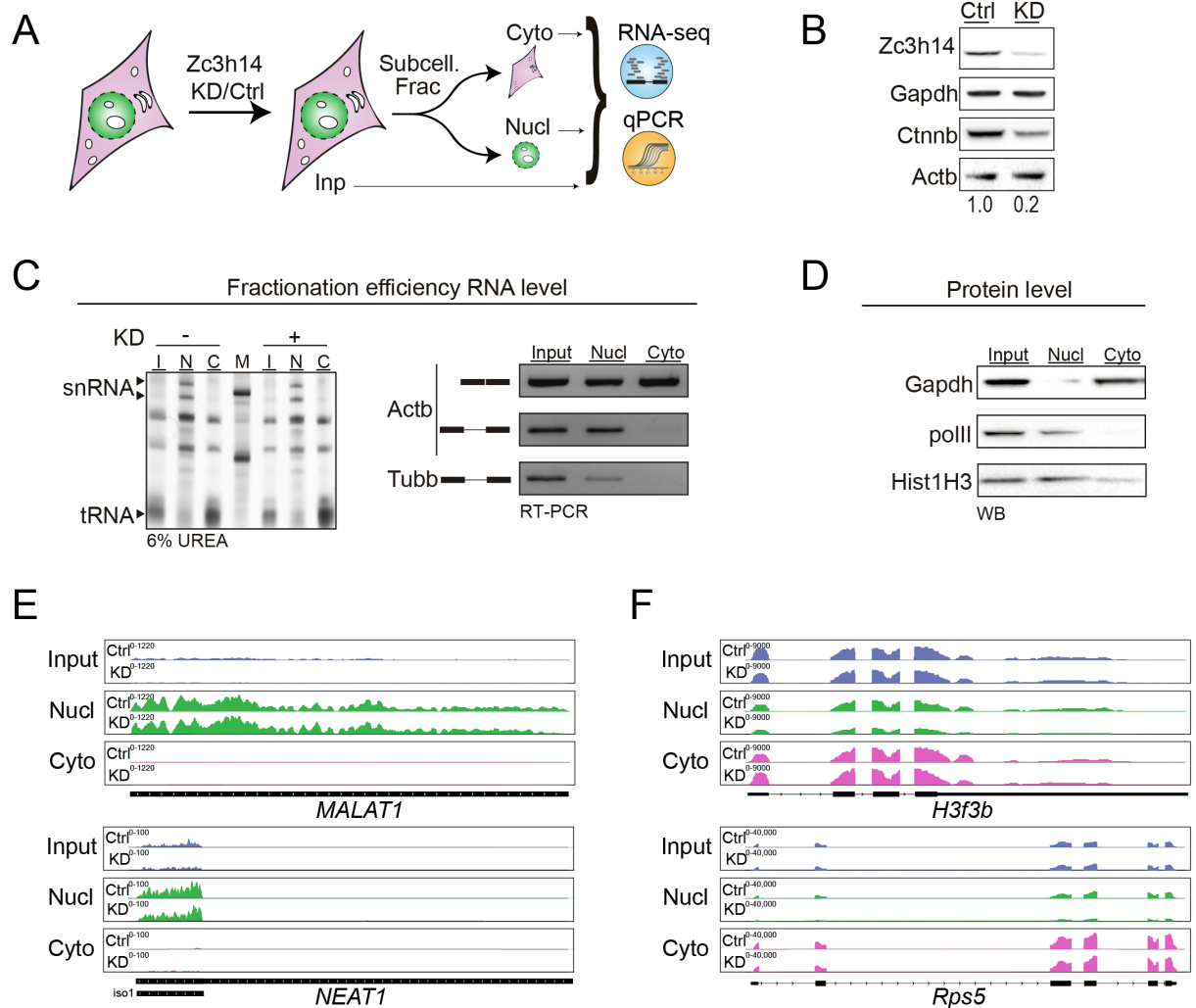


Figure 29: Subcellular fractionation upon Zc3h14 depletion. A) Workflow of the fractionation experiment. Zc3h14 KD was performed with specific siRNAs (KD) and control cells were transfected with siRNAs against *Luciferase* (Ctrl). After fractionation, polyA+ RNA was sequenced, and validation was performed by qPCR. B) Representative WB image displaying the KD efficiency in total cell lysates. Zc3h14 KD efficiency was quantified at the protein level relative to the control (values are indicated below the blot). Beta actin (ActB) and Gapdh were used as loading controls. C) Validation of fractionation efficiency at the RNA level. Left panel: 6% Urea gel loaded with RNA extracted from Input, nuclear (Nuc) and cytoplasmic (Cyt) fractions. The enrichment of small nuclear RNAs (snRNAs) and transfer RNAs (tRNAs) was used to assess the purity of the subcellular fractions (indicated by black arrows beside the image). Right panel: RT-PCR splicing gels (1.5% agarose) detecting pre-mRNAs (intron-containing) and mRNAs of the *Beta-actin* and the *Tubulin* genes in each subcellular fraction (Ctrl samples). Amplified isoforms are shown beside the gel. C) Representative WB image validating subcellular fractionation efficiency at the protein level (Ctrl samples). Antibodies against the cytoplasmic protein Gapdh and nuclear proteins RNA polymerase II (polII) and Histone1H3 (Hist1H3) were used to detect those proteins in each subcellular fraction. E) Browser shots with RNA-Seq read coverage on the nuclear retained lncRNAs *Malat1* and *Neat1*. F) Browser shots with RNA-Seq read coverage on efficiently exported *H3f3b* and *Rps5* transcripts for each subcellular fraction of Ctrl and Zc3h14 KD samples using IGV. Constitutive exons of the main protein coding isoform are shown as black boxes and introns as black lines. The scale represents the maximum number of reads per nucleotide position.

The other nuclear marker RNA *Neat1* expresses two main isoforms. The long isoform functions as a protein scaffold to assemble paraspeckles. However, in pluripotent P19 cells, only the short isoform of *Neat1* is expressed. Read coverage of the short isoform is restricted to the nuclear fraction, confirming the pluripotency of P19 cells and fractionation efficiency (Figure 29E). For comparison, we visualized the read coverage of two efficiently exported transcripts, the H3 histone family member 3B (*H3f3b*) and the ribosomal protein S5 (*Rps5*) (Figure 29F). Indeed, both transcripts are enriched in the cytoplasmic fractions of Ctrl and KD samples compared to nucleus and input.

We selected five transcripts that were strongly down-regulated upon Zc3h14 KD (*Smc4*, *Fmr1*, *Kif20b*, *Cdc25a* and *Sept7*) for export validation. Their RNA-seq read coverage was visualized in input, nuclear and cytoplasmic fractions. *ActB* was included as a control, since its mRNA levels were not affected upon Zc3h14 KD (Figure 30A). Confirming the differential expression analyses, all selected transcripts showed a strong decrease in read coverage in the input fraction upon Zc3h14 KD compared to the control, whereas *ActB* showed no change. Strikingly, all five Zc3h14 targets - *Smc4*, *Fmr1*, *Kif20b*, *Cdc25a* and *Sept7* - showed increased read coverage in the nuclear fraction and a strong decrease in the cytoplasmic fraction compared to Ctrl samples, strongly suggesting that they are export deficient upon Zc3h14 KD. In contrast, only minor changes could be seen for the *ActB* transcript (Figure 30A).

To validate this, we designed specific primer sets for the selected target transcripts and performed quantitative real time PCRs (qPCR) of input, nuclear and cytoplasmic RNA. To adjust for variations in total cDNA levels, we normalized mRNA levels within each fraction using the replication-dependent Histone transcript *Hist1h1e*. Replication dependent histones are exported by a different export pathway and are unaffected by Zc3h14 depletion (Marzluff et al., 2008) (Section 9 Table 25 and Table 26).

qPCR confirmed that *Smc4*, *Fmr1*, *Kif20b*, *Cdc25a* and *Sept7* transcripts were strongly decreased after Zc3h14 depletion compared to the Ctrl in the input samples, while *ActB* was unaffected (Figure 30B). Moreover, Zc3h14 depletion led indeed to increased nuclear levels of all target transcripts (1 to 5-fold) and a massive decrease in the cytoplasmic levels. This is in contrast to *ActB*, where no significant differences in mRNA levels between both fractions could be detected (Figure 30C).

Next, we tested whether the observed expression and export phenotype could be reverted by overexpression (Oex) of Zc3h14. We performed subcellular fractionation on WT and Zc3h14-GFP Oex cells and quantified mRNA levels of the five target genes in the fractions using qPCRs. Indeed, Zc3h14 Oex showed the opposite effect on expression of the target transcripts (Figure 30D).

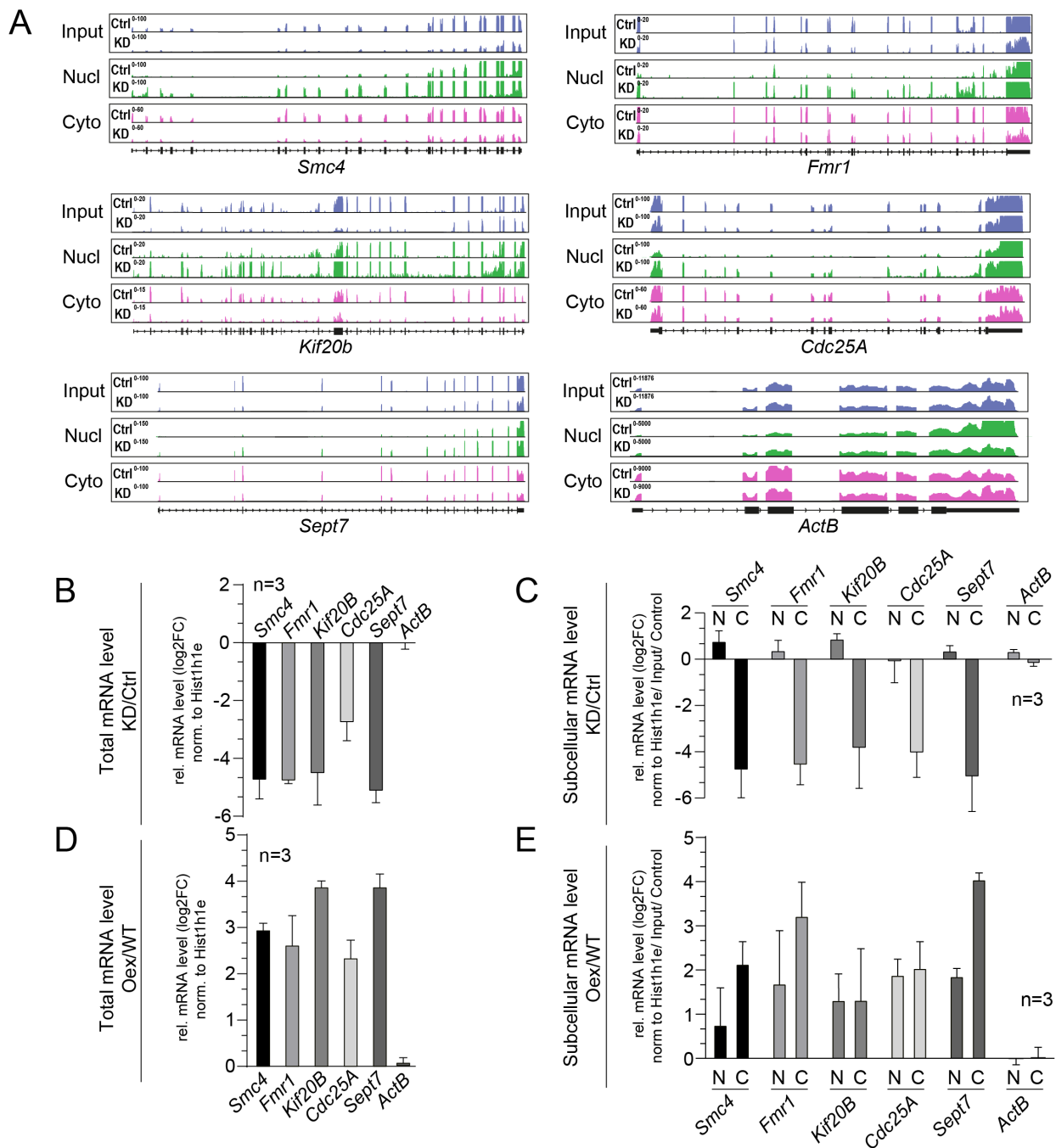


Figure 30: Zc3h14 levels modulate nuclear export of its targets. A) IGV browser shots showing RNA-Seq read coverage of five transcripts, which were down-regulated upon Zc3h14 KD and selected for validation (*Smc4*, *Fmr1*, *Kif20b*, *Cdc25a* and *Sept7*). The non-regulated *Beta-actin* transcript is shown as control. Read coverage is shown for each subcellular fraction in Ctrl and KD samples. Inp = Input; Nuc = nucleus; Cyt = cytoplasm. Constitutive exons of the main protein-coding isoforms are shown as black boxes and introns as black lines. The scale represents the maximum number of reads per nucleotide position. B & D) RT-qPCR validation of total mRNA levels of down-regulated Zc3h14 targets, and *Beta-actin* transcript as non-regulated control. Total mRNA levels were quantified from the Input fraction and normalized to *Histone3H13* mRNA in Zc3h14 Ctrl/ KD cells (B) and WT/Zc3h14 Oex cell

lines (D). The graphics shows log₂ fold changes (log₂FC) from Zc3h14 KD/Oex relative to Ctrl/WT samples. C & E RT-qPCR validation of down-regulated transcripts in nuclear and cytoplasmic fractions in Zc3h14 Ctrl/KD cells (C) and WT/ Zc3h14 Oex (E) cell lines. mRNA levels were normalized within each fraction by *Histone3H13* mRNA and to the Input. The graphic shows log₂ fold changes (log₂FC) from Zc3h14 Kd/Oex relative to Ctrl/WT samples. N = nucleus; C = cytoplasm.

Smc4, *Fmr1*, *Kif20b*, *Cdc25a* and *Sept7* mRNAs are increased (2.5- to 4.0-fold) in Zc3h14 Oex cells compared to WT cells, while again no significant difference was detected for the *ActB* transcript. Moreover, all target mRNAs were more efficiently exported, evidenced by a strong increase in cytoplasmic mRNA levels compared to the WT (Figure 30E). Surprisingly nuclear mRNA levels were also up-regulated upon Zc3h14 Oex, but to a lesser degree. This phenotype might be due to an increase in the stability of nuclear target RNAs at high Zc3h14 protein levels, similar to what has been observed for Nab2 (Tudek et al., 2018; Schmid et al., 2015; Haruki et al., 2008).

We next aimed to validate the observed export deficiency upon Zc3h14 depletion by RNA FISH. We chose *Smc4*, which is strongly regulated by Zc3h14, and designed fluorophore labeled FISH probes. Zc3h14 was depleted for 48 h and Ctrl and KD cells were imaged. In agreement with our RNA-seq and qPCR data, we detected a substantial change in the cellular *Smc4* mRNA distribution. In control cells *Smc4* accumulates in the cytoplasm, whereas KD cells show accumulation of *Smc4* in the nucleus (Figure 31A/B). Interestingly, nuclear *Smc4* transcripts are concentrated in defined foci, suggesting that *Smc4* mRNA is sequestered in nuclear bodies, most likely NS. As a control, we determined the distribution of replication-dependent histone mRNAs that do not contain polyA tails and that were not affected by Zc3h14 depletion. Indeed histone transcripts were efficiently exported to the cytoplasm in Ctrl and KD cells (Figure 31C/D).

To validate the observed decrease in *Smc4* levels and the shift in its subcellular distribution, we quantified total, nuclear and cytoplasmic signal in 90 cells. For the nuclear signal we first defined the nuclear area from Hoechst-stained regions. For the cytoplasmic signal intensity, we subtracted total *Smc4* signal from the nuclear signal, as indicated in the representative cell inset (Figure 31A/B, bottom image). Quantification of total fluorescence intensity showed only a slight decrease of *Smc4* mRNA in KD cells compared to the Ctrl (Figure 31E). However, quantification of nuclear and cytoplasmic fluorescence confirmed the significant decrease of *Smc4* transcripts in the cytoplasm in KD cells and concomitantly, an increase in nuclear *Smc4* levels (Figure 31F).

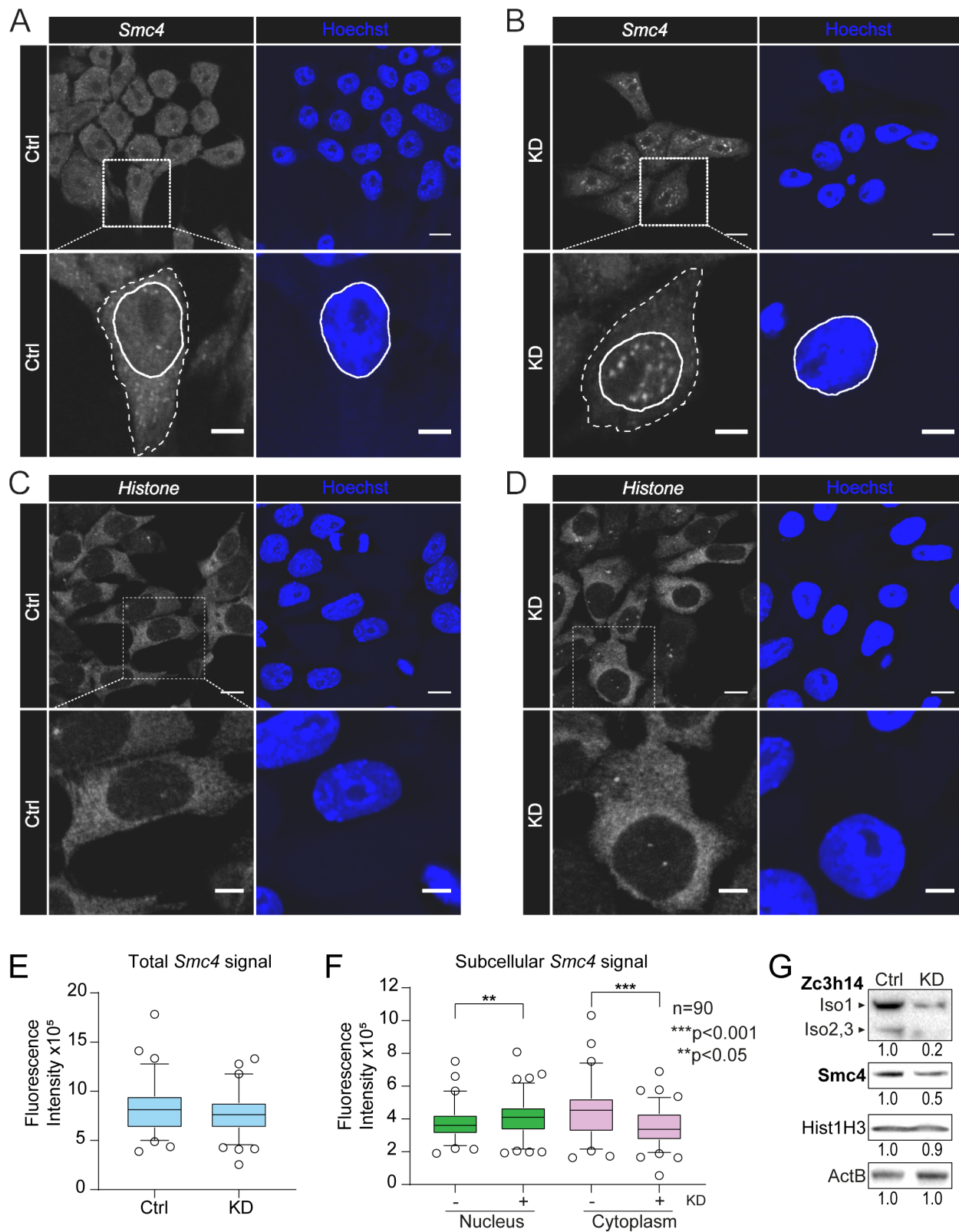


Figure 31: Zc3h14 KD impairs nuclear export of *Smc4* mRNA leading to decreased protein expression. A-B) Panels displaying representative RNA-FISH images of Ctrl (A) and Zc3h14 KD (B) P19 cells hybridized with a *Smc4* specific FISH probe set. Upper panels display wide field images and bottom panels show zooms of representative cells

(indicated with a white square). Cytoplasmic and nuclear areas used for *Smc4* fluorescence quantification are drawn in white. *Smc4* signal is shown in gray and Hoechst DNA staining in blue. Scale bars = 10 μm (upper panels) and 5 μm (bottom panels). C) Mean total *Smc4* fluorescence intensity values in Ctrl and Zc3h14 KD cells (n = 90). D) Mean *Smc4* fluorescence signal intensities in each subcellular fraction were quantified and differences of cytoplasmic and nuclei signal in KD cells were calculated relative to the Ctrl using t-test (n= 90, **p<0.01; ***p<0.001). E) Representative WB images showing the efficiency of Zc3h14 KD using a specific antibody against Zc3h14 (three isoforms indicated in the right side). *Smc4* and Histone H3 protein expression was visualized in Ctrl and KD samples using specific antibody. Beta actin antibody was used as loading control (ActinB). F-G) Panels displaying representative RNA-FISH images of Ctrl (F) and Zc3h14 KD (G) P19 cells hybridized with *Histone* probes (shown in gray). Upper panels display wide field images and bottom panels show zooms of representative cells (indicated in the wide field images with a white square). Scale bars = 10 μm .

In line with an impaired *Smc4* mRNA export Zc3h14 KD also led to a 2-fold decrease in *Smc4* protein expression, while Histone H3 levels did not change (Figure 31G). In summary, we used three different molecular techniques (RNA-seq, qPCR and FISH) to demonstrate that Zc3h14 selectively modulates the mRNA export of a subset of transcripts and introduce Zc3h14 as a novel mRNA export adaptor in pluripotent P19 cells.

5.8. Zc3h14 binds preferentially to polyA stretches and polyA tails

Studies in yeast reported a high affinity of Nab2 for polyadenosines, which led to its classification as a polyA binding protein (PABP). Zc3h14 is also involved in polyA tail length control (Kelly et al., 2014; Rha et al., 2017). However, the global *in vivo* RNA-binding landscape of Zc3h14 has not yet been reported.

Our data showed that Zc3h14 shuttling and SRSF3 interaction was strongly decreased after splicing inhibition, suggesting that Zc3h14 recruitment to its mRNA targets might be also splicing dependent. To test this hypothesis, we set out to determine and compare the global RNA binding landscape of Zc3h14 upon splicing inhibition. For this we performed UV Cross-linking and Immunoprecipitation (iCLIP) in Zc3h14-GFP cells in the presence or absence of IsoG (Figure 32A).

Since cross-linking to adenosines is very inefficient compared to uridine residues, we first optimized the cross-linking efficiency of Zc3h14 at different UV intensities. For this, Zc3h14 was immunopurified and the cross-linked RNA was radio-labeled and visualized by phosphor-imaging (Figure 32B). As expected, the

cross-linking efficiency positively correlated with the UV irradiation intensity at constant levels of the Zc3h14-GFP bait. Since previous studies showed that intensive UV irradiation can lead to mutations at the cross-link site (Stork & Zheng, 2016), we chose 300 mJ/cm² as optimal conditions for our Zc3h14 iCLIP study (Figure 32B).

For the iCLIP experiment, UV cross-linked cell lysates were briefly treated with RNaseI to fragment the crosslinked RNAs. Subsequently, RNA-protein complexes were immunoprecipitated using an anti-GFP antibody, labelled with P³², stringently purified and separated by SDS-PAGE and membrane transfer (Figure 32C). Interestingly, the RNA signal in the IsoG samples were strongly decreased, suggesting that Zc3h14 binds less to RNA upon splicing inhibition (Figure 32C). Bound RNA fragments were subsequently isolated, reverse transcribed, size selected (50-300 nt) and PCR-amplified, to generate the final iCLIP libraries for deep sequencing (Figure 32D). iCLIP reads were mapped to the mouse genome (mm10) using STAR (Dobin et al., 2013) and unique cross-links events were obtained for control and IsoG samples. All unmapped reads were also kept and analyzed for their A-content (Figure 32F).

We obtained indeed less mapped reads for the IsoG samples compared to the control and much less spliced reads in line with a successful splicing inhibition by IsoG (Figure 32E). The reduced number of Zc3h14 cross-link events (reads) upon IsoG treatment can be either due to a reduced RNA-binding capacity of Zc3h14 or to an increased binding to polyA tails. To investigate whether Zc3h14 binds to polyA tails, we quantified the prevalence of adenosines within iCLIP reads that could not be mapped to the genome (Figure 32F). We found that the majority of unmapped reads indeed contained a high proportion of adenosines. Specifically, 22% of all unmapped reads exhibited an A-content greater than 50%. This fraction is notably higher compared to the A-content in unmapped reads of the splicing factor HNRNPH, where only 3% of the unmapped reads exhibit an A-content of greater 50%. Strikingly, the A-content in Zc3h14 iCLIP reads was even higher than for MKRN1, an RBP that was recently demonstrated to bind immediately upstream of polyA tails (Figure 32F). To test whether Zc3h14 binding to polyA tails is affected upon IsoG treatment, we compared the A-content of unmapped reads in the presence and absence of IsoG and found a small increase in the binding of Zc3h14 to adenosines when splicing is inhibited (Figure 32G).

We next investigated whether Zc3h14 also binds to genomically encoded A-stretches. For this, we determined the *in vivo* binding motif using the mapped reads and a K-mer enrichment analysis (Figure 32H). We analyzed enriched 5-mers around crosslink events (first nucleotide of the read) and identified a consensus-binding motif of Zc3h14 rich in adenosine and cytosines (Figure 32H).

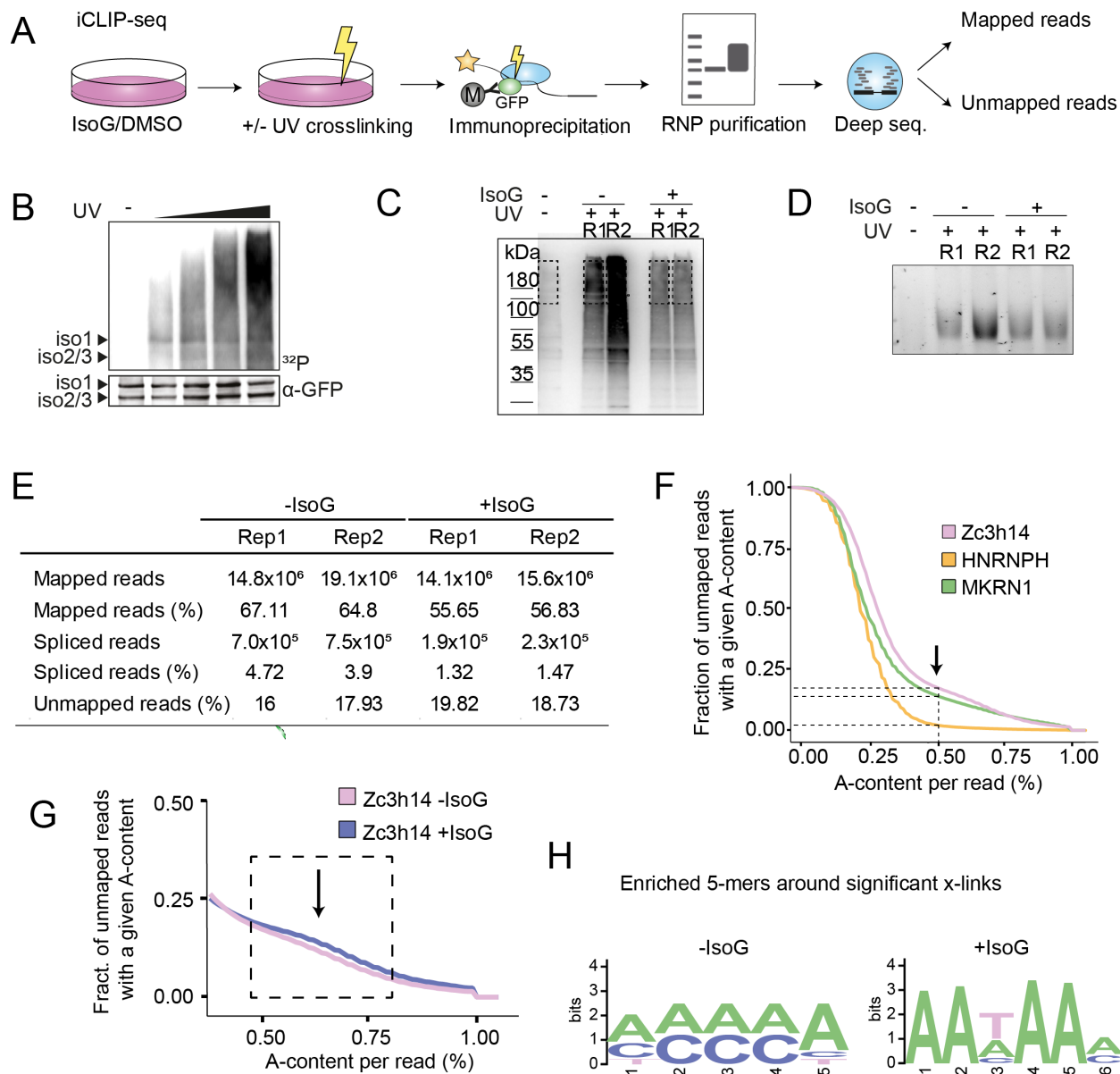


Figure 32: Global identification of the *in vivo* Zc3h14 binding landscape. A) Workflow of the iCLIP experiment using Zc3h14-GFP cells treated with IsoG or DMSO as control for 16 h (33 μM). B) Autoradiograph showing the RNA cross-linked to purified Zc3h14-GFP for increased UV intensities (isoforms shown beside the image) labeled with ^{32}P . Below, is an image of the membrane probed with an antibody against GFP showing the Zc3h14-GFP protein isoforms (indicated by black arrows). UV- = non-crosslinked samples. C) Autoradiograph of RNA cross-linked to purified Zc3h14-GFP protein in IsoG/DMSO treated cells (IsoG +/-). Squares indicate where the RNA was cut and purified. UV- = non-crosslinked samples, R1-2 = replicate 1 and 2. D) 6% TBE-Urea gel stained with SYBR Gold showing the final iCLIP library (22 cycles). E) Table listing the number of spliced, mapped and unmapped reads obtained from the iCLIP libraries for each replicate. F) Plot showing the cumulative fractions of unmapped reads and their A-content comparing Zc3h14 to HNRNPH and MKRN1. G) Plot showing the cumulative fractions of unmapped reads and their A-content comparing Zc3h14 with and without IsoG. H) Weblogo showing the *in vivo* binding motifs of Zc3h14 with and without IsoG treatment.

Interestingly, upon splicing inhibition the consensus motif changed to a homopolymeric adenosine stretch (AA A/T AA), which could be interpreted as elevated binding of Zc3h14 to polyA-stretches upon splicing inhibition. Altogether, this demonstrates that Zc3h14 binds preferentially to polyA tails and polyA-stretches *in vivo* in pluripotent P19 cells and suggests that its RNA binding capacity and specificity is reduced upon splicing inhibition.

5.9. Zc3h14 binding to its regulated target RNAs is sensitive to splicing inhibition

Next, we tested whether transcripts that were down-regulated upon Zc3h14 depletion are bound by Zc3h14. For this, we counted all mapped iCLIP reads into annotated genes using the gencode_v18.gtf annotation and htSeq. Then we normalized and compared the read numbers between Ctrl and IsoG samples using DESeq2. Subsequently, we divided the normalized Zc3h14 iCLIP read numbers of each transcript by their normalized RNA-seq read counts (DESeq2) to control for transcript expression level. Applying a cut-off of >2-fold we defined transcripts as bound over background. Using this analysis pipeline, we found 1243 Zc3h14 targets with decreased binding upon IsoG treatment, which were enriched for the GO-term categories 'cell cycle', 'cell division' and 'mitotic nuclear division' in line with the proposed function of Zc3h14 in cell cycle control (Figure 33A).

To observe if those transcripts, which are down-regulated upon Zc3h14 depletion are also bound by Zc3h14, we interrogated the iCLIP data set for the presence of binding sites in targets and non-target transcripts. The number of binding sites were normalized by transcript expression using the number of RNA-seq reads per transcript. The presence of Zc3h14 Clip tags was considered when at least 2 iCLIP peaks per 100 RNA-Seq reads per transcript was detected. This analysis showed, that 87% (6708) of all transcripts that were down-regulated upon Zc3h14 depletion are also bound by Zc3h14. This is in contrast to the non-regulated transcripts, where only 22% of transcripts contain iCLIP tags, while the vast majority 78% (14,161) of non-regulated transcripts are also not bound to Zc3h14 (Figure 33B). This observation suggests that binding of Zc3h14 to down-regulated transcripts normally promotes their expression and/or nuclear export.

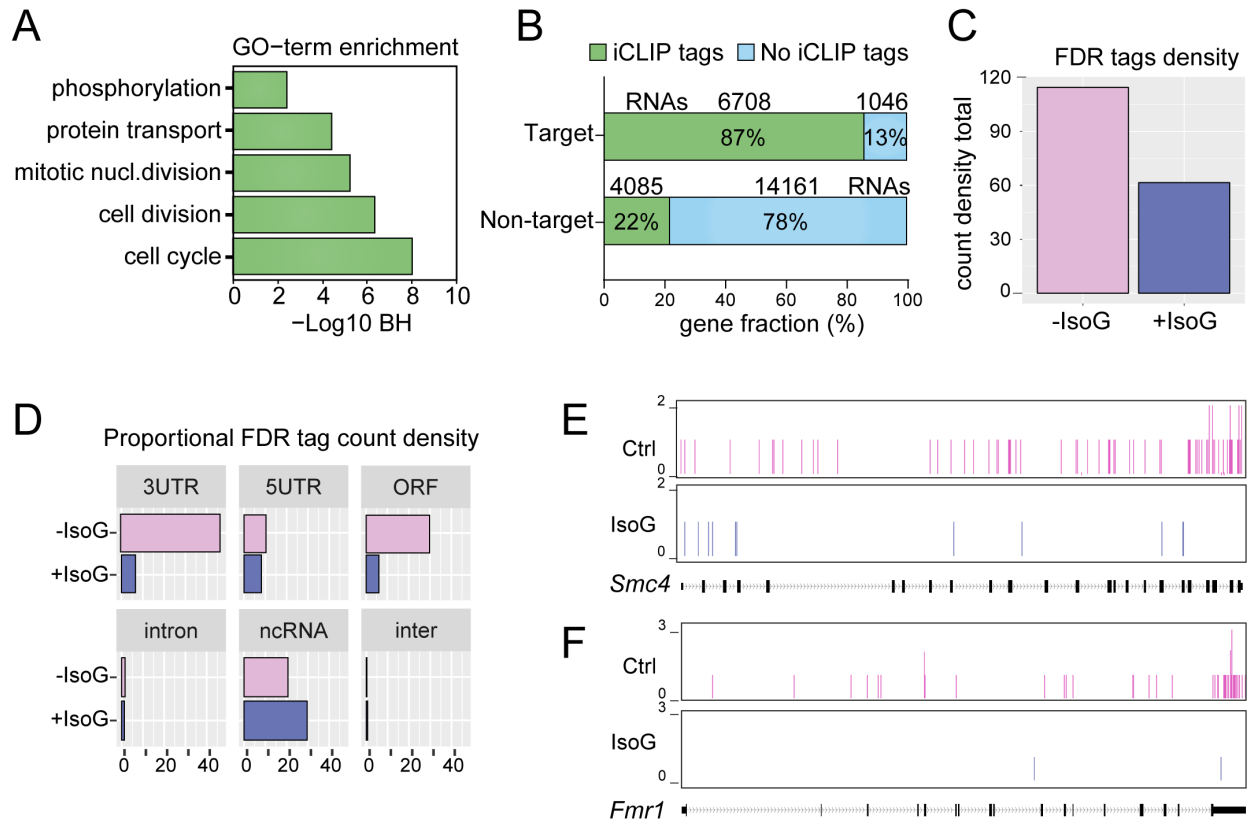


Figure 33: Zc3h14 RNA binding specificity is modulated upon IsoG treatment. A) GO-term analysis of biological processes (BP) for genes that presented significantly decreased Zc3h14 iCLIP tags in IsoG treatment compared to control using DAVID. BH = Benjamini-Hochberg corrected P-value. B) Percentage of Zc3h14 iCLIP reads in up-regulated and non-regulated transcripts acquired from Deseq2 analyses upon Zc3h14 KD. The number of binding sites were normalized by transcript expression using the number of RNA-seq reads per transcript. Zc3h14 binding was defined when at least 2 iCLIP peaks per 100 RNA-Seq reads were detected and are grouped as “iCLIP tags”. C) Graphic displaying total iCLIP tags counts from Zc3h14 in DMSO (-IsoG) and IsoG treated (+IsoG) cells. D) Significant X-link enrichment of Zc3h14 in different genomic regions in control and IsoG treated samples. ORF – open reading frame; ncRNA – non-coding RNA; inter – intergenic regions. E-F) Browser shots showing the distribution of significant Zc3h14 X-links on 2 genes (*Smc4* and *Fmr1*) which were identified as down regulated upon Zc3h14 KD.

To investigate to which transcript regions Zc3h14 binds preferentially, we pooled the replicates and counted all X-link events (X-links) into transcript features (5’UTR, ORF, 3’UTR, introns and intergenic regions) using iCOUNT (<http://icount.fri.uni-lj.si/groups.html>). In line with a reduced RNA binding capacity of Zc3h14, the total number of X-links was drastically reduced in the IsoG sample (Figure 33C). Interestingly, X-link density (X-link counts normalized to feature length) was highest in 3’UTRs and ORFs, but decreased strongly upon splicing inhibition, while binding to introns, 5’UTRs and intergenic regions increased or remained unchanged (Figure 33D).

As exemplified in (Figure 33E-F) we detect Zc3h14-iCLIP reads at the 3' end of *Smc4* and *Fmr1* in the absence of splicing inhibition, however binding is lost upon IsoG treatment. Taken together our global RNA-binding analysis revealed that Zc3h14 binds preferentially to polyA tails or genomically encoded A-stretches. Zc3h14 also binds to coding regions and 3'UTRs of export targets *in vivo*. Splicing inhibition decreases binding to 3'UTRs and ORFs but increases binding to A-stretches or polyA tails. Altogether, this suggests a mechanism, by which Zc3h14 acts as a surveillance factor that selectively stimulates mRNA export in a splicing-dependent manner.

5.10. Zc3h14 recruitment to mRNPs requires SRSF3 and is inhibited by SRSF3-hyperphosphorylation

Our data showed that Zc3h14 is involved in nuclear mRNA export. However, its interaction with SRSF3, its RNA-binding capacity and its shuttling activity are strongly decreased after splicing inhibition, suggesting that Zc3h14 might act as an export licensing factor for specific transcripts. To confirm the splicing dependent recruitment of Zc3h14 to mRNPs and understand its interplay with SRSF3, we performed a comparative RNA binding capacity assay upon IsoG treatment (Figure 34A).

P19 cell lines expressing GFP-tagged SRSF3, Zc3h14 and Nxf1 were treated with IsoG or DMSO for 16 h. Bound RNAs were UV cross-linked and the protein-RNA complexes were stringently purified similar to the iCLIP procedure (Figure 34A). Radioactively labeled RNA that co-purified with SRSF3, Zc3h14 and Nxf1 was visualized using a phosphor imager. The membrane was subsequently probed with an anti-GFP antibody to quantify the protein levels of the respective baits. Quantification of RNA binding capacities revealed that Zc3h14 and Nxf1 are highly sensitive to splicing inhibition by IsoG and show a 26% and 42% decrease in bound RNAs upon IsoG treatment (Figure 34B). Interestingly, the RNA binding capacity of SRSF3 was not affected by splicing inhibition. These results confirm that SRSF3 stays bound to unspliced transcripts after splicing inhibition. In contrast, the association of the export factors Zc3h14 and Nxf1 with the mRNPs is dependent on the completion of splicing.

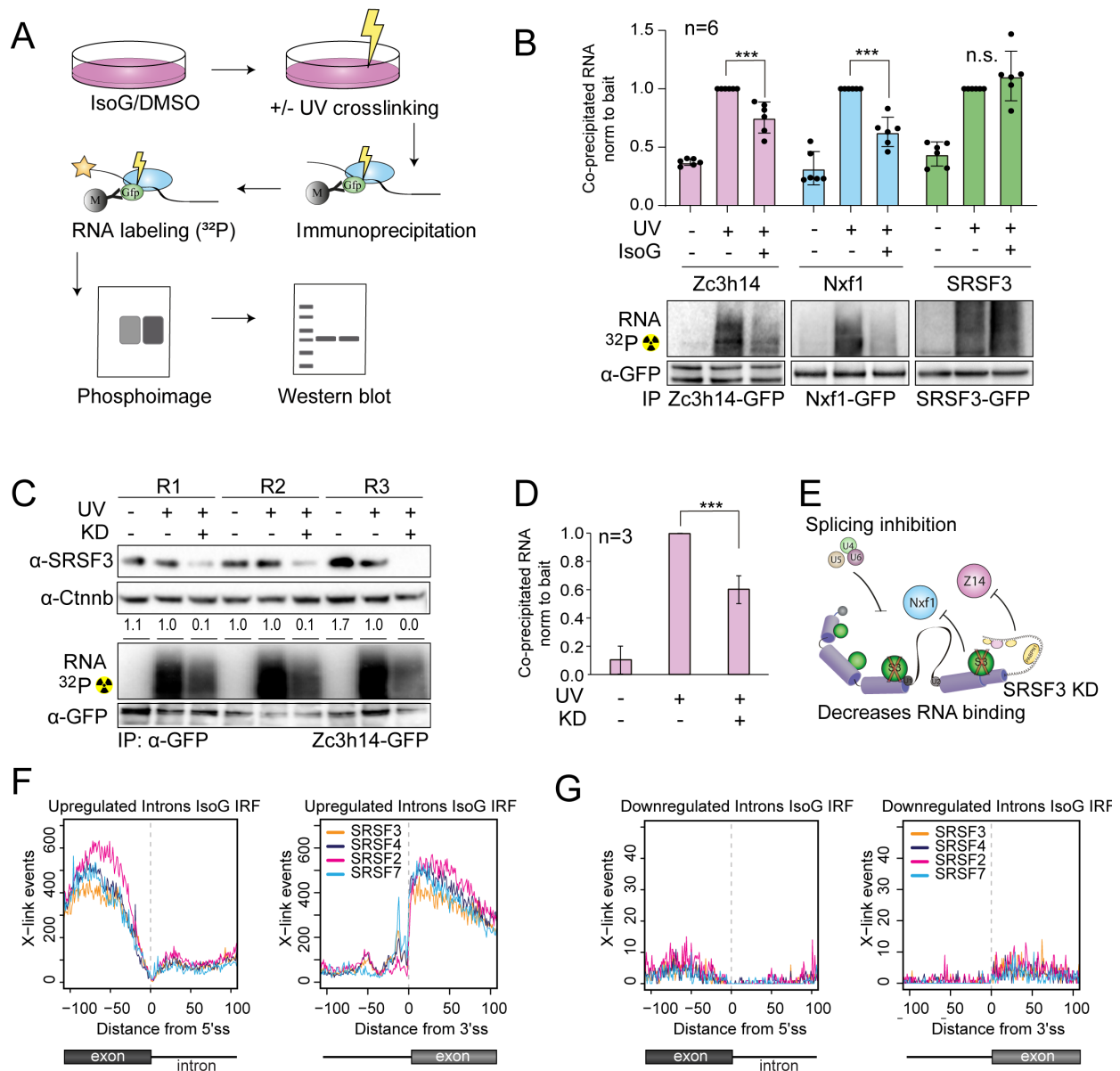


Figure 34: Zc3h14 binding to RNA requires SRSF3 and is decreased upon splicing inhibition. A) Workflow of the RNA binding assay using cells treated with IsoG or DMSO control for 16 h (33 μ M). B) Quantification of RNA cross-linked to purified Zc3h14-GFP, NXF1-GFP and SRSF3-GFP proteins in the presence or absence of IsoG. Differences in total cross-linked RNA levels between IsoG- and IsoG+ samples for each purified protein were analysed using t-test ($n = 6$, $***p < 0.01$, ns = non-significant). A representative autoradiograph with labelled RNA cross-linked to purified proteins is shown below. Membranes were probed with an anti-GFP antibody to quantify the levels of each purified protein (bait). IP = Immunoprecipitation. C) Validation of SRSF3 KD in Zc3h14-GFP cells transfected with siRNAs against SRSF3 (KD+) and Luciferase as control (KD-), cross-linked or not (+UV/-UV) using an antibody against SRSF3. Beta catenin was used as loading control (Ctnnb). A representative autoradiograph is shown below. Membranes were probed with an anti-GFP antibody to quantify total levels of Zc3h14. IP = Immunoprecipitation. D) Quantification of RNA bound by purified Zc3h14 (samples from C). E) Scheme of RNA binding loss of Zc3h14 and Nxf1 upon SRSF3 KD and splicing inhibition due to impaired recruitment by SRSF3. F/G) Number of cross-link events of individual SR proteins mapping window of +/- 100 nt around the 5'ss (left) and 3'ss (right) of upregulated (F) or downregulated (G) introns upon IsoG treatment. SR protein iClip data sets originate from (Müller-McNicoll et al., 2016).

We next investigated whether Zc3h14 recruitment to mRNPs is dependent on SRSF3 and performed RNA binding assays with Zc3h14-GFP cells in the presence and absence of SRSF3. Analysis of the Zc3h14 RNA binding capacity upon SRSF3 depletion (KD) in three biological replicates revealed a strong decrease in the bound RNA. This suggests that SRSF3 recruits Zc3h14 to mRNPs in a splicing dependent manner (Figure 34C/D).

To test if SR proteins bind to introns which are retained upon IsoG treatment, we mapped iCLIP reads of SRSF2, SRSF3, SRSF4 and SRSF7 (Müller-McNicoll et al., 2016) to introns, which were upregulated upon splicing inhibition. As expected all four SR proteins show a high RNA binding sites at the exonic 5' and 3'ss (Figure 34F). This is in contrast to the low SR protein binding profile of introns, which are downregulated upon IsoG treatment (Figure 34G), indicating that SR proteins preferentially bind splice sites of introns which are retained upon splicing inhibition.

How could the splicing-dependent recruitment of Zc3h14 by SRSF3 be regulated? One possibility would be through phosphorylation. SR proteins are recruited to nascent pre-mRNAs in a hyper-phosphorylated state and become hypo-phosphorylated during the splicing process. Consequently, splicing inhibition is expected to lead to an accumulation of hyper-phosphorylated SR proteins. To test this, we performed an IsoG time course experiment and analyzed SRSF3 phosphorylation levels using SDS-PAGE phostag® gels (Figure 35A). Phostag® is a dinuclear metal complex that binds to phosphate monoesters with high affinity and reduces the electrophoretic mobility of phosphorylated proteins. Slower migration improves the separation of different phosphorylation states (Ito et al., 2016). Immunoblotting of a 12% SDS-PAGE phostag® gel with an antibody against total SRSF3 detected two distinct SRSF3 phosphorylation states, corresponding to hyper- and hypo-phosphorylated SRSF3 (Figure 35A). In agreement with two phosphorylation states, a recent study revealed that SRSF3 phosphorylation dynamics are minimal compared to SRSF1 and are restricted to few phosphorylation sites within the RS domain (Long et al., 2019). Interestingly, the hyper-phosphorylated form of SRSF3 increased over time upon splicing inhibition. We quantified the ratio between hyper- and hypo-phosphorylated SRSF3, which confirmed that upon splicing inhibition, hyper-phosphorylated SRSF3 increased significantly and is maximal at 16 h (Figure 35B). To confirm that the observed size shift is due to phosphorylation, we completely de-phosphorylated SRSF3 in cell lysates using the Shrimp Alkaline Phosphatase (SAP). The hyper- and hypo-phosphorylated SRSF3 forms disappeared and de-phosphorylated SRSF3 was migrating much faster than the observed bands, confirming that we indeed monitored phosphorylated SRSF3. However, this phosphorylation status does

not reflect a SRSF3 phosphorylation status that exist in cellular conditions (Long et al., 2019). Phostag[®] efficiency was verified by comparing the migration shifts in a 12% SDS-PAGE without phostag. Here we detected only small shifts between phosphorylated and SAP-treated SRSF3 (Figure 35A, right panel). These data suggest that SRSF3 has two distinct phosphorylation states whose proportions change upon splicing inhibition.

To confirm this result, we monitored changes in SRSF3 phosphorylation by WB using the monoclonal antibody mAb104, which recognizes only phosphorylated SR proteins. We compared the levels of hyper-phosphorylated SRSF3 to its total levels using an antibody against total SRSF3. In agreement with the phostag gel analysis, the IsoG time course experiment revealed, that SRSF3 phosphorylation increases over time upon splicing inhibition, while total levels remain constant (Figure 35C). Quantification of 3 experiments confirmed the relative increase in hyper-phosphorylated SRSF3 levels upon IsoG treatment with highest phosphorylation differences after 16 h (1.5-fold increase) (Figure 35D).

Previous studies have shown that SRSF1 and SRSF7 interaction with Nxf1 is highly phosphorylation dependent (Huang et al., 2004). Our results show that SRSF3 phosphorylation is increased upon splicing inhibition, thus the impaired interaction with export factors can be due to SRSF3 hyper-phosphorylation.

To test if the interactions of SRSF3 with the export factors Zc3h14 and Nxf1 is phosphorylation- and splicing-dependent, we performed co-immunoprecipitation assays using P19 Zc3h14- and Nxf1 GFP-tagged cell lines in the presence and absence of the splicing inhibitor IsoG and compared co-purified hyper-phosphorylated (SRSF3_{phos}) with total SRSF3 (SRSF3_{tot}) using the antibodies mAb104 and total anti-SRSF3 (Figure 35E/F).

Indeed, Nxf1 efficiently co-purifies total SRSF3, in a RNA-independent manner, but not hyper-phosphorylated SRSF3 (Figure 35E). Zc3h14 interactions shows the same tendency as Nxf1, with an even higher selectivity for the different SRSF3 phosphorylation states. While total SRSF3 is efficiently co-purified independently of RNA, hyper-phosphorylated SRSF3 is completely absent in Zc3h14 pull-downs (Figure 35F). In agreement with our SRSF3 interactome, the interaction of Nxf1 and Zc3h14 with SRSF3 decreased upon splicing inhibition. Again, Zc3h14 is more sensitive to IsoG with respect to the SRSF3 interaction, which in agreement with our mass spectrometry analysis.

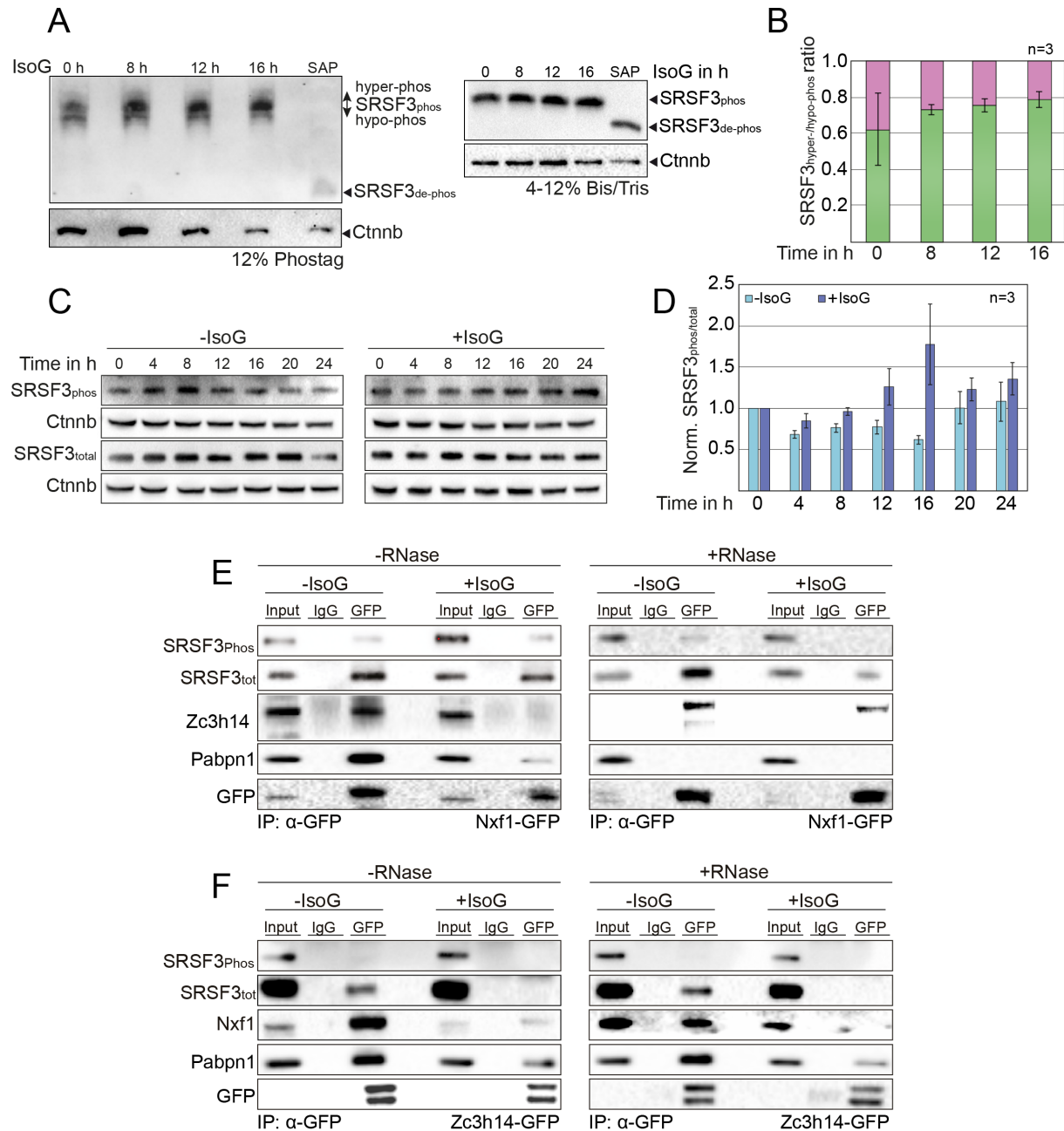


Figure 35: Splicing inhibition leads to hyper-phosphorylation of SRSF3 and impairs its interaction with Zc3h14 and Nxf1. A) Left panel: representative image of a WB from a 12% SDS-PAGE gel containing 10 μ l Phostag[®]. P19 cells were treated with IsoG and protein lysates were acquired at the indicated time points. The membrane was probed with anti-SRSF3 antibody and different SRSF3 phosphorylation states are indicated beside the blot. SAP = Shrimp Alkaline Phosphatase. Right: the same samples were loaded in a normal 4-12% gradient Bis-tris gel and probed with anti-SRSF3. B) Quantification of SRSF3 hyper/hypo phosphorylated SRSF3 bands from Phostag[®] gels. C) Representative WB from a 24 h time course experiment with IsoG treated/untreated P19 WT cells probed with antibodies against phosphorylated SR proteins (mAb104) showing SRSF3 phosphorylation and total SRSF3. Beta catenin (Ctnnb) was used as loading control. D) Quantification of the ration between phosphorylated and total SRSF3 in IsoG+/- samples for each time point relative to 0 h treatment. E-F) Co-IP of purified Nxf1-GFP (E) and Zc3h14-GFP (F) with or without RNaseA treatment upon IsoG treatment (IsoG+) or DMSO control (IsoG-) (33 μ M for 16 h). WBs were probed with antibodies against total and phosphorylated SRSF3 (mAb104), NXF1 and Zc3h14 to analyze

interactions differences between control and IsoG treated samples as well as RNase treated/untreated samples. Anti-GFP antibody was used to confirm the purification of the IP protein. PABPN1 was used to control for successful RNase treatment. IgG = unspecific antibody control.

Finally, we tested whether Zc3h14 is an Nxf1 adaptor or acts independently of Nxf1 in mRNA export. Co-immunoprecipitations revealed that both proteins interact RNA-independently with each other (Figure 35E/F). Strikingly splicing inhibition by IsoG treatment leads to a complete loss of this interaction in both, suggesting that Zc3h14 is an Nxf1 adaptor and that both proteins are part of the same mRNP. RNase treatment was controlled by re-probing the membranes with an antibody against the polyA-binding protein Pabpn1. Interestingly, while the interaction of Nxf1 and Pabpn1 is highly RNase sensitive, the Zc3h14-Pabpn1 interaction is clearly RNA-independent. This indicates that Zc3h14 and Pabpn1 interact and likely co-bind in close proximity to polyA tails of mRNAs (Figure 35F). In addition, both, Nxf1 and Zc3h14 interactions with Pabpn1 are highly IsoG sensitive, which confirms that the association of Zc3h14 and Nxf1 to mature mRNPs is highly splicing dependent.

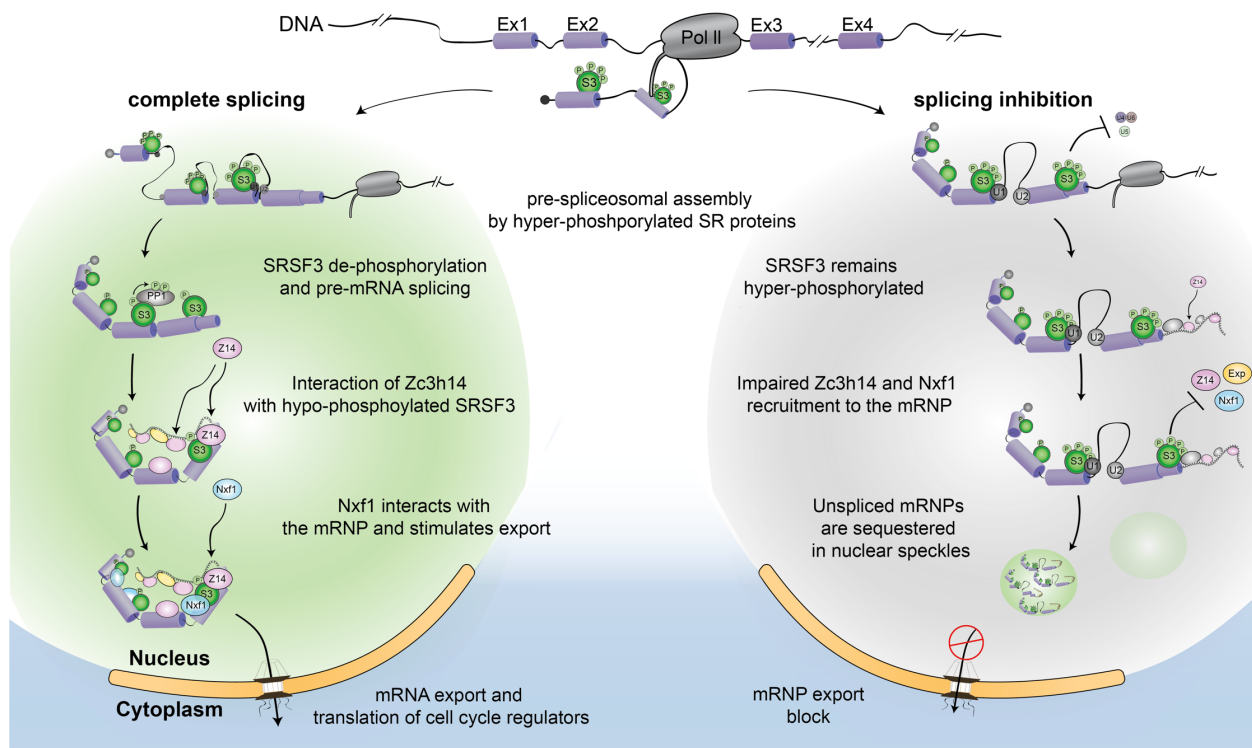


Figure 36: The role of SRSF3 in splicing surveillance. Hyper-phosphorylated SRSF3 (S3) binds co-transcriptionally to the nascent transcript. In case of splicing completion SRSF3 gets hypo-phosphorylated by SR specific phosphatases (PP1). Hypo-phosphorylated SRSF3 recruits Zc3h14 (Z14) and Nxf1 to the mRNP, which stimulates the cytoplasmic transport of the completely processed and export competent mRNP. In case of incomplete splicing/splicing inhibition (U4,U5,U6) SRSF3 remains hyper-phosphorylated leading to an impaired recruitment of export adaptors/factors

(Exp), such as Zc3h14 and Nxf1 at the transcript 3' end, due to a blocked SRSF3 interaction with the pre-spliceosome (U1, U2) and to a nuclear sequestration of intronic transcripts in nuclear speckles.

Taken together, our data lead us to propose a model, in which SRSF3 monitors and communicates the splicing status of transcripts *via* phosphorylation and thereby discriminates between fully spliced and an aberrantly processed transcripts. While hypo-phosphorylated SRSF3 recruits the export factors Nxf1 and Zc3h14 to a subset of mRNAs and stimulate the export of transcripts coding for cell cycle regulators, splicing inhibition lead to the accumulation of hyper-phosphorylated SRSF3 bound on the aberrantly processed transcript. This causes an impaired export factor recruitment und nuclear retention of export-incompetent RNA species in nuclear speckles. This splicing surveillance mechanism might be limited to a subset of mRNAs, but is important for the regulation of the cell cycle in pluripotent P19 cells.

6. Discussion

6.1. Isoginkgetin as a tool to investigate splicing surveillance in P19 cells

Although multiple studies have described, that inhibition of splicing by small molecule inhibitors leads to intron retention and cause an export block of polyadenylated RNA at defined nuclear sites, the molecular retention mechanism remained unclear (Carvalho et al., 2017; Kaida et al., 2007; Pawellek et al., 2017). Insights in the formation and composition of these nuclear sites could be the key to identifying the regulatory players and understanding the cellular splicing surveillance mechanisms.

We validated Isoginkgetin as a potent splicing inhibitor in pluripotent P19 cells. Our splicing analysis revealed that intron retention is detectable at lower IsoG concentrations and incubation times, when compared to HeLa cells (O'Brien et al., 2008). The high sensitivity of P19 cells to the splicing inhibitor could be due to its high cell metabolism and low doubling times. Indeed, the efficiency of small molecule inhibitors has been shown to be selective and affect preferentially cells with high proliferation rates, which makes IsoG a potential drug for cancer therapy (Salton & Misteli, 2016).

Our global analysis in P19 cells revealed that thousands of introns are retained upon IsoG treatment. Short introns seem to be more susceptible to IsoG than long intronic sequences. This is in agreement with a recent study characterizing features of retained introns in more than 40 human and mouse tissue types (Braunschweig et al., 2014). This study subcategorized introns according to their percent intron retention (PIR) value. Higher PIR values were displayed by introns, which were short in length, had a high C/G content and weak splice sites (Braunschweig et al., 2014). A recent transcriptome-wide study of cells treated with SSA showed that a significant fraction of intron-containing transcripts leak to the cytoplasm (Yoshimoto et al., 2017). These leaked transcripts displayed weak 5' splice sites and significantly shorter intronic sequences. Thus, short introns generally seem to be more vulnerable in the presence of a splicing inhibitor. Moreover, transcripts with short retained introns tend to escape nuclear retention, remain stable in the cytoplasm and are less affected by cytoplasmic surveillance mechanisms such as NMD nonsense-mediated decay, most likely due to lower frequencies of premature termination codons (PTCs) (Yoshimoto et al., 2017).

Previous studies have shown, that complex E inhibitors, such as SSA (Carvalho et al., 2017; Martins et al., 2011; Kaida et al., 2007; Roybal & Jurica, 2010; Yoshimoto et al., 2017) and its derivatives, as well as complex A inhibitors, such as Hinokiflavone (Pawellek et al., 2017) lead to the retention of pA+RNA in nuclear bodies. For both classes of inhibitors, these retained pA+RNAs co-localize with SC35 in nuclear speckles, which were referred to as “enlarged speckles” (Carvalho et al., 2017), “pA+ bodies” or “megaspeckles” (Pawellek et al., 2017). Most of these observations are based on FISH experiments using either oligodT probes or probes that hybridize to introns of transgenic *Beta-globin* transcripts (Carvalho et al., 2017; Brody et al., 2011; Martins et al., 2011; Takemura et al., 2011; Pawellek et al., 2017). The *Beta-globin* mRNA is 1600 nt long and contains two short introns of around 150 and 800 nt. Therefore, *Beta-globin* mRNA does not reflect the characteristic features and mRNP compositions of a typical transcript in higher eukaryotes. It remained thus unclear whether pA+ bodies actually contain improperly spliced endogenous transcripts.

Our transcriptome wide data set enabled us to identify introns that were highly susceptible to the splicing inhibitor IsoG. From those we selected *Nip7* to visualize intron retention by FISH in the presence of the splicing inhibitor. We found that *Nip7* transcripts with retained intron 3 massively accumulated in enlarged nuclear speckles in a time-dependent manner and co-localized with pA+RNA. At the same time, bulk mRNA export of pA+RNA ceased over time. Our recovery experiments indicated that RNA sequestration and export block are reversible and point to a retention mechanism where the cell postpones mRNA export until the splicing stress is relieved, without degrading the transcripts. This is in agreement with studies, which demonstrated that some intron containing transcripts are stably retained in the nucleus and are post-transcriptionally spliced and subsequently exported upon various stimuli (Boutz et al., 2015; Braunschweig et al., 2014; Jacob & Smith, 2017). Regulated intron detention enables the cell to quickly respond to certain stress conditions and rapidly recover to physiological RNA homeostasis (Boutz et al., 2015). Although *Nip7* intron 3 was not previously described as being detained, further investigations are required to understand whether intron retention through splicing inhibitors follows the same pathways as intron detention.

The rapid decrease of the *Nip7* intronic signal upon splicing stress release could be due to post-transcriptional splicing or degradation of the intron-containing transcript. However, the steady decrease in the nucleus in combination with the restoration of the cytoplasmic pA+RNA signal pattern until

physiological distributions are reached, strongly suggests that sequestered intron-containing transcripts are post-transcriptionally spliced and subsequently released to the cytoplasm. Previous studies showed that a significant fraction of transcripts are still bound to active spliceosomes when they enter NS, suggesting that post-transcriptional splicing occurs within NS (Girard et al., 2012). In agreement with this, studies using Hinokiflavone or SSA reported that splicing factors and all five snRNPs associate with nascent transcripts prior to complex A formation and accumulate together with pA+RNA in ENS (Pawellek et al., 2017)(Roybal & Jurica, 2010). In contrast, splicing factors that assemble with the spliceosome after complex A formation were not affected in their localization (Pawellek et al., 2017), confirming that intron-containing pA+RNAs are loaded with pre-spliceosomal complexes and are retained in NS until splicing completion (Roybal & Jurica, 2010).

Release from nuclear retention is highly dependent on active splicing: studies using SV40 reporter transcripts clearly demonstrated that not the presence of introns, but the splicing activity is essential to release mature RNAs from NS (Ryu & Mertz, 1989; Valencia et al., 2008). In addition, post-transcriptional splicing was shown to release anchored transcripts from NS, since their nuclear export was up to 10-fold enhanced when the intron was removed by splicing (Luo 1999; Zhou et al. 2000; Masuda et al. 2005; Cheng et al. 2006; Dufu et al. 2010; Chi et al. 2013; Valencia, 2008).

It was claimed previously in several studies using different methodologies and splicing reporters that splicing inhibition retains incompletely spliced transcripts at the chromatin (Almeida et al., 2010; Martins et al., 2011). We find here that endogenous intron-containing transcripts after IsoG treatment accumulate in ENS, demonstrating that they are not sequestered at the chromatin. Our findings are in line with Martins and collaborators that showed that SSA treatment lead to a reduced polIII occupancy towards the 3'end of genes and an increased release of intron containing transcripts to the nucleoplasm (Martins et al., 2011). Moreover multiple pA+ FISH studies demonstrated that splicing inhibition by SMIs (Kaida et al., 2007; Carvalho et al., 2017), depletion of splicing factors or sequestration of snRNAs by antisense morpholinos (O'Keefe, 1994; Hett & West, 2014) lead to the accumulation of cleaved and polyadenylated transcripts in ENS. Further investigation describing the nuclear dynamics of pre-mature RNA, led to the assignment of NS as quality control hubs, through which all processed mRNAs transit prior to nuclear export (Girard et al., 2012; Dias et al., 2010; Ishihama et al., 2008).

NS are classified in two domains: while inactive splicing factors accumulate in interchromatin granule clusters (IGC), perichromatin fibrils (PFs) are sites of active transcription and co-transcriptional splicing (Mintz et al., 1999; Spector & Lamond, 2011). NS exhibit an irregular speckly geometry, which arises from the high cellular dynamics of stored processing factors (Kim et al., 2018; Fei et al., 2017; Fu & Maniatis, 1990). NS are organized in a shell shaped structure. While inactive splicing factors such as SR proteins and the long non-coding RNA (lncRNA) *Malat1* form the core, NS are surrounded by pA+RNA (Kim et al., 2018). Our FISH analysis revealed that the organization of ENS follows the same structure, but they have a rather round donut-like shape. This can be explained by the NS domain organization. When splicing is inhibited, the dynamics and activities of splicing factors decrease, and inactive splicing factors accumulate in IGCs leading to a shift from the PF structure towards the IGC structure, causing a round geometry. This is in line with numerous reports studying splicing inhibition by splicing factor knockdowns (Dias et al., 2010; Tripathi et al., 2012), snRNA depletion (Hett & West, 2014; O'Keefe, 1994) and small molecule inhibitors (Kaida et al., 2007; Carvalho et al., 2017; Pawellek et al., 2017; Fan et al., 2011). Although we cannot exclude that IsoG treatment causes a slight transcription inhibition, which could contribute to the round shape of ENS (Kim et al., 2019), microscopic assays, measuring the synthesis of nascent transcripts revealed that a treatment with the related flavonoid hinokiflavone does not affect polII transcription (Pawellek et al., 2017).

Not all pA+RNAs are sequestered in ENS. We found that *Malat1*, which is normally concentrated in NS (Tripathi et al., 2010), is excluded from NS in IsoG treated cells and thus exhibits the opposite behavior as pA+RNA. This suggests, that splicing factors, which bind massively to *Malat1* under normal conditions, are now occupied with pA+RNA within ENS and therefore can no longer bind to *Malat1*. Interestingly, a recent study reported, that treatment with the RNA processing and export inhibitor tubercidin in U2OS cells, also led to a redistribution of the lncRNAs *Malat1* and *Neat1* to the nucleoplasm (Hochberg-Laufer et al., 2019). Since tubercidin also caused an accumulation of mRNAs in nuclear speckles, the authors suggested that this redistribution is due to a displacement of *Malat1* by pA+ mRNAs. These and our results further suggests that splicing factors need to bind to pA+RNAs to stay in phase and to be able to concentrate within NS without aggregation.

In addition to a nuclear reorganization, we also observed the disruption of Cajal bodies in the presence of IsoG. This finding is in agreement with previous studies using other complex A inhibitors such as Madrasin and Hinokiflavone, where both treatments led to Cajal body disruption (Pawellek et al., 2017; Pawellek et

al., 2014). Cajal bodies are the processing factories of snRNPs. Since pre-mature spliceosomes are retained on incomplete spliced RNAs, one possible explanation is that Cajal bodies are disrupted due to lower amounts of snRNPs within those nuclear sites.

An alternative explanation could be pleiotropic effects of splicing inhibitors by influencing the cell cycle. The formation of Cajal bodies is highly cell cycle dependent. Cajal bodies disassemble in the mitosis phase and reappear again as multiple small foci in early G1 phase. It was previously shown that IsoG affects multiple proliferation pathways such as the NF-kappaB pathway (Zhou et al., 2011; Kwak et al., 2002). Furthermore, other complex A inhibitors have been shown to cause a massive cell cycle arrest in S/G₂ and M phase (Lagisetti et al., 2013; Sakai et al., 2002; Salton & Misteli, 2016; Pawellek et al., 2014).

Our FISH analysis revealed that a prolonged IsoG treatment (>16h) leads to the formation of smaller pA⁺ foci besides ENS. Similar bodies have recently been reported to form when HeLa cells were treated with Hinokiflavone in high concentrations and incubation times. Although we do not know which type of pA⁺RNA accumulates in these pA⁺foci, recent reports in human cells described similar nuclear foci upon depletion of the nuclear exosome (Fan et al., 2018; Silla et al., 2018). Knockdown of either the exosomal core subunit Rrp40, the catalytically active subunits Exosc10 and Exosc11 or depletion of the helicase Mtr4 caused the formation of such small pA⁺foci. These foci were distinct from other nuclear bodies such as NS, paraspeckles or Cajal bodies (Silla et al., 2018). We assume that the small pA⁺RNA foci that we observed at incubation times >16h upon IsoG are sites of exosomal decay. Either intron-containing transcripts are degraded only at later time points of IsoG treatment, or they are degraded all the time, but we only see pA⁺ decay foci, when the exosomal machinery is overwhelmed and decay targets accumulate. Under normal conditions exosomal decay is highly efficient and thus pA⁺ decay foci are not detectable. Two recent studies attempted to identify the RNA species content of these pA⁺ decay foci, but their findings were contradictory. Thus, it is currently not clear if unspliced mRNAs or rather other cryptic RNA species accumulate in these foci (Silla et al., 2018; Fan et al., 2018).

In conclusion, we show that pluripotent P19 cells are highly susceptible to the splicing inhibitor IsoG. We demonstrate that IsoG treatment leads to global intron retention with concomitant nuclear reorganization of nuclear bodies. ENS form reversibly and sequester intron-containing pA⁺RNAs until stress release. Studies using this inhibitor will thus provide new insights in the molecular mechanism of the interplay between splicing, export and nuclear surveillance.

6.2. The involvement of SRSF3 in nuclear splicing surveillance

Prior to their cytoplasmic export pre-mRNAs undergo extensive processing, which is tightly regulated by SR proteins (Cui et al., 2008; Müller-McNicoll et al., 2016; Lou et al., 1998). In particular, SRSF3 participates in multiple mRNA maturation processes such as pre-mRNA splicing and alternative polyadenylation and it modulates the nuclear export of numerous mRNAs by recruiting the export factor Nxf1 (Müller-McNicoll et al., 2016; Änkö et al., 2012; Botti et al., 2017). Thus SRSF3 connects mRNA processing to nuclear export and might also control the selective export/retention of improperly processed transcripts. Despite its essential role in mRNA processing and export very little is known about the role of SRSF3 in nuclear surveillance. In this thesis, we provide evidence that SRSF3 indeed monitors the splicing status of transcripts and likely inhibits the export of improperly processed mRNAs: i) SRSF3 accumulates together with intron-containing transcripts in ENS upon IsoG treatment; ii) SRSF3 binds close to IsoG-sensitive introns; iii) SRSF3 remains hyper-phosphorylated upon IsoG-treatment; iv) SRSF3 stays bound to RNA in its hyper-phosphorylated state; v) SRSF3 interaction with Nxf1 and numerous other mRNA export adaptors is strongly decreased when splicing is inhibited; vi) SRSF3 recruits Nxf1 to pA+RNA (Müller-McNicoll et al., 2016); viii) RNA binding of Nxf1 is reduced upon splicing inhibition; viii) SRSF3 interacts only with Nxf1 in its hypo-phosphorylated state; ix) Depletion of SRSF3 causes a partial export block.

Several studies have shown that SR protein activity and its interactome is highly phosphorylation dependent (Huang et al., 2004; Botti et al., 2017; Taniguchi et al., 2007; Hargous et al., 2006; Misteli et al., 1997; Duncan et al., 1998; Aubol et al., 2018b). SR proteins bind to nascent transcripts in their hyper-phosphorylated state and become hypo-phosphorylated during the splicing reaction (Keshwani et al., 2015; Ghosh & Adams, 2011; Zhou & Fu, 2013; Duncan et al., 1998). The increased SRSF3 phosphorylation levels upon IsoG treatment strongly suggest, that IsoG affects splicing catalysis, but not SRSF3 binding to the nascent transcript and thus the recruitment of the early pre-spliceosome complex E. In contrast, the RNA binding capacity of Nxf1 and its interaction with SRSF3 is strongly decreased upon splicing inhibition, which suggests that SRSF3 no longer recruits Nxf1 to the mRNP. In agreement with this finding, recent studies in *S. cerevisiae* demonstrated that the Nxf1 orthologue Mex67 and its adaptors exhibited reduced RNA binding capacities upon certain stress conditions and dissociate from the mRNAs leading to a global nuclear export block and nuclear retention of bulk pA+RNA (Zander et al., 2016; Saavedra et al., 1997a; Saavedra et al., 1996).

Hyper-phosphorylated SRSF3 promotes the recruitment of the U2 snRNP constituents such as the U2af2 and the SF3b1 complex during complex E formation *via* its RS domain. Its Nxf1 binding site is within the adjacent linker region. The decreased interaction of Nxf1 with hyper-phosphorylated SRSF3 could be due to the inaccessibility of the Nxf1 binding site as long as splicing associated factors bind to its RS domain. In agreement with this idea, we found that the SF3b1 and the U2af2 complex subunits are enriched in our SRSF3 interactome upon IsoG treatment. Furthermore, it has been shown that mRNAs are associated with pre-spliceosomal complexes when entering NS (Roybal & Jurica, 2010; Pawellek et al., 2014; Girard et al., 2012). Thus, pre-spliceosomes bound to immature mRNPs could prevent SRSF3 from interacting directly with Nxf1 (Cho et al., 2011), even though both proteins accumulate in ENS.

The decreased interaction of SRSF3 with Nxf1 along with its increased hyper-phosphorylation strongly suggests that a splicing dependent SRSF3 hypo-phosphorylation and the release of the spliceosome are essential for Nxf1 recruitment to the mRNP. In support to this model our co-immunoprecipitation experiments demonstrated, that only hypo-phosphorylated SRSF3 co-purified with Nxf1 under normal conditions. This is in agreement with previous studies, which showed that only hypo-phosphorylated SRSF1 and SRSF7 co-purified with Nxf1 (Hargous et al., 2006).

Nxf1 recruitment to its mRNA targets is dependent on export adaptors, which bind to the transcript at different maturation stages. One of the most studied export adaptor complexes that is recruited to the 5' end of transcripts early in the mRNA lifecycle is the TREX-1 complex (Chen & Carmichael, 2009). Accordingly, we found multiple TREX-1 complex constituents enriched in the SRSF3 interactome. Interestingly, in the presence of IsoG some TREX-complex subunits, such as the Tho complex or the associated factor UIF are highly decreased, while other subunits such as Uap56 or Alyref remained unchanged. This could be explained by the sequential association of the TREX subunits with the nascent transcript: while Uap56 and Alyref bind to the nascent transcript first, the ATPase activity of Uap56 stimulates the subsequent recruitment of the Tho complex. This suggests that IsoG impairs the assembly of the export machinery after Uap56 association and only inhibits the recruitment of the Tho complex or UIF. Indeed, both adaptors have been shown to be essential for Nxf1 recruitment. While UIF recruits Nxf1 by displacing Uap56 (Hautbergue et al., 2009), Thoc5 stimulates a conformational change of Nxf1 from an closed to an open conformation with elevated RNA binding capacity (Viphakone et al., 2012).

The exon junction complex (EJC) is deposited on exon junctions post-splicing and thus at a later step of pre-mRNA maturation (Kataoka et al., 2001; Kim et al., 2001; Le Hir et al., 2001; Stutz et al., 2000). Interestingly, EJC interactome studies revealed that EJC multimerizes with SR proteins and forms a mega-Dalton complex enclosing the mRNA. The authors of this study proposed that this formation promotes the compaction of the mRNP, protects the mRNP from exonucleolytic cleavage and stimulates mRNP export (Singh et al., 2012). Recent studies demonstrated that treatment with tubercidin caused the dissociation of EJCs from pA+RNAs and the retention of fully spliced mRNAs in NS (Hochberg-Laufer et al., 2019). This indicates that stable EJC association after splicing is essential for export competency and the release of mRNPs from NS. Our comprehensive SRSF3 mass spectrometry data confirmed that all nuclear EJC complex subunits, Magoh, Rbm8A and eIF4A3 were strongly decreased in SRSF3 mRNPs in line with impaired splicing. Furthermore, we observed that intronic pA+RNAs are retained in ENS upon IsoG treatment. The diminished interaction of SRSF3 and the EJC might contribute to an impaired recruitment of Nxf1 to the mRNPs and their retention in ENS.

Although our study solely focussed on the post-translational modification (PTM) phosphorylation, a recent study investigated the effect of bioflavonoids on protein SUMOylation and found that IsoG increases the sumoylation of multiple splicing factors, such as SRSF1, by inhibiting the SENP1 deconjugation reaction (Pawellek et al., 2017). Elevated SUMOylation of splicing factors, such as PRPF3 and SRSF1 has been associated with spliceosome assembly inhibition by preventing the recruitment of the U4–U6–U5 tri-snRNP (Pawellek et al., 2017; Pozzi et al., 2017). The increased SUMOylation of SRSF1 could for example interfere with the phosphatase activity of PP1. Impaired SR protein SUMO-deconjugation upon IsoG treatment could inhibit the PP1 release from its inactive N-terminal bound state, which keeps SRSF1 in a hyper-phosphorylated state. Our mass spectrometry data showed that SRSF3 interaction with Sumo3 is strongly increased upon IsoG treatment. This raises the possibility that SRSF3 might also be sumoylated under splicing stress conditions, which would hinder phosphatases such as PP1 to interact with the RS domain and instead remain inactive bound to the RRM domain. Surprisingly, we did not identify any phosphatases in our SRSF3 interactome. Since our SRSF3 IsoG timeline experiments reveal, that SRSF3 undergoes different phosphorylation states, the lack of phosphatases in our SRSF3 interactome is most likely due to their transient binding to SRSF3. This indicates that our stringent IP solely co-purifies with strong SRSF3 interactors, while transiently interacting proteins are lost and cannot be taken into account in our analysis.

6.2.1. SRSF3: Its role between exosomal decay and nuclear export

Several transcriptome-wide studies in yeast demonstrated that deficiently processed mRNAs are targeted by the nuclear exosome and degraded (Bousquet-Antonelli et al., 2000; Gudipati et al., 2012; Schneider et al., 2012; Almeida et al., 2011; Almeida et al., 2010; Bresson & Tollervey, 2018). Exosomal targeting is achieved by co-factors that recognize different RNA substrates and guide the degradation machinery to its targets (Meola & Jensen, 2017). All exosome co-factors were identified and characterized in yeast, but they are not conserved and differ in higher eukaryotes. Only very recently two co-factors have been described in higher eukaryotes, named Nuclear Exosome Targeting complex (NEXT) (Lubas et al., 2015; Andersen et al., 2013) and the poly(A) tail exosome targeting connection (PAXT) (Meola & Jensen, 2017; Meola et al., 2016), but so far it is not clear whether they target and degrade mis-spliced mRNAs.

Constituents of both the NEXT complex (Rbm7, Zcchc8, Ars2 and Zc3h18) and the PAXT connection (Zfc3h1, PABPN1, Zc3h3, Rbm26 and Rbm27) were identified by quantitative mass spectrometry experiments. These interactome data sets revealed, that NEXT and PAXT co-purify with multiple members of the SR protein family (Meola et al., 2016; Lubas et al., 2011; Lubas et al., 2015; Andersen et al., 2013) whereby SRSF3 was the most enriched interactor. The connection between exosomal co-factors and SRSF3 was further functionally characterized in a recent study. The authors demonstrated that binding of SRSF3 to viral intron-less mRNAs destabilized them by recruiting Rbm7 together with the NEXT complex to the RNA (Mure et al., 2018). Thus, SRSF3-binding marks certain RNA species for decay in a splicing-independent manner by stimulating the recruitment of the nuclear exosome, but it remained unclear whether this is also the case for cellular intron-less or intron-containing mRNAs. In agreement with previous studies, NEXT and PAXT complex constituents were also enriched in our SRSF3 interactome. However, the interactions with Rbm7, Zc3h18 and Pabpn1 were decreased upon splicing inhibition, suggesting that SRSF3 might not target intron-containing mRNAs for exosomal decay at this time-point (16h).

In the presence of small molecule splicing inhibitors, a fraction of intron-containing transcripts escape nuclear splicing surveillance. These transcripts leak to the cytoplasm and are efficiently translated (O'Brien et al., 2008; Kaida et al., 2007; Yoshimoto et al., 2017; Carvalho et al., 2017). This indicates that these intron-containing mRNAs are not targeted by the cytoplasmic surveillance machinery NMD. Thus their quality must be controlled prior to nuclear export *via* nuclear surveillance mechanisms. The retained

introns of these transcripts are rather short and have been shown to associate with the export adaptors Alyref or the Tho complex (Carvalho et al., 2017; Morris & Corbett, 2018). This suggests that these unspliced transcripts are considered export competent and are not actively retained in nuclear speckles.

But how are the mis-spliced transcripts with longer introns retained in ENS? RNA FISH experiments using an intron-containing GFP reporter gene revealed, that depletion of splicing factors such as U2af2 and U1-70K caused the cytoplasmic leakage of the unspliced RNA assigning these splicing factors a role in nuclear splicing surveillance (Takemura et al., 2011). Similar to other regulatory splicing factors, U2af2 and U1-70K contain a region with multiple arginine and serine repeats (Hedley et al., 1995; Takemura et al., 2011). These low-complexity regions have been shown to have high affinity to hyper-phosphorylated SR proteins such as SRSF1 (Cho et al., 2011; Yeakley et al., 1999). It is thought that the interaction of low-complexity domain-containing splicing factors such as U1-70K and U2af2 with SR proteins anchor them together with associated RNAs to NS (Takemura et al., 2011; Lai & Tarn, 2004; Yeakley et al., 1999; Cho et al., 2011) and thereby control the export of fully spliced transcripts *via* NS release. In agreement with these studies, we found that the interaction between U2af2 and SRSF3 increases upon IsoG treatment, which could indicate that the U2af2-SRSF3 interaction anchors transcripts in NS. However, we did not identify U1-70K in our SRSF3 mass spectrometry data set, neither in the absence, nor in the presence of IsoG. This indicates that the splicing factor, only interact with specific SR proteins such as SRSF1 or the interaction with SRSF3 is transient and can not be detected using stringent IPs.

We found SRSF3 highly enriched in ENS together with intron-containing RNAs. This suggests a mechanism, where SRSF3 retains improperly spliced RNAs in ENS and rather protects them from exosomal degradation. Indeed the nuclear exosome seems to target aberrant pA+RNAs at early steps of maturation before they enter the NS (Fan et al., 2018). NS shield these RNAs from exosomal targeting and/or degradation, allowing for post-transcriptional splicing and the assembly of export-competent mRNPs (Fan et al., 2018). This is in agreement with multiple studies, which reported that most mRNAs are stabilized and pass through NS prior to nuclear export (Visa et al., 1993; Huang et al., 1994; Carter et al., 1991; Mor et al., 2016; Akef et al., 2013; Dias et al., 2010).

In conclusion, we show for the first time that SRSF3 recruitment of Nxf1 is both splicing and phosphorylation dependent. These findings imply that SRSF3 mediates the interplay between pre-mRNA splicing and mRNA export. Hypo-phosphorylation of SRSF3 promotes the association of Nxf1 and triggers

nuclear export of export competent mRNAs while hyper-phosphorylated SRSF3 retains incomplete spliced transcripts in ENS, where they are shielded from exosomal decay to allow post-transcriptional splicing after splicing stress release.

6.3. Zc3h14: A novel export adaptor in higher eukaryotes

Studies in the last decade indicate that mRNA export in higher eukaryotes is more complex and is dependent on a larger pool of export adaptors compared to yeast (Wegener & Müller-McNicoll, 2018). These export adaptors can be responsible for the export of specific subset of transcripts. They are sensitive to certain cellular stimuli and could thereby selectively regulate gene expression. The identification of novel export adaptors and their RNA targets can provide new insights in the dynamics of post-transcriptional gene expression control.

We showed here that SRSF3 is a nuclear surveillance factor, which controls mRNA export by recruiting Nxf1 in a splicing dependent manner. When we screened the SRSF3 interactome data set for other potential splicing-dependent export adaptors, we identified Zc3h14 as one of the most affected interactors by splicing inhibition. Zc3h14 is the orthologue of Nab2, which is an essential export adaptor in *Saccharomyces cerevisiae*. Nab2 prevents exosomal decay by facilitating a rapid and efficient RNA export through the NPC (Tudek et al., 2018; Soucek et al., 2012). A recent study showed that Zc3h14 co-purified with the Tho complex in mouse brain (Morris & Corbett, 2018), indicating that the Zc3h14 export function might be conserved in higher eukaryotes. However, its role in mRNA export had not been studied so far.

We investigated a potential Zc3h14 export function in P19 cells by depletion experiments combined with pA+RNA FISH. We found that Zc3h14 knockdown leads to the retention of pA+RNA in the nucleus, although to a lesser extent when compared to Nxf1 depletion. Both, Nxf1 and Zc3h14 knockdowns, lead to the accumulation of pA+RNA at the nuclear rim. This phenotype is in agreement with confocal microscopy studies in HEK293 and HeLa cells upon Nxf1 depletion (Katahira et al., 2009; Viphakone et al., 2012) and its mutagenesis, respectively (Aibara et al., 2015). The accumulation of RNA at the nuclear rim could be based on the gatekeeper function of Tpr1 at the nuclear basket. Tpr1 associates with mRNPs co-transcriptionally and actively retains unspliced RNAs at the nuclear basket until splicing has been completed or export-incompetent mRNPs are loaded with sufficient Nxf1 export factors (Coyle et al.,

2011; Fasken & Corbett, 2016; Carmody et al., 2010; Galy et al., 2004). In contrast, SRSF3 depletion results in pA+RNA accumulation in NS, which is in agreement with previous studies and a common phenotype when splicing is impaired (Fei et al., 2017; Escudero-Paunetto et al., 2010). The distinct phenotypes of SRSF3 and Zc3h14/Nxf1 depletion indicate that SRSF3 acts earlier in the pathway of export competency control or that NS speckle release is also controlled by other factors, such as retention factors. The recruitment of Zc3h14 and Nxf1 by hypo-phosphorylated SRSF3 might be important later to pass the final nuclear checkpoint at the NPC, prior to nuclear exit. Since this retention mechanism is the final quality check point in the nuclear mRNA life cycle and is coupled to Nxf1 facilitated export, Nxf1 depletion causes an inefficient nuclear export due to the lack of an export-competent “label” and could lead to an active transcript sequestration by Tpr1 interaction (Wegener & Müller-McNicoll, 2018).

In Zc3h14 depleted cells we observed a similar phenotype, suggesting that Zc3h14 is required for mRNA translocation through the NPC similar to Nxf1. Interestingly, its orthologue Nab2 has been shown to interact with Mex67, nucleoporins, Gfd1 and Mlp1 and thereby stimulates conformational changes within the NPC and direct mRNPs to the cytoplasmic face (Green et al., 2003; Fasken et al., 2008; Suntharalingam et al., 2004; Zheng et al., 2010). Additionally, Nab2 depletion in yeast displays a similar phenotype causing accumulation of pA+RNA at the nuclear basket, which suggests a conserved export function of Zc3h14 in eukaryotes (Green et al., 2002; Chekanova et al., 2001).

A high shuttling capacity has been shown to be a common feature of multiple factors involved in export (Botti et al., 2017). Indeed, our HKA assays demonstrate that Zc3h14 has a highly shuttling capacity, which is comparable to Nxf1 and SRSF3. Moreover, our comparative HKA analysis revealed, that Zc3h14 and Nxf1 shuttling dynamics are highly sensitive to splicing inhibition by IsoG. This supports our finding that Zc3h14 is a potential export adapter that may co-shuttle with Nxf1 and SRSF3.

Our transcriptome wide analysis of Zc3h14 depleted cells revealed, that the levels of thousands of transcripts were decreased. This decrease is not due to a normalization artifact as we used ERCC Spike-ins for normalization in our RNA-seq experiment. In contrast, we observed only a minor export defect in our RNA-FISH experiments upon Zc3h14 depletion. **Global down-regulation of transcript abundance can be either due to an inhibition of transcription or due to a decreased RNA half-life.** Recent studies in *S. cerevisiae* described the global mRNA loss upon Nab2 depletion and showed that Nab2 plays a crucial role in mRNA half-life by protecting mRNAs from exosomal decay rather than affecting polII transcription

(Schmid et al., 2015). In higher eukaryotes the involvement of Zc3h14 in transcription or mRNA half-life control is not known. But interestingly, Zc3h14 co-purifies with Zfc3h1, the core protein of the exosomal adapter complex PAXT (Meola & Jensen, 2017), suggesting it might function in exosomal decay. Depletion of PAXT subunits increased the stability of snoRNA host genes (SNHG), an RNA species, which is heavily polyadenylated. However, we observed that Zc3H14 depletion rather decreased mRNAs globally.

Although we do not understand the discrepancy between the RNA-seq and pA+FISH data, one possibility would be that Zc3h14 depletion globally blocks mRNA export, but the retained mRNAs do not accumulate in the nucleus because they become unstable. Transcript instability could be due to extended polyA tails (Jensen et al., 2001). Indeed Zc3h14 was proposed to function in polyA-tail length control. Using polyA assays in mouse neuroblastoma cell lines, cortex, hippocampus and liver tissue previous studies have shown that Zc3h14 depletion result in polyA tail lengthening (Rha et al., 2017; Pak et al., 2011).

Although, we found a large overlap between Nxf1 and Zc3h14 regulated targets, nearly six thousand transcripts are downregulated independent from each other. This suggests that i) Zc3h14 depletion has pleiotropic effects and decreases the half-life of RNAs of non-Nxf1 targets; ii) the Nxf1 export function is not exclusively dependent on Zc3h14 and is rather restricted to a smaller subset of transcripts; or iii) the differences are due to differences in data analysis. Export adaptors in higher eukaryotes have been shown to facilitate the export of subsets of mRNAs involved in specific cellular processes (Yamazaki et al., 2010; Tran et al., 2014; Katahira et al., 2009; Wang et al., 2013). For instance, the AREX complex has been shown to facilitate the export of a small subset of transcripts, which are distinct from TREX complex targets. Gene ontology analysis revealed that these AREX targets are highly enriched in cell cycle regulation and mitosis (Yamazaki et al., 2010). Similarly, our GO-term analysis suggested that transcripts that were down-regulated upon Zc3h14 depletion were enriched for DNA repair, mRNA processing, mitotic cell cycle regulation and chromatin modification.

Using subcellular fractionation RNA-seq (FRAC-seq), we aimed to globally identify Zc3h14 export targets. Unfortunately, metablots (data not shown) to evaluate the quality of the RNA-seq data set pointed to a partial degradation towards 3' and 5' end of transcripts in the nuclear and cytoplasmic fraction, which made an analysis of differential gene expression in these fraction unreliable. However, the FRAC-seq browser shots were used as an indication if Zc3h14 regulated genes display an export phenotype. Using a combination of quantitative PCR and confocal microscopy, we confirmed that five Zc3h14 targets down-

regulation is accompanied with an impaired nuclear export, indicating that the decrease of Zc3h14 targets are caused by nuclear export deficiencies.

Our cell proliferation assays showed that the doubling time of P19 cells is significantly decreased upon Zc3h14 depletion. This phenotype is in line with depletion studies of other export adaptors; e.g. Uap56 depletion has been shown to cause a premature sister chromatid separation, while Urh49 knock down led to chromosome arm resolution defects (Yamazaki et al., 2010). In addition, we found that Zc3h14 Oex strongly decreases the cell size, increases P19 cell proliferation and we observed an increase of total mRNA target levels upon Zc3h14 Oex. Quantitative PCR experiments revealed that this increase is mainly found in the cytoplasmic fraction, indicating a highly efficient mRNA export when Zc3h14 protein levels are high. In contrast, we did not observe a significant change of the pA+RNA signal in subcellular compartments in Oex cells, likely because Zc3h14 facilitates the export of a subset of transcripts. These subsets could not be detectable in polyA FISH experiments, where bulk polyA RNA is labeled. We additionally observed elevated levels of Zc3h14 targets in the nuclear fraction of Oex cells. This can be explained by two mechanisms: i) Zc3h14 Oex stimulates transcription and the synthesis of its RNA targets, or ii) high Zc3h14 levels increase the stability of its targets by modulating their polyA tail length. Although we have no evidence for either scenario, in yeast it was shown that Nab2 controls polyA tail length and thereby regulates mRNA export and exosomal decay (Hector et al., 2002; Soucek et al., 2012; Soucek et al., 2016). Nab2 mutants with low RNA-binding affinity caused polyA tail extension in transcripts, which lead to their nuclear retention and decreased stability due to the stimulation of exosomal decay (Hector et al., 2002; Marfatia et al., 2003). On the other hand, Nab2 overexpression rescued mRNA export deficient mutants and inhibited hyper-adenylation (Gallardo et al., 2003; Hector et al., 2002). polyA tail length greatly influences the export potential of mRNAs. Transcripts with short polyA tails are efficiently exported, while transcripts with long polyA tails are nuclear retained and/or highly unstable (Fuke & Ohno, 2007; Gudde et al., 2017). polyA tail length control by Nab2 might be conserved among eukaryotes, since studies in mouse brain have shown that Zc3h14 functional depletion causes polyA tail lengthening (Rha et al., 2017; Pak et al., 2011), albeit only to a small extent. However, the export function of Zc3h14 might be cell type- specific: Microarray studies in human breast adenocarcinoma cells (MCF7) revealed that only 1% of the analyzed genes (171 genes) were differentially expressed upon Zc3h14 knock down with the majority being up-regulated (Morris & Corbett, 2018), which is in contrast to our findings. Cell type specificity of Zc3h14 was suggested previously, as its expression levels differ strongly between tissues with the highest concentrations in testes and the brain (Leung et al., 2009; Rha et al., 2017; Kelly et al., 2012;

Pak et al., 2011), and in particular in the hippocampus, cerebral cortex and cerebellum (Rha et al., 2017; Kelly et al., 2012; Pak et al., 2011). The expression levels of Zc3h14 in breast cancer cells are much lower compared to testes tissue. In addition, induced pluripotent stem cells exhibit a higher expression profile, compared to differentiated cells (Lin et al., 2011), which suggests that Zc3h14 depletion might have a superior impact in P19 cells compared to MCF7 cells (Morris & Corbett, 2018). Interestingly, genes, which were regulated by Zc3h14 in MCF7 cells displayed also export deficits, which resembles our FRAC-seq, qPCR and FISH results.

Fluorescent *in situ* hybridization (FISH) studies in *Schizosaccharomyces pombe* (Grenier St-Sauveur et al., 2013), *Drosophila melongaster* (Pak et al., 2011) and mammalian cells (Kelly et al., 2014) that were treated with Zc3h14 siRNAs showed little or no accumulation of pA+RNA in the nuclei. Similarly, our FISH experiments revealed only slight changes in the distribution of pA+RNA signal. However, quantification of signal intensities in more than 100 cells showed that pA+RNAs are significantly enriched in the nucleus. FISH quantification was not performed in the previous studies and conclusions were drawn from representative cell images. The analysis of a high number of cells is crucial for knockdown FISH experiments, since Zc3h14 might not be efficiently depleted in the selected cells (Kelly et al., 2014).

Using iCLIP, we characterized for the first time the *in vivo* binding landscape of Zc3h14 in mouse cells. Initially, we found that the majority of the iCLIP library reads did not map to the genome. Since Zc3H14 is suggested to be a polyA binding protein, we used a previously described approach to confirm the preferential binding to A-rich regions. Hildebrandt and collaborators recently demonstrated that Makorin 1 (MKRN1) binds to polyA tails by quantifying the A-content of unmapped reads obtained from MKRN1 iCLIP data (Hildebrandt et al., 2019). The A-content of MKRN1 unmapped reads was significantly higher compared to other RNA binding proteins. Strikingly, the A-content of Zc3H14 unmapped reads was even higher than of MKRN1. This result, in combination with the binding motif of Zc3h14 (AAA/TAA) confirmed that this protein binds preferentially polyA tails and polyA stretches in higher eukaryotes *in vivo*. Analysis of Zc3h14 binding in genomic regions showed a major binding to 3'UTRs and to ORFs. The enriched 3'UTR binding could be due to the high A-content in this transcript region. This idea is supported by a microarray analysis, which revealed that Nab2 targets exhibit enriched intragenic polyA-stretches (Kim Guisbert et al., 2005).

6.3.1. Zc3h14 facilitates the export of cell cycle regulators

In this study, we identified thousands of Zc3h14 regulated targets. Many of these targets are involved in cell cycle regulation and related bioprocesses. We validated five of those targets and confirmed that their expression levels and cytoplasmic abundance is highly dependent on Zc3h14 protein levels. These targets were selected according the following criteria: I) highly regulated upon Zc3h14 depletion in the RNA-seq data, II) increased nuclear and decreased cytoplasmic read coverage in the FRAC-seq data, III) intermediate expression levels, IV) Zc3h14 binding sites according to Zc3h14 iCLIP-seq data, and V) known function in cell cycle regulation. In this section, we discuss the functions of the five validated Zc3h14 targets and their impact on cellular growth and proliferation.

Smc4 (structural maintenance of chromosomes) codes for the SMC4 protein, a conserved ATPase, which is part of the Condensin enzyme complex. The Condensin complex is composed of SMC4, SMC2, a Kleisin subunit (Brn1/chromosome-associated protein H CAP-H), and two HEAT repeat-containing subunits (Ycg1/CAP-G and Ycs4/CAP-D). This complex is essential for the compaction of chromatin in the interphase of the cell cycle. Chromosomal rearrangement is a complex process, which determines the successful entry into mitosis and correct chromosomal segregation. SMC4 expression levels have been shown to be tightly regulated in normal conditions and during the cell cycle (Wei-Shan et al., 2019). During mitosis, SMC4 is highly expressed while it decreases massively in the interphase (Takemoto et al., 2004; Thadani et al., 2018). In embryonic stem cells, SMC4 has been shown to control the pluripotent gene expression profile by altering the chromatin structure and thereby maintains the stem cell identity (Fazio & Panning, 2010; Fazio et al., 2008; van Bortle et al., 2014). Disturbances in SMC4 expression levels lead to aberrant cell division and accelerated growth (Feng et al., 2014; Jiang et al., 2017; Palou et al., 2018; Zhou et al., 2012). Accordingly, SMC4 is considered a pro-oncogene, and its overexpression has been reported in a variety of cancers, such as hepatocellular carcinoma, glioma and lung adenocarcinoma, and is correlated with poor prognosis and tumor aggressiveness (Jiang et al., 2017; Shen et al., 2019; Zhang et al., 2016a). Although the mechanism is not clear, it has been shown that SMC4 overexpression leads to increased proliferation and tumor de-differentiation (Jiang et al., 2017). Concordantly, SMC4 down-regulation in skin fibroblasts led to rapid senescence and diminished proliferation potential. Knockdown of SMC4 also led to decreased proliferation and migration of normal and cancer cells (Meng et al., 2018).

Fmr1: The fragile X mental retardation 1 codes for FMRP. This RBP is ubiquitously expressed but shows high expression in brain, testes, and ovaries (Ferder et al., 2013). It binds to numerous synaptic mRNAs

involved in neuronal maturation, proper synaptic signaling and plasticity (Darnell et al., 2011; Richter et al., 2015), and controls their translation by ribosome stalling (Darnell et al., 2011). Upon certain neuronal stimuli, FMRP is de-phosphorylated (Ceman et al., 2003; Narayanan et al., 2008; Muddashetty et al., 2011), dissociates from polysomes and thereby allows the synthesis of synaptic transcripts. In the absence of FMRP, total protein synthesis in the hippocampus is increased by nearly 20% and thus result in different neuronal diseases (Udagawa et al., 2013; Dölen et al., 2007; Qin et al., 2013; Muddashetty et al., 2007; Weiler et al., 2004). The fragile X syndrome (FXS) is an inherited form of intellectual disability (ID) frequently associated with a broad spectrum of autistic phenotypes such as intellectual, cognitive, and social deficits (Bhakar et al., 2012; Santoro et al., 2012) and causes developmental problems including learning disabilities and cognitive impairment (Bassell & Warren, 2008). FXS is caused by triplet repeat expansion of up to 200 polymorphic CGG repeats in the 5' UTR of *Fmr1* exon 1 (Nelson et al., 2013). These repeats are methylated, leading to the inactivation of the gene and the loss of FMRP (Nelson et al., 2013). FMRP has been shown recently to physically and functionally interact with the Zc3h14 orthologue dNab2 in *Drosophila melanogaster* (Bienkowski et al., 2017). This study showed that FMRP and dNab2 mRNA targets overlap. In addition, FMRP restricts polyA tail length in a similar manner as dNab2 and strikingly rescues a rough eye phenotype caused by dNab2 transgenic expression, which demonstrate their tight cross-regulation (Bienkowski et al., 2017).

Kif20b: The vertebrate-specific Kinesin-6 (also called MPHOSPH1 or MPP1) is one of the three members of the Kinesin-6 family and plays an essential role in regulating cytokinesis in the late telophase of mitosis (Abaza et al., 2003; Janisch et al., 2018; Janisch et al., 2013; Kanehira et al., 2007). It controls the cytokinetic furrow ingression and the separation of the cytoplasm between the daughter cells, which are connected through an intercellular bridge. During the last step of the cytokinesis KIF20B aids in the maturation of midbodies. Midbodies form during final stages of cytokinesis and are rich in microtubules that are stabilized by KIF20B (Janisch et al., 2018). In ESCs KIF20B expression levels are tightly regulated by Symplekin, which together with Oct4 control stem cell pluripotency expression profiles (Yu et al., 2019). *Kif20b* knockdown disrupts cellular polarization and cells display cytokinetic defects leading to the accumulation of apoptotic multinucleated cells (Georges et al., 2019). Furthermore, KIF20B loss of function mouse mutants have been shown to display a decreased cerebral cortex, with a reduced number of neurons and neuronal progenitors (Janisch et al., 2018; Kanehira et al., 2007; Chavoshi et al., 2016; Scolnick & Halazonetis, 2000).

So far, very little is known about the *Ccdc25* (Coiled-Coil Domain Containing 25) gene. *CCDC25* overexpression has been reported in cholangiocarcinoma (CCA) tissue samples (Proungvitaya et al., 2017). Protein interaction predictions showed that this protein interacts with the endothelial growth factor (EGFR) signalling pathway, which is responsible for cellular proliferation and migration. Accordingly, CCA cells with overexpression of *CCDC25* displayed fast growth and migration potential (Proungvitaya et al., 2017).

Septin 7 (SEPT7) is an important member of the septins family. It co-purifies in different septin complexes and is associated with diverse cellular processes in human cells (Wang et al., 2018). Septins are GTP binding proteins that form homo and heterodimers, which leads to the formation of filament structures (Sirajuddin et al., 2007). SEPT7 filament formation has been associated with chromosome assembly and mitosis progression. Loss of SEPT7 expression leads to chromosome mis-segregation and loss of the centrosome-associated protein E (CENP-E). Interestingly, SEPT7 not only plays a role in the mitotic spindle assembly, but additionally functions as a mitosis check point. Its depletion triggers the mitosis arrest response by activation of the mitotic arrest deficient protein 2 (Mad2) (Zhu et al., 2008). SEPT7 is also an essential protein in neurons and has been shown to be the most highly expressed septin in rat neurons (Peng et al., 2004). SEPT7 is expressed in all developmental neuronal stages and localizes at the bases of filopodia and at branch points in developing hippocampal neurons. SEPT7 down-regulation leads to impaired dendrite branching and elongated spines in developing hippocampal neurons (Xie et al., 2007). Mechanistically, SEPT7 phosphorylation by the TAOK2 kinase leads to its translocation to neuronal spines where it promotes dendritic spine maturation (Yadav et al., 2017). In addition to SEPT7 functions in neurons, this protein has been described to be important for axonal myelination. Schwann cells deprived of SEPT7 exhibit disorganization of the actin cytoskeleton and are not able to wrap around the axons (Roth et al., 2013). In agreement with the important roles of SEPT7 in neuronal cells and neuronal synapse formation and maintenance, SEPT7 de-regulation has been associated with a variety of neuronal diseases. Down-regulation of SEPT7 was described in patients with schizophrenia, neuropsychiatric systemic lupus erythematosus (NPSLE) and mouse models of early Alzheimer's disease (Zhu et al., 2008).

6.3.2. Zc3h14 export activity is splicing and SRSF3 dependent

Pre-mRNA splicing highly differs between higher eukaryotes and yeast. More than 95% of human genes contain introns. Human genes contain on average 9 exons, which can be all alternatively spliced (Lander

et al., 2001). This is in stark contrast to the genome of *Saccharomyces cerevisiae*, which contain only around 250 introns in 6,000 genes (4%) (Parenteau et al., 2008). In *S. cerevisiae* only six genes have two introns, what makes alternative splicing events very rare (Ast, 2004). Apart from occurring much more frequently in higher eukaryotes, the mechanism of splicing and its regulation also differs from yeast: First, the recognition of exons/introns is achieved *via* an interplay across exons and/or introns termed exon or intron definition respectively. While the splice site recognition in yeast is achieved *via* intron definition, exon definition is thought to initiate splicing in higher eukaryotes (Ast, 2004). The reason for that is the relatively short introns in yeast (40-75 nt in *S. pombe*; ~270 nt in *S. cerevisiae* (Ast, 2004), which enables a communication network across the intron, while in higher eukaryotes introns are much longer (5,000-6,000 nt in *homo sapiens* (Abebrese et al., 2017)) and splicing interactions evolved rather across the relatively short exons (~120 nt in *homo sapiens* (Abebrese et al., 2017)). Second, in higher eukaryotes splice site recognition is regulated by numerous splicing factors such as SR proteins, which bind to exonic/intronic splicing enhancer/silencer and thereby regulate alternative splicing by strengthening or weakening splice sites. SR proteins are either not present or are poorly conserved in yeast. Instead, the splice site recognition is achieved *via* perfect base pairing of the U1 snRNP to the highly conserved 5'ss (Keren et al., 2010; Conti et al., 2013). Third, yeast lack nuclear speckles, which are highly enriched in splicing factors and serve as a quality hub for final RNA maturation processes, such as post-transcriptional splicing (Potashkin et al., 1990). Fourth, nuclear export and decay is linked to transcription in yeast (Jensen et al., 2001), while nuclear export in higher eukaryotes is interconnected to pre-mRNA processing events such as splicing (Wegener & Müller-McNicoll, 2018). The mechanistical and functional discrepancy of splicing between yeast and higher eukaryotes suggest that splicing surveillance pathways that couple splicing and mRNA export most likely differ (Wegener & Müller-McNicoll, 2018).

In this study we showed, that SRSF3 hypo-phosphorylation upon splicing completion is important for the recruitment of export factors/adaptors, and thereby couples pre-mRNA splicing to mRNA export. iCLIP analysis showed that the binding landscape of Zc3h14 is affected by splicing inhibition. We found that Zc3h14 RNA binding generally decreases. Interestingly, binding to ORFs decreases and is likely shifted towards 3'UTR and polyA tail binding. This is evidenced by the exclusively adenosine containing 5-mer motif and the increased number of unmapped reads with high A-content. We validated the decreased RNA binding capacity of Zc3h14 upon IsoG treatment using comparative RNA binding assays and found that this decrease is comparable to Nxf1. In line with this, the Zc3h14 shuttling capacity is also affected by IsoG. Our shuttling assays showed that shuttling of Zc3h14 is highly sensitive to IsoG as it dramatically

decreases already at early time points of splicing inhibition. This indicates that Zc3h14 export targets seem to be highly susceptible to inhibition of splicing. Surprisingly, Nxf1 and SRSF3 shuttling is more robust and less sensitive to splicing inhibition at early timepoints.

Since SRSF3 RNA binding is not affected by IsoG treatment, we speculated that SRSF3 recruits Nxf1 and Zc3h14 to its targets. In support of this idea, comparative iCLIP of SRSF3 and Nxf1 identified an overlap of the binding sites of Nxf1 and SRSF3 and a similar binding motif in last exons. Moreover overexpression of SRSF3 enhanced the RNA binding of Nxf1 (Müller-McNicoll et al., 2016). SRSF3 and Zc3h14 do not share the same binding motif in last exons, since the Zc3h14 binding motif is dominated by A-stretches. However, we show here that SRSF3 and Zc3h14 interact RNA-independently and that this interaction decreases upon IsoG treatment. Moreover, the RNA binding capacity of Zc3h14 decreases upon IsoG treatment. SRSF3 depletion also caused a strong decrease of Zc3h14 RNA binding capacity, which demonstrates that the recruitment of Zc3h14 to the mRNP occurs in a SRSF3- and splicing-dependent manner.

We further investigated the molecular mechanism of Zc3h14 recruitment by SRSF3 using Co-immunoprecipitation assays and found that Zc3h14 exclusively interacts with hypo-phosphorylated SRSF3 in a similar manner as Nxf1. This interaction is lost upon splicing inhibition, which explains the decreased RNA binding capacity of Zc3h14 in this condition. Nxf1 co-purifies with Zc3h14 and *vice versa*, in an RNA-independent manner, which strongly suggests that both proteins associate with the same mRNPs. Studies in yeast described that Nab2 export activity is also dependent on TREX-1 and Mex67 (Nxf1) (Soucek et al., 2012). However, in yeast the Nab2-Mex67 pathway promotes the export of bulk pA+RNA, indicating that the pathway *per se* is conserved, while its targets are distinct in higher eukaryotes (Soucek et al., 2012). We speculate that the discrepancy between Nab2 and Zc3h14 export specificity is achieved through SRSF3-dependent recruitment. Since SR proteins are not present in yeast, monitoring of the splicing through SRSF3 phosphorylation state as well as SRSF3 recruitment of export adaptors to specific and fully processed targets is absent. Taken together, our findings indicate that Zc3h14 facilitates the export of a subset of transcripts *via* the Nxf1 export pathway; still it remains unclear how pA+RNA is released from NS as well as whether SRSF3 recruits both proteins Zc3h14 and Nxf1 together or independently to overcome a final quality control at the nuclear rim.

6.4. The role of Zc3h14 and SRSF3 export function in neurological diseases

Although the functions of Zc3h14 in higher eukaryotes have been described in only few studies, loss-of-function mutants and decreased Zc3h14 expression levels have been connected to multiple neurological disorders such as non-syndromic autosomal recessive intellectual disability (ARID) (Pak et al., 2011) and Alzheimer's disease (AD) (Guthrie et al., 2011). So far, the functional contribution and the molecular mechanism of Zc3h14 causing those disorders is limited to *in vitro* studies using polyadenylation assays presenting minor shifts of polyA tail extension of total RNAs (Rha et al., 2017). In this study we elucidate the Zc3h14 function and propose an export model, which could aid to understand the cause of several diseases.

Patients suffering from FXS or SEPT7 associated AD and neuropsychiatric systemic lupus erythematosus (NPSLE) show the same disease symptoms as patients expressing a truncated Zc3h14 isoform (Pak et al., 2011; Guthrie et al., 2011; Bassell & Warren, 2008; Zhu et al., 2008). Since we found that *Fmr1* and *Sept7* export is facilitated *via* Zc3h14, the disease pattern and loss of normal synaptic plasticity of patients expressing a mutated Zc3h14 form, could be due to secondary effects and an impaired export of *Fmr1* and *Sept7*.

Zc3h14 export target associated diseases seem to preferentially affect neurodevelopmental disorders, which correlates with the high tissue specific expression of Zc3h14 in the hippocampus (Rha et al., 2017; Pak et al., 2011), suggesting that Zc3h14 export activity should have a great impact in neuronal cells. Neurons display a specific gene expression signature, which is characterized by a cell cycle arrest at the S-phase (Felfly et al., 2011). Since our data point out, that the expression of numerous cell cycle regulators is controlled by the Zc3h14 export activity, a loss-of-function mutant of Zc3h14 could dysregulate the cell cycle maintenance and modify the neuronal expression profile.

SRSF3 plays an important role in pluripotency maintenance and regulates cellular reprogramming of induced pluripotent stem cells (iPSC) (Ratnadiwakara et al., 2018). Its expression levels sequentially increase during iPSC reprogramming leading to a stimulated export of essential pluripotency factors (Ratnadiwakara et al., 2018). Thus, a dysregulation of SRSF3 expression levels might cause deficits in the neuronal differentiation and cause a variety of neurodevelopmental defects. Indeed, SRSF3 has been

implicated in AD by regulating the splicing of *Trkb* to generate the *TrkB-Shc* transcripts, one driver of the disease (Majerciak et al., 2014). Moreover, SRSF3 has been shown to be involved in cell cycle progression (Shirahata-Adachi et al., 2017; He et al., 2011). Its expression profile correlates with cellular growth rates and has been shown to be elevated in various cancer types (He et al., 2011; Ibrahim et al., 2005; Ibrahim et al., 2014). With regards to our findings, SRSF3 dependent cell cycle dysregulation and tumor initiation could be at least partially due a mis-regulated recruitment of export adaptors causing elevated cellular proliferation rates.

In the last decade numerous studies demonstrated, that pathogenesis could be at least partly due to an impaired export of disease driving transcripts. Lethal congenital contracture syndrome (LCCS) and lethal arthrogryposis with anterior horn cell disease (LAAHD) describe a series of autosomal recessive genetic disorders leading to early fetal death, characterized by a degeneration of motoneurons in the spinal cord (Folkmann et al., 2014; Narkis et al., 2007; Nousiainen et al., 2008). Both diseases have been assigned with a genetic mutation of *Gle1* intron 3, which generates a cryptic 3' splice site (Nousiainen et al., 2008). *Gle1* is an essential export associated factor in the Nxf1 pathway and facilitates tethering of the mRNP to the NPC by interacting with CG1 and Nup155 (Rayala et al., 2004; Kendirgi et al., 2005). Interestingly, the *Gle1* yeast orthologue has been shown to control mRNA export by interacting with Nab2. Furthermore, after the cytoplasmic mRNP translocation, the ATP-dependent RNA helicase Dbp5 is activated by *Gle1* and promotes the dissociation of Nab2, Mex67 and other export (associated) adaptors/factors (Tran et al., 2007; Lund & Guthrie, 2005). Although it is not known if the Nab2 and *Gle1* interplay is evolutionary conserved, *Gle1* mutations could cause an impaired recruitment and/or a defective dissociation of Zc3h14 from the mRNP. In addition, we found *Gle1* among Zc3h14 regulated targets indicating an involvement of Zc3h14 in LCCS associated diseases.

Multiple diseases are caused by triplet repeat expansions, such as oculopharyngeal muscular dystrophy (OPMD) (Raz & Raz, 2014), myotonic dystrophy type 1 (DM1) (Pettersson et al., 2015) and the huntington's disease (HD) (Mezer et al., 2011). These triplet repeats cause the formation of insoluble aggregates or cytotoxic foci and sequesters multiple pre-mRNA processing and export factors such as SR proteins and Pabps (Raz & Raz, 2014). This sequestration leads to mis-processing and nuclear retention of numerous transcripts. Although SRSF3 and Zc3h14 have not been identified in those aggregates, we identified *Mbnl1* among the Zc3h14 regulated targets. Since previous studies showed, that *Mbnl1* disrupt these cytotoxic

foci (Sun et al., 2015), Zc3h14 deficient cells could display reduced Mbnl1 expression levels and increased nuclear aggregate formation.

7. Conclusion and outlook

Isoginkgetin is a potent splicing inhibitor in pluripotent P19 cells and causes the retention of thousands of introns due to the impairment of the spliceosome assembly. Incompletely spliced intron-containing RNAs are cleaved and polyadenylated and are sequestered in enlarged nuclear speckles (ENS). Since the formation of these ENS is reversible, the cell is able to rapidly respond to stress release and post-transcriptionally splice sequestered mRNAs and return to cellular homeostasis. Post-transcriptional splicing implies a high stability of intron-containing transcripts. To investigate if the stability of transcripts, which are retained in ENS is affected, mRNA half-life studies could be performed. In addition, a depletion of catalytic exosomal subunits should not influence the abundance of ENS sequestered mRNAs. We show that SRSF3 remains bound to intron-containing transcripts and accumulates in ENS upon splicing inhibition. However, the SRSF3 interactome is altered and is characterized by a decreased interaction with mRNA export adaptors/factors as well as exosomal co-factors, which supports the activation of a retention pathway rather than a decay pathways as surveillance mechanism in response to splicing stress.

Our IsoG SRSF3 interactome led to the identification of Zc3h14 as a novel export adaptor. Zc3h14 is recruited to the mRNP *via* SRSF3 in a splicing dependent manner. Our global transcriptome analysis identified thousands of transcripts that are down-regulated upon Zc3h14 depletion. Zc3h14 targets show a large overlap with Nxf1 export targets. In addition, Zc3h14 and Nxf1 interact in an RNase independent manner, which strongly suggest that they are acting in the same export pathway. We confirmed for five Zc3h14 targets that their nuclear export is impaired when Zc3h14 is depleted. However, we currently do not know if all transcripts that are affected by Zc3h14 depletion are impaired in their nuclear export. A transcriptome-wide analysis of subcellular fractions could identify all Zc3h14 export targets and reveal whether Nxf1 and SRSF3 export targets overlap.

Our data revealed for the first time the *in vivo* binding landscape of Zc3h14. Zc3h14 shows enriched binding within 3'UTRs with a preference for polyA tails and polyA stretches. Upon splicing inhibition, the

Zc3h14 RNA binding capacity is decreased accompanied with a loss of RNA binding specificity and preferential association to polyA tails. In light of the function of Zc3h14 to control the length of polyA tails, an impaired export could be due a dysregulation of polyA tail length. Further studies could be performed to elucidate whether splicing inhibition affects the polyA tail length. Since IsoG treatment decreases the RNA binding capacity of Zc3h14, splicing inhibition might mimick the effect of Zc3h14 knock down - an impaired export of its targets. Depletion of Zc3h14 is usually accompanied with polyA tail lengthening, but it is currently not clear if prolonged polyA tails are cause or effect of impaired mRNA export. To uncouple polyA tail length control and mRNA export, co-depletion of other polyA tail regulators, such as Pabpn1, which has been shown to lead to polyA tail shortening, could rescue the polyA tail lengthening and clarify if Zc3h14 export functions are independent to its activity in polyA tail length control.

Nab2 has been shown to be phosphorylated upon cellular stress and dissociate from the mRNP. Since our data reveal that Zc3h14 also dissociates from the mRNP upon splicing stress, an analysis of post-translational modifications, such as phosphorylation, methylation or sumoylation of Zc3h14 and Nxf1 could serve as an additional explanation for the impaired association of both factors.

Patients with ARID or AD express a truncated Zc3h14 isoform. To elucidate whether this mutation causes neurodevelopmental developmental disorders, the differentiation of pluripotent mouse P19 cells depleted of Zc3h14 could be investigated with regards of the following characteristics:

- Differentiation efficiency could be analyzed by monitoring the expression levels of differentiation markers, such as Nestin, Synapsin, Tuj1, MAP2 or NF200 by immunofluorescence and immunoblotting.
- Zc3h14 export activity during neuronal differentiation could be observed by Fish experiments, detecting the export of *Fmr1* mRNA. This would provide insights if the Zc3h14 depletion is accompanied by an impaired *Fmr1* export and could establish a connection between the fragile X syndrome and Zc3h14 dependent neurological diseases.
- Multiple neurological diseases exhibit characteristic morphological alterations of neurons. The investigation of the neuromorphology during P19 differentiation with regards of the soma area, neurite length and number of neurite branches could be important parameters to identify a neuronal phenotype.

- The neuronal functionality can be observed by neuronal transmission potential after neurogenesis. Determining the expression levels of ionotropic and metabotropic glutamate and GABAergic receptors, such as GluA2, GluA3, GluK5, mGluR7 and GABA will give first hints if Zc3h14 causes aberrant calcium currents. Additionally, the electrophysiological activities could be displayed by whole-cell patch-clamp analyses in differentiated P19 cells.

Our study showed that the interplay between SRSF3 and Zc3h14/Nxf1 is phosphorylation dependent. Splicing inhibition increases the hyper-phosphorylated state of SRSF3. In this hyper-phosphorylated state, SRSF3 does not recruit Zc3h14 and Nxf1. To elucidate if SRSF3 phosphorylation is *per se* the driver of the splicing surveillance mechanism that blocks export of intron-containing transcripts, the following studies could be performed:

- A global screening for SRSF3-specific phosphatases and the identification of specific and potent SRSF3 phosphatase inhibitors/activators. Using these inhibitors/activators SRSF3-phosphorylation levels could be modulated and give first insights in the phosphorylation dynamics of SRSF3.
- A thio-phosphorylated SRSF3 RS domain would be insensitive to de-phosphorylation and thus SRSF3 would remain hyper-phosphorylated. By visualizing Zc3h14 targets by FISH, this technique would answer the question whether SRSF3 hyper-phosphorylation is sufficient to retain mRNAs in the nucleus. An alternative approach could be the use of phospho-mimetics. Amino acid substitutions within the RS domain with negatively charged or uncharged amino acids can be used to mimic different SRSF3 phosphorylation states to confirm the phosphorylation-dependent interaction with Nxf1 and Zc3h14. Joining both techniques, thio-phosphorylation assays and phosphor-mimetics, would clarify whether the SRSF3 interaction with Nxf1 and Zc3h14 is dependent on phosphorylation *per se* or due to the different charges that SRSF3 exhibits during mRNA processing.
- To exclude that SRSF3 hyper-phosphorylation is a pleiotropic effect of Isoginkgetin treatment alternative small molecule inhibitors or depletion of core spliceosomal factors could confirm, that SRSF3 remains hyper-phosphorylated when splicing is inhibited.

What are the minimal requirements for Zc3h14-mediated export? To answer this question an inducible tethering system can be useful to attach specific export factors/adaptors to an RNA reporter. Tethering Nxf1 or Zc3h14 directly to the RNA would answer the question if their recruitment by SRSF3 is sufficient to transport Zc3h14 targets to the cytoplasm. Moreover, using the tethering system with SRSF3 phosphorylation mimics in combination with RNA binding experiments would elucidate if the mRNA binding capability of Zc3h14 and Nxf1 is dependent on the phosphorylation state of SRSF3.

We have shown that SRSF3 binds to the mRNP and recruits Zc3h14 and Nxf1. However, we currently do not know whether Zc3h14 is important for Nxf1 recruitment or whether it associates with the mRNP independently of Nxf1. Co-immunoprecipitation experiments and RNA binding assays of Nxf1 in Zc3h14 depleted cells and *vice versa* could be useful to understand whether Zc3h14 acts as a bona fide export adaptor by recruiting Nxf1, or whether it promotes mRNA export independently of Nxf1 and rather acts as an mRNA export receptor for specific transcripts. These studies could also uncover the sequential order in which export adaptors and receptors associate with the mRNP and unveil the molecular mechanism of a splicing-dependent mRNA export.

Currently it is not known, which proteins/complexes are targeted by Isoginkgetin. An Isoginkgetin pull-down coupled with mass spectrometry analysis could be used to identify Isoginkgetin targets and could be useful to identify the affected splicing step.

8. References

- Abaza, A., Soleilhac, J.-M., Westendorf, J., Piel, M., Crevel, I., Roux, A., and Pirollet, F. (2003). M phase phosphoprotein 1 is a human plus-end-directed kinesin-related protein required for cytokinesis. *The Journal of biological chemistry* 278, 27844–27852.
- Abebrese, E.L., Ali, S.H., Arnold, Z.R., Andrews, V.M., Armstrong, K., Burns, L., Crowder, H.R., Day, R.T., Hsu, D.G., Jarrell, K., Lee, G., Luo, Y., Mugayo, D., Raza, Z., and Friend, K. (2017). Identification of human short introns. *PloS one* 12.
- Aibara, S., Gordon, J.M.B., Riesterer, A.S., McLaughlin, S.H., and Stewart, M. (2017). Structural basis for the dimerization of Nab2 generated by RNA binding provides insight into its contribution to both poly(A) tail length determination and transcript compaction in *Saccharomyces cerevisiae*. *Nucleic acids research* 45, 1529–1538.
- Aibara, S., Katahira, J., Valkov, E., and Stewart, M. (2015). The principal mRNA nuclear export factor NXF1:NXT1 forms a symmetric binding platform that facilitates export of retroviral CTE-RNA. *Nucleic acids research* 43, 1883–1893.
- Ajiro, M., Jia, R., Yang, Y., Zhu, J., and Zheng, Z.-M. (2015). A genome landscape of SRSF3-regulated splicing events and gene expression in human osteosarcoma U2OS cells. *Genes & Development* 44, 1854–1870.
- Akef, A., Zhang, H., Masuda, S., and Palazzo, F.A. (2013). Trafficking of mRNAs containing ALREX-promoting elements through nuclear speckles. *Nucleus* 4, 326–340.
- Albert, B.J., McPherson, P.A., O'Brien, K., Czaicki, N.L., Destefino, V., Osman, S., Li, M., Day, B.W., Grabowski, P.J., Moore, M.J., Vogt, A., and Koide, K. (2009). Meayamycin inhibits pre-messenger RNA splicing and exhibits picomolar activity against multidrug-resistant cells. *Molecular cancer therapeutics* 8, 2308–2318.
- Allmang, C., Petfalski, E., Podtelejnikov, A., Mann, M., Tollervey, D., and Mitchell, P. (1999). The yeast exosome and human PM-Scl are related complexes of 3' → 5' exonucleases. *Genes & Development* 13, 2148–2158.
- Almeida, F.S. de, García-Sacristán, A., Custódio, N., and Carmo-Fonseca, M. (2010). A link between nuclear RNA surveillance, the human exosome and RNA polymerase II transcriptional termination. *Nucleic acids research* 38, 8015–8026.
- Almeida, S.F. de, Grosso, A.R., Koch, F., Fenouil, R., Carvalho, S., Andrade, J., Levezinho, H., Gut, M., Eick, D., Gut, I., Andrau, J.-C., Ferrier, P., and Carmo-Fonseca, M. (2011). Splicing enhances recruitment of methyltransferase HYPB/Setd2 and methylation of histone H3 Lys36. *Nature structural & molecular biology* 18, 977–983.
- Anczuków, O., Akerman, M., Cléry, A., Wu, J., Shen, C., Shirole, N.H., Raimer, A., Sun, S., Jensen, M.A., Hua, Y., Allain, F.H.-T., and Krainer, A.R. (2015). SRSF1-Regulated Alternative Splicing in Breast Cancer. *Molecular cell* 60, 105–117.
- Andersen, R.P., Domanski, M., Kristiansen, S.M., Storvall, H., Ntini, E., Verheggen, C., Schein, A., Bunkenborg, J., Poser, I., Hallais, M., Sandberg, R., Hyman, A., LaCava, J., Rout, P.M., Andersen, S.J.,

- Bertrand, E., and Jensen, H.T. (2013). The human cap-binding complex is functionally connected to the nuclear RNA exosome. *Nature structural & molecular biology* *20*, 1367–1376.
- Anderson, T.J., Wilson, M.S., Datar, V.K., and Swanson, S.M. (1993). NAB2: a yeast nuclear polyadenylated RNA-binding protein essential for cell viability. *Molecular and cellular biology* *13*, 2730–2741.
- Ando, T., Yamayoshi, S., Tomita, Y., Watanabe, S., Watanabe, T., and Kawaoka, Y. (2016). The host protein CLUH participates in the subnuclear transport of influenza virus ribonucleoprotein complexes. *Nature microbiology* *1*, 16062.
- Änkö, M.-L., Morales, L., Henry, I., Beyer, A., and Neugebauer, K.M. (2010). Global analysis reveals SRp20- and SRp75-specific mRNPs in cycling and neural cells. *Nature structural & molecular biology* *17*, 962–970.
- Änkö, M.-L., Müller-McNicoll, M., Brandl, H., Curk, T., Gorup, C., Henry, I., Ule, J., and Neugebauer, K.M. (2012). The RNA-binding landscapes of two SR proteins reveal unique functions and binding to diverse RNA classes. *Genome biology* *13*, R17.
- Aramburu, I.V., and Lemke, E.A. (2017). Floppy but not sloppy: Interaction mechanism of FG-nucleoporins and nuclear transport receptors. *Seminars in cell & developmental biology* *68*, 34–41.
- Ast, G. (2004). How did alternative splicing evolve? *Nature reviews. Genetics* *5*, 773–782.
- Aubol, B.E., and Adams, J.A. (2011). Applying the brakes to multisite SR protein phosphorylation: substrate-induced effects on the splicing kinase SRPK1. *Biochemistry* *50*, 6888–6900.
- Aubol, B.E., Chakrabarti, S., Ngo, J., Shaffer, J., Nolen, B., Fu, X.-D., Ghosh, G., and Adams, J.A. (2003). Processive phosphorylation of alternative splicing factor/splicing factor 2. *Proceedings of the National Academy of Sciences of the United States of America* *100*, 12601–12606.
- Aubol, B.E., Hailey, K.L., Fattet, L., Jennings, P.A., and Adams, J.A. (2017). Redirecting SR Protein Nuclear Trafficking through an Allosteric Platform. *Journal of molecular biology* *429*, 2178–2191.
- Aubol, B.E., Keshwani, M.M., Fattet, L., and Adams, J.A. (2018a). Mobilization of a splicing factor through a nuclear kinase-kinase complex. *The Biochemical journal* *475*, 677–690.
- Aubol, B.E., Serrano, P., Fattet, L., Wuthrich, K., and Adams, J.A. (2018b). Molecular Interactions Connecting the Function of the Serine-Arginine-rich protein SRSF1 to Protein Phosphatase 1. *The Journal of biological chemistry*.
- Audibert, A., Weil, D., and Dautry, F. (2002). In Vivo Kinetics of mRNA Splicing and Transport in Mammalian Cells. *Molecular and Cellular Biology* *22*, 6706–6718.
- Bachi, A., Braun, I.C., Rodrigues, J.P., Pante, N., Ribbeck, K., Kobbe, C. von, Kutay, U., Wilm, M., Gorlich, D., Carmo-Fonseca, M., and Izaurralde, E. (2000). The C-terminal domain of TAP interacts with the nuclear pore complex and promotes export of specific CTE-bearing RNA substrates. *RNA (New York, N.Y.)* *6*, 136–158.
- Bassell, G.J., and Warren, S.T. (2008). Fragile X Syndrome: Loss of Local mRNA Regulation Alters Synaptic Development and Function. *Neuron* *60*, 201–214.
- Bastide, B., Mouly, V., and Trollet, C. (2016). Nuclear poly(A)-binding protein aggregates misplace a pre-mRNA outside of SC35 speckle causing its abnormal splicing. *Nucleic Acids Research* *44*.

- Baurén, G., and Wieslander, L. (1994). Splicing of Balbiani ring 1 gene pre-mRNA occurs simultaneously with transcription. *Cell* 76, 183–192.
- Bear, J., Tan, W., Zolotukhin, A.S., Taberner, C., Hudson, E.A., and Felber, B.K. (1999). Identification of Novel Import and Export Signals of Human TAP, the Protein That Binds to the Constitutive Transport Element of the Type D Retrovirus mRNAs. *Molecular and cellular biology* 19, 6306–6317.
- Bengoechea, R., Tapia, O., Casafont, I., Berciano, J., Lafarga, M., and Berciano, M.T. (2012). Nuclear speckles are involved in nuclear aggregation of PABPN1 and in the pathophysiology of oculopharyngeal muscular dystrophy. *Neurobiology of Disease* 46, 118–129.
- Benoit, B., Nemeth, A., Aulner, N., Khn, U., Simonelig, M., Wahle, E., and Bourbon, M.H. (1999). The *Drosophila* poly(A)-binding protein II is ubiquitous throughout *Drosophila* development and has the same function in mRNA polyadenylation as its bovine homolog in vitro. *Nucleic acids research* 27, 3771–3778.
- Bentley, D.L. (2005). Rules of engagement: co-transcriptional recruitment of pre-mRNA processing factors. *Current opinion in cell biology* 17, 251–256.
- Bentley, D.L. (2014). Coupling mRNA processing with transcription in time and space. *Nature Reviews Genetics* 15, 163.
- Berg, M.G., Wan, L., Younis, I., Diem, M.D., Soo, M., Wang, C., and Dreyfuss, G. (2012). A Quantitative High-Throughput In Vitro Splicing Assay Identifies Inhibitors of Spliceosome Catalysis. *Molecular and Cellular Biology* 32, 1271–1283.
- Berget, S.M., Moore, C., and Sharp, P.A. (1977). Spliced segments at the 5' terminus of adenovirus 2 late mRNA. *Proceedings of the National Academy of Sciences* 74, 3171–3175.
- Bernstein, J., Patterson, N.D., Wilson, M.G., and Toth, A.E. (2007). Characterization of the Essential Activities of *Saccharomyces cerevisiae* Mtr4p, a 3'->5' Helicase Partner of the Nuclear Exosome. *The Journal of biological chemistry* 283.
- Beyer, A.L., Bouton, A.H., and Miller, O.L. (1981). Correlation of hnRNP structure and nascent transcript cleavage. *Cell* 26, 155–165.
- Beyer, A.L., and Osheim, Y.N. (1988). Splice site selection, rate of splicing, and alternative splicing on nascent transcripts. *Genes & Development* 2, 754–765.
- Beyer, K., Dandekar, T., and Keller, W. (1997). RNA ligands selected by cleavage stimulation factor contain distinct sequence motifs that function as downstream elements in 3'-end processing of pre-mRNA. *The Journal of biological chemistry* 272, 26769–26779.
- Bhakar, A.L., Dölen, G., and Bear, M.F. (2012). The Pathophysiology of Fragile X (and What It Teaches Us about Synapses). *Annual review of neuroscience* 35, 417–443.
- Bienkowski, R.S., Banerjee, A., Rounds, J.C., Rha, J., Omotade, O.F., Gross, C., Morris, K.J., Leung, S.W., Pak, C., Jones, S.K., Santoro, M.R., Warren, S.T., Zheng, J.Q., Bassell, G.J., Corbett, A.H., and Moberg, K.H. (2017). The Conserved, Disease-Associated RNA Binding Protein dNab2 Interacts with the Fragile X Protein Ortholog in *Drosophila* Neurons. *Cell reports* 20, 1372–1384.
- Bienroth, S., Keller, W., and Wahle, E. (1993). Assembly of a processive messenger RNA polyadenylation complex. *The EMBO journal* 12, 585–594.

- Black, D.L. (2003). Mechanisms of alternative pre-messenger RNA splicing. *Annual review of biochemistry* 72, 291–336.
- Blencowe, B.J., Baurén, G., Eldridge, A.G., Issner, R., Nickerson, J.A., Rosonina, E., and Sharp, P.A. (2000). The SRm160/300 splicing coactivator subunits. *RNA* 6, 111–120.
- Blencowe, B.J., Bowman, J.A., McCracken, S., and Rosonina, E. (1999). SR-related proteins and the processing of messenger RNA precursors. *Biochemistry and cell biology = Biochimie et biologie cellulaire* 77, 277–291.
- Blencowe, B.J., Issner, R., Nickerson, J.A., and Sharp, P.A. (1998). A coactivator of pre-mRNA splicing. *Genes & Development* 12, 996–1009.
- Bodoor, K., Shaikh, S., Salina, D., Raharjo, W.H., Bastos, R., Lohka, M., and Burke, B. (1999). Sequential recruitment of NPC proteins to the nuclear periphery at the end of mitosis. *Journal of cell science* 112 (Pt 13), 2253–2264.
- Botti, V., McNicoll, F., Steiner, M.C., Richter, F.M., Solovyeva, A., Wegener, M., Schwich, O.D., Poser, I., Zarnack, K., Wittig, I., Neugebauer, K.M., and Müller-McNicoll, M. (2017). Cellular differentiation state modulates the mRNA export activity of SR proteins. *The Journal of cell biology* 216, 1993–2009.
- Boukris, L.A., Liu, N., Furuyama, S., and Bruzik, J.P. (2004). Ser/Arg-rich protein-mediated communication between U1 and U2 small nuclear ribonucleoprotein particles. *The Journal of biological chemistry* 279, 29647–29653.
- Bousquet-Antonelli, C., Presutti, C., and Tollervey, D. (2000). Identification of a regulated pathway for nuclear pre-mRNA turnover. *Cell* 102, 765–775.
- Boutz, P.L., Bhutkar, A., and Sharp, P.A. (2015). Detained introns are a novel, widespread class of post-transcriptionally spliced introns. *Genes & Development* 29, 63–80.
- Bradley, T., Cook, M.E., and Blanchette, M. (2015). SR proteins control a complex network of RNA-processing events. *RNA* 21, 75–92.
- Braunschweig, U., Barbosa-Morais, N.L., Pan, Q., Nachman, E.N., Alipanahi, B., Gonatopoulos-Pournatzis, T., Frey, B., Irimia, M., and Blencowe, B.J. (2014). Widespread intron retention in mammals functionally tunes transcriptomes. *Genome research* 24, 1774–1786.
- Breathnach, R., Mandel, J.L., and Chambon, P. (1977). Ovalbumin gene is split in chicken DNA. *Nature* 270, 314.
- Bresson, S., and Tollervey, D. (2018). Surveillance-ready transcription: nuclear RNA decay as a default fate. *Open biology* 8.
- Bresson, S., Tuck, A., Staneva, D., and Tollervey, D. (2017). Nuclear RNA Decay Pathways Aid Rapid Remodeling of Gene Expression in Yeast. *Molecular cell* 65, 787-800.e5.
- Brockmann, C., Soucek, S., Kuhlmann, S.I., Mills-Lujan, K., Kelly, S.M., Yang, J.-C., Iglesias, N., Stutz, F., Corbett, A.H., Neuhaus, D., and Stewart, M. (2012). Structural Basis for Polyadenosine-RNA Binding by Nab2 Zn Fingers and Its Function in mRNA Nuclear Export. *Structure(London, England:1993)* 20-540, 1007–1018.

- Brody, Y., Neufeld, N., Bieberstein, N., Causse, S.Z., Bohnlein, E.-M., Neugebauer, K.M., Darzacq, X., and Shav-Tal, Y. (2011). The in vivo kinetics of RNA polymerase II elongation during co-transcriptional splicing. *PLoS biology* *9*, e1000573.
- Brugiolo, M., Botti, V., Liu, N., Müller-McNicoll, M., and Neugebauer, K.M. (2017). Fractionation iCLIP detects persistent SR protein binding to conserved, retained introns in chromatin, nucleoplasm and cytoplasm. *Nucleic acids research* *45*, 10452–10465.
- Buratti, E. (2015). Functional Significance of TDP-43 Mutations in Disease. *0065-2660* *91*, 1–53.
- Cáceres, J.F., and Krainer, A.R. (1993). Functional analysis of pre-mRNA splicing factor SF2/ASF structural domains. *The EMBO journal* *12*, 4715–4726.
- Cannon, D., and Chubb, J.R. (2011). Pol II caught speeding by single gene imaging. *EMBO reports* *12*, 1208–1210.
- Cao, W., Jamison, S.F., and Garcia-Blanco, M.A. (1997). Both phosphorylation and dephosphorylation of ASF/SF2 are required for pre-mRNA splicing in vitro. *RNA* *3*, 1456–1467.
- Cardinali, B., Cohen, P.T.W., and Lamond, A.I. (1994). Protein phosphatase 1 can modulate alternative 5' splice site selection in a HeLa splicing extract. *FEBS Letters* *352*, 276–280.
- Carmody, R.S., Tran, J.E., Apponi, H.L., Corbett, H.A., and Wenthe, R.S. (2010). The mitogen-activated protein kinase Slt2 regulates nuclear retention of non-heat shock mRNAs during heat shock-induced stress. *Molecular and cellular biology* *30*, 5168–5179.
- Carter, Taneja, and Lawrence (1991). Discrete nuclear domains of poly(A) RNA and their relationship to the functional organization of the nucleus. *The Journal of cell biology* *115*, 1191–1202.
- Carter, K.C., Bowman, D., Carrington, W., Fogarty, K., McNeil, J.A., Fay, F.S., and Lawrence, J.B. (1993). A three-dimensional view of precursor messenger RNA metabolism within the mammalian nucleus. *Science (New York, N.Y.)* *259*, 1330–1335.
- Carvalho, T., Martins, S., Rino, J., Marinho, S., and Carmo-Fonseca, M. (2017). Pharmacological inhibition of the spliceosome subunit SF3b triggers exon junction complex-independent nonsense-mediated decay. *Journal of cell science* *130*, 1519–1531.
- Cavaloc, Y., Bourgeois, C.F., Kister, L., and Stévenin, J. (1999). The splicing factors 9G8 and SRp20 transactivate splicing through different and specific enhancers. *RNA* *5*, 468–483.
- Cazalla, D., Zhu, J., Manche, L., Huber, E., Krainer, A.R., and Cáceres, J.F. (2002). Nuclear Export and Retention Signals in the RS Domain of SR Proteins. *Molecular and Cellular Biology* *22*, 6871–6882.
- Ceman, S., O'Donnell, W.T., Reed, M., Patton, S., Pohl, J., and Warren, S.T. (2003). Phosphorylation influences the translation state of FMRP-associated polyribosomes. *Human molecular genetics* *12*, 3295–3305.
- Chandler, S.D., Mayeda, A., Yeakley, J.M., Krainer, A.R., and Fu, X.-D. (1997). RNA splicing specificity determined by the coordinated action of RNA recognition motifs in SR proteins. *Proceedings of the National Academy of Sciences* *94*, 3596–3601.
- Chang, D.D., and Sharp, A.P. (1989). Regulation by HIV Rev depends upon recognition of splice sites. *Cell* *59*, 789–795.

- Chang, H., Lim, J., Ha, M., and Kim, V.N. (2014). TAIL-seq: Genome-wide Determination of Poly(A) Tail Length and 3' End Modifications. *Molecular cell* *53*, 1044–1052.
- Chavoshi, S., Egorova, O., Lacdao, I.K., Farhadi, S., Sheng, Y., and Saridakis, V. (2016). Identification of Kaposi Sarcoma Herpesvirus (KSHV) vIRF1 Protein as a Novel Interaction Partner of Human Deubiquitinase USP7. *The Journal of biological chemistry* *291*, 6281–6291.
- Chekanova, A.J., Shaw, J.R., and Belostotsky, A.D. (2001). Analysis of an essential requirement for the poly(A) binding protein function using cross-species complementation. *Current Biology* *11*, 1207–1214.
- Chen, L.-L., and Carmichael, G.G. (2009). Altered nuclear retention of mRNAs containing inverted repeats in human embryonic stem cells: functional role of a nuclear noncoding RNA. *Molecular cell* *35*, 467–478.
- Cheng, H., Dufu, K., Lee, C.-S., Hsu, J.L., Dias, A., and Reed, R. (2006). Human mRNA Export Machinery Recruited to the 5' End of mRNA. *Cell* *127*, 1389–1400.
- Cho, S., Hoang, A., Sinha, R., Zhong, X.-Y., Fu, X.-D., Krainer, A.R., and Ghosh, G. (2011). Interaction between the RNA binding domains of Ser-Arg splicing factor 1 and U1-70K snRNP protein determines early spliceosome assembly. *Proceedings of the National Academy of Sciences of the United States of America* *108*, 8233–8238.
- Chow, L.T., Gelinias, R.E., Broker, T.R., and Roberts, R.J. (1977). An amazing sequence arrangement at the 5' ends of adenovirus 2 messenger RNA. *Cell* *12*, 1–8.
- Conti, L.D., Baralle, M., and Buratti, E. (2013). Exon and intron definition in pre-mRNA splicing. *Wiley Interdisciplinary Reviews: RNA* *4*, 49–60.
- Convertini, P., Shen, M., Potter, M.P., Palacios, G., Lagisetti, C., La Grange, P. de, Horbinski, C., Fondufe-Mittendorf, N.Y., Webb, R.T., and Stamm, S. (2014). Sudemycin E influences alternative splicing and changes chromatin modifications. *Nucleic acids research* *42*, 4947–4961.
- Corkery, D.P., Holly, A.C., Lahsaee, S., and Dellaire, G. (2015). Connecting the speckles: Splicing kinases and their role in tumorigenesis and treatment response. *Nucleus (Austin, Tex.)* *6*, 279–288.
- Corrionero, A., Miñana, B., and Valcárcel, J. (2011). Reduced fidelity of branch point recognition and alternative splicing induced by the anti-tumor drug spliceostatin A. *Genes & Development* *25*, 445–459.
- Coyle, J.H., Bor, Y.-C., Rekosh, D., and Hammarskjold, M.-L. (2011). The Tpr protein regulates export of mRNAs with retained introns that traffic through the Nxf1 pathway. *RNA* *17*, 1344–1356.
- Cui, M., Allen, M.A., Larsen, A., MacMorris, M., Han, M., and Blumenthal, T. (2008). Genes involved in pre-mRNA 3'-end formation and transcription termination revealed by a lin-15 operon Muv suppressor screen. *Proceedings of the National Academy of Sciences* *105*, 16665–16670.
- Culjkovic-Kraljacic, B., Baguet, A., Volpon, L., Amri, A., and Borden, K.L.B. (2012). The oncogene eIF4E reprograms the nuclear pore complex to promote mRNA export and oncogenic transformation. *Cell reports* *2*, 207–215.
- Cullen, B.R. (1998). Retroviruses as model systems for the study of nuclear RNA export pathways. *Virology* *249*, 203–210.

- Danko, C.G., Hah, N., Luo, X., Martins, A.L., Core, L., Lis, J.T., Siepel, A., and Kraus, W.L. (2013). Signaling pathways differentially affect RNA polymerase II initiation, pausing, and elongation rate in cells. *Molecular cell* *50*, 212–222.
- Darnell, J.C., van Driesche, S.J., Zhang, C., Hung, K.Y.S., Mele, A., Fraser, C.E., Stone, E.F., Chen, C., Fak, J.J., Chi, S.W., Licatalosi, D.D., Richter, J.D., and Darnell, R.B. (2011). FMRP stalls ribosomal translocation on mRNAs linked to synaptic function and autism. *Cell* *146*, 247–261.
- Darzacq, X., Shav-Tal, Y., Turris, V. de, Brody, Y., Shenoy, S.M., Phair, R.D., and Singer, R.H. (2007). In vivo dynamics of RNA polymerase II transcription. *Nature structural & molecular biology* *14*, 796–806.
- Dassi, E. (2017). Handshakes and Fights: The Regulatory Interplay of RNA-Binding Proteins. *Frontiers in Molecular Biosciences* *4*.
- Datta, S., Snow, C.J., and Paschal, B.M. (2014). A pathway linking oxidative stress and the Ran GTPase system in progeria. *Molecular biology of the cell* *25*, 1202–1215.
- Dehm, S.M. (2013). Test-firing ammunition for spliceosome inhibition in cancer. *Clinical cancer research an official journal of the American Association for Cancer Research* *19*.
- Dembowski, J.A., An, P., Scoulos-Hanson, M., Yeo, G., Han, J., Fu, X.-D., and Grabowski, P.J. (2012). Alternative Splicing of a Novel Inducible Exon Diversifies the CASK Guanylate Kinase Domain. *Journal of nucleic acids* *2012*, 816237.
- Dez, C., Houseley, J., and Tollervey, D. (2006). Surveillance of nuclear-restricted pre-ribosomes within a subnucleolar region of *Saccharomyces cerevisiae*. *The EMBO journal* *25*, 1534–1546.
- Dias, A.P., Dufu, K., Lei, H., and Reed, R. (2010). A role for TREX components in the release of spliced mRNA from nuclear speckle domains. *Nature communications* *1*, 97.
- Ding, J.-H., Zhong, X.-Y., Hagopian, J.C., Cruz, M.M., Ghosh, G., Feramisco, J., Adams, J.A., and Fu, X.-D. (2006). Regulated Cellular Partitioning of SR Protein-specific Kinases in Mammalian Cells. *Molecular biology of the cell* *17*, 876–885.
- Dobin, A., Davis, C.A., Schlesinger, F., Drenkow, J., Zaleski, C., Jha, S., Batut, P., Chaisson, M., and Gingeras, T.R. (2013). STAR: ultrafast universal RNA-seq aligner. *Bioinformatics (Oxford, England)* *29*, 15–21.
- Dölen, G., Osterweil, E., Shankaranarayana Rao, B.S., Smith, G.B., Auerbach, B.D., Chattarji, S., and Bear, M.F. (2007). Correction of fragile X syndrome in mice. *Neuron* *56*, 955–962.
- Duncan, P.I., Stojdl, D.F., Marius, R.M., and Bell, J.C. (1997). In vivo regulation of alternative pre-mRNA splicing by the Clk1 protein kinase. *Molecular and Cellular Biology* *17*, 5996–6001.
- Duncan, P.I., Stojdl, D.F., Marius, R.M., Scheit, K.H., and Bell, J.C. (1998). The Clk2 and Clk3 dual-specificity protein kinases regulate the intranuclear distribution of SR proteins and influence pre-mRNA splicing. *Experimental cell research* *241*, 300–308.
- Duncan Kent, Umen JG, and Guthrie C (2000). A putative ubiquitin ligase required for efficient mRNA export differentially affects hnRNP transport. *Current Biology* *10*, 687–696.
- Edwards, M.K., Harris, J.F., and McBurney, M.W. (1983). Induced muscle differentiation in an embryonal carcinoma cell line. *Molecular and Cellular Biology* *3*, 2280–2286.

- Edwards, M.K., and McBurney, M.W. (1983). The concentration of retinoic acid determines the differentiated cell types formed by a teratocarcinoma cell line. *Developmental Biology* *98*, 187–191.
- Effenberger, A.K., Anderson, D.D., Bray, M.W., Prichard, E.B., Ma, N., Adams, S.M., Ghosh, K.A., and Jurica, S.M. (2014). Coherence between cellular responses and in vitro splicing inhibition for the anti-tumor drug pladienolide B and its analogs. *The Journal of biological chemistry* *289*, 1938–1947.
- Ellison, W.J., Rosenfeld, A.J., and Shaffer, G.L. (2013). Genetic basis of intellectual disability. *Annual review of medicine* *64*, 441–450.
- Engreitz, J.M., Sirokman, K., McDonel, P., Shishkin, A.A., Surka, C., Russell, P., Grossman, S.R., Chow, A.Y., Guttman, M., and Lander, E.S. (2014). RNA-RNA interactions enable specific targeting of noncoding RNAs to nascent Pre-mRNAs and chromatin sites. *Cell* *159*, 188–199.
- Erkelenz, S., Mueller, W.F., Evans, M.S., Busch, A., Schöneweis, K., Hertel, K.J., and Schaal, H. (2013). Position-dependent splicing activation and repression by SR and hnRNP proteins rely on common mechanisms. *RNA (New York, N.Y.)* *19*, 96–102.
- Ernst, R.K., Bray, M., Rekosh, D., and Hammarskjöld, M.L. (1997). A structured retroviral RNA element that mediates nucleocytoplasmic export of intron-containing RNA. *Molecular and Cellular Biology* *17*, 135–144.
- Escudero-Paunetto, L., Li, L., Hernandez, F.P., and Sandri-Goldin, R.M. (2010). SR proteins SRp20 and 9G8 contribute to efficient export of herpes simplex virus 1 mRNAs. *Virology* *401*, 155–164.
- Eskens, Ferry, Ramos, F.J., Burger, H., O'Brien, J.P., Piera, A., de Jonge, Maja J A, Mizui, Y., Wiemer, E.A.C., Carreras, M.J., Baselga, J., and Tabernero, J. (2013). Phase I pharmacokinetic and pharmacodynamic study of the first-in-class spliceosome inhibitor E7107 in patients with advanced solid tumors. *Clinical cancer research an official journal of the American Association for Cancer Research* *19*, 6296–6304.
- Fakan, S., and van Driel, R. (2007). The perichromatin region: a functional compartment in the nucleus that determines large-scale chromatin folding. *Seminars in cell & developmental biology* *18*, 676–681.
- Fan, J., Kuai, B., Wang, K., Wang, L., Wang, Y., Wu, X., Chi, B., Li, G., and Cheng, H. (2018). mRNAs are sorted for export or degradation before passing through nuclear speckles. *Nucleic acids research*.
- Fan, L., Lagisetti, C., Edwards, C.C., Webb, T.R., and Potter, P.M. (2011). Sudemycins, novel small molecule analogues of FR901464, induce alternative gene splicing. *ACS chemical biology* *6*, 582–589.
- Fasken, M.B., and Corbett, A.H. (2016). Links between mRNA splicing, mRNA quality control, and intellectual disability. *RNA & disease (Houston, Tex.)* *3*.
- Fasken, M.B., Stewart, M., and Corbett, A.H. (2008). Functional Significance of the Interaction between the mRNA-binding Protein, Nab2, and the Nuclear Pore-associated Protein, Mlp1, in mRNA Export. *The Journal of biological chemistry* *283*, 27130–27143.
- Fazio, T.G., Huff, J.T., and Panning, B. (2008). An RNAi screen of chromatin proteins identifies Tip60-p400 as a regulator of embryonic stem cell identity. *Cell* *134*, 162–174.
- Fazio, T.G., and Panning, B. (2010). Condensin complexes regulate mitotic progression and interphase chromatin structure in embryonic stem cells. *The Journal of cell biology* *188*, 491–503.

- Fei, J., Jadhavi, M., Harmon, T.S., Li, I.T.S., Hua, B., Hao, Q., Holehouse, A.S., Reyer, M., Sun, Q., Freier, S.M., Pappu, R.V., Prasanth, K.V., and Ha, T. (2017). Quantitative analysis of multilayer organization of proteins and RNA in nuclear speckles at super resolution. *Journal of cell science* *130*, 4180–4192.
- Felfly, H., Xue, J., Zamboni, A.C., Muotri, A., Zhou, D., and Haddad, G.G. (2011). Identification of a neuronal gene expression signature: role of cell cycle arrest in murine neuronal differentiation in vitro. *American journal of physiology. Regulatory, integrative and comparative physiology* *301*, R727-45.
- Feng, X.-D., Song, Q., Li, C.-W., Chen, J., Tang, H.-M., Peng, Z.-H., and Wang, X.-C. (2014). Structural maintenance of chromosomes 4 is a predictor of survival and a novel therapeutic target in colorectal cancer. *Asian Pacific journal of cancer prevention APJCP* *15*, 9459–9465.
- Ferder, I., Parborell, F., Sundblad, V., Chiauzzi, V., Gomez, K., Charreau, E.H., Tesone, M., and Dain, L. (2013). Expression of fragile X mental retardation protein and Fmr1 mRNA during folliculogenesis in the rat. *Reproduction (Cambridge, England)* *145*, 335–343.
- Fica, S.M., Tuttle, N., Novak, T., Li, N.-S., Lu, J., Koodathingal, P., Dai, Q., Staley, J.P., and Piccirilli, J.A. (2013). RNA catalyses nuclear pre-mRNA splicing. *Nature* *503*, 229–234.
- Folkmann, A.W., Dawson, T.R., and Wenthe, S.R. (2014). Insights into mRNA export-linked molecular mechanisms of human disease through a Gle1 structure–function analysis. *Advances in Biological Regulation* *54*, 74–91.
- Freibaum, B.D., Lu, Y., Lopez-Gonzalez, R., Kim, N.C., Almeida, S., Lee, K.-H., Badders, N., Valentine, M., Miller, B.L., Wong, P.C., Petrucelli, L., Kim, H.J., Gao, F.-B., and Taylor, J.P. (2015). GGGGCC repeat expansion in *C9orf72* compromises nucleocytoplasmic transport. *Nature* *525*, 129.
- Fu, X.D. (1995). The superfamily of arginine/serine-rich splicing factors. *RNA* *1*, 663–680.
- Fu, X.D., and Maniatis, T. (1992a). Isolation of a complementary DNA that encodes the mammalian splicing factor SC35. *Science (New York, N.Y.)* *256*, 535–538.
- Fu, X.D., and Maniatis, T. (1992b). The 35-kDa mammalian splicing factor SC35 mediates specific interactions between U1 and U2 small nuclear ribonucleoprotein particles at the 3' splice site. *Proceedings of the National Academy of Sciences* *89*, 1725–1729.
- Fu, X.-D., and Ares, M. (2014). Context-dependent control of alternative splicing by RNA-binding proteins. *Nature reviews. Genetics* *15*, 689–701.
- Fu, X.-D., and Maniatis, T. (1990). Factor required for mammalian spliceosome assembly is localized to discrete regions in the nucleus. *Nature* *343*, 437.
- Fuke, H., and Ohno, M. (2007). Role of poly (A) tail as an identity element for mRNA nuclear export. *Genes & Development* *36*, 1037–1049.
- Furuta, M., Kose, S., Koike, M., Shimi, T., Hiraoka, Y., Yoneda, Y., Haraguchi, T., and Imamoto, N. (2004). Heat-shock induced nuclear retention and recycling inhibition of importin alpha. *Genes to cells devoted to molecular & cellular mechanisms* *9*, 429–441.
- Galiana-Arnoux, D., Lejeune, F., Gesnel, M.-C., Stevenin, J., Breathnach, R., and Gatto-Konczak, F.D. (2003). The CD44 Alternative v9 Exon Contains a Splicing Enhancer Responsive to the SR Proteins 9G8, ASF/SF2, and SRp20. *Journal of Biological Chemistry* *278*, 32943–32953.

- Gallardo, M., Luna, R., Erdjument-Bromage, H., Tempst, P., and Aguilera, A. (2003). Nab2p and the Thp1p-Sac3p complex functionally interact at the interface between transcription and mRNA metabolism. *The Journal of biological chemistry* 278, 24225–24232.
- Gallouzi, I.E., Brennan, C.M., and Steitz, J.A. (2001). Protein ligands mediate the CRM1-dependent export of HuR in response to heat shock. *RNA (New York, N.Y.)* 7, 1348–1361.
- Galy, V., Gadad, O., Fromont-Racine, M., Romano, A., Jacquier, A., and Nehrbass, U. (2004). Nuclear retention of unspliced mRNAs in yeast is mediated by perinuclear Mlp1. *Cell* 116, 63–73.
- Ge, H., and Manley, J.L. (1990). A protein factor, ASF, controls cell-specific alternative splicing of SV40 early pre-mRNA in vitro. *Cell* 62, 25–34.
- Ge, H., Zuo, P., and Manley, J.L. (1991). Primary structure of the human splicing factor ASF reveals similarities with Drosophila regulators. *Cell* 66, 373–382.
- Georges, A., Coyaud, E., Marcon, E., Greenblatt, J., Raught, B., and Frappier, L. (2019). USP7 Regulates Cytokinesis through FBXO38 and KIF20B. *Scientific reports* 9, 2724.
- Gerstberger, S., Hafner, M., and Tuschl, T. (2014). A census of human RNA-binding proteins. *Nature reviews. Genetics* 15, 829–845.
- Ghosh, A., Shuman, S., and Lima, C.D. (2011). Structural insights to how mammalian capping enzyme reads the CTD code. *Molecular cell* 43, 299–310.
- Ghosh, G., and Adams, J.A. (2011). Phosphorylation mechanism and structure of serine-arginine protein kinases. *The FEBS journal* 278, 587–597.
- Gilbert, W. (1978). Why genes in pieces? *Nature* 271, 501.
- Girard, C., Will, C.L., Peng, J., Makarov, E.M., Kastner, B., Lemm, I., Urlaub, H., Hartmuth, K., and Lührmann, R. (2012). Post-transcriptional spliceosomes are retained in nuclear speckles until splicing completion. *Nature communications* 3, 994.
- Gonçalves, V., Matos, P., and Jordan, P. (2008). The beta-catenin/TCF4 pathway modifies alternative splicing through modulation of SRp20 expression. *RNA (New York, N.Y.)* 14, 2538–2549.
- Goss, J.D., and Kleiman, E.F. (2013). Poly(A) binding proteins: are they all created equal? *Wiley interdisciplinary reviews. RNA* 4, 167–179.
- Grant, R.P., Marshall, N.J., Yang, J.-C., Fasken, M.B., Kelly, S.M., Harreman, M.T., Neuhaus, D., Corbett, A.H., and Stewart, M. (2008). Structure of the N-terminal Mlp1-binding domain of the *Saccharomyces cerevisiae* mRNA-binding protein, Nab2. *Journal of molecular biology* 376, 1048–1059.
- Graveley, B.R. (2000). Sorting out the complexity of SR protein functions. *RNA* 6, 1197–1211.
- Graveley, B.R., and Maniatis, T. (1998). Arginine/serine-rich domains of SR proteins can function as activators of pre-mRNA splicing. *Molecular cell* 1, 765–771.
- Green, D.M., Johnson, C.P., Hagan, H., and Corbett, A.H. (2003). The C-terminal domain of myosin-like protein 1 (Mlp1p) is a docking site for heterogeneous nuclear ribonucleoproteins that are required for mRNA export. *Proceedings of the National Academy of Sciences of the United States of America* 100, 1010–1015.

- Green, D.M., Marfatia, K.A., Crafton, E.B., Zhang, X., Cheng, X., and Corbett, A.H. (2002). Nab2p is required for poly(A) RNA export in *Saccharomyces cerevisiae* and is regulated by arginine methylation via Hmt1p. *The Journal of biological chemistry* *277*, 7752–7760.
- Grenier St-Sauveur, V., Soucek, S., Corbett, A.H., and Bachand, F. (2013). Poly(A) tail-mediated gene regulation by opposing roles of Nab2 and Pab2 nuclear poly(A)-binding proteins in pre-mRNA decay. *Molecular and cellular biology* *33*, 4718–4731.
- Grudzien, E., Kalek, M., Jemielity, J., Darzynkiewicz, E., and Rhoads, R.E. (2006). Differential inhibition of mRNA degradation pathways by novel cap analogs. *The Journal of biological chemistry* *281*, 1857–1867.
- Grünwald, D., and Singer, R.H. (2010). In Vivo Imaging of Labelled Endogenous β -actin mRNA During Nucleocytoplasmic Transport. *Nature* *467*, 604–607.
- Gruter, P., Tabernero, C., Kobbe, C. von, Schmitt, C., Saavedra, C., Bachi, A., Wilm, M., Felber, B.K., and Izaurralde, E. (1998). TAP, the human homolog of Mex67p, mediates CTE-dependent RNA export from the nucleus. *Molecular cell* *1*, 649–659.
- Gudde, A., van Kessel, Ingeborg D G, Andre, L.M., Wieringa, B., and Wansink, D.G. (2017). Trinucleotide-repeat expanded and normal DMPK transcripts contain unusually long poly(A) tails despite differential nuclear residence. *Biochimica et biophysica acta. Gene regulatory mechanisms* *1860*, 740–749.
- Gudipati, K.R., Xu, Z., Lebreton, A., Séraphin, B., Steinmetz, M.L., Jacquier, A., and Libri, D. (2012). Extensive degradation of RNA precursors by the exosome in wild-type cells. *Molecular cell* *48*, 409–421.
- Guthrie, R.C., Greenup, L., Leverenz, B.J., and Kraemer, C.B. (2011). MSUT2 is a determinant of susceptibility to tau neurotoxicity. *Human molecular genetics* *20*, 1989–1999.
- Guthrie, R.C., Schellenberg, D.G., and Kraemer, C.B. (2009). SUT-2 potentiates tau-induced neurotoxicity in *Caenorhabditis elegans*. *Human molecular genetics* *18*, 1825–1838.
- Hall, L.L., Smith, K.P., Byron, M., and Lawrence, J.B. (2006). Molecular anatomy of a speckle. *The Anatomical Record Part A: Discoveries in Molecular, Cellular, and Evolutionary Biology* *288A*, 664–675.
- Hammarskjöld, M.-L., and Rekosh, D. (2017). SR proteins: To shuttle or not to shuttle, that is the question. *The Journal of cell biology* *216*, 1875–1877.
- Han, J., and van Hoof, A. (2016). The RNA Exosome Channeling and Direct Access Conformations Have Distinct In Vivo Functions. *Cell reports* *16*, 3348–3358.
- Han, J., Xiong, J., Wang, D., and Fu, X.-D. (2011). Pre-mRNA splicing: Where and when in the nucleus. *Trends in cell biology* *21*, 336–343.
- Hargous, Y., Hautbergue, G.M., Tintaru, A.M., Skrisovska, L., Golovanov, A.P., Stevenin, J., Lian, L.-Y., Wilson, S.A., and Allain, F.H.-T. (2006). Molecular basis of RNA recognition and TAP binding by the SR proteins SRp20 and 9G8. *The EMBO journal* *25*, 5126–5137.
- HARRIS, H., and Watts, J.W. (1962). The relationship between nuclear and cytoplasmic ribonucleic acid. *Proceedings of the Royal Society of London. Series B, Biological sciences* *156*, 109–121.
- Hartmann, A.M., Rujescu, D., Giannakouros, T., Nikolakaki, E., Goedert, M., Mandelkow, E.M., Gao, Q.S., Andreadis, A., and Stamm, S. (2001). Regulation of alternative splicing of human tau exon 10 by phosphorylation of splicing factors. *Molecular and cellular neurosciences* *18*, 80–90.

- Haruki, H., Nishikawa, J., and Laemmli, U.K. (2008). The Anchor-Away Technique: Rapid, Conditional Establishment of Yeast Mutant Phenotypes. *Molecular cell* *31*, 925–932.
- Hasegawa, M., Miura, T., Kuzuya, K., Inoue, A., Won Ki, S., Horinouchi, S., Yoshida, T., Kunoh, T., Koseki, K., Mino, K., Sasaki, R., Yoshida, M., and Mizukami, T. (2011). Identification of SAP155 as the target of GEX1A (Herboxidiene), an antitumor natural product. *ACS chemical biology* *6*, 229–233.
- Hauer, C., Sieber, J., Schwarzl, T., Hollerer, I., Curk, T., Alleaume, A.-M., Hentze, M.W., and Kulozik, A.E. (2016). Exon Junction Complexes Show a Distributional Bias toward Alternatively Spliced mRNAs and against mRNAs Coding for Ribosomal Proteins. *Cell reports* *16*, 1588–1603.
- Hautbergue, G.M., Hung, M.-L., Walsh, M.J., Snijders, A.P.L., Chang, C.-T., Jones, R., Ponting, C.P., Dickman, M.J., and Wilson, S.A. (2009). UIF, a New mRNA Export Adaptor that Works Together with REF/ALY, Requires FACT for Recruitment to mRNA. *Current Biology* *19*, 1918–1924.
- He, X., Arslan, A.D., Pool, M.D., Ho, T.-T., Darcy, K.M., Coon, J.S., and Beck, W.T. (2011). Knockdown of splicing factor SRp20 causes apoptosis in ovarian cancer cells and its expression is associated with malignancy of epithelial ovarian cancer. *Oncogene* *30*, 356–365.
- Hector, R.E., Nykamp, K.R., Dheur, S., Anderson, J.T., Non, P.J., Urbinati, C.R., Wilson, S.M., Minvielle-Sebastia, L., and Swanson, M.S. (2002). Dual requirement for yeast hnRNP Nab2p in mRNA poly(A) tail length control and nuclear export. *The EMBO journal* *21*, 1800–1810.
- Hedley, L.M., Amrein, H., and Maniatis, T. (1995). An amino acid sequence motif sufficient for subnuclear localization of an arginine/serine-rich splicing factor. *Proceedings of the National Academy of Sciences of the United States of America* *92*, 11524–11528.
- Henschel, A., Buchholz, F., and Habermann, B. (2004). DEQOR: a web-based tool for the design and quality control of siRNAs. *Nucleic acids research* *32*, W113-20.
- Herold, A., Suyama, M., Rodrigues, J.P., Braun, I.C., Kutay, U., Carmo-Fonseca, M., Bork, P., and Izaurralde, E. (2000a). TAP (NXF1) Belongs to a Multigene Family of Putative RNA Export Factors with a Conserved Modular Architecture. *Molecular and Cellular Biology* *20*, 8996–9008.
- Herold, A., Suyama, M., Rodrigues, J.P., Braun, I.C., Kutay, U., Carmo-Fonseca, M., Bork, P., and Izaurralde, E. (2000b). TAP (NXF1) Belongs to a Multigene Family of Putative RNA Export Factors with a Conserved Modular Architecture. *Molecular and Cellular Biology* *20*, 8996–9008.
- Herold, A., Teixeira, L., and Izaurralde, E. (2003). Genome-wide analysis of nuclear mRNA export pathways in *Drosophila*. *The EMBO journal* *22*, 2472–2483.
- Hertel, K.J., and Maniatis, T. (1999). Serine–arginine (SR)-rich splicing factors have an exon-independent function in pre-mRNA splicing. *Proceedings of the National Academy of Sciences* *96*, 2651–2655.
- Herzel, L., Straube, K., and Neugebauer, K.M. (2018). Long-read sequencing of nascent RNA reveals coupling among RNA processing events. *Genome research* *28*, 1008–1019.
- Hett, A., and West, S. (2014). Inhibition of U4 snRNA in human cells causes the stable retention of polyadenylated pre-mRNA in the nucleus. *PLoS one* *9*, e96174.

- Hildebrandt, A., Brüggemann, M., Boerner, S., Rücklé, C., Heidelberger, J. B., Dold, A., Busch, A., Hänel, H., Voigt, A., Ebersberger, S., Ebersberger, I., Roignant, J.-Y., Zarnack, K., König, J., & Beli, P. (2019). The RNA-binding ubiquitin ligase MKRN1 functions in ribosome-associated quality control of poly(A)-translation.
- Hirschfeld, M., Zur Hausen, A., Bettendorf, H., Jäger, M., and Stickeler, E. (2009). Alternative splicing of *Cyr61* is regulated by hypoxia and significantly changed in breast cancer. *Cancer research* 69, 2082–2090.
- Ho, D.N., Coburn, G.A., Kang, Y., Cullen, B.R., and Georgiadis, M.M. (2002). The crystal structure and mutational analysis of a novel RNA-binding domain found in the human Tap nuclear mRNA export factor. *Proceedings of the National Academy of Sciences of the United States of America* 99, 1888–1893.
- Hochberg-Laufer, H., Schwed-Gross, A., Neugebauer, K.M., and Shav-Tal, Y. (2019). Uncoupling of nucleocytoplasmic RNA export and localization during stress. *Nucleic acids research* 47, 4778–4797.
- Hong, D.S., Kurzrock, R., Naing, A., Wheler, J.J., Falchook, G.S., Schiffman, J.S., Faulkner, N., Pilat, M.J., O'Brien, J., and LoRusso, P. (2014). A phase I, open-label, single-arm, dose-escalation study of E7107, a precursor messenger ribonucleic acid (pre-mRNA) spliceosome inhibitor administered intravenously on days 1 and 8 every 21 days to patients with solid tumors. *Investigational new drugs* 32, 436–444.
- Houseley, J., Kotovic, K., El Hage, A., and Tollervey, D. (2007). Trf4 targets ncRNAs from telomeric and rDNA spacer regions and functions in rDNA copy number control. *The EMBO journal* 26, 4996–5006.
- Hsu, T.Y.-T., Simon, L.M., Neill, N.J., Marcotte, R., Sayad, A., Bland, C.S., Echeverria, G.V., Sun, T., Kurley, S.J., Tyagi, S., Karlin, K.L., Dominguez-Vidaña, R., Hartman, J.D., Renwick, A., Scorsone, K., Bernardi, R.J., Skinner, S.O., Jain, A., Orellana, M., Lagiseti, C., Golding, I., Jung, S.Y., Neilson, J.R., Zhang, X.H.-F., Cooper, T.A., Webb, T.R., Neel, B.G., Shaw, C.A., and Westbrook, T.F. (2015). The spliceosome is a therapeutic vulnerability in MYC-driven cancer. *Nature* 525, 384–388.
- Hu, Y., Plutz, M., and Belmont, A.S. (2010). Hsp70 gene association with nuclear speckles is Hsp70 promoter specific. *The Journal of cell biology* 191, 711–719.
- Huang, S., Deerinck, J.T., Ellisman, H.M., and Spector, L.D. (1994). In vivo analysis of the stability and transport of nuclear poly(A)+ RNA. *The Journal of cell biology* 126, 877–899.
- Huang, Y., and Steitz, J.A. (2005). SRprises along a messenger's journey. *Molecular cell* 17, 613–615.
- Huang, Y., Yario, T.A., and Steitz, J.A. (2004). A molecular link between SR protein dephosphorylation and mRNA export. *Proceedings of the National Academy of Sciences* 101, 9666–9670.
- Huppertz, I., Attig, J., D'Ambrogio, A., Easton, L.E., Sibley, C.R., Sugimoto, Y., Tajnik, M., König, J., and Ule, J. (2014). iCLIP: protein-RNA interactions at nucleotide resolution. *Methods (San Diego, Calif.)* 65, 274–287.
- Hyjek, M., Wojciechowska, N., Rudzka, M., Kołowerzo-Lubnau, A., and Smoliński, D.J. (2015). Spatial regulation of cytoplasmic snRNP assembly at the cellular level. *Journal of Experimental Botany* 66, 7019–7030.
- Ibrahim, E.C., Schaal, T.D., Hertel, K.J., Reed, R., and Maniatis, T. (2005). Serine/arginine-rich protein-dependent suppression of exon skipping by exonic splicing enhancers. *Proceedings of the National Academy of Sciences* 102, 5002–5007.

- Ibrahim, M.Y., Mohd Hashim, N., Mohan, S., Abdulla, M.A., Abdelwahab, S.I., Kamalidehghan, B., Ghaderian, M., Dehghan, F., Ali, L.Z., Karimian, H., Yahayu, M., Ee, G.C.L., Farjam, A.S., and Mohd Ali, H. (2014). Involvement of NF-kappaB and HSP70 signaling pathways in the apoptosis of MDA-MB-231 cells induced by a prenylated xanthone compound, alpha-mangostin, from *Cratoxylum arborescens*. *Drug design, development and therapy* 8, 2193–2211.
- Iglesias, N., Tutucci, E., Gwizdek, C., Vinciguerra, P., Dach, E. von, Corbett, A.H., Dargemont, C., and Stutz, F. (2010). Ubiquitin-mediated mRNP dynamics and surveillance prior to budding yeast mRNA export. *Genes & Development* 24, 1927–1938.
- Imamoto, N. (2018). Heat stress-induced nuclear transport mediated by Hikeshi confers nuclear function of Hsp70s. *Current opinion in cell biology* 52, 82–87.
- Irwin, S., Vandelft, M., Pinchev, D., Howell, J.L., Graczyk, J., Orr, H.T., and Truant, R. (2005). RNA association and nucleocytoplasmic shuttling by ataxin-1. *Journal of cell science* 118, 233–242.
- Ishihama, Y., Tadakuma, H., Tani, T., and Funatsu, T. (2008). The dynamics of pre-mRNAs and poly(A)+ RNA at speckles in living cells revealed by iFRAP studies. *Experimental cell research* 314, 748–762.
- Ito, G., Katsemonova, K., Tonelli, F., Lis, P., Baptista, M.A.S., Shpiro, N., Duddy, G., Wilson, S., Ho, P.W.-L., Ho, S.-L., Reith, A.D., and Alessi, D.R. (2016). Phos-tag analysis of Rab10 phosphorylation by LRRK2: a powerful assay for assessing kinase function and inhibitors. *Biochemical Journal* 473, 2671–2685.
- Izaurralde, E. (2002). A novel family of nuclear transport receptors mediates the export of messenger RNA to the cytoplasm. *European journal of cell biology* 81, 577–584.
- Izaurralde, E., Lewis, J., McGuigan, C., Jankowska, M., Darzynkiewicz, E., and Mattaj, I.W. (1994). A nuclear cap binding protein complex involved in pre-mRNA splicing. *Cell* 78, 657–668.
- Jacob, A.G., and Smith, C.W.J. (2017). Intron retention as a component of regulated gene expression programs. *Human genetics*.
- Jády, B.E., Darzacq, X., Tucker, K.E., Matera, A.G., Bertrand, E., and Kiss, T. (2003). Modification of Sm small nuclear RNAs occurs in the nucleoplasmic Cajal body following import from the cytoplasm. *The EMBO journal* 22, 1878–1888.
- Jamison, S.F., Pasmán, Z., Wang, J., Will, C., Lührmann, R., Manley, J.L., and Garcia-Blanco, M.A. (1995). U1 snRNP-ASF/SF2 interaction and 5' splice site recognition: characterization of required elements. *Genes & Development* 23, 3260–3267.
- Janisch, K.M., McNeely, K.C., Dardick, J.M., Lim, S.H., and Dwyer, N.D. (2018). Kinesin-6 KIF20B is required for efficient cytokinetic furrowing and timely abscission in human cells. *Molecular biology of the cell* 29, 166–179.
- Janisch, K.M., Vock, V.M., Fleming, M.S., Shrestha, A., Grimsley-Myers, C.M., Rasoul, B.A., Neale, S.A., Cupp, T.D., Kinchen, J.M., Liem, K.F., JR, and Dwyer, N.D. (2013). The vertebrate-specific Kinesin-6, Kif20b, is required for normal cytokinesis of polarized cortical stem cells and cerebral cortex size. *Development (Cambridge, England)* 140, 4672–4682.
- Jensen, T.H., Patricio, K., McCarthy, T., and Rosbash, M. (2001). A Block to mRNA Nuclear Export in *S. cerevisiae* Leads to Hyperadenylation of Transcripts that Accumulate at the Site of Transcription. *Molecular cell* 7, 887–898.

- Jeong, S. (2017). SR Proteins: Binders, Regulators, and Connectors of RNA. *Molecules and cells* *40*, 1–9.
- Jia, H., Wang, X., Anderson, T.J., and Jankowsky, E. (2012). RNA unwinding by the Trf4/Air2/Mtr4 polyadenylation (TRAMP) complex. *Proceedings of the National Academy of Sciences of the United States of America* *109*, 7292–7297.
- Jia, R., Li, C., McCoy, J.P., Deng, C.-X., and Zheng, Z.-M. (2010). SRp20 is a proto-oncogene critical for cell proliferation and tumor induction and maintenance. *International Journal of Biological Sciences* *6*, 806–826.
- Jiang, L., Zhou, J., Zhong, D., Zhou, Y., Zhang, W., Wu, W., Zhao, Z., Wang, W., Xu, W., He, L., Ma, Y., Hu, Y., and Li, J. (2017). Overexpression of SMC4 activates TGF β /Smad signaling and promotes aggressive phenotype in glioma cells. *Oncogenesis* *6*, e301.
- Johnson, C., Primorac, D., McKinstry, M., McNeil, J., Rowe, D., and Lawrence, J.B. (2000). Tracking COL1A1 RNA in osteogenesis imperfecta. splice-defective transcripts initiate transport from the gene but are retained within the SC35 domain. *The Journal of cell biology* *150*, 417–432.
- Jones-Villeneuve, E.M., McBurney, M.W., Rogers, K.A., and Kalnins, V.I. (1982). Retinoic acid induces embryonal carcinoma cells to differentiate into neurons and glial cells. *The Journal of cell biology* *94*, 253–262.
- Jones-Villeneuve, E.M., Rudnicki, M.A., Harris, J.F., and McBurney, M.W. (1983). Retinoic acid-induced neural differentiation of embryonal carcinoma cells. *Molecular and Cellular Biology* *3*, 2271–2279.
- Jumaa, H., Guénet, J.L., and Nielsen, P.J. (1997). Regulated expression and RNA processing of transcripts from the Srp20 splicing factor gene during the cell cycle. *Molecular and Cellular Biology* *17*, 3116–3124.
- Jumaa, H., and Nielsen, P.J. (1997). The splicing factor SRp20 modifies splicing of its own mRNA and ASF/SF2 antagonizes this regulation. *The EMBO journal* *16*, 5077–5085.
- Jumaa, H., and Nielsen, P.J. (2000). Regulation of SRp20 exon 4 splicing. *Biochimica et Biophysica Acta (BBA) - Gene Structure and Expression* *1494*, 137–143.
- Kadaba, S., Krueger, A., Trice, T., Krecic, M.A., Hinnebusch, G.A., and Anderson, J. (2004). Nuclear surveillance and degradation of hypomodified initiator tRNAMet in *S. cerevisiae*. *Genes & Development* *18*, 1227–1240.
- Kaida, D., Motoyoshi, H., Tashiro, E., Nojima, T., Hagiwara, M., Ishigami, K., Watanabe, H., Kitahara, T., Yoshida, T., Nakajima, H., Tani, T., Horinouchi, S., and Yoshida, M. (2007). Spliceostatin A targets SF3b and inhibits both splicing and nuclear retention of pre-mRNA. *Nature chemical biology* *3*, 576–583.
- Kanehira, M., Katagiri, T., Shimo, A., Takata, R., Shuin, T., Miki, T., Fujioka, T., and Nakamura, Y. (2007). Oncogenic role of MPHOSPH1, a cancer-testis antigen specific to human bladder cancer. *Cancer research* *67*, 3276–3285.
- Kanopka, A., Mühlemann, O., Petersen-Mahrt, S., Estmer, C., Ohrmalm, C., and Akusjärvi, G. (1998). Regulation of adenovirus alternative RNA splicing by dephosphorylation of SR proteins. *Nature* *393*, 185–187.
- Kanungo, J. (2017). Retinoic Acid Signaling in P19 Stem Cell Differentiation. *Anti-cancer agents in medicinal chemistry* *17*, 1184–1198.

- Katahira, J., Inoue, H., Hurt, E., and Yoneda, Y. (2009). Adaptor Aly and co-adaptor Thoc5 function in the Tap-p15-mediated nuclear export of HSP70 mRNA. *The EMBO journal* *28*, 556–567.
- Katahira, J., Strässer, K., Podtelejnikov, A., Mann, M., Jung, J.U., and Hurt, E. (1999). The Mex67p-mediated nuclear mRNA export pathway is conserved from yeast to human. *The EMBO journal* *18*, 2593–2609.
- Kataoka, N., Bachorik, J.L., and Dreyfuss, G. (1999). Transportin-SR, a Nuclear Import Receptor for SR Proteins. *The Journal of cell biology* *145*, 1145–1152.
- Kataoka, N., Diem, D.M., Kim, N.V., Yong, J., and Dreyfuss, G. (2001). Magoh, a human homolog of *Drosophila mago nashi* protein, is a component of the splicing-dependent exon-exon junction complex. *The EMBO journal* *20*, 6424–6433.
- Kaufman, L., Ayub, M., and Vincent, B.J. (2010). The genetic basis of non-syndromic intellectual disability: a review. *Journal of neurodevelopmental disorders* *2*, 182–209.
- Kelich, J.M., and Yang, W. (2014). High-Resolution Imaging Reveals New Features of Nuclear Export of mRNA through the Nuclear Pore Complexes. *International Journal of Molecular Sciences* *15*, 14492–14504.
- Kelley, J.B., and Paschal, B.M. (2007). Hyperosmotic stress signaling to the nucleus disrupts the Ran gradient and the production of RanGTP. *Molecular biology of the cell* *18*, 4365–4376.
- Kelly, M.S., Bienkowski, R., Banerjee, A., Melicharek, J.D., Brewer, A.Z., Marendza, R.D., Corbett, H.A., and Moberg, H.K. (2016). The *Drosophila* ortholog of the Zc3h14 RNA binding protein acts within neurons to pattern axon projection in the developing brain. *Developmental neurobiology* *76*, 93–106.
- Kelly, M.S., Leung, W.S., Apponi, H.L., Bramley, M.A., Tran, J.E., Chekanova, A.J., Wenthe, R.S., and Corbett, H.A. (2010). Recognition of polyadenosine RNA by the zinc finger domain of nuclear poly(A) RNA-binding protein 2 (Nab2) is required for correct mRNA 3'-end formation. *The Journal of biological chemistry* *285*, 26022–26032.
- Kelly, M.S., Pabit, A.S., Kitchen, M.C., Guo, P., Marfatia, A.K., Murphy, J.T., Corbett, H.A., and Berland, M.K. (2007). Recognition of polyadenosine RNA by zinc finger proteins. *Proceedings of the National Academy of Sciences of the United States of America* *104*, 12306–12311.
- Kelly, S., Pak, C., Garshasbi, M., Kuss, A., Corbett, A.H., and Moberg, K. (2012). New kid on the ID block: neural functions of the Nab2/ZC3H14 class of Cys₃His tandem zinc-finger polyadenosine RNA binding proteins. *RNA biology* *9*, 555–562.
- Kelly, S.M., Leung, S.W., Pak, C., Banerjee, A., Moberg, K.H., and Corbett, A.H. (2014). A conserved role for the zinc finger polyadenosine RNA binding protein, ZC3H14, in control of poly(A) tail length. *RNA (New York, N.Y.)* *20*, 681–688.
- Kendirgi, F., Rexer, D.J., Alcázar-Román, A.R., Onishko, H.M., and Wenthe, S.R. (2005). Interaction between the shuttling mRNA export factor Gle1 and the nucleoporin hCG1: a conserved mechanism in the export of Hsp70 mRNA. *Molecular biology of the cell* *16*, 4304–4315.
- Keren, H., Lev-Maor, G., and Ast, G. (2010). Alternative splicing and evolution: diversification, exon definition and function. *Nature reviews. Genetics* *11*, 345–355.

- Keshwani, M.M., Aubol, B.E., Fattet, L., Ma, C.-T., Qiu, J., Jennings, P.A., Fu, X.-D., and Adams, J.A. (2015). Conserved proline-directed phosphorylation regulates SR protein conformation and splicing function. *Biochemical Journal* *466*, 311–322.
- Khanna, N., Hu, Y., and Belmont, A.S. (2014). HSP70 transgene directed motion to nuclear speckles facilitates heat shock activation. *Current biology CB* *24*, 1138–1144.
- Kilchert, C., Wittmann, S., and Vasiljeva, L. (2016). The regulation and functions of the nuclear RNA exosome complex. *Nature reviews. Molecular cell biology* *17*, 227–239.
- Kim, J., Han, K. Y., Khanna, N., Ha, T., & Belmont, A. S. (2018). Nuclear speckle fusion via long-range directional motion regulates the number and size of speckles.
- Kim, J., Han, K.Y., Khanna, N., Ha, T., and Belmont, A.S. (2019). Nuclear speckle fusion via long-range directional motion regulates speckle morphology after transcriptional inhibition. *Journal of cell science* *132*.
- Kim, N.V., Yong, J., Kataoka, N., Abel, L., Diem, D.M., and Dreyfuss, G. (2001). The Y14 protein communicates to the cytoplasm the position of exon-exon junctions. *The EMBO journal* *20*, 2062–2068.
- Kim Guisbert, Karen Duncan, Li, H., and Guthrie, C. (2005). Functional specificity of shuttling hnRNPs revealed by genome-wide analysis of their RNA binding profiles. *RNA* *11*, 383–393.
- Klein, P., Oloko, M., Roth, F., Montel, V., Malerba, A., Jarmin, S., Gidaro, T., Popplewell, L., Perie, S., Lacau St Guily, J., La Grange, P. de, Antoniou, M.N., Dickson, G., Butler-Browne, G., Bastide, B., Mouly, V., and Trollet, C. (2016). Nuclear poly(A)-binding protein aggregates misplace a pre-mRNA outside of SC35 speckle causing its abnormal splicing. *Nucleic Acids Research* *44*, 10929–10945.
- Knowles, B.B., Aden, D.P., and Solter, D. (1978). Monoclonal antibody detecting a stage-specific embryonic antigen (SSEA-1) on preimplantation mouse embryos and teratocarcinoma cells. *Current topics in microbiology and immunology* *81*, 51–53.
- Kodiha, M., Banski, P., Ho-Wo-Cheong, D., and Stochaj, U. (2008). Dissection of the molecular mechanisms that control the nuclear accumulation of transport factors importin-alpha and CAS in stressed cells. *Cellular and molecular life sciences CMLS* *65*, 1756–1767.
- Koguchi, Y., Nishio, M., Kotera, J., Omori, K., Ohnuki, T., and Komatsubara, S. (1997). Trichostatin A and herboxidiene up-regulate the gene expression of low density lipoprotein receptor. *The Journal of antibiotics* *50*, 970–971.
- Kohtz, J.D., Jamison, S.F., Will, C.L., Zuo, P., Lührmann, R., Garcia-Blanco, M.A., and Manley, J.L. (1994). Protein-protein interactions and 5'-splice-site recognition in mammalian mRNA precursors. *Nature* *368*, 119–124.
- Kong, L., Wang, S., Wu, X., Zuo, F., Qin, H., and Wu, J. (2016). Paeoniflorin attenuates ultraviolet B-induced apoptosis in human keratinocytes by inhibiting the ROS-p38-p53 pathway. *Molecular Medicine Reports* *13*, 3553–3558.
- König, J., Zarnack, K., Rot, G., Curk, T., Kayikci, M., Zupan, B., Turner, D.J., Luscombe, N.M., and Ule, J. (2010). iCLIP reveals the function of hnRNP particles in splicing at individual nucleotide resolution. *Nature structural & molecular biology* *17*, 909–915.

- Kota, K.P., Wagner, S.R., Huerta, E., Underwood, J.M., and Nickerson, J.A. (2008). Binding of ATP to UAP56 is necessary for mRNA export. *Journal of cell science* *121*, 1526–1537.
- Kotake, Y., Sagane, K., Owa, T., Mimori-Kiyosue, Y., Shimizu, H., Uesugi, M., Ishihama, Y., Iwata, M., and Mizui, Y. (2007). Splicing factor SF3b as a target of the antitumor natural product pladienolide. *Nature chemical biology* *3*, 570–575.
- Krainer, A.R., Conway, G.C., and Kozak, D. (1990a). Purification and characterization of pre-mRNA splicing factor SF2 from HeLa cells. *Genes & Development* *4*, 1158–1171.
- Krainer, A.R., Conway, G.C., and Kozak, D. (1990b). The essential pre-mRNA splicing factor SF2 influences 5' splice site selection by activating proximal sites. *Cell* *62*, 35–42.
- Krainer, A.R., and Maniatis, T. (1985). Multiple factors including the small nuclear ribonucleoproteins U1 and U2 are necessary for pre-mRNA splicing in vitro. *Cell* *42*, 725–736.
- Krainer, A.R., Mayeda, A., Kozak, D., and Binns, G. (1991). Functional expression of cloned human splicing factor SF2: homology to RNA-binding proteins, U1 70K, and *Drosophila* splicing regulators. *Cell* *66*, 383–394.
- Kruhlak, M.J., Lever, M.A., Fischle, W., Verdin, E., Bazett-Jones, D.P., and Hendzel, M.J. (2000). Reduced Mobility of the Alternate Splicing Factor (Asf) through the Nucleoplasm and Steady State Speckle Compartments. *The Journal of cell biology* *150*, 41–52.
- Kuhlmann, S.I., Valkov, E., and Stewart, M. (2014). Structural basis for the molecular recognition of polyadenosine RNA by Nab2 Zn fingers. *Nucleic acids research* *42*, 672–680.
- Kwak, W.-J., Han, C.K., Son, K.H., Chang, H.W., Kang, S.S., Park, B.K., and Kim, H.P. (2002). Effects of Ginkgetin from *Ginkgo biloba* Leaves on cyclooxygenases and in vivo skin inflammation. *Planta medica* *68*, 316–321.
- Lacadie, S.A., Tardiff, D.F., Kadener, S., and Rosbash, M. (2006). In vivo commitment to yeast cotranscriptional splicing is sensitive to transcription elongation mutants. *Genes & Development* *20*, 2055–2066.
- Lagisetti, C., Palacios, G., Goronga, T., Freeman, B., Caufield, W., and Webb, T.R. (2013). Optimization of antitumor modulators of pre-mRNA splicing. *Journal of medicinal chemistry* *56*, 10033–10044.
- Lai, M.C., Lin, R.I., Huang, S.Y., Tsai, C.W., and Tarn, W.Y. (2000). A human importin-beta family protein, transportin-SR2, interacts with the phosphorylated RS domain of SR proteins. *The Journal of biological chemistry* *275*, 7950–7957.
- Lai, M.-C., Lin, R.-I., and Tarn, W.-Y. (2001). Transportin-SR2 mediates nuclear import of phosphorylated SR proteins. *Proceedings of the National Academy of Sciences of the United States of America* *98*, 10154–10159.
- Lai, M.-C., and Tarn, W.-Y. (2004). Hypophosphorylated ASF/SF2 binds TAP and is present in messenger ribonucleoproteins. *The Journal of biological chemistry* *279*, 31745–31749.
- Lander, S.E., Linton, M.L., Birren, B., Nusbaum, C., Zody, C.M., Baldwin, J., Devon, K., Dewar, K., Doyle, M., FitzHugh, W., Funke, R., Gage, D., Harris, K., Heaford, A., Howland, J., Kann, L., Lehoczy, J., LeVine, R., McEwan, P., McKernan, K., Meldrim, J., Mesirov, P.J., Miranda, C., Morris, W., Naylor, J., Raymond, C.,

- Rosetti, M., Santos, R., Sheridan, A., Sougnez, C., Stange-Thomann, Y., Stojanovic, N., Subramanian, A., Wyman, D., Rogers, J., Sulston, J., Ainscough, R., Beck, S., Bentley, D., Burton, J., Clee, C., Carter, N., Coulson, A., Deadman, R., Deloukas, P., Dunham, A., Dunham, I., Durbin, R., French, L., Grafham, D., Gregory, S., Hubbard, T., Humphray, S., Hunt, A., Jones, M., Lloyd, C., McMurray, A., Matthews, L., Mercer, S., Milne, S., Mullikin, C.J., Mungall, A., Plumb, R., Ross, M., Shownkeen, R., Sims, S., Waterston, H.R., Wilson, K.R., Hillier, W.L., McPherson, D.J., Marra, A.M., Mardis, R.E., Fulton, A.L., Chinwalla, T.A., Pepin, H.K., Gish, R.W., Chissoe, L.S., Wendl, C.M., Delehaunty, D.K., Miner, L.T., Delehaunty, A., Kramer, B.J., Cook, L.L., Fulton, S.R., Johnson, L.D., Minx, J.P., Clifton, W.S., Hawkins, T., Branscomb, E., Predki, P., Richardson, P., Wenning, S., Slezak, T., Doggett, N., Cheng, F.J., Olsen, A., Lucas, S., Elkin, C., Uberbacher, E., Frazier, M., Gibbs, A.R., Muzny, M.D., Scherer, E.S., Bouck, B.J., Sodergren, J.E., Worley, C.K., Rives, M.C., Gorrell, H.J., Metzker, L.M., Naylor, L.S., Kucherlapati, S.R., Nelson, L.D., Weinstock, M.G., Sakaki, Y., Fujiyama, A., Hattori, M., Yada, T., Toyoda, A., Itoh, T., Kawagoe, C., Watanabe, H., Totoki, Y., Taylor, T., Weissbach, J., Heilig, R., Saurin, W., Artiguenave, F., Brottier, P., Bruls, T., Pelletier, E., Robert, C., Wincker, P., Smith, R.D., Doucette-Stamm, L., Rubenfield, M., Weinstock, K., Lee, M.H., Dubois, J., Rosenthal, A., Platzer, M., Nyakatura, G., Taudien, S., Rump, A., Yang, H., Yu, J., Wang, J., Huang, G., Gu, J., Hood, L., Rowen, L., Madan, A., Qin, S., Davis, W.R., Federspiel, A.N., Abola, P.A., Proctor, J.M., Myers, M.R., Schmutz, J., Dickson, M., Grimwood, J., Cox, R.D., Olson, V.M., Kaul, R., Shimizu, N., Kawasaki, K., Minoshima, S., Evans, A.G., Athanasiou, M., Schultz, R., Roe, A.B., Chen, F., Pan, H., Ramser, J., Lehrach, H., Reinhardt, R., McCombie, R.W., La Bastide, M. de, Dedhia, N., Blcker, H., Hornischer, K., Nordsiek, G., Agarwala, R., Aravind, L., Bailey, A.J., Bateman, A., Batzoglou, S., Birney, E., Bork, P., Brown, G.D., Burge, B.C., Cerutti, L., Chen, C.H., Church, D., Clamp, M., Copley, R.R., Doerks, T., Eddy, R.S., Eichler, E.E., Furey, S.T., Galagan, J., Gilbert, G.J., Harmon, C., Hayashizaki, Y., Haussler, D., Hermjakob, H., Hokamp, K., Jang, W., Johnson, S.L., Jones, A.T., Kasif, S., Kasprzyk, A., Kennedy, S., Kent, J.W., Kitts, P., Koonin, V.E., Korf, I., Kulp, D., Lancet, D., Lowe, M.T., McLysaght, A., Mikkelsen, T., Moran, V.J., Mulder, N., Pollara, J.V., Ponting, P.C., Schuler, G., Schultz, J., Slater, G., Smit, F.A., Stupka, E., Szustakowki, J., Thierry-Mieg, D., Thierry-Mieg, J., Wagner, L., Wallis, J., Wheeler, R., Williams, A., Wolf, I.Y., Wolfe, H.K., Yang, P.S., Yeh, F.R., Collins, F., Guyer, S.M., Peterson, J., Felsenfeld, A., Wetterstrand, A.K., Patrinos, A., Morgan, J.M., Jong, P. de, Catanese, J.J., Osoegawa, K., Shizuya, H., Choi, S., Chen, J.Y., and Consortium, International Human Genome Sequencing (2001). Initial sequencing and analysis of the human genome. *Nature* 409, 860–921.
- Le Hir, H., Gatfield, D., Braun, C.I., Forler, D., and Izaurralde, E. (2001). The protein Mago provides a link between splicing and mRNA localization. *EMBO reports* 2, 1119–1124.
- Le Hir, H., Izaurralde, E., Maquat, L.E., and Moore, M.J. (2000). The spliceosome deposits multiple proteins 20–24 nucleotides upstream of mRNA exon–exon junctions. *The EMBO journal* 19, 6860–6869.
- Lebreton, A., Tomecki, R., Dziembowski, A., and Séraphin, B. (2008). Endonucleolytic RNA cleavage by a eukaryotic exosome. *Nature* 456, 993–996.
- Lee, H., Pine, P.S., McDaniel, J., Salit, M., and Oliver, B. (2016). External RNA Controls Consortium Beta Version Update. *Journal of Genomics* 4, 19–22.
- Leonard, H., and Wen, X. (2002). The epidemiology of mental retardation: challenges and opportunities in the new millennium. *Mental retardation and developmental disabilities research reviews* 8, 117–134.

- Leung, S.W., Apponi, L.H., Cornejo, O.E., Kitchen, C.M., Valentini, S.R., Pavlath, G.K., Dunham, C.M., and Corbett, A.H. (2009). Splice Variants of the Human ZC3H14 Gene Generate Multiple Isoforms of a Zinc Finger Polyadenosine RNA Binding Protein. *Gene* 439, 71–78.
- Levine, J.M., and Flynn, P. (1986). Cell surface changes accompanying the neural differentiation of an embryonal carcinoma cell line. *Journal of Neuroscience* 6, 3374–3384.
- Li, C., Goryaynov, A., and Yang, W. (2016a). The selective permeability barrier in the nuclear pore complex. *Nucleus* 7, 430–446.
- Li, P., Banjade, S., Cheng, H.-C., Kim, S., Chen, B., Guo, L., Llaguno, M., Hollingsworth, J.V., King, D.S., Banani, S.F., Russo, P.S., Jiang, Q.-X., Nixon, B.T., and Rosen, M.K. (2012). Phase Transitions in the Assembly of Multi-Valent Signaling Proteins. *Nature* 483, 336–340.
- Li, Y., and Blencowe, B.J. (1999). Distinct Factor Requirements for Exonic Splicing Enhancer Function and Binding of U2AF to the Polypyrimidine Tract. *Journal of Biological Chemistry* 274, 35074–35079.
- Li, Y., Bor, Y.-C., Fitzgerald, M.P., Lee, K.S., Rekosh, D., and Hammarskjöld, M.-L. (2016b). An NXF1 mRNA with a retained intron is expressed in hippocampal and neocortical neurons and is translated into a protein that functions as an Nxf1 cofactor. *Molecular biology of the cell* 27, 3903–3912.
- Li, Y., Bor, Y.-C., Misawa, Y., Xue, Y., Rekosh, D., and Hammarskjöld, M.-L. (2006). An intron with a constitutive transport element is retained in a Tap messenger RNA. *Nature* 443, 234.
- Lin, M., Pedrosa, E., Shah, A., Hrabovsky, A., Maqbool, S., Zheng, D., and Lachman, H.M. (2011). RNA-Seq of Human Neurons Derived from iPS Cells Reveals Candidate Long Non-Coding RNAs Involved in Neurogenesis and Neuropsychiatric Disorders. *PLoS one* 6.
- Lin, S., Xiao, R., Sun, P., Xu, X., and Fu, X.-D. (2005). Dephosphorylation-dependent sorting of SR splicing factors during mRNP maturation. *Molecular cell* 20, 413–425.
- Listerman, I., Sapra, A.K., and Neugebauer, K.M. (2006). Cotranscriptional coupling of splicing factor recruitment and precursor messenger RNA splicing in mammalian cells. *Nature structural & molecular biology* 13, 815–822.
- Liu, H.-X., Chew, S.L., Cartegni, L., Zhang, M.Q., and Krainer, A.R. (2000). Exonic Splicing Enhancer Motif Recognized by Human SC35 under Splicing Conditions. *Molecular and Cellular Biology* 20, 1063–1071.
- Liu, H.-X., Zhang, M., and Krainer, A.R. (1998). Identification of functional exonic splicing enhancer motifs recognized by individual SR proteins. *Genes & Development* 12, 1998–2012.
- Long, J.C., and Caceres, J.F. (2009). The SR protein family of splicing factors: master regulators of gene expression. *The Biochemical journal* 417, 15–27.
- Long, Y., Sou, W.H., Yung, K.W.Y., Liu, H., Wan, S.W.C., Li, Q., Zeng, C., Law, C.O.K., Chan, G.H.C., Lau, T.C.K., and Ngo, J.C.K. (2019). Distinct mechanisms govern the phosphorylation of different SR protein splicing factors. *The Journal of biological chemistry* 294, 1312–1327.
- Los Angeles, A. de, Ferrari, F., Xi, R., Fujiwara, Y., Benvenisty, N., Deng, H., Hochedlinger, K., Jaenisch, R., Lee, S., Leitch, H.G., Lensch, M.W., Lujan, E., Pei, D., Rossant, J., Wernig, M., Park, P.J., and Daley, G.Q. (2015). Hallmarks of pluripotency. *Nature* 525, 469–478.

- Losh, S.J., King, K.A., Bakelar, J., Taylor, L., Loomis, J., Rosenzweig, A.J., Johnson, J.S., and van Hoof, A. (2015). Interaction between the RNA-dependent ATPase and poly(A) polymerase subunits of the TRAMP complex is mediated by short peptides and important for snoRNA processing. *Nucleic acids research* *43*, 1848–1858.
- Lou, H., Neugebauer, K.M., Gagel, R.F., and Berget, S.M. (1998). Regulation of Alternative Polyadenylation by U1 snRNPs and SRp20. *Molecular and cellular biology* *18*, 4977–4985.
- Love, M.I., Huber, W., and Anders, S. (2014). Moderated estimation of fold change and dispersion for RNA-seq data with DESeq2. *Genome biology* *15*.
- Lu, Z., Zhang, Q.C., Lee, B., Flynn, R.A., Smith, M.A., Robinson, J.T., Davidovich, C., Gooding, A.R., Goodrich, K.J., Mattick, J.S., Mesirov, J.P., Cech, T.R., and Chang, H.Y. (2016). RNA Duplex Map in Living Cells Reveals Higher-Order Transcriptome Structure. *Cell* *165*, 1267–1279.
- Lubas, M., Andersen, R.P., Schein, A., Dziembowski, A., Kudla, G., and Jensen, H.T. (2015). The human nuclear exosome targeting complex is loaded onto newly synthesized RNA to direct early ribonucleolysis. *Cell reports* *10*, 178–192.
- Lubas, M., Christensen, S.M., Kristiansen, S.M., Domanski, M., Falkenby, G.L., Lykke-Andersen, S., Andersen, S.J., Dziembowski, A., and Jensen, H.T. (2011). Interaction profiling identifies the human nuclear exosome targeting complex. *Molecular cell* *43*, 624–637.
- Lubelsky, Y., and Ulitsky, I. (2018). Sequences enriched in Alu repeats drive nuclear localization of long RNAs in human cells. *Nature* *555*, 107–111.
- Lukasiewicz, R., Velazquez-Dones, A., Huynh, N., Hagopian, J., Fu, X.-D., Adams, J., and Ghosh, G. (2007). Structurally unique yeast and mammalian serine-arginine protein kinases catalyze evolutionarily conserved phosphorylation reactions. *The Journal of biological chemistry* *282*, 23036–23043.
- Lun, A.T.L., Calero-Nieto, F.J., Haim-Vilmovsky, L., Göttgens, B., and Marioni, J.C. (2017). Assessing the reliability of spike-in normalization for analyses of single-cell RNA sequencing data. *Genome research* *27*, 1795–1806.
- Lund, K.M., and Guthrie, C. (2005). The DEAD-box protein Dbp5p is required to dissociate Mex67p from exported mRNPs at the nuclear rim. *Molecular cell* *20*, 645–651.
- Lunde, B.M., Moore, C., and Varani, G. (2007). RNA-binding proteins: modular design for efficient function. *Nature reviews. Molecular cell biology* *8*, 479–490.
- Ma, C.-T., Ghosh, G., Fu, X.-D., and Adams, J.A. (2010). Mechanism of dephosphorylation of the SR protein ASF/SF2 by protein phosphatase 1. *Journal of molecular biology* *403*, 386–404.
- Ma, C.-T., Hagopian, J.C., Ghosh, G., Fu, X.-D., and Adams, J.A. (2009). Regiospecific phosphorylation control of the SR protein ASF/SF2 by SRPK1. *Journal of molecular biology* *390*, 618–634.
- Magnuson, D.S., Morassutti, D.J., McBurney, M.W., and Marshall, K.C. (1995a). Neurons derived from P19 embryonal carcinoma cells develop responses to excitatory and inhibitory neurotransmitters. *Brain research. Developmental brain research* *90*, 141–150.

- Magnuson, D.S., Morassutti, D.J., Staines, W.A., McBurney, M.W., and Marshall, K.C. (1995b). In vivo electrophysiological maturation of neurons derived from a multipotent precursor (embryonal carcinoma) cell line. *Brain research. Developmental brain research* *84*, 130–141.
- Mahajan, R., Delphin, C., Guan, T., Gerace, L., and Melchior, F. (1997). A Small Ubiquitin-Related Polypeptide Involved in Targeting RanGAP1 to Nuclear Pore Complex Protein RanBP2. *Cell* *88*, 97–107.
- Majerciak, V., Lu, M., Li, X., and Zheng, Z.-M. (2014). Attenuation of the suppressive activity of cellular splicing factor SRSF3 by Kaposi sarcoma-associated herpesvirus ORF57 protein is required for RNA splicing. *RNA* *20*, 1747–1758.
- Makino, L.D., Schuch, B., Stegmann, E., Baumgärtner, M., Basquin, C., and Conti, E. (2015). RNA degradation paths in a 12-subunit nuclear exosome complex. *Nature* *524*, 54–58.
- Mandel, C.R., Bai, Y., and Tong, L. (2008). Protein factors in pre-mRNA 3'-end processing. *Cellular and molecular life sciences: CMLS* *65*, 1099–1122.
- Manley, J.L., and Krainer, A.R. (2010). A rational nomenclature for serine/arginine-rich protein splicing factors (SR proteins). *Genes & Development* *24*, 1073–1074.
- Marfatia, A.K., Crafton, B.E., Green, M.D., and Corbett, H.A. (2003). Domain analysis of the *Saccharomyces cerevisiae* heterogeneous nuclear ribonucleoprotein, Nab2p. Dissecting the requirements for Nab2p-facilitated poly(A) RNA export. *The Journal of biological chemistry* *278*, 6731–6740.
- Martin, S.A., and Ouchi, T. (2005). BRCA1 phosphorylation regulates caspase-3 activation in UV-induced apoptosis. *Cancer research* *65*, 10657–10662.
- Martínez-Lumbreras, S., Santiveri, C.M., Mirassou, Y., Zorrilla, S., and Pérez-Cañadillas, J.M. (2013). Two singular types of CCCH tandem zinc finger in Nab2p contribute to polyadenosine RNA recognition. *Structure (London, England 1993)* *21*, 1800–1811.
- Martins, B.S., Rino, J., Carvalho, T., Carvalho, C., Yoshida, M., Klose, M.J., Almeida, F.S. de, and Carmo-Fonseca, M. (2011). Spliceosome assembly is coupled to RNA polymerase II dynamics at the 3' end of human genes. *Nature structural & molecular biology* *18*, 1115–1123.
- Marzluff, W.F., Wagner, E.J., and Duronio, R.J. (2008). Metabolism and regulation of canonical histone mRNAs: life without a poly(A) tail. *Nature reviews. Genetics* *9*, 843–854.
- Masuda, S., Das, R., Cheng, H., Hurt, E., Dorman, N., and Reed, R. (2005). Recruitment of the human TREX complex to mRNA during splicing. *Genes & Development* *19*, 1512–1517.
- Matera, A.G., and Wang, Z. (2014). A day in the life of the spliceosome. *Nature reviews. Molecular cell biology* *15*, 108–121.
- Matsu-ura, T., Dovzhenok, A., Aihara, E., Rood, J., Le, H., Ren, Y., Rosselot, A.E., Zhang, T., Lee, C., Obrietan, K., Montrose, M.H., Lim, S., Moore, S.R., and Hong, C.I. (2016). Intercellular Coupling of the Cell Cycle and Circadian Clock in Adult Stem Cell Culture. *Molecular cell* *64*, 900–912.
- Mauger, O., Lemoine, F., and Scheiffele, P. (2016). Targeted Intron Retention and Excision for Rapid Gene Regulation in Response to Neuronal Activity. *Neuron* *92*, 1266–1278.

- Maulik, K.P., Mascarenhas, N.M., Mathers, D.C., Dua, T., and Saxena, S. (2011). Prevalence of intellectual disability: a meta-analysis of population-based studies. *Research in developmental disabilities* 32, 419–436.
- Mayeda, A., and Krainer, A.R. (1992). Regulation of alternative pre-mRNA splicing by hnRNP A1 and splicing factor SF2. *Cell* 68, 365–375.
- McBurney, M.W., Jones-Villeneuve, E.M.V., Edwards, M.K.S., and Anderson, P.J. (1982). Control of muscle and neuronal differentiation in a cultured embryonal carcinoma cell line. *Nature* 299, 165.
- McBurney, M.W., and Rogers, B.J. (1982). Isolation of male embryonal carcinoma cells and their chromosome replication patterns. *Developmental Biology* 89, 503–508.
- McNicoll, F., and Müller-McNicoll, M. (2018). A Quantitative Heterokaryon Assay to Measure the Nucleocytoplasmic Shuttling of Proteins. *BIO-PROTOCOL* 8.
- Meng, Q., Gao, J., Zhu, H., He, H., Lu, Z., Hong, M., and Zhou, H. (2018). The proteomic study of serially passaged human skin fibroblast cells uncovers down-regulation of the chromosome condensin complex proteins involved in replicative senescence. *Biochemical and Biophysical Research Communications* 505, 1112–1120.
- Meola, N., Domanski, M., Karadoulama, E., Chen, Y., Gentil, C., Pultz, D., Vitting-Seerup, K., Lykke-Andersen, S., Andersen, S.J., Sandelin, A., and Jensen, H.T. (2016). Identification of a Nuclear Exosome Decay Pathway for Processed Transcripts. *Molecular cell* 64, 520–533.
- Meola, N., and Jensen, H.T. (2017). Targeting the nuclear RNA exosome: Poly(A) binding proteins enter the stage. *RNA biology* 14, 820–826.
- Meredith, L.J., Wang, C.-M., Nascimento, L., Liu, R., Wang, L., and Yang, W.-H. (2016). The Key Regulator for Language and Speech Development, FOXP2, is a Novel Substrate for SUMOylation. *Journal of cellular biochemistry* 117, 426–438.
- Mermoud, J.E., Cohen, P., and Lamond, A.I. (1992). Ser/Thr-specific protein phosphatases are required for both catalytic steps of pre-mRNA splicing. *Genes & Development* 20, 5263–5269.
- Mermoud, J.E., Cohen, P.T., and Lamond, A.I. (1994). Regulation of mammalian spliceosome assembly by a protein phosphorylation mechanism. *The EMBO journal* 13, 5679–5688.
- Mezer, M. de, Wojciechowska, M., Napierala, M., Sobczak, K., and Krzyzosiak, W.J. (2011). Mutant CAG repeats of Huntingtin transcript fold into hairpins, form nuclear foci and are targets for RNA interference. *Nucleic Acids Research* 39, 3852–3863.
- Michlewski, G., Sanford, J.R., and Cáceres, J.F. (2008). The splicing factor SF2/ASF regulates translation initiation by enhancing phosphorylation of 4E-BP1. *Molecular cell* 30, 179–189.
- Middleton, R., Gao, D., Thomas, A., Singh, B., Au, A., Wong, J.J.-L., Bomane, A., Cosson, B., Eyra, E., Rasko, J.E.J., and Ritchie, W. (2017). IRFinder: assessing the impact of intron retention on mammalian gene expression. *Genome biology* 18, 51.
- Miller-Wideman, M., Makkar, N., Tran, M., Isaac, B., Biest, N., and Stonard, R. (1992). Herboxidiene, a new herbicidal substance from *Streptomyces chromofuscus* A7847. Taxonomy, fermentation, isolation, physico-chemical and biological properties. *The Journal of antibiotics* 45, 914–921.

- Mintz, P.J., Patterson, S.D., Neuwald, A.F., Spahr, C.S., and Spector, D.L. (1999). Purification and biochemical characterization of interchromatin granule clusters. *The EMBO journal* *18*, 4308–4320.
- Misteli, T. (2000). Cell biology of transcription and pre-mRNA splicing: nuclear architecture meets nuclear function. *Journal of cell science* *113 (Pt 11)*, 1841–1849.
- Misteli, T., Cáceres, J.F., and Spector, D.L. (1997). The dynamics of a pre-mRNA splicing factor in living cells. *Nature* *387*, 523–527.
- Misteli, T., and Spector, D.L. (1996). Serine/threonine phosphatase 1 modulates the subnuclear distribution of pre-mRNA splicing factors. *Molecular biology of the cell* *7*, 1559–1572.
- Miyagawa, R., Tano, K., Mizuno, R., Nakamura, Y., Ijiri, K., Rakwal, R., Shibato, J., Masuo, Y., Mayeda, A., Hirose, T., and Akimitsu, N. (2012). Identification of cis- and trans-acting factors involved in the localization of MALAT-1 noncoding RNA to nuclear speckles. *RNA (New York, N.Y.)* *18*, 738–751.
- Miyamoto, Y., Saiwaki, T., Yamashita, J., Yasuda, Y., Kotera, I., Shibata, S., Shigeta, M., Hiraoka, Y., Haraguchi, T., and Yoneda, Y. (2004). Cellular stresses induce the nuclear accumulation of importin alpha and cause a conventional nuclear import block. *The Journal of cell biology* *165*, 617–623.
- Moen, P.T., Johnson, C.V., Byron, M., Shopland, L.S., La Serna, I.L. de, Imbalzano, A.N., and Lawrence, J.B. (2004). Repositioning of muscle-specific genes relative to the periphery of SC-35 domains during skeletal myogenesis. *Molecular biology of the cell* *15*, 197–206.
- Mor, A., White, A., Zhang, K., Thompson, M., Esparza, M., Muñoz-Moreno, R., Koide, K., Lynch, K.W., García-Sastre, A., and Fontoura, B.M.A. (2016). Influenza Virus mRNA Trafficking Through Host Nuclear Speckles. *Nature microbiology* *2016*.
- Morris, J.K., and Corbett, H.A. (2018). The polyadenosine RNA-binding protein ZC3H14 interacts with the THO complex and coordinately regulates the processing of neuronal transcripts. *Nucleic acids research* *46*, 6561–6575.
- Muddashetty, R.S., Kelic, S., Gross, C., Xu, M., and Bassell, G.J. (2007). Dysregulated metabotropic glutamate receptor-dependent translation of AMPA receptor and postsynaptic density-95 mRNAs at synapses in a mouse model of fragile X syndrome. *The Journal of neuroscience the official journal of the Society for Neuroscience* *27*, 5338–5348.
- Muddashetty, R.S., Nalavadi, V.C., Gross, C., Yao, X., Xing, L., Laur, O., Warren, S.T., and Bassell, G.J. (2011). Reversible inhibition of PSD-95 mRNA translation by miR-125a, FMRP phosphorylation, and mGluR signaling. *Molecular cell* *42*, 673–688.
- Müller-McNicoll, M., Botti, V., Jesus Domingues, A.M. de, Brandl, H., Schwich, O.D., Steiner, M.C., Curk, T., Poser, I., Zarnack, K., and Neugebauer, K.M. (2016). SR proteins are NXF1 adaptors that link alternative RNA processing to mRNA export. *Genes & Development* *30*, 553–566.
- Mummery, C.L., Feijen, A., Moolenaar, W.H., van den Brink, C.E., and Laats, S.W. de (1986). Establishment of a differentiated mesodermal line from P19 EC cells expressing functional PDGF and EGF receptors. *Experimental cell research* *165*, 229–242.
- Muraki, M., Ohkawara, B., Hosoya, T., Onogi, H., Koizumi, J., Koizumi, T., Sumi, K., Yomoda, J.-i., Murray, M.V., Kimura, H., Furuichi, K., Shibuya, H., Krainer, A.R., Suzuki, M., and Hagiwara, M. (2004). Manipulation

- of alternative splicing by a newly developed inhibitor of Clks. *The Journal of biological chemistry* 279, 24246–24254.
- Mure, F., Corbin, A., Benbahouche, N.E.H., Bertrand, E., Manet, E., and Gruffat, H. (2018). The splicing factor SRSF3 is functionally connected to the nuclear RNA exosome for intronless mRNA decay. *Scientific reports* 8.
- Nakielnny, S., and Dreyfuss, G. (1996). The hnRNP C proteins contain a nuclear retention sequence that can override nuclear export signals. *The Journal of cell biology* 134, 1365–1373.
- Narayanan, U., Nalavadi, V., Nakamoto, M., Thomas, G., Ceman, S., Bassell, G.J., and Warren, S.T. (2008). S6K1 phosphorylates and regulates fragile X mental retardation protein (FMRP) with the neuronal protein synthesis-dependent mammalian target of rapamycin (mTOR) signaling cascade. *The Journal of biological chemistry* 283, 18478–18482.
- Narkis, G., Ofir, R., Manor, E., Landau, D., Elbedour, K., and Birk, O.S. (2007). Lethal Congenital Contractural Syndrome Type 2 (LCCS2) Is Caused by a Mutation in ERBB3 (Her3), a Modulator of the Phosphatidylinositol-3-Kinase/Akt Pathway. *The American Journal of Human Genetics* 81, 589–595.
- Naro, C., Jolly, A., Di Persio, S., Bielli, P., Setterblad, N., Alberdi, J.A., Vicini, E., Geremia, R., La Grange, P. de, and Sette, C. (2017). An Orchestrated Intron Retention Program in Meiosis Controls Timely Usage of Transcripts during Germ Cell Differentiation. *Developmental cell* 41, 82-93.e4.
- Nau, H., Hauck, R.-S., and Ehlers, K. (1991). Valproic Acid-Induced Neural Tube Defects in Mouse and Human: Aspects of Chirality, Alternative Drug Development, Pharmacokinetics and Possible Mechanisms. *Pharmacology & Toxicology* 69, 310–321.
- Nelson, D.L., Orr, H.T., and Warren, S.T. (2013). The Unstable Repeats - Three Evolving Faces of Neurological Disease. *Neuron* 77, 825–843.
- Neugebauer, K.M., and Roth, M.B. (1997). Distribution of pre-mRNA splicing factors at sites of RNA polymerase II transcription. *Genes & Development* 11, 1148–1159.
- Ngo, J.C.K., Chakrabarti, S., Ding, J.-H., Velazquez-Dones, A., Nolen, B., Aubol, B.E., Adams, J.A., Fu, X.-D., and Ghosh, G. (2005). Interplay between SRPK and Clk/Sty kinases in phosphorylation of the splicing factor ASF/SF2 is regulated by a docking motif in ASF/SF2. *Molecular cell* 20, 77–89.
- Nguyen, T.C., Cao, X., Yu, P., Xiao, S., Lu, J., Biase, F.H., Sridhar, B., Huang, N., Zhang, K., and Zhong, S. (2016). Mapping RNA-RNA interactome and RNA structure in vivo by MARIO. *Nature communications* 7, 12023.
- Nguyen, T.H.D., Galej, W.P., Bai, X.-c., Savva, C.G., Newman, A.J., Scheres, S.H.W., and Nagai, K. (2015). The architecture of the spliceosomal U4/U6.U5 tri-snRNP. *Nature* 523, 47–52.
- Nousiainen, H.O., Kestilä, M., Pakkasjärvi, N., Honkala, H., Kuure, S., Tallila, J., Vuopala, K., Ignatius, J., Herva, R., and Peltonen, L. (2008). Mutations in mRNA export mediator *GLE1* result in a fetal motoneuron disease. *Nature genetics* 40, 155.
- Novoyatleva, T., Heinrich, B., Tang, Y., Benderska, N., Butchbach, M.E.R., Lorson, C.L., Lorson, M.A., Bendov, C., Fehlbauer, P., Bracco, L., Burghes, A.H.M., Bollen, M., and Stamm, S. (2008). Protein phosphatase 1 binds to the RNA recognition motif of several splicing factors and regulates alternative pre-mRNA processing. *Human molecular genetics* 17, 52–70.

- O'Brien, K., Matlin, A.J., Lowell, A.M., and Moore, M.J. (2008). The biflavonoid isoginkgetin is a general inhibitor of Pre-mRNA splicing. *The Journal of biological chemistry* 283, 33147–33154.
- Ohta, S., Nishida, E., Yamanaka, S., and Yamamoto, T. (2013). Global splicing pattern reversion during somatic cell reprogramming. *Cell reports* 5, 357–366.
- O'Keefe, R.T. (1994). Disruption of pre-mRNA splicing in vivo results in reorganization of splicing factors. *The Journal of cell biology* 124, 249–260.
- Pak, C., Garshasbi, M., Kahrizi, K., Gross, C., Apponi, L.H., Noto, J.J., Kelly, S.M., Leung, S.W., Tzschach, A., Behjati, F., Abedini, S.S., Mohseni, M., Jensen, L.R., Hu, H., Huang, B., Stahley, S.N., Liu, G., Williams, K.R., Burdick, S., Feng, Y., Sanyal, S., Bassell, G.J., Ropers, H.-H., Najmabadi, H., Corbett, A.H., Moberg, K.H., and Kuss, A.W. (2011). Mutation of the conserved polyadenosine RNA binding protein, ZC3H14/dNab2, impairs neural function in *Drosophila* and humans. *Proceedings of the National Academy of Sciences of the United States of America* 108, 12390–12395.
- Palou, R., Dhanaraman, T., Marrakchi, R., Pascariu, M., Tyers, M., and D'Amours, D. (2018). Condensin ATPase motifs contribute differentially to the maintenance of chromosome morphology and genome stability. *PLOS Biology* 16, e2003980.
- Pandit, S., Zhou, Y., Shiue, L., Coutinho-Mansfield, G., Li, H., Qiu, J., Huang, J., Yeo, G.W., Ares, M., and Fu, X.-D. (2013). Genome-wide Analysis Reveals SR Protein Cooperation and Competition in Regulated Splicing. *Molecular cell* 50, 223–235.
- Pandya-Jones, A., and Black, D.L. (2009). Co-transcriptional splicing of constitutive and alternative exons. *RNA (New York, N.Y.)* 15, 1896–1908.
- Parenteau, J., Durand, M., Vronneau, S., Lacombe, A.-A., Morin, G., Gurin, V., Cecez, B., Gervais-Bird, J., Koh, C.-S., Brunelle, D., Wellinger, J.R., Chabot, B., and Abou Elela, S. (2008). Deletion of many yeast introns reveals a minority of genes that require splicing for function. *Molecular biology of the cell* 19, 1932–1941.
- Pasquinelli, A.E., Ernst, R.K., Lund, E., Grimm, C., Zapp, M.L., Rekosh, D., Hammarskjold, M.L., and Dahlberg, J.E. (1997). The constitutive transport element (CTE) of Mason-Pfizer monkey virus (MPMV) accesses a cellular mRNA export pathway. *The EMBO journal* 16, 7500–7510.
- Patrick, M.E., Srinivasan, S., Jankowsky, E., and Comstock, J.M. (2017). The RNA helicase Mtr4p is a duplex-sensing translocase. *Nature chemical biology* 13, 99–104.
- Pawellek, A., McElroy, S., Samatov, T., Mitchell, L., Woodland, A., Ryder, U., Gray, D., Lührmann, R., and Lamond, A.I. (2014). Identification of Small Molecule Inhibitors of Pre-mRNA Splicing*. *The Journal of biological chemistry* 289, 34683–34698.
- Pawellek, A., Ryder, U., Tammsalu, T., King, L.J., Kreinin, H., Ly, T., Hay, R.T., Hartley, R.C., and Lamond, A.I. (2017). Characterisation of the biflavonoid hinokiflavone as a pre-mRNA splicing modulator that inhibits SENP. *eLife* 6.
- Peng, J., Kim, M.J., Cheng, D., Duong, D.M., Gygi, S.P., and Sheng, M. (2004). Semiquantitative proteomic analysis of rat forebrain postsynaptic density fractions by mass spectrometry. *The Journal of biological chemistry* 279, 21003–21011.

- Pettersson, O.J., Aagaard, L., Jensen, T.G., and Damgaard, C.K. (2015). Molecular mechanisms in DM1 — a focus on foci. *Nucleic Acids Research* *43*, 2433–2441.
- Popp, M.W.-L., and Maquat, L.E. (2014). The dharma of nonsense-mediated mRNA decay in mammalian cells. *Molecules and cells* *37*, 1–8.
- Poser, I., Sarov, M., Hutchins, J.R.A., Heriche, J.-K., Toyoda, Y., Pozniakovsky, A., Weigl, D., Nitzsche, A., Hegemann, B., Bird, A.W., Pelletier, L., Kittler, R., Hua, S., Naumann, R., Augsburg, M., Sykora, M.M., Hofemeister, H., Zhang, Y., Nasmyth, K., White, K.P., Dietzel, S., Mechtler, K., Durbin, R., Stewart, A.F., Peters, J.-M., Buchholz, F., and Hyman, A.A. (2008). BAC TransgeneOmics: a high-throughput method for exploration of protein function in mammals. *Nature methods* *5*, 409–415.
- Potashkin, J.A., Derby, R.J., and Spector, D.L. (1990). Differential distribution of factors involved in pre-mRNA processing in the yeast cell nucleus. *Molecular and cellular biology* *10*, 3524–3534.
- Pozzi, B., Bragado, L., Will, C.L., Mammi, P., Risso, G., Urlaub, H., Lührmann, R., and Srebrow, A. (2017). SUMO conjugation to spliceosomal proteins is required for efficient pre-mRNA splicing. *Genes & Development* *45*, 6729–6745.
- Prasanth, K.V., Prasanth, S.G., Xuan, Z., Hearn, S., Freier, S.M., Bennett, C.F., Zhang, M.Q., and Spector, D.L. (2005). Regulating gene expression through RNA nuclear retention. *Cell* *123*, 249–263.
- Price, A.M., Görnemann, J., GUTHRIE, C., and Brow, D.A. (2014). An unanticipated early function of DEAD-box ATPase Prp28 during commitment to splicing is modulated by U5 snRNP protein Prp8. *RNA (New York, N.Y.)* *20*, 46–60.
- Proungvitaya, S., Klinthong, W., Proungvitaya, T., Limpiboon, T., Jearanaikoon, P., Roytrakul, S., Wongkham, C., Nimboriboonporn, A., and Wongkham, S. (2017). High expression of CCDC25 in cholangiocarcinoma tissue samples. *Oncology Letters* *14*, 2566–2572.
- Puno, M.R., and Lima, C.D. (2018). Structural basis for MTR4–ZCCHC8 interactions that stimulate the MTR4 helicase in the nuclear exosome-targeting complex. *Proceedings of the National Academy of Sciences* *115*, E5506–E5515.
- Qin, M., Schmidt, K.C., Zometkin, A.J., Bishu, S., Horowitz, L.M., Burlin, T.V., Xia, Z., Huang, T., Quezado, Z.M., and Smith, C.B. (2013). Altered cerebral protein synthesis in fragile X syndrome: studies in human subjects and knockout mice. *Journal of Cerebral Blood Flow & Metabolism* *33*, 499–507.
- Query, C.C., Bentley, R.C., and Keene, J.D. (1989). A common RNA recognition motif identified within a defined U1 RNA binding domain of the 70K U1 snRNP protein. *Cell* *57*, 89–101.
- Rappsilber, J., Ryder, U., Lamond, A.I., and Mann, M. (2002). Large-Scale Proteomic Analysis of the Human Spliceosome. *Genome research* *12*, 1231–1245.
- Ratnadiwakara, M., Archer, S.K., Dent, C.I., Ruiz De Los Mozos, I., Beilharz, T.H., Knaupp, A.S., Nefzger, C.M., Polo, J.M., and Anko, M.-L. (2018). SRSF3 promotes pluripotency through Nanog mRNA export and coordination of the pluripotency gene expression program. *eLife* *7*.
- Rayala, H.J., Kendirgi, F., Barry, D.M., Majerus, P.W., and Wenthe, S.R. (2004). The mRNA Export Factor Human Gle1 Interacts with the Nuclear Pore Complex Protein Nup155. *Molecular & Cellular Proteomics* *3*, 145–155.

- Raz, Y., and Raz, V. (2014). Oculopharyngeal Muscular Dystrophy as a Paradigm for Muscle Aging. *Frontiers in Aging Neuroscience* 6, 317.
- Rha, J., Jones, S.K., Fidler, J., Banerjee, A., Leung, S.W., Morris, K.J., Wong, J.C., Inglis, G.A.S., Shapiro, L., Deng, Q., Cutler, A.A., Hanif, A.M., Pardue, M.T., Schaffer, A., Seyfried, N.T., Moberg, K.H., Bassell, G.J., Escayg, A., García, P.S., and Corbett, A.H. (2017). The RNA-binding protein, ZC3H14, is required for proper poly(A) tail length control, expression of synaptic proteins, and brain function in mice. *Human molecular genetics* 26, 3663–3681.
- Ribbeck, K., and Görlich, D. (2001). Kinetic analysis of translocation through nuclear pore complexes. *The EMBO journal* 20, 1320–1330.
- Richter, J.D., Bassell, G.J., and Klann, E. (2015). Dysregulation and restoration of translational homeostasis in fragile X syndrome. *Nature reviews. Neuroscience* 16, 595–605.
- Riordan, D.P., Herschlag, D., and Brown, P.O. (2010). Identification of RNA recognition elements in the *Saccharomyces cerevisiae* transcriptome. *Nucleic acids research* 39, 1501–1509.
- Robberson, B.L., Cote, G.J., and Berget, S.M. (1990). Exon definition may facilitate splice site selection in RNAs with multiple exons. *Molecular and Cellular Biology* 10, 84–94.
- Rodrigues, P.J., Rode, M., Gatfield, D., Blencowe, J.B., Carmo-Fonseca, M., and Izaurralde, E. (2001). REF proteins mediate the export of spliced and unspliced mRNAs from the nucleus. *Proceedings of the National Academy of Sciences of the United States of America* 98, 1030–1035.
- Ropers, H.H. (2008). Genetics of intellectual disability. *Current opinion in genetics & development* 18, 241–250.
- Roscigno, R.F., and Garcia-Blanco, M.A. (1995). SR proteins escort the U4/U6.U5 tri-snRNP to the spliceosome. *RNA* 1, 692–706.
- Roth, Zahler, and Stolk (1991). A conserved family of nuclear phosphoproteins localized to sites of polymerase II transcription. *The Journal of cell biology* 115, 587–596.
- Roth, A.D., Liazoghli, D., Perez De Arce, F., and Colman, D.R. (2013). Septin 7: actin cross-organization is required for axonal association of Schwann cells. *Biological research* 46, 243–249.
- Roth, M.K., Byam, J., Fang, F., and Butler, S.J. (2009). Regulation of NAB2 mRNA 3'-end formation requires the core exosome and the Trf4p component of the TRAMP complex. *RNA* 15, 1045–1058.
- Roybal, G.A., and Jurica, M.S. (2010). Spliceostatin A inhibits spliceosome assembly subsequent to prespliceosome formation. *Nucleic acids research* 38, 6664–6672.
- Ruvolo, P.P., Deng, X., and May, W.S. (2001). Phosphorylation of Bcl2 and regulation of apoptosis. *Leukemia* 15, 515.
- Ryu, W.S., and Mertz, J.E. (1989). Simian virus 40 late transcripts lacking excisable intervening sequences are defective in both stability in the nucleus and transport to the cytoplasm. *Journal of virology* 63, 4386–4394.
- Saavedra, A.C., Hammell, M.C., Heath, V.C., and Cole, N.C. (1997a). Yeast heat shock mRNAs are exported through a distinct pathway defined by Rip1p. *Genes & Development* 11, 2845–2856.

- Saavedra, C., Felber, B., and Izaurralde, E. (1997b). The simian retrovirus-1 constitutive transport element, unlike the HIV-1 RRE, uses factors required for cellular mRNA export. *Current biology CB* 7, 619–628.
- Saavedra, C., Tung, S.K., Amberg, C.D., Hopper, K.A., and Cole, N.C. (1996). Regulation of mRNA export in response to stress in *Saccharomyces cerevisiae*. *Genes & Development* 10, 1608–1620.
- Saitoh, N., Spahr, C.S., Patterson, S.D., Bubulya, P., Neuwald, A.F., and Spector, D.L. (2004). Proteomic Analysis of Interchromatin Granule Clusters. *Molecular biology of the cell* 15, 3876–3890.
- Sakai, Y., Yoshida, T., Ochiai, K., Uosaki, Y., Saitoh, Y., Tanaka, F., Akiyama, T., Akinaga, S., and Mizukami, T. (2002). GEX1 compounds, novel antitumor antibiotics related to herboxidiene, produced by *Streptomyces* sp. I. Taxonomy, production, isolation, physicochemical properties and biological activities. *The Journal of antibiotics* 55, 855–862.
- Sakharkar, K.M., Chow, K.V.T., and Kanguene, P. (2004). Distributions of exons and introns in the human genome. *In silico biology* 4, 387–393.
- Salton, M., and Misteli, T. (2016). Small Molecule Modulators of Pre-mRNA Splicing in Cancer Therapy. *Trends in molecular medicine* 22, 28–37.
- Samatov, T.R., Wolf, A., Odenwalder, P., Bessonov, S., Deraeve, C., Bon, R.S., Waldmann, H., and Luhrmann, R. (2012). Psoromic acid derivatives: a new family of small-molecule pre-mRNA splicing inhibitors discovered by a stage-specific high-throughput in vitro splicing assay. *Chembiochem a European journal of chemical biology* 13, 640–644.
- Sanford, J.R., Ellis, J., and Caceres, J.F. (2005). Multiple roles of arginine/serine-rich splicing factors in RNA processing. *Biochemical Society transactions* 33, 443–446.
- Sanford, J.R., Gray, N.K., Beckmann, K., and Caceres, J.F. (2004). A novel role for shuttling SR proteins in mRNA translation. *Genes & Development* 18, 755–768.
- Sanford, J.R., Wang, X., Mort, M., VanDuyn, N., Cooper, D.N., Mooney, S.D., Edenberg, H.J., and Liu, Y. (2009). Splicing factor SFRS1 recognizes a functionally diverse landscape of RNA transcripts. *Genome research* 19, 381–394.
- Santoro, M.R., Bray, S.M., and Warren, S.T. (2012). Molecular mechanisms of fragile X syndrome: a twenty-year perspective. *Annual review of pathology* 7, 219–245.
- Sapra, A.K., anko, M.-L., Grishina, I., Lorenz, M., Pabis, M., Poser, I., Rollins, J., Weiland, E.-M., and Neugebauer, K.M. (2009). SR Protein Family Members Display Diverse Activities in the Formation of Nascent and Mature mRNPs In Vivo. *Molecular cell* 34, 179–190.
- Sarkissian, M., Winne, A., and Lafyatis, R. (1996). The mammalian homolog of suppressor-of-white-apricot regulates alternative mRNA splicing of CD45 exon 4 and fibronectin IIICS. *The Journal of biological chemistry* 271, 31106–31114.
- Saroufim, M.-A., Bensidoun, P., Raymond, P., Rahman, S., Krause, M.R., Oeffinger, M., and Zenklusen, D. (2015). The nuclear basket mediates perinuclear mRNA scanning in budding yeast. *The Journal of cell biology* 211, 1131–1140.
- Schaal, T.D., and Maniatis, T. (1999a). Multiple Distinct Splicing Enhancers in the Protein-Coding Sequences of a Constitutively Spliced Pre-mRNA. *Molecular and cellular biology* 19, 261–273.

- Schaal, T.D., and Maniatis, T. (1999b). Selection and Characterization of Pre-mRNA Splicing Enhancers: Identification of Novel SR Protein-Specific Enhancer Sequences. *Molecular and Cellular Biology* *19*, 1705–1719.
- Schaeffer, D., Tsanova, B., Barbas, A., Reis, P.F., Dastidar, G.E., Sanchez-Rotunno, M., Arraiano, M.C., and van Hoof, A. (2009). The exosome contains domains with specific endoribonuclease, exoribonuclease and cytoplasmic mRNA decay activities. *Nature structural & molecular biology* *16*, 56–62.
- Scherrer, K., Latham, H., and Darnell, J.E. (1963). DEMONSTRATION OF AN UNSTABLE RNA AND OF A PRECURSOR TO RIBOSOMAL RNA IN HELA CELLS*. *Proceedings of the National Academy of Sciences* *49*, 240–248.
- Schindelin, J., Arganda-Carreras, I., Frise, E., Kaynig, V., Longair, M., Pietzsch, T., Preibisch, S., Rueden, C., Saalfeld, S., Schmid, B., Tinevez, J.-Y., White, D.J., Hartenstein, V., Eliceiri, K., Tomancak, P., and Cardona, A. (2012). Fiji: an open-source platform for biological-image analysis. *Nature methods* *9*, 676–682.
- Schmid, M., Olszewski, P., Pelechano, V., Gupta, I., Steinmetz, M.L., and Jensen, H.T. (2015). The Nuclear PolyA-Binding Protein Nab2p Is Essential for mRNA Production. *Cell reports* *12*, 128–139.
- Schmid, M., Poulsen, M.B., Olszewski, P., Pelechano, V., Saguez, C., Gupta, I., Steinmetz, L.M., Moore, C., and Jensen, T.H. (2012). Rrp6p controls mRNA polyA tail length and its decoration with polyA binding proteins. *Molecular cell* *47*, 267–280.
- Schmidt, U., Basyuk, E., Robert, M.-C., Yoshida, M., Villemin, J.-P., Auboeuf, D., Aitken, S., and Bertrand, E. (2011). Real-time imaging of cotranscriptional splicing reveals a kinetic model that reduces noise: Implications for alternative splicing regulation. *The Journal of cell biology* *193*, 819–829.
- Schmidt-Kastner, P.K., Jardine, K., Cormier, M., and McBurney, M.W. (1996). Genes transfected into embryonal carcinoma stem cells are both lost and inactivated at high frequency. *Somatic Cell and Molecular Genetics* *22*, 383–392.
- Schmidt-Kastner, P.K., Jardine, K., Cormier, M., and McBurney, M.W. (1998). Absence of p53-dependent cell cycle regulation in pluripotent mouse cell lines. *Oncogene* *16*, 3003–3011.
- Schneider, C., Kudla, G., Wlotzka, W., Tuck, A., and Tollervey, D. (2012). Transcriptome-wide analysis of exosome targets. *Molecular cell* *48*, 422–433.
- Schneider, C., Leung, E., Brown, J., and Tollervey, D. (2009). The N-terminal PIN domain of the exosome subunit Rrp44 harbors endonuclease activity and tethers Rrp44 to the yeast core exosome. *Nucleic acids research* *37*, 1127–1140.
- Schwartz, D.C., and Parker, R. (2000). mRNA decapping in yeast requires dissociation of the cap binding protein, eukaryotic translation initiation factor 4E. *Molecular and Cellular Biology* *20*, 7933–7942.
- Scolnick, D.M., and Halazonetis, T.D. (2000). Chfr defines a mitotic stress checkpoint that delays entry into metaphase. *Nature* *406*, 430–435.
- Segref, A., Sharma, K., Doye, V., Hellwig, A., Huber, J., Luhrmann, R., and Hurt, E. (1997). Mex67p, a novel factor for nuclear mRNA export, binds to both poly(A)⁺ RNA and nuclear pores. *The EMBO journal* *16*, 3256–3271.

- Sharma, S., and Notter, M.F. (1988). Characterization of neurotransmitter phenotype during neuronal differentiation of embryonal carcinoma cells. *Developmental Biology* *125*, 246–254.
- Shen, M., and Mattox, W. (2011). Activation and repression functions of an SR splicing regulator depend on exonic versus intronic-binding position. *Genes & Development* *40*, 428–437.
- Shen, S., Kong, J., Qiu, Y., Yang, X., Wang, W., and Yan, L. (2019). Identification of core genes and outcomes in hepatocellular carcinoma by bioinformatics analysis. *Journal of cellular biochemistry* *120*, 10069–10081.
- Shepard, J., Reick, M., Olson, S., and Graveley, B.R. (2002). Characterization of U2AF6, a Splicing Factor Related to U2AF35. *Molecular and Cellular Biology* *22*, 221–230.
- Shepard, P.J., and Hertel, K.J. (2009). The SR protein family. *Genome biology* *10*, 242.
- Shi, Y., Reddy, B., and Manley, J.L. (2006). PP1/PP2A Phosphatases Are Required for the Second Step of Pre-mRNA Splicing and Target Specific snRNP Proteins. *Molecular cell* *23*, 819–829.
- Shiomi, T., Fukushima, K., Suzuki, N., Nakashima, N., Noguchi, E., and Nishimoto, T. (1998). Human dis3p, which binds to either GTP- or GDP-Ran, complements *Saccharomyces cerevisiae* dis3. *Journal of biochemistry* *123*, 883–890.
- Shirahata-Adachi, M., Iriyama, C., Tomita, A., Suzuki, Y., Shimada, K., and Kiyoi, H. (2017). Altered EZH2 splicing and expression is associated with impaired histone H3 lysine 27 tri-Methylation in myelodysplastic syndrome. *Leukemia research* *63*, 90–97.
- Shopland, L.S., Johnson, C.V., and Lawrence, J.B. (2002). Evidence that all SC-35 domains contain mRNAs and that transcripts can be structurally constrained within these domains. *Journal of Structural Biology* *140*, 131–139.
- Shukla, C.J., McCorkindale, A.L., Gerhardinger, C., Korthauer, K.D., Cabili, M.N., Shechner, D.M., Irizarry, R.A., Maass, P.G., and Rinn, J.L. (2018). High-throughput identification of RNA nuclear enrichment sequences. *The EMBO journal* *37*.
- Silla, T., Karadoulama, E., Mąkosa, D., Lubas, M., and Jensen, T.H. (2018). The RNA Exosome Adaptor ZFC3H1 Functionally Competes with Nuclear Export Activity to Retain Target Transcripts. *Cell reports* *23*, 2199–2210.
- Singh, G., Kucukural, A., Cenik, C., Leszyk, D.J., Shaffer, A.S., Weng, Z., and Moore, J.M. (2012). The cellular EJC interactome reveals higher-order mRNP structure and an EJC-SR protein nexus. *Cell* *151*, 750–764.
- Singh, J., and Padgett, R.A. (2009). Rates of in situ transcription and splicing in large human genes. *Nature structural & molecular biology* *16*, 1128–1133.
- Sirajuddin, M., Farkasovsky, M., Hauer, F., Kühlmann, D., Macara, I.G., Weyand, M., Stark, H., and Wittinghofer, A. (2007). Structural insight into filament formation by mammalian septins. *Nature* *449*, 311.
- Smith, K.P., Moen, P.T., Wydner, K.L., Coleman, J.R., and Lawrence, J.B. (1999). Processing of Endogenous Pre-mRNAs in Association with SC-35 Domains Is Gene Specific. *The Journal of cell biology* *144*, 617–629.
- Soheilypour, M., and Mofrad, M.R.K. Regulation of RNA-binding proteins affinity to export receptors enables the nuclear basket proteins to distinguish and retain aberrant mRNAs. *Scientific reports* *6*, 35380.

- Solnestam, B.W., Stranneheim, H., Hallman, J., Kaller, M., Lundberg, E., Lundeberg, J., and Akan, P. (2012). Comparison of total and cytoplasmic mRNA reveals global regulation by nuclear retention and miRNAs. *BMC Genomics* 13, 574.
- Solter, D., and Knowles, B.B. (1978). Monoclonal antibody defining a stage-specific mouse embryonic antigen (SSEA-1). *Proceedings of the National Academy of Sciences of the United States of America* 75, 5565–5569.
- Soucek, S., Corbett, H.A., and Fasken, B.M. (2012). The long and the short of it: the role of the zinc finger polyadenosine RNA binding protein, Nab2, in control of poly(A) tail length. *Biochimica et biophysica acta* 1819, 546–554.
- Soucek, S., Zeng, Y., Bellur, L.D., Bergkessel, M., Morris, J.K., Deng, Q., Duong, D., Seyfried, T.N., GUTHRIE, C., Staley, P.J., Fasken, B.M., and Corbett, H.A. (2016). The Evolutionarily-conserved Polyadenosine RNA Binding Protein, Nab2, Cooperates with Splicing Machinery to Regulate the Fate of pre-mRNA. *Molecular and cellular biology*.
- Spector, D.L. (1993). Macromolecular domains within the cell nucleus. *Annual review of cell biology* 9, 265–315.
- Spector, D.L. (1996). Nuclear organization and gene expression. *Experimental cell research* 229, 189–197.
- Spector, D.L., and Lamond, A.I. (2011). Nuclear Speckles. *Cold Spring Harbor Perspectives in Biology* 3, a000646.
- Staals, J.R.H., Bronkhorst, W.A., Schilders, G., Slomovic, S., Schuster, G., Heck, R.A.J., Raijmakers, R., and Pruijn, M.G.J. (2010). Dis3-like 1: a novel exoribonuclease associated with the human exosome. *The EMBO journal* 29, 2358–2367.
- Stark, J.M., Bazett-Jones, D.P., Herfort, M., and Roth, M.B. (1998). SR proteins are sufficient for exon bridging across an intron. *Molecular and Cellular Biology* 18, 2163–2168.
- Stevens, S.W., Ryan, D.E., Ge, H.Y., Moore, R.E., Young, M.K., Lee, T.D., and Abelson, J. (2002). Composition and functional characterization of the yeast spliceosomal penta-snRNP. *Molecular cell* 9, 31–44.
- Stojdl, D.F., and Bell, J.C. (1999). SR protein kinases: the splice of life. *Biochemistry and cell biology = Biochimie et biologie cellulaire* 77, 293–298.
- Stork, C., and Zheng, S. (2016). Genome-Wide Profiling of RNA–Protein Interactions Using CLIP-Seq. *Methods in molecular biology (Clifton, N.J.)* 1421, 137–151.
- Strasser, K., Masuda, S., Mason, P., Pfannstiel, J., Oppizzi, M., Rodriguez-Navarro, S., Rondon, A.G., Aguilera, A., Struhl, K., Reed, R., and Hurt, E. (2002). TREX is a conserved complex coupling transcription with messenger RNA export. *Nature* 417, 304–308.
- Stutz, F., Bachi, A., Doerks, T., Braun, C.I., Sraphin, B., Wilm, M., Bork, P., and Izaurralde, E. (2000). REF, an evolutionary conserved family of hnRNP-like proteins, interacts with TAP/Mex67p and participates in mRNA nuclear export. *RNA* 6, 638–650.
- Suh, M.-H., Meyer, P.A., Gu, M., Ye, P., Zhang, M., Kaplan, C.D., Lima, C.D., and Fu, J. (2010). A Dual Interface Determines the Recognition of RNA Polymerase II by RNA Capping Enzyme*. *The Journal of biological chemistry* 285, 34027–34038.

- Sun, X., Li, P.P., Zhu, S., Cohen, R., Marque, L.O., Ross, C.A., Pulst, S.M., Chan, H.Y.E., Margolis, R.L., and Rudnicki, D.D. (2015). Nuclear retention of full-length HTT RNA is mediated by splicing factors MBNL1 and U2AF65. *Scientific reports* 5, 12521.
- Suntharalingam, M., Alczar-Romn, R.A., and Wente, R.S. (2004). Nuclear export of the yeast mRNA-binding protein Nab2 is linked to a direct interaction with Gfd1 and to Gle1 function. *The Journal of biological chemistry* 279, 35384–35391.
- Tacke, R., Chen, Y., and Manley, J.L. (1997). Sequence-specific RNA binding by an SR protein requires RS domain phosphorylation: Creation of an SRp40-specific splicing enhancer. *Proceedings of the National Academy of Sciences* 94, 1148–1153.
- Tacke, R., and Manley, J.L. (1995). The human splicing factors ASF/SF2 and SC35 possess distinct, functionally significant RNA binding specificities. *The EMBO journal* 14, 3540–3551.
- Takagaki, Y., and Manley, J.L. (1997). RNA recognition by the human polyadenylation factor CstF. *Molecular and Cellular Biology* 17, 3907–3914.
- Takemoto, A., Kimura, K., Yokoyama, S., and Hanaoka, F. (2004). Cell cycle-dependent phosphorylation, nuclear localization, and activation of human condensin. *The Journal of biological chemistry* 279, 4551–4559.
- Takemura, R., Takeiwa, T., Taniguchi, I., McCloskey, A., and Ohno, M. (2011). Multiple factors in the early splicing complex are involved in the nuclear retention of pre-mRNAs in mammalian cells. *Genes to cells devoted to molecular & cellular mechanisms* 16, 1035–1049.
- Taniguchi, I., Masuyama, K., and Ohno, M. (2007). Role of purine-rich exonic splicing enhancers in nuclear retention of pre-mRNAs. *Proceedings of the National Academy of Sciences of the United States of America* 104, 13684–13689.
- Taniguchi, I., and Ohno, M. (2008). ATP-Dependent Recruitment of Export Factor Aly/REF onto Intronless mRNAs by RNA Helicase UAP56. *Molecular and cellular biology* 28, 601–608.
- Tazi, J., Kornstädt, U., Rossi, F., Jeanteur, P., Cathala, G., Brunel, C., and Lührmann, R. (1993). Thiophosphorylation of U1-70K protein inhibits pre-mRNA splicing. *Nature* 363, 283–286.
- Thadani, R., Kamenz, J., Heeger, S., Munoz, S., and Uhlmann, F. (2018). Cell-Cycle Regulation of Dynamic Chromosome Association of the Condensin Complex. *Cell reports* 23, 2308–2317.
- Thiry, M. (1995a). Behavior of interchromatin granules during the cell cycle. *European journal of cell biology* 68, 14–24.
- Thiry, M. (1995b). The interchromatin granules. *Histology and histopathology* 10, 1035–1045.
- Tomecki, R., Kristiansen, S.M., Lykke-Andersen, S., Chlebowski, A., Larsen, M.K., Szczesny, J.R., Drazkowska, K., Pastula, A., Andersen, S.J., Stepień, P.P., Dziembowski, A., and Jensen, H.T. (2010). The human core exosome interacts with differentially localized processive RNases: hDIS3 and hDIS3L. *The EMBO journal* 29, 2342–2357.
- Tran, D.D.H., Koch, A., and Tamura, T. (2014). THOC5, a member of the mRNA export complex: a novel link between mRNA export machinery and signal transduction pathways in cell proliferation and differentiation. *Cell Communication and Signaling CCS* 12, 3.

- Tran, H.T., Ulke, A., Morrice, N., Johannes, C.J., and Moorhead, G.B.G. (2004). Proteomic characterization of protein phosphatase complexes of the mammalian nucleus. *Molecular & cellular proteomics MCP* 3, 257–265.
- Tran, J.E., Zhou, Y., Corbett, H.A., and Wenthe, R.S. (2007). The DEAD-box protein Dbp5 controls mRNA export by triggering specific RNA: protein remodeling events. *Molecular cell* 28, 850–859.
- Tripathi, V., Ellis, J.D., Shen, Z., Song, D.Y., Pan, Q., Watt, A.T., Freier, S.M., Bennett, C.F., Sharma, A., Bubulya, P.A., Blencowe, B.J., Prasanth, S.G., and Prasanth, K.V. (2010). The nuclear-retained noncoding RNA MALAT1 regulates alternative splicing by modulating SR splicing factor phosphorylation. *Molecular cell* 39, 925–938.
- Tripathi, V., Song, D.Y., Zong, X., Shevtsov, S.P., Hearn, S., Fu, X.-D., Dundr, M., and Prasanth, K.V. (2012). SRSF1 regulates the assembly of pre-mRNA processing factors in nuclear speckles. *Molecular biology of the cell* 23, 3694–3706.
- Truant, R., Kang, Y., and Cullen, B.R. (1999). The human tap nuclear RNA export factor contains a novel transportin-dependent nuclear localization signal that lacks nuclear export signal function. *The Journal of biological chemistry* 274, 32167–32171.
- Tudek, A., Schmid, M., Makaras, M., Barrass, J.D., Beggs, J.D., and Jensen, T.H. (2018). A Nuclear Export Block Triggers the Decay of Newly Synthesized Polyadenylated RNA. *Cell reports* 24, 2457-2467.e7.
- Twyffels, L., Gueydan, C., and Kruijs, V. (2011). Shuttling SR proteins: more than splicing factors. *The FEBS journal* 278, 3246–3255.
- Udagawa, T., Farny, N.G., Jakovcevski, M., Kaphzan, H., Alarcon, J.M., Anilkumar, S., Ivshina, M., Hurt, J.A., Nagaoka, K., Nalavadi, V.C., Lorenz, L.J., Bassell, G.J., Akbarian, S., Chattarji, S., Klann, E., and Richter, J.D. (2013). Genetic and Acute CPEB Depletion Ameliorate Fragile X Pathophysiology. *Nature medicine* 19, 1473–1477.
- Valencia, P., Dias, A.P., and Reed, R. (2008). Splicing promotes rapid and efficient mRNA export in mammalian cells. *Proceedings of the National Academy of Sciences* 105, 3386–3391.
- van Bortle, K., Nichols, M.H., Li, L., Ong, C.-T., Takenaka, N., Qin, Z.S., and Corces, V.G. (2014). Insulator function and topological domain border strength scale with architectural protein occupancy. *Genome biology* 15, R82.
- van der Heyden, Marcel A G, and Defize, L.H.K. (2003). Twenty one years of P19 cells: what an embryonal carcinoma cell line taught us about cardiomyocyte differentiation. *Cardiovascular research* 58, 292–302.
- Vanáčová, S., Wolf, J., Martin, G., Blank, D., Dettwiler, S., Friedlein, A., Langen, H., Keith, G., and Keller, W. (2005). A new yeast poly(A) polymerase complex involved in RNA quality control. *PLoS biology* 3.
- Vargas, D.Y., Shah, K., Batish, M., Levandoski, M., Sinha, S., Marras, S.A.E., Schedl, P., and Tyagi, S. (2011). Single-molecule imaging of transcriptionally coupled and uncoupled splicing. *Cell* 147, 1054–1065.
- Vega-Naredo, I., Loureiro, R., Mesquita, K.A., Barbosa, I.A., Tavares, L.C., Branco, A.F., Erickson, J.R., Holy, J., Perkins, E.L., Carvalho, R.A., and Oliveira, P.J. (2014). Mitochondrial metabolism directs stemness and differentiation in P19 embryonal carcinoma stem cells. *Cell death and differentiation* 21, 1560–1574.

- Vinciguerra, P., Iglesias, N., Camblong, J., Zenklusen, D., and Stutz, F. (2005). Perinuclear Mlp proteins downregulate gene expression in response to a defect in mRNA export. *The EMBO journal* *24*, 813–823.
- Viphakone, N., Cumberbatch, M.G., Livingstone, M.J., Heath, P.R., Dickman, M.J., Catto, J.W., and Wilson, S.A. (2015). Lusz4 defines a new mRNA export pathway in cancer cells. *Nucleic acids research* *43*, 2353–2366.
- Viphakone, N., Hautbergue, G.M., Walsh, M., Chang, C.-T., Holland, A., Folco, E.G., Reed, R., and Wilson, S.A. (2012). TREX exposes the RNA-binding domain of Nxf1 to enable mRNA export. *Nature communications* *3*, 1006.
- Viphakone, N., Sudbery, I., Griffith, L., Heath, C.G., Sims, D., and Wilson, S.A. (2019). Co-transcriptional Loading of RNA Export Factors Shapes the Human Transcriptome. *Molecular cell*.
- Viphakone, N., Voisinet-Hakil, F., and Minvielle-Sebastia, L. (2008). Molecular dissection of mRNA poly(A) tail length control in yeast. *Nucleic acids research* *36*, 2418–2433.
- Visa, N., Puvion-Dutilleul, F., Harper, F., Bachellerie, P.J., and Puvion, E. (1993). Intranuclear distribution of poly(A) RNA determined by electron microscope in situ hybridization. *Experimental cell research* *208*, 19–34.
- Wada, Y., Ohta, Y., Xu, M., Tsutsumi, S., Minami, T., Inoue, K., Komura, D., Kitakami, J.'i., Oshida, N., Papantonis, A., Izumi, A., Kobayashi, M., Meguro, H., Kanki, Y., Mimura, I., Yamamoto, K., Mataka, C., Hamakubo, T., Shirahige, K., Aburatani, H., Kimura, H., Kodama, T., Cook, P.R., and Ihara, S. (2009). A wave of nascent transcription on activated human genes. *Proceedings of the National Academy of Sciences of the United States of America* *106*, 18357–18361.
- Wagner, S., Chiosea, S., Ivshina, M., and Nickerson, J.A. (2004). In vitro FRAP reveals the ATP-dependent nuclear mobilization of the exon junction complex protein SRm160. *The Journal of cell biology* *164*, 843–850.
- Wahl, M.C., Will, C.L., and Lührmann, R. (2009). The spliceosome: design principles of a dynamic RNP machine. *Cell* *136*, 701–718.
- Wahle, E. (1991). Purification and characterization of a mammalian polyadenylate polymerase involved in the 3' end processing of messenger RNA precursors. *The Journal of biological chemistry* *266*, 3131–3139.
- Wahle, E., and Regsegger, U. (1999). 3'-End processing of pre-mRNA in eukaryotes. *FEMS microbiology reviews* *23*, 277–295.
- Wallace, J.E.W., Kear-Scott, L.J., Pilipenko, V.E., Schwartz, H.M., Laskowski, R.P., Rojek, E.A., Katanski, D.C., Riback, A.J., Dion, F.M., Franks, M.A., Airoidi, M.E., Pan, T., Budnik, A.B., and Drummond, A.D. (2015). Reversible, Specific, Active Aggregates of Endogenous Proteins Assemble upon Heat Stress. *Cell* *162*, 1286–1298.
- Walsh, M.J., Hautbergue, G.M., and Wilson, S.A. (2010). Structure and function of mRNA export adaptors. *Biochemical Society transactions* *38*, 232–236.
- Wang, B., Rekosh, D., and Hammarskjöld, M.-L. (2015). Evolutionary conservation of a molecular machinery for export and expression of mRNAs with retained introns. *RNA* *21*, 426–437.

- Wang, H.-W., Wang, J., Ding, F., Callahan, K., Bratkowski, A.M., Butler, S.J., Nogales, E., and Ke, A. (2007). Architecture of the yeast Rps44 exosome complex suggests routes of RNA recruitment for 3' end processing. *Proceedings of the National Academy of Sciences of the United States of America* *104*, 16844–16849.
- Wang, J., Xiao, S.-H., and Manley, J.L. (1998). Genetic analysis of the SR protein ASF/SF2: interchangeability of RS domains and negative control of splicing. *Genes & Development* *12*, 2222–2233.
- Wang, L., Miao, Y.-L., Zheng, X., Lackford, B., Zhou, B., Han, L., Yao, C., Ward, J.M., Burkholder, A., Lipchina, I., Fargo, D.C., Hochedlinger, K., Shi, Y., Williams, C.J., and Hu, G. (2013). The THO complex regulates pluripotency gene mRNA export and controls embryonic stem cell self-renewal and somatic cell reprogramming. *Cell stem cell* *13*, 676–690.
- Wang, X., Fei, F., Qu, J., Li, C., Li, Y., and Zhang, S. (2018). The role of septin 7 in physiology and pathological disease: A systematic review of current status. *Journal of cellular and molecular medicine* *22*, 3298–3307.
- Wang, Z., Hoffmann, H.M., and Grabowski, P.J. (1995). Intrinsic U2AF binding is modulated by exon enhancer signals in parallel with changes in splicing activity. *RNA* *1*, 21–35.
- Wang, Z., Xiao, X., van Nostrand, E., and Burge, C.B. (2006). General and Specific Functions of Exonic Splicing Silencers in Splicing Control. *Molecular cell* *23*, 61–70.
- Wegener, M., and Müller-McNicoll, M. (2018). Nuclear retention of mRNAs - quality control, gene regulation and human disease. *Seminars in cell & developmental biology* *79*, 131–142.
- Wegener, M., and Müller-McNicoll, M. (2020). View from an mRNP: The Roles of SR Proteins in Assembly, Maturation and Turnover. In *The biology of mRNA: Structure and function*, M. Oeffinger, and D. Zenklusen, eds. (Cham: Springer), pp. 83–112.
- Weiler, I.J., Spangler, C.C., Klintsova, A.Y., Grossman, A.W., Kim, S.H., Bertaina-Anglade, V., Khaliq, H., Vries, F.E. de, Lambers, F.A.E., Hatia, F., Base, C.K., and Greenough, W.T. (2004). Fragile X mental retardation protein is necessary for neurotransmitter-activated protein translation at synapses. *Proceedings of the National Academy of Sciences of the United States of America* *101*, 17504–17509.
- Wei-Shan, H., Amit, V.C., and Clarke, D.J. (2019). Cell cycle regulation of condensin Smc4. *Oncotarget* *10*, 263–276.
- Wente, S.R., and Rout, M.P. (2010). The Nuclear Pore Complex and Nuclear Transport. *Cold Spring Harbor Perspectives in Biology* *2*.
- Wickramasinghe, V.O., Andrews, R., Ellis, P., Langford, C., Gurdon, J.B., Stewart, M., Venkitaraman, A.R., and Laskey, R.A. (2014). Selective nuclear export of specific classes of mRNA from mammalian nuclei is promoted by GANP. *Nucleic acids research* *42*, 5059–5071.
- Wickramasinghe, V.O., Savill, J.M., Chavali, S., Jonsdottir, A.B., Rajendra, E., Gruner, T., Laskey, R.A., Babu, M.M., and Venkitaraman, A.R. (2013). Human inositol polyphosphate multikinase regulates transcript-selective nuclear mRNA export to preserve genome integrity. *Molecular cell* *51*, 737–750.
- Wigington, P.C., Morris, J.K., Newman, E.L., and Corbett, H.A. (2016). The Polyadenosine RNA-binding Protein, Zinc Finger Cys3His Protein 14 (ZC3H14), Regulates the Pre-mRNA Processing of a Key ATP Synthase Subunit mRNA. *The Journal of biological chemistry* *291*, 22442–22459.

- Will, C.L., and Lührmann, R. (2011). Spliceosome Structure and Function. *Cold Spring Harbor Perspectives in Biology* 3.
- Wlotzka, W., Kudla, G., Granneman, S., and Tollervey, D. (2011). The nuclear RNA polymerase II surveillance system targets polymerase III transcripts. *The EMBO journal* 30, 1790–1803.
- Wolf, B.B., Schuler, M., Echeverri, F., and Green, D.R. (1999). Caspase-3 Is the Primary Activator of Apoptotic DNA Fragmentation via DNA Fragmentation Factor-45/Inhibitor of Caspase-activated DNase Inactivation. *Journal of Biological Chemistry* 274, 30651–30656.
- Wong, C.-M., Qiu, H., Hu, C., Dong, J., and Hinnebusch, A.G. (2007). Yeast cap binding complex impedes recruitment of cleavage factor IA to weak termination sites. *Molecular and Cellular Biology* 27, 6520–6531.
- Wu, J.Y., and Maniatis, T. (1993). Specific interactions between proteins implicated in splice site selection and regulated alternative splicing. *Cell* 75, 1061–1070.
- Wyers, F., Rougemaille, M., Badis, G., Rousselle, J.-C., Dufour, M.-E., Boulay, J., Régnault, B., Devaux, F., Namane, A., Séraphin, B., Libri, D., and Jacquier, A. (2005). Cryptic pol II transcripts are degraded by a nuclear quality control pathway involving a new poly(A) polymerase. *Cell* 121, 725–737.
- Xiao, S.H., and Manley, J.L. (1997). Phosphorylation of the ASF/SF2 RS domain affects both protein-protein and protein-RNA interactions and is necessary for splicing. *Genes & Development* 11, 334–344.
- Xie, Y., Vessey, J.P., Konecna, A., Dahm, R., Macchi, P., and Kiebler, M.A. (2007). The GTP-binding protein Septin 7 is critical for dendrite branching and dendritic-spine morphology. *Current biology CB* 17, 1746–1751.
- Xu, Q., Walker, D., Bernardo, A., Brodbeck, J., Balestra, M.E., and Huang, Y. (2008). Intron-3 retention/splicing controls neuronal expression of apolipoprotein E in the CNS. *The Journal of neuroscience the official journal of the Society for Neuroscience* 28, 1452–1459.
- Xu, Z., Wei, W., Gagneur, J., Perocchi, F., Clauder-Münster, S., Camblong, J., Guffanti, E., Stutz, F., Huber, W., and Steinmetz, M.L. (2009). Bidirectional promoters generate pervasive transcription in yeast. *Nature* 457, 1033–1037.
- Yadav, S., Osés-Prieto, J.A., Peters, C.J., Zhou, J., Pleasure, S.J., Burlingame, A.L., Jan, L.Y., and Jan, Y.-N. (2017). TAOK2 Kinase Mediates PSD95 Stability and Dendritic Spine Maturation through Septin7 Phosphorylation. *Neuron* 93, 379–393.
- Yamazaki, T., Fujiwara, N., Yukinaga, H., Ebisuya, M., Shiki, T., Kurihara, T., Kioka, N., Kambe, T., Nagao, M., Nishida, E., and Masuda, S. (2010). The closely related RNA helicases, UAP56 and URH49, preferentially form distinct mRNA export machineries and coordinately regulate mitotic progression. *Molecular biology of the cell* 21, 2953–2965.
- Yang, L., Lin, C., Liu, W., Zhang, J., Ohgi, K.A., Grinstein, J.D., Dorrestein, P.C., and Rosenfeld, M.G. (2011). ncRNA- and Pc2 methylation-dependent gene relocation between nuclear structures mediates gene activation programs. *Cell* 147, 773–788.
- Yap, K., Lim, Z.Q., Khandelwa, P., Friedman, B., and Makeyev, E.V. (2012). Coordinated regulation of neuronal mRNA steady-state levels through developmentally controlled intron retention. *Genes & Development* 26, 1209–1223.

- Yeakley, J.M., Tronchère, H., Olesen, J., Dyck, J.A., Wang, H.Y., and Fu, X.D. (1999). Phosphorylation regulates in vivo interaction and molecular targeting of serine/arginine-rich pre-mRNA splicing factors. *The Journal of cell biology* *145*, 447–455.
- Yean, S.L., Wuenschell, G., Termini, J., and Lin, R.J. (2000). Metal-ion coordination by U6 small nuclear RNA contributes to catalysis in the spliceosome. *Nature* *408*, 881–884.
- Yokoi, A., Kotake, Y., Takahashi, K., Kadowaki, T., Matsumoto, Y., Minoshima, Y., Sugi, N.H., Sagane, K., Hamaguchi, M., Iwata, M., and Mizui, Y. (2011). Biological validation that SF3b is a target of the antitumor macrolide pladienolide. *The FEBS journal* *278*, 4870–4880.
- Yoon, S.-O., Shin, S., Lee, H.-J., Chun, H.-K., and Chung, A.-S. (2006). Isoginkgetin inhibits tumor cell invasion by regulating phosphatidylinositol 3-kinase/Akt-dependent matrix metalloproteinase-9 expression. *Molecular Cancer Therapeutics* *5*, 2666–2675.
- Yoshimoto, R., Kaida, D., Furuno, M., Burroughs, M.A., Noma, S., Suzuki, H., Kawamura, Y., Hayashizaki, Y., Mayeda, A., and Yoshida, M. (2017). Global analysis of pre-mRNA subcellular localization following splicing inhibition by spliceostatin A. *RNA* *23*, 47–57.
- Yoshimura, S.H., Otsuka, S., Kumeta, M., Taga, M., and Takeyasu, K. (2013). Intermolecular disulfide bonds between nucleoporins regulate karyopherin-dependent nuclear transport. *Journal of cell science* *126*, 3141–3150.
- Yost, H.J., and Lindquist, S. (1986). RNA splicing is interrupted by heat shock and is rescued by heat shock protein synthesis. *Cell* *45*, 185–193.
- Yost, H.J., and Lindquist, S. (1991). Heat shock proteins affect RNA processing during the heat shock response of *Saccharomyces cerevisiae*. *Molecular and Cellular Biology* *11*, 1062–1068.
- Yu, J., Lu, W., Ge, T., Huang, R., Chen, B., Ye, M., Bai, Y., Shi, G., Songyang, Z., Ma, W., and Huang, J. (2019). Interaction Between Sympk and Oct4 Promotes Mouse Embryonic Stem Cell Proliferation. *STEM CELLS* *37*, 743–753.
- Yu, Q., Guo, J., and Zhou, J. (2004). A minimal length between tau exon 10 and 11 is required for correct splicing of exon 10. *Journal of neurochemistry* *90*, 164–172.
- Yun, C.Y., and Fu, X.-D. (2000). Conserved Sr Protein Kinase Functions in Nuclear Import and Its Action Is Counteracted by Arginine Methylation in *Saccharomyces cerevisiae*. *The Journal of cell biology* *150*, 707–718.
- Zahler, A.M., Lane, W.S., Stolk, J.A., and Roth, M.B. (1992). SR proteins: a conserved family of pre-mRNA splicing factors. *Genes & Development* *6*, 837–847.
- Zahler, A.M., and Roth, M.B. (1995). Distinct functions of SR proteins in recruitment of U1 small nuclear ribonucleoprotein to alternative 5' splice sites. *Proceedings of the National Academy of Sciences* *92*, 2642–2646.
- Zamore, P.D., Patton, J.G., and Green, M.R. (1992). Cloning and domain structure of the mammalian splicing factor U2AF. *Nature* *355*, 609–614.
- Zander, G., Hackmann, A., Bender, L., Becker, D., Lingner, T., Salinas, G., and Krebber, H. (2016). mRNA quality control is bypassed for immediate export of stress-responsive transcripts. *Nature*.

- Zemp, I., and Kutay, U. (2007). Nuclear export and cytoplasmic maturation of ribosomal subunits. *FEBS Letters* 581, 2783–2793.
- Zhang, C., Kuang, M., Li, M., Feng, L., Zhang, K., and Cheng, S. (2016a). SMC4, which is essentially involved in lung development, is associated with lung adenocarcinoma progression. *Scientific reports* 6, 34508.
- Zhang, M., Zamore, P.D., Carmo-Fonseca, M., Lamond, A.I., and Green, M.R. (1992). Cloning and intracellular localization of the U2 small nuclear ribonucleoprotein auxiliary factor small subunit. *Proceedings of the National Academy of Sciences of the United States of America* 89, 8769–8773.
- Zhang, Q., Kota, K.P., Alam, S.G., Nickerson, J.A., Dickinson, R.B., and Lele, T.P. (2016b). Coordinated Dynamics of RNA Splicing Speckles in the Nucleus. *Journal of cellular physiology* 231, 1269–1275.
- Zheng, C., Fasken, M.B., Marshall, N.J., Brockmann, C., Rubinson, M.E., Wentz, S.R., Corbett, A.H., and Stewart, M. (2010). Structural Basis for the Function of the *Saccharomyces cerevisiae* Gfd1 Protein in mRNA Nuclear Export. *The Journal of biological chemistry* 285, 20704–20715.
- Zhou, B., Yuan, T., Liu, M., Liu, H., Xie, J., Shen, Y., and Chen, P. (2012). Overexpression of the structural maintenance of chromosome 4 protein is associated with tumor de-differentiation, advanced stage and vascular invasion of primary liver cancer. *Oncology reports* 28, 1263–1268.
- Zhou, H.-F., Xie, C., Jian, R., Kang, J., Li, Y., Zhuang, C.-L., Yang, F., Zhang, L.-L., Lai, L., Wu, T., and Wu, X. (2011). Biflavonoids from Caper (*Capparis spinosa* L.) fruits and their effects in inhibiting NF-kappa B activation. *Journal of agricultural and food chemistry* 59, 3060–3065.
- Zhou, Z., and Fu, X.-D. (2013). Regulation of Splicing by SR proteins and SR Protein-Specific Kinases. *Chromosoma* 122, 191–207.
- Zhou, Z., Licklider, L.J., Gygi, S.P., and Reed, R. (2002). Comprehensive proteomic analysis of the human spliceosome. *Nature* 419, 182–185.
- Zhou, Z., Luo, J.M., Straesser, K., Katahira, J., Hurt, E., and Reed, R. (2000). The protein Aly links pre-messenger-RNA splicing to nuclear export in metazoans. *Nature* 407, 401–405.
- Zhu, M., Wang, F., Yan, F., Yao, P.Y., Du, J., Gao, X., Wang, X., Wu, Q., Ward, T., Li, J., Kioko, S., Hu, R., Xie, W., Ding, X., and Yao, X. (2008). Septin 7 interacts with centromere-associated protein E and is required for its kinetochore localization. *The Journal of biological chemistry* 283, 18916–18925.
- Zuo, P., and Maniatis, T. (1996). The splicing factor U2AF35 mediates critical protein-protein interactions in constitutive and enhancer-dependent splicing. *Genes & Development* 10, 1356–1368.
- Zuo, P., and Manley, J.L. (1993). Functional domains of the human splicing factor ASF/SF2. *The EMBO journal* 12, 4727–4737.
- Zuo, P., and Manley, J.L. (1994). The human splicing factor ASF/SF2 can specifically recognize pre-mRNA 5' splice sites. *Proceedings of the National Academy of Sciences* 91, 3363–3367.

9. Supplementary tables

Table 22: The SRSF3 interactome. Top 200 SRSF3 interaction partners identified by mass spectrometry.

Gene Symbol	Log ratio SRSF3/NLS	adj p-value	Gene Symbol	Log ratio SRSF3/NLS	adj p-value
<i>Hnrnpc</i>	4.27	2.02803E-06	<i>Pnn</i>	2.66	1.70162E-07
<i>Snrpf</i>	4.01	1.00283E-06	<i>Rpl36</i>	2.66	6.37041E-06
<i>4933434E20Rik</i>	3.87	3.05019E-05	<i>Eif4a3</i>	2.65	7.72945E-08
<i>Rbm22</i>	3.72	5.54285E-06	<i>Ftsj3</i>	2.63	7.38025E-05
<i>Hist1h1c</i>	3.26	1.64339E-07	<i>Mrpl38</i>	2.62	4.29744E-06
<i>Fyttl1</i>	3.22	5.3825E-08	<i>Hnrnpa0</i>	2.61	2.22694E-07
<i>Srsf3</i>	3.19	0.000578377	<i>Rpl27;</i> <i>LOC108167922</i>	2.61	1.85955E-08
<i>Rpl26;</i> <i>Gm15772</i>	3.19	5.25665E-09	<i>Lyar</i>	2.60	1.66476E-06
<i>Mrpl27;</i> <i>Gm6304</i>	3.19	1.20247E-05	<i>Rpl18a</i>	2.56	0.000197778
<i>Hnrnpa3</i>	3.17	0.001177954	<i>Snw1</i>	2.54	2.56623E-06
<i>Krr1</i>	3.17	1.8425E-09	<i>Rpl35</i>	2.54	6.64276E-05
<i>Ints3</i>	3.14	0.000184652	<i>Rpl27a</i>	2.54	2.78958E-08
<i>Rbm8a</i>	3.06	1.9178E-05	<i>Mrps34</i>	2.52	5.91966E-06
<i>Rbmx</i>	3.00	6.60194E-05	<i>Bclaf1</i>	2.51	1.23328E-09
<i>Rpl36al; Rpl36a;</i> <i>Rpl36a-ps3</i>	3.00	3.19773E-06	<i>H2afz</i>	2.51	4.90205E-06
<i>Snrpe</i>	2.98	0.000194091	<i>Raly</i>	2.51	1.92521E-05
<i>Hist1h1a</i>	2.96	1.17175E-05	<i>Rpl10; Rpl10-</i> <i>ps1</i>	2.48	6.1567E-09
<i>Ddx50</i>	2.93	8.87146E-07	<i>Dgcr8</i>	2.48	0.000129561
<i>Mrps31</i>	2.90	4.69696E-06	<i>Rpl21</i>	2.48	7.13302E-06
<i>Fmn13</i>	2.90	0.000218161	<i>Rpl23a</i>	2.47	2.77397E-07
<i>Myef2</i>	2.87	6.14089E-07	<i>Rpl32; Rpl32p</i>	2.46	8.46905E-07
<i>Mrpl3</i>	2.86	1.12753E-05	<i>Fxr1</i>	2.45	1.41351E-05
<i>Hist1h3i;</i> <i>Hist1h3a;</i> <i>Hist1h3g;</i> <i>Hist1h3h</i>	2.84	1.19993E-05	<i>Hnrnpab</i>	2.44	0.000127775
<i>Igf2bp1</i>	2.84	5.65548E-06	<i>Rps13; Rps13-</i> <i>ps1;</i> <i>LOC102642137</i>	2.43	0.001842249
<i>Mrpl28</i>	2.82	9.2615E-07	<i>Ctnnd1</i>	2.42	9.30801E-06
<i>Rps19</i>	2.78	0.000954693	<i>Srfbp1</i>	2.42	7.35618E-06
<i>Rps9</i>	2.77	3.43183E-06	<i>Rpl14</i>	2.41	6.76405E-09
<i>Wdr3</i>	2.77	1.71692E-08	<i>Evpl</i>	2.40	0.000453793
<i>Thrap3</i>	2.76	2.01449E-06	<i>Hist1h3d;</i> <i>Hist1h3f;</i> <i>Hist2h3c1;</i> <i>Hist2h3b;</i> <i>Hist2h3c2;</i> <i>Hist1h3c;</i> <i>Hist1h3e;</i> <i>Hist1h3b</i>	2.40	0.001809327
<i>Grwd1</i>	2.73	7.262E-08	<i>Rpl30; Rpl30-</i> <i>ps8; Gm12191</i>	2.40	2.3935E-07
<i>Hnrnpa2b1</i>	2.72	1.37245E-06			
<i>Hist2h2be</i>	2.72	1.217E-06			
<i>Hist1h1b</i>	2.70	0.021783324			
<i>Caprin1</i>	2.68	0.001220148			
<i>Srsf9</i>	2.66	3.81333E-05			

Gene Symbol	Log ratio SRSF3/NLS	adj p-value
<i>Ddx21</i>	2.40	9.83188E-08
<i>Rps27a</i> ; <i>Rps27a-ps2</i> ; <i>LOC100042019</i>	2.39	4.22454E-06
<i>Rpl13a</i>	2.39	4.63645E-07
<i>Ncl</i>	2.38	1.04773E-05
<i>Rpl28</i>	2.37	1.84209E-09
<i>1810009A15Rik</i> ; <i>LOC105242733</i>	2.37	4.48424E-07
<i>Hist1h1e</i>	2.36	1.22397E-05
<i>Rps4x</i>	2.36	5.70619E-06
<i>Srpk1</i>	2.36	3.02064E-06
<i>Mrpl19</i>	2.35	1.48304E-05
<i>Slc16a3</i>	2.35	6.80264E-05
<i>Rpl15</i>	2.34	2.65846E-06
<i>Rbm7</i>	2.34	0.000151014
<i>Mrpl24</i>	2.33	1.36222E-05
<i>Rpl35a-ps4</i> ; <i>Rpl35a</i> ; <i>Rpl35a-ps2</i> ; <i>Gm10243</i> ; <i>Rpl35a-ps5</i> ; <i>LOC100862595</i> ; <i>Gm14279</i> ; <i>LOC100048620</i>	2.31	2.62712E-08
<i>Esrp2</i>	2.31	5.67656E-05
<i>Srsf10</i>	2.30	4.42512E-06
<i>Rpl11</i>	2.30	1.42285E-08
<i>Rplp2</i>	2.30	1.01853E-05
<i>Hist1h2ae</i> ; <i>Hist1h2ao</i> ; <i>Hist1h2ab</i> ; <i>Hist1h2ai</i> ; <i>Hist1h2ac</i> ; <i>Hist1h2ad</i> ; <i>Hist1h2an</i> ; <i>Hist1h2aa</i> ; <i>Hist1h2ag</i> ; <i>Hist1h2ap</i>	2.28	5.20707E-05
<i>Rbmx1</i>	2.26	3.50071E-05
<i>Igf2bp3</i>	2.25	5.81406E-05
<i>Srsf7</i>	2.25	3.91078E-06
<i>Rps15a</i>	2.24	5.33626E-06
<i>Prpf19</i>	2.24	2.45878E-05

Gene Symbol	Log ratio SRSF3/NLS	adj p-value
<i>Rbm14</i>	2.23	8.26915E-10
<i>Mrpl39</i>	2.23	1.09023E-06
<i>Syncrip</i>	2.23	9.73836E-07
<i>Nufip2</i>	2.22	0.000138646
<i>Nol11</i>	2.22	4.33445E-05
<i>Pcbp1</i>	2.21	4.24483E-06
<i>Npm1</i>	2.21	1.15333E-06
<i>Hnrnrm</i>	2.18	3.60317E-06
<i>Zc3h18</i>	2.16	0.000386984
<i>Ddx18</i>	2.16	1.36106E-09
<i>Hnrnpl</i>	2.15	9.39931E-05
<i>Zc3h13</i>	2.15	2.06114E-05
<i>Hnrnpl</i>	2.14	4.40401E-06
<i>Upf1</i>	2.13	6.22807E-08
<i>Slc25a5</i>	2.12	6.52404E-07
<i>Vdac1</i>	2.12	6.44723E-05
<i>Rexo4</i>	2.12	2.13161E-06
<i>Luc7l3</i>	2.12	0.000106035
<i>L1td1</i>	2.11	1.57015E-05
<i>Erh</i>	2.09	0.000465719
<i>Tardbp</i>	2.09	8.60006E-05
<i>Utp6</i>	2.08	1.69846E-05
<i>Dhx9</i>	2.08	2.46353E-07
<i>Gnl2</i>	2.08	1.48972E-08
<i>Pgam5</i>	2.07	5.18252E-08
<i>Sf3a2</i>	2.07	2.14808E-05
<i>Cherp</i>	2.07	7.04301E-07
<i>Wdr33</i>	2.06	4.45173E-05
<i>G3bp2</i>	2.06	0.000137763
<i>Mrps35</i>	2.05	2.22593E-05
<i>Rpl3</i>	2.04	1.60998E-08
<i>Imp4</i>	2.04	9.39822E-08
<i>Lbr</i>	2.04	1.20717E-05
<i>Ptbp1</i>	2.04	0.000127398
<i>Hist1h2bm</i>	2.02	1.10846E-06
<i>Pphl1</i>	2.02	6.55508E-06
<i>Rps2</i> ; <i>Rps2-ps13</i>	2.01	3.71121E-06
<i>Luc7l</i>	2.01	2.18887E-05
<i>Matr3</i>	1.99	2.80915E-05

Gene Symbol	Log ratio SRSF3/NLS	adj p-value
<i>Mrps16</i>	1.99	2.04683E-05
<i>Mak16</i>	1.98	0.000106506
<i>Tra2a</i>	1.98	1.80219E-05
<i>Xab2</i>	1.97	1.44701E-06
<i>Acin1</i>	1.97	1.47408E-08
<i>Srsf6</i>	1.97	4.80439E-05
<i>Rpf2</i>	1.97	5.29234E-06
<i>Hnrnpf</i>	1.96	1.13947E-07
<i>Rpl37a</i>	1.96	1.20634E-05
<i>Coil</i>	1.95	9.6234E-07
<i>Sf3b1</i>	1.95	9.3764E-05
<i>Atxn2l</i>	1.95	0.000525871
<i>Nsa2;</i> <i>LOC636306;</i> <i>LOC102642514</i>	1.95	6.92891E-06
<i>Sart1</i>	1.94	2.55748E-05
<i>Eif4g1</i>	1.94	1.4685E-05
<i>Celf1</i>	1.94	5.70164E-05
<i>Snrnp70</i>	1.93	4.55874E-08
<i>Srsf1;</i> <i>LOC102641923</i>	1.93	0.000162033
<i>Zfml; Zfp638</i>	1.93	1.7345E-08
<i>Ddx54</i>	1.93	4.55558E-06
<i>Hnrnp2</i>	1.93	6.4748E-07
<i>Rbm17</i>	1.92	6.87901E-05
<i>Rpl7a</i>	1.92	5.67924E-10
<i>Fau</i>	1.92	0.000178978
<i>Srp2k</i>	1.92	0.000232412
<i>Ostc</i>	1.91	0.000255467
<i>Pabpc1</i>	1.91	1.96918E-06
<i>Nop14</i>	1.91	4.03289E-07
<i>Safb</i>	1.91	0.000128406
<i>Cpsf3</i>	1.91	0.000264292
<i>Hnrpd1;</i> <i>Hnrnpdl;</i> <i>Hnrnpdl1</i>	1.91	2.26868E-05
<i>Srrm2</i>	1.90	1.81619E-06
<i>Atp1b1</i>	1.90	4.26814E-06
<i>Thoc2</i>	1.90	3.15281E-05
<i>Rpl6</i>	1.89	5.46256E-06
<i>Hnrnpd</i>	1.89	2.40636E-05

Gene Symbol	Log ratio SRSF3/NLS	adj p-value
<i>Hspd1</i>	1.89	0.000247978
<i>Mrps6</i>	1.88	0.000149071
<i>Snrpa1</i>	1.88	3.2165E-07
<i>Hnrnpu</i>	1.88	7.76742E-07
<i>Hsp90b1</i>	1.88	0.000382885
<i>Surf6</i>	1.88	0.000106212
<i>G3bp1</i>	1.88	0.000230699
<i>Rps11</i>	1.88	9.39079E-08
<i>Prpf4b</i>	1.88	5.12277E-05
<i>Mrpl21</i>	1.86	1.6587E-05
<i>Gm13826;</i> <i>Rpl37rt; Rpl37</i>	1.86	0.001178968
<i>Rpl7</i>	1.85	0.002630816
<i>Wdr46</i>	1.85	3.4357E-05
<i>Ppil1</i>	1.84	0.000273719
<i>Tra2b</i>	1.84	1.14728E-05
<i>Nono</i>	1.83	6.33366E-06
<i>Srsf5</i>	1.83	0.000315726
<i>Sltm</i>	1.83	1.1622E-07
<i>Ythdc1</i>	1.83	3.51965E-06
<i>Rbbp6</i>	1.82	0.000495522
<i>Gtf2i</i>	1.82	0.000477488
<i>Mrps22</i>	1.82	0.000222342
<i>Nol9</i>	1.81	5.49444E-05
<i>Mrps5</i>	1.81	2.09139E-06
<i>Hnrnpa3</i>	1.80	2.38247E-05
<i>Rps3a; Rps3a1</i>	1.80	1.51451E-05
<i>Rps14</i>	1.80	0.010695774
<i>Top2a</i>	1.79	6.95511E-06
<i>Nop2</i>	1.78	2.05078E-07
<i>Chtop</i>	1.78	0.000872923
<i>Ddx39b</i>	1.77	1.17806E-05
<i>Rpl10a</i>	1.77	5.82609E-06
<i>Ilf3</i>	1.77	2.21962E-06
<i>Srrt</i>	1.76	9.85911E-06

Table 23: The SRSF3 interactome upon IsoG treatment. Top 200 SRSF3 interactors which change upon IsoG.

Ratio IsoG/DMSO	Pval	log10_Pval	Gene name	MGI description
-1.72	2.4E-05	4.621	<i>Fytd1</i>	forty-two-three domain containing 1
-1.64	1.4E-04	3.844	<i>Rbm22</i>	RNA binding motif protein 22
-1.61	9.2E-05	4.038	<i>Snw1</i>	SNW domain containing 1
-1.54	4.3E-05	4.370	<i>Ptcd1</i>	pentatricopeptide repeat domain 1
-1.48	2.9E-04	3.531	<i>Wdr33</i>	WD repeat domain 33
-1.45	9.1E-04	3.039	<i>Ppil1</i>	peptidylprolyl isomerase (cyclophilin)-like 1
-1.40	1.5E-03	2.826	<i>Rbbp6</i>	retinoblastoma binding protein 6, ubiquitin ligase
-1.34	3.7E-03	2.429	<i>Ncbp3</i>	nuclear cap binding subunit 3
-1.34	1.9E-04	3.716	<i>Cdc40</i>	cell division cycle 40
-1.30	2.2E-03	2.658	<i>Rbm8a</i>	RNA binding motif protein 8a
-1.29	3.1E-06	5.515	<i>Ppie</i>	peptidylprolyl isomerase E (cyclophilin E)
-1.29	4.8E-06	5.323	<i>Upf1</i>	UPF1 regulator of nonsense transcripts homolog (yeast)
-1.25	2.3E-04	3.646	<i>Mrps31</i>	mitochondrial ribosomal protein S31
-1.22	1.2E-02	1.933	<i>Hnrnpa3</i>	heterogeneous nuclear ribonucleoprotein A3
-1.21	5.1E-04	3.292	<i>Mrpl3</i>	mitochondrial ribosomal protein L3
-1.20	7.1E-04	3.148	<i>Mrps11</i>	mitochondrial ribosomal protein S11
-1.18	1.3E-03	2.878	<i>Cpsf3</i>	cleavage and polyadenylation specificity factor 3
-1.18	4.0E-04	3.396	<i>Mrps35</i>	mitochondrial ribosomal protein S35
-1.17	2.2E-04	3.660	<i>Cpsf2</i>	cleavage and polyadenylation specific factor 2
-1.13	1.5E-02	1.817	<i>Caprin1</i>	cell cycle associated protein 1
-1.11	1.4E-04	3.867	<i>Mrpl2</i>	mitochondrial ribosomal protein L2
-1.09	4.2E-04	3.372	<i>Mrps34</i>	mitochondrial ribosomal protein S34
-1.08	1.9E-05	4.729	<i>Fip11</i>	FIP1 like 1 (<i>S. cerevisiae</i>)
-1.07	1.5E-03	2.838	<i>Mrpl17</i>	mitochondrial ribosomal protein L17
-1.07	4.2E-04	3.378	<i>Mrps16</i>	mitochondrial ribosomal protein S16
-1.06	1.6E-04	3.799	<i>Mrpl39</i>	mitochondrial ribosomal protein L39
-1.05	3.7E-03	2.433	<i>G3bp2</i>	GTPase activating protein (SH3 domain) binding protein 2
-1.05	2.8E-04	3.548	<i>Hnrnpa2b1</i>	heterogeneous nuclear ribonucleoprotein A2/B1
-1.05	3.5E-04	3.457	<i>Mrpl28</i>	mitochondrial ribosomal protein L28
-1.05	1.4E-04	3.869	<i>Mrps2</i>	mitochondrial ribosomal protein S2
-1.05	2.4E-05	4.628	<i>Crnk1</i>	crooked neck pre-mRNA splicing factor 1
-1.04	2.0E-03	2.707	<i>Nufip2</i>	Nuc. fragile X mental retardation protein interacting protein 2
-1.04	3.9E-04	3.408	<i>Mrps10</i>	mitochondrial ribosomal protein S10
-1.02	2.9E-04	3.539	<i>Rbm7</i>	RNA binding motif protein 7
-1.00	1.9E-04	3.726	<i>Xab2</i>	XPA binding protein 2
-0.99	7.8E-04	3.107	<i>Mrpl19</i>	mitochondrial ribosomal protein L19
-0.99	2.6E-03	2.593	<i>Mfap1a</i>	microfibrillar-associated protein 1A
-0.97	1.8E-04	3.734	<i>Pphln1</i>	periphilin 1
-0.95	8.6E-04	3.067	<i>Prpf19</i>	pre-mRNA processing factor 19

Ratio IsoG/DMSO	Pval	log10_Pval	Gene name	MGI description
-0.95	3.8E-04	3.416	<i>Pabpn1</i>	poly(A) binding protein, nuclear 1
-0.95	3.9E-05	4.407	<i>Ptcd3</i>	pentatricopeptide repeat domain 3
-0.93	4.9E-04	3.305	<i>Mrpl49</i>	mitochondrial ribosomal protein L49
-0.93	1.0E-04	3.982	<i>Pabpc1</i>	poly(A) binding protein, cytoplasmic 1
-0.93	7.5E-04	3.122	<i>Mrpl24</i>	mitochondrial ribosomal protein L24
-0.93	7.4E-05	4.130	<i>Ik</i>	IK cytokine
-0.92	1.5E-04	3.819	<i>Eif4a3</i>	eukaryotic translation initiation factor 4A3
-0.92	8.0E-03	2.095	<i>Fmn13</i>	formin-like 3
-0.92	6.9E-06	5.161	<i>Mrps5</i>	mitochondrial ribosomal protein S5
-0.91	4.2E-05	4.374	<i>Dap3</i>	death associated protein 3
-0.91	1.3E-05	4.877	<i>Rrbp1</i>	ribosome binding protein 1
-0.91	3.0E-04	3.517	<i>Mrpl15</i>	mitochondrial ribosomal protein L15
-0.90	3.3E-04	3.476	<i>Hnrnpa1</i>	heterogeneous nuclear ribonucleoprotein A1
-0.90	4.9E-04	3.306	<i>Thoc3</i>	THO complex 3
-0.90	9.4E-06	5.028	<i>Mrps9</i>	mitochondrial ribosomal protein S9
-0.88	2.5E-03	2.601	<i>Mrpl27</i>	mitochondrial ribosomal protein L27
-0.87	2.6E-03	2.591	<i>Mrps6</i>	mitochondrial ribosomal protein S6
-0.86	4.4E-05	4.352	<i>Pgam5</i>	phosphoglycerate mutase family member 5
-0.86	1.1E-04	3.944	<i>Syncrip</i>	synaptotagmin binding, cytoplasmic RNA interacting protein
-0.85	2.9E-04	3.541	<i>Zc3h14</i>	zinc finger CCCH type containing 14
-0.85	6.6E-03	2.178	<i>Mrpl45</i>	mitochondrial ribosomal protein L45
-0.85	6.7E-03	2.172	<i>Mrpl22</i>	mitochondrial ribosomal protein L22
-0.85	3.3E-03	2.478	<i>Hnrnpab</i>	heterogeneous nuclear ribonucleoprotein A/B
-0.84	2.1E-03	2.684	<i>Plrg1</i>	pleiotropic regulator 1
-0.84	7.1E-04	3.146	<i>Hnrnpd</i>	heterogeneous nuclear ribonucleoprotein D
-0.82	1.6E-05	4.789	<i>Mrps7</i>	mitochondrial ribosomal protein S7
-0.81	1.6E-04	3.805	<i>Cdc5l</i>	cell division cycle 5-like (<i>S. pombe</i>)
-0.81	3.2E-03	2.489	<i>Mrps27</i>	mitochondrial ribosomal protein S27
-0.80	1.6E-03	2.794	<i>Mrpl38</i>	mitochondrial ribosomal protein L38
-0.79	2.4E-05	4.613		
-0.79	1.9E-02	1.719	<i>Magoh</i>	mago homolog, exon junction complex core component
-0.78	1.6E-04	3.800	<i>Ssbp1</i>	single-stranded DNA binding protein 1
-0.78	1.3E-03	2.878	<i>Mrps17</i>	mitochondrial ribosomal protein S17
-0.77	5.0E-03	2.302	<i>Mrpl44</i>	mitochondrial ribosomal protein L44
-0.77	9.0E-05	4.044	<i>Bclaf1</i>	BCL2-associated transcription factor 1
-0.77	1.3E-03	2.876	<i>Thoc2</i>	THO complex 2
-0.77	9.0E-05	4.047	<i>Strbp</i>	spermatid perinuclear RNA binding protein
-0.76	4.3E-03	2.368	<i>Thoc7</i>	THO complex 7
-0.76	6.3E-03	2.197	<i>G3bp1</i>	GTPase activating protein (SH3 domain) binding protein 1

Ratio IsoG/DMSO	Pval	log10_Pval	Gene name	MGI description
-0.76	3.6E-03	2.443	<i>Clk4</i>	CDC like kinase 4
-0.75	1.5E-02	1.810	<i>Atxn2l</i>	ataxin 2-like
-0.75	2.2E-04	3.665	<i>Mrpl13</i>	mitochondrial ribosomal protein L13
-0.73	1.4E-03	2.840	<i>Mrps33</i>	mitochondrial ribosomal protein S33
-0.73	2.2E-03	2.660	<i>Thoc5</i>	THO complex 5
-0.72	2.4E-03	2.612	<i>Elavl1</i>	ELAV (embryonic lethal, abnormal vision)-like 1 (Hu antigen R)
-0.72	1.7E-03	2.779	<i>Isy1</i>	ISY1 splicing factor homolog
-0.72	2.0E-03	2.696	<i>Mrpl20</i>	mitochondrial ribosomal protein L20
-0.71	2.5E-03	2.606	<i>Pnn</i>	pinin
-0.69	1.5E-03	2.823	<i>Rbm45</i>	RNA binding motif protein 45
-0.69	2.2E-02	1.650	<i>Thoc1</i>	THO complex 1
-0.69	1.7E-04	3.764	<i>Mrpl1</i>	mitochondrial ribosomal protein L1
-0.69	2.4E-02	1.613	<i>Hnrnpk</i>	heterogeneous nuclear ribonucleoprotein K
-0.69	6.0E-04	3.220	<i>Mrpl21</i>	mitochondrial ribosomal protein L21
-0.69	1.7E-04	3.780	<i>Larp4</i>	La ribonucleoprotein domain family, member 4
-0.67	1.3E-04	3.893	<i>Mrps22</i>	mitochondrial ribosomal protein S22
-0.67	8.5E-03	2.073	<i>Fubp1</i>	far upstream element (FUSE) binding protein 1
-0.66	3.9E-03	2.406	<i>Esrp2</i>	epithelial splicing regulatory protein 2
-0.65	4.3E-05	4.367	<i>Bcas2</i>	breast carcinoma amplified sequence 2
-0.65	7.6E-05	4.117	<i>Dhx36</i>	DEAH (Asp-Glu-Ala-His) box polypeptide 36
-0.64	3.2E-03	2.499	<i>Ddx3x</i>	DEAD/H (Asp-Glu-Ala-Asp/His) box polypeptide 3, X-linked
-0.64	2.3E-03	2.636	<i>Cpsf1</i>	cleavage and polyadenylation specific factor 1
-0.63	2.2E-02	1.657	<i>Evpl</i>	envoplakin
-0.62	1.1E-03	2.943	<i>Mrpl9</i>	mitochondrial ribosomal protein L9
-0.61	8.4E-04	3.075	<i>Cpsf4</i>	cleavage and polyadenylation specific factor 4
-0.61	5.2E-04	3.280	<i>Nxf1</i>	nuclear RNA export factor 1
-0.61	6.0E-04	3.223	<i>Zcchc8</i>	zinc finger, CCHC domain containing 8
-0.60	2.5E-03	2.608	<i>Larp1</i>	La ribonucleoprotein domain family, member 1
-0.60	1.7E-03	2.777	<i>L1td1</i>	LINE-1 type transposase domain containing 1
-0.59	5.5E-03	2.260	<i>Snrnp40</i>	small nuclear ribonucleoprotein 40 (U5)
-0.59	1.3E-03	2.886	<i>Thrap3</i>	thyroid hormone receptor associated protein 3
-0.58	3.0E-03	2.519	<i>Smu1</i>	smu-1 suppressor of mec-8 and unc-52 homolog (C. elegans)
-0.58	1.3E-03	2.894	<i>Zfr</i>	zinc finger RNA binding protein
-0.58	2.7E-02	1.564	<i>Zc3h18</i>	zinc finger CCCH-type containing 18
-0.56	1.7E-03	2.770	<i>Igf2bp1</i>	insulin-like growth factor 2 mRNA binding protein 1
-0.55	2.1E-03	2.671	<i>Mrpl41</i>	mitochondrial ribosomal protein L41
-0.55	5.9E-03	2.228	<i>Polr2a</i>	polymerase (RNA) II (DNA directed) polypeptide A
-0.55	1.1E-02	1.958	<i>Fxr1</i>	fragile X mental retardation gene 1, autosomal homolog
-0.54	5.0E-04	3.303	<i>Myef2</i>	myelin basic protein expression factor 2, repressor

Ratio IsoG/DMSO	Pval	log10_Pval	Gene name	MGI description
-0.54	7.0E-04	3.156	<i>Hnrnpa0</i>	heterogeneous nuclear ribonucleoprotein A0
-0.54	1.3E-04	3.901	<i>Aqr</i>	aquarius
-0.53	1.2E-03	2.909	<i>Nsa2</i>	NSA2 ribosome biogenesis homolog
-0.53	3.4E-04	3.471	<i>Rbm10</i>	RNA binding motif protein 10
-0.52	1.9E-05	4.720	<i>Sfpq</i>	splicing factor proline/glutamine rich (polypyrimidine tract binding protein associated)
-0.52	2.2E-02	1.653	<i>Chtop</i>	chromatin target of PRMT1
-0.51	9.1E-04	3.040	<i>Ilf3</i>	interleukin enhancer binding factor 3
-0.51	3.5E-02	1.458	<i>Aak1</i>	AP2 associated kinase 1
-0.50	1.2E-02	1.921	<i>Tardbp</i>	TAR DNA binding protein
0.50	1.5E-03	2.824	<i>Nkrf</i>	NF-kappaB repressing factor
0.50	8.9E-03	2.052	<i>Psip1</i>	PC4 and SFRS1 interacting protein 1
0.50	5.4E-03	2.270	<i>Rpl6</i>	ribosomal protein L6
0.51	1.2E-03	2.925	<i>Tmpo</i>	thymopoietin
0.51	1.8E-02	1.740	<i>Uba2</i>	ubiquitin-like modifier activating enzyme 2
0.51	2.6E-03	2.592	<i>Tubb4b</i>	tubulin, beta 4B class IVB
0.51	1.8E-02	1.747	<i>Ipo7</i>	importin 7
0.52	3.0E-02	1.525	<i>Rpl7</i>	ribosomal protein L7
0.52	6.9E-04	3.159	<i>Nhp2</i>	NHP2 ribonucleoprotein
0.52	1.1E-02	1.950	<i>Rpl13</i>	ribosomal protein L13
0.52	4.4E-04	3.355	<i>Rrs1</i>	ribosome biogenesis regulator 1
0.52	1.3E-03	2.877	<i>Ssb</i>	Sjogren syndrome antigen B
0.53	1.9E-03	2.726	<i>Rpl23a</i>	ribosomal protein L23A
0.53	3.4E-03	2.469	<i>Nop58</i>	NOP58 ribonucleoprotein
0.53	2.8E-04	3.555	<i>Rpl35a-ps4</i>	ribosomal protein 35A, pseudogene 4
0.53	4.0E-03	2.403	<i>Top2a</i>	topoisomerase (DNA) II alpha
0.53	2.7E-03	2.568	<i>Rpl9</i>	ribosomal protein L9
0.53	4.2E-04	3.373	<i>Rpl28</i>	ribosomal protein L28
0.53	2.4E-03	2.614	<i>Lyar</i>	Ly1 antibody reactive clone
0.53	1.8E-04	3.733	<i>Ruvb1</i>	RuvB-like protein 1
0.54	9.6E-03	2.019	<i>Rpl31</i>	ribosomal protein L31
0.54	1.6E-02	1.803	<i>Utp15</i>	UTP15 small subunit processome component
0.54	1.9E-03	2.728	<i>Rpl4</i>	ribosomal protein L4
0.55	1.4E-03	2.865	<i>Rpl15</i>	ribosomal protein L15
0.55	3.2E-03	2.494	<i>Rpl36al</i>	ribosomal protein L36A-like
0.56	1.3E-02	1.891	<i>Rrp9</i>	RRP9, small subunit (SSU) processome component, homolog (yeast)
0.56	2.1E-03	2.671	<i>Atp5b</i>	ATP synthase, H ⁺ transporting mitochondrial F1 complex, beta subunit
0.56	1.1E-02	1.950	<i>Coil</i>	coilin

Ratio IsoG/DMSO	Pval	log10_Pval	Gene name	MGI description
0.56	1.8E-02	1.757	<i>Rpl35</i>	ribosomal protein L35
0.57	2.0E-02	1.705	<i>Rps5</i>	ribosomal protein S5
0.57	1.2E-02	1.922	<i>Psmc5</i>	protease (prosome, macropain) 26S subunit, ATPase 5
0.57	7.1E-04	3.146	<i>Ddx25</i>	DEAD (Asp-Glu-Ala-Asp) box polypeptide 25
0.57	1.4E-02	1.862	<i>Rpl22</i>	ribosomal protein L22
0.57	9.4E-03	2.027	<i>Mat2a</i>	methionine adenosyltransferase II, alpha
0.57	1.5E-02	1.823	<i>Psm12</i>	proteasome (prosome, macropain) 26S subunit, non-ATPase, 12
0.57	5.2E-04	3.282	<i>Rpl14</i>	ribosomal protein L14
0.58	3.5E-02	1.452	<i>Rplp2</i>	ribosomal protein, large P2
0.58	1.6E-03	2.807	<i>Tuba4a</i>	tubulin, alpha 4A
0.58	1.3E-03	2.892	<i>Psmc2</i>	proteasome (prosome, macropain) 26S subunit, ATPase 2
0.58	5.3E-04	3.273	<i>Rps26</i>	ribosomal protein S26
0.58	1.9E-02	1.732	<i>Rpl18a</i>	ribosomal protein L18A
0.59	1.7E-03	2.779	<i>Snd1</i>	staphylococcal nuclease and tudor domain containing 1
0.59	2.4E-04	3.614	<i>Psm13</i>	proteasome (prosome, macropain) 26S subunit, non-ATPase, 13
0.59	7.6E-03	2.117	<i>Prrc2a</i>	proline-rich coiled-coil 2A
0.60	1.5E-03	2.817	<i>Cct5</i>	chaperonin containing Tcp1, subunit 5 (epsilon)
0.60	2.7E-03	2.575	<i>Cse1l</i>	chromosome segregation 1-like (<i>S. cerevisiae</i>)
0.60	3.5E-03	2.455	<i>Psm3</i>	proteasome (prosome, macropain) activator subunit 3 (PA28 gamma, Ki)
0.61	2.6E-03	2.578	<i>Dnmt3b</i>	DNA methyltransferase 3B
0.61	8.7E-03	2.059	<i>Rpl34-ps1</i>	ribosomal protein L34, pseudogene 1
0.61	2.6E-02	1.580	<i>Fau</i>	Finkel-Biskis-Reilly murine sarcoma virus (FBR-MuSV) ubiquitously expressed (fox derived)
0.61	1.4E-03	2.848	<i>Rpl13a</i>	ribosomal protein L13A
0.61	7.0E-05	4.155	<i>Rpl8</i>	ribosomal protein L8
0.61	2.7E-03	2.571	<i>Sf3a3</i>	splicing factor 3a, subunit 3
0.61	8.0E-04	3.099	<i>Hspa8</i>	heat shock protein 8
0.62	2.5E-03	2.598	<i>Fasn</i>	fatty acid synthase
0.63	2.3E-02	1.635	<i>Rps19</i>	ribosomal protein S19
0.63	4.3E-03	2.367	<i>Npm1</i>	nucleophosmin 1
0.63	2.5E-04	3.597	<i>Rpl24</i>	ribosomal protein L24
0.63	2.6E-05	4.583	<i>Rpl27</i>	ribosomal protein L27
0.64	3.4E-02	1.469	<i>Rpl30</i>	ribosomal protein L30
0.64	3.9E-03	2.412	<i>Leng8</i>	leukocyte receptor cluster (LRC) member 8
0.64	3.0E-04	3.523	<i>Rpl21</i>	ribosomal protein L21
0.56	1.8E-02	1.757	<i>Rpl35</i>	ribosomal protein L35
0.57	2.0E-02	1.705	<i>Rps5</i>	ribosomal protein S5

Ratio IsoG/DMSO	Pval	log10_Pval	Gene name	MGI description
0.56	1.8E-02	1.757	<i>Rpl35</i>	ribosomal protein L35
0.57	2.0E-02	1.705	<i>Rps5</i>	ribosomal protein S5
0.57	1.2E-02	1.922	<i>Psmc5</i>	protease (prosome, macropain) 26S subunit, ATPase 5
0.57	7.1E-04	3.146	<i>Ddx25</i>	DEAD (Asp-Glu-Ala-Asp) box polypeptide 25
0.57	1.4E-02	1.862	<i>Rpl22</i>	ribosomal protein L22
0.57	9.4E-03	2.027	<i>Mat2a</i>	methionine adenosyltransferase II, alpha
0.57	1.5E-02	1.823	<i>Psm12</i>	proteasome (prosome, macropain) 26S subunit, non-ATPase, 12
0.57	5.2E-04	3.282	<i>Rpl14</i>	ribosomal protein L14
0.58	3.5E-02	1.452	<i>Rplp2</i>	ribosomal protein, large P2
0.58	1.6E-03	2.807	<i>Tuba4a</i>	tubulin, alpha 4A
0.58	1.3E-03	2.892	<i>Psmc2</i>	proteasome (prosome, macropain) 26S subunit, ATPase 2
0.58	5.3E-04	3.273	<i>Rps26</i>	ribosomal protein S26
0.58	1.9E-02	1.732	<i>Rpl18a</i>	ribosomal protein L18A
0.59	1.7E-03	2.779	<i>Snd1</i>	staphylococcal nuclease and tudor domain containing 1
0.59	2.4E-04	3.614	<i>Psm13</i>	proteasome (prosome, macropain) 26S subunit, non-ATPase, 13
0.59	7.6E-03	2.117	<i>Prrc2a</i>	proline-rich coiled-coil 2A
0.60	1.5E-03	2.817	<i>Cct5</i>	chaperonin containing Tcp1, subunit 5 (epsilon)
0.60	2.7E-03	2.575	<i>Cse1l</i>	chromosome segregation 1-like (<i>S. cerevisiae</i>)
0.60	3.5E-03	2.455	<i>Psm3</i>	proteasome (prosome, macropain) activator subunit 3 (PA28 gamma, Ki)
0.61	2.6E-03	2.578	<i>Dnmt3b</i>	DNA methyltransferase 3B
0.61	8.7E-03	2.059	<i>Rpl34-ps1</i>	ribosomal protein L34, pseudogene 1
0.61	2.6E-02	1.580	<i>Fau</i>	Finkel-Biskis-Reilly murine sarcoma virus (FBR-MuSV) ubiquitously expressed (fox derived)
0.61	1.4E-03	2.848	<i>Rpl13a</i>	ribosomal protein L13A
0.61	7.0E-05	4.155	<i>Rpl8</i>	ribosomal protein L8
0.61	2.7E-03	2.571	<i>Sf3a3</i>	splicing factor 3a, subunit 3
0.61	8.0E-04	3.099	<i>Hspa8</i>	heat shock protein 8
0.62	2.5E-03	2.598	<i>Fasn</i>	fatty acid synthase
0.63	2.3E-02	1.635	<i>Rps19</i>	ribosomal protein S19
0.63	4.3E-03	2.367	<i>Npm1</i>	nucleophosmin 1
0.63	2.5E-04	3.597	<i>Rpl24</i>	ribosomal protein L24
0.63	2.6E-05	4.583	<i>Rpl27</i>	ribosomal protein L27
0.64	3.4E-02	1.469	<i>Rpl30</i>	ribosomal protein L30
0.64	3.9E-03	2.412	<i>Leng8</i>	leukocyte receptor cluster (LRC) member 8
0.64	3.0E-04	3.523	<i>Rpl21</i>	ribosomal protein L21
0.64	2.0E-02	1.689	<i>Hsp90ab1</i>	heat shock protein 90 alpha (cytosolic), class B member 1
0.65	4.0E-04	3.398	<i>Tuba1c</i>	tubulin, alpha 1C

Ratio IsoG/DMSO	Pval	log10_Pval	Gene name	MGI description
0.65	1.6E-03	2.806	<i>Cct2</i>	chaperonin containing Tcp1, subunit 2 (beta)
0.65	2.5E-04	3.599	<i>Rpl10a</i>	ribosomal protein L10A
0.66	6.6E-03	2.181	<i>Cct8</i>	chaperonin containing Tcp1, subunit 8 (theta)
0.66	4.5E-03	2.349	<i>Gm12033</i>	predicted gene 12033
0.66	5.9E-03	2.230	<i>Aimp2</i>	aminoacyl tRNA synthetase complex-interacting multifunctional protein 2
0.67	1.3E-02	1.880	<i>Nono</i>	non-POU-domain-containing, octamer binding protein
0.67	4.8E-02	1.316	<i>Gmps</i>	guanine monophosphate synthetase
0.68	8.2E-03	2.085	<i>Actb</i>	actin, beta
0.68	1.3E-04	3.877	<i>Rplp0</i>	ribosomal protein, large, P0
0.69	1.9E-02	1.723	<i>Cpsf6</i>	cleavage and polyadenylation specific factor 6
0.69	5.3E-04	3.275	<i>Trim28</i>	tripartite motif-containing 28
0.69	2.5E-05	4.597	<i>Psmc6</i>	proteasome (prosome, macropain) 26S subunit, ATPase, 6
0.70	1.6E-02	1.805	<i>Rbm25</i>	RNA binding motif protein 25
0.72	2.5E-02	1.600	<i>Wbp11</i>	WW domain binding protein 11
0.72	9.5E-04	3.023	<i>Rps25</i>	ribosomal protein S25
0.73	8.2E-04	3.085	<i>Tcp1</i>	t-complex protein 1
0.73	3.3E-03	2.488	<i>Dkc1</i>	dyskeratosis congenita 1, dyskerin
0.73	2.8E-02	1.552	<i>Rfc4</i>	replication factor C (activator 1) 4
0.73	4.5E-03	2.347	<i>Rpl36</i>	ribosomal protein L36
0.73	5.2E-03	2.287	<i>Ccar1</i>	cell division cycle and apoptosis regulator 1
0.74	4.1E-04	3.382	<i>Rpf2</i>	ribosome production factor 2 homolog
0.75	8.9E-04	3.051	<i>Mrto4</i>	mRNA turnover 4, ribosome maturation factor
0.75	4.6E-03	2.338	<i>Eef2</i>	eukaryotic translation elongation factor 2
0.75	3.1E-03	2.510	<i>Sf3a1</i>	splicing factor 3a, subunit 1
0.76	2.2E-05	4.653	<i>Psmc3</i>	proteasome (prosome, macropain) 26S subunit, ATPase 3
0.76	8.0E-03	2.099	<i>Hsp90aa1</i>	heat shock protein 90, alpha (cytosolic), class A member 1
0.77	1.3E-02	1.896	<i>Ldha</i>	lactate dehydrogenase A
0.77	3.7E-03	2.437	<i>Cct6a</i>	chaperonin containing Tcp1, subunit 6a (zeta)
0.77	9.9E-03	2.005	<i>Cherp</i>	calcium homeostasis endoplasmic reticulum protein
0.78	5.5E-03	2.263	<i>Prpf40a</i>	pre-mRNA processing factor 40A
0.78	1.1E-03	2.969	<i>Lig1</i>	ligase I, DNA, ATP-dependent
0.79	1.0E-03	2.998	<i>Eif3m</i>	eukaryotic translation initiation factor 3, subunit M
0.79	3.1E-03	2.505	<i>Cnn3</i>	calponin 3, acidic
0.80	1.9E-02	1.716	<i>Rpl37a</i>	ribosomal protein L37a
0.82	1.1E-02	1.951	<i>Nsun2</i>	NOL1/NOP2/Sun domain family member 2
0.84	2.6E-03	2.587	<i>Supt16</i>	suppressor of Ty 16

Ratio IsoG/DMSO	Pval	log10_Pval	Gene name	MGI description
0.84	6.4E-03	2.194	<i>Sf3a2</i>	splicing factor 3a, subunit 2
0.84	2.2E-03	2.658	<i>Mcm7</i>	minichromosome maintenance complex component 7
0.85	3.6E-04	3.440	<i>Rps27a</i>	ribosomal protein S27A
0.85	2.0E-04	3.704	<i>Ssrp1</i>	structure specific recognition protein 1
0.86	6.1E-04	3.213	<i>Ddx46</i>	DEAD (Asp-Glu-Ala-Asp) box polypeptide 46
0.87	3.8E-03	2.415	<i>Rcc2</i>	regulator of chromosome condensation 2
0.89	4.5E-03	2.345	<i>Mlf2</i>	myeloid leukemia factor 2
0.91	1.0E-03	2.979	<i>Usp5</i>	ubiquitin specific peptidase 5 (isopeptidase T)
0.93	4.8E-05	4.317	<i>Umps</i>	uridine monophosphate synthetase
0.93	3.1E-04	3.511	<i>Eif3f</i>	eukaryotic translation initiation factor 3, subunit F
0.95	1.1E-03	2.950	<i>Mcm4</i>	minichromosome maintenance complex component 4
0.95	1.0E-02	1.980	<i>Khsrp</i>	KH-type splicing regulatory protein
0.95	1.5E-03	2.828	<i>Pou5f1</i>	POU domain, class 5, transcription factor 1
0.96	7.0E-03	2.152	<i>Scaf8</i>	SR-related CTD-associated factor 8
0.97	6.3E-03	2.203	<i>Ywhae</i>	tyrosine 3-monooxygenase/tryptophan 5-monooxygenase activation protein, epsilon polypeptide
1.00	2.6E-03	2.587	<i>Hat1</i>	histone aminotransferase 1
1.02	2.1E-03	2.684	<i>Rbpms</i>	RNA binding protein gene with multiple splicing
1.03	9.3E-05	4.030	<i>Maged1</i>	melanoma antigen, family D, 1
1.08	8.1E-04	3.093	<i>Eif4a1</i>	eukaryotic translation initiation factor 4A1
1.14	1.7E-03	2.765	<i>Eif5a</i>	eukaryotic translation initiation factor 5A
1.14	1.9E-04	3.714	<i>Sfn</i>	stratifin
1.18	4.8E-04	3.321	<i>Eef1a1</i>	eukaryotic translation elongation factor 1 alpha 1
1.19	1.2E-03	2.906	<i>Mcm5</i>	minichromosome maintenance complex component 5
1.20	5.2E-04	3.288	<i>Galk1</i>	galactokinase 1
1.22	4.2E-04	3.380	<i>Glrx3</i>	glutaredoxin 3
1.22	1.3E-03	2.877	<i>Nap1l1</i>	nucleosome assembly protein 1-like 1
1.24	8.9E-04	3.051	<i>Actc1</i>	actin, alpha, cardiac muscle 1
1.36	3.1E-03	2.502	<i>Aars</i>	alanyl-tRNA synthetase
1.59	3.7E-04	3.438	<i>Srsf2</i>	serine/arginine-rich splicing factor 2
1.59	5.0E-04	3.300	<i>Ptges3</i>	prostaglandin E synthase 3
1.60	9.6E-04	3.017	<i>Eif2s1</i>	eukaryotic translation initiation factor 2, subunit 1 alpha
1.71	6.7E-04	3.171	<i>Gapdh</i>	glyceraldehyde-3-phosphate dehydrogenase
1.93	1.2E-03	2.911	<i>Tcerg1</i>	transcription elongation regulator 1 (CA150)
2.05	2.1E-03	2.674	<i>Ppia</i>	peptidylprolyl isomerase A
2.33	1.7E-03	2.781	<i>Sumo3</i>	small ubiquitin-like modifier 3
2.50	3.9E-03	2.411	<i>Bub3</i>	BUB3 mitotic checkpoint protein
2.81	1.7E-03	2.779	<i>Anp32b</i>	acidic (leucine-rich) nuclear phosphoprotein 32 family, member B

Table 24: Top 240 DEG upon Zc3h14 depletion.

Gene Name	log2FC	padj
<i>Zc3h14</i>	-2.84	8.67E-100
<i>Kif20b</i>	-2.54	1.023E-50
<i>Tpr</i>	-1.96	4.276E-43
<i>Smc4</i>	-2.08	4.276E-43
<i>Dek</i>	-2.07	1.014E-41
<i>Ppig</i>	-1.96	3.448E-40
<i>Zfp638</i>	-2.24	4.067E-40
<i>Top2b</i>	-1.77	2.511E-38
<i>Atrx</i>	-2.07	1.103E-36
<i>Hmgn5</i>	-1.84	7.105E-36
<i>Eif3a</i>	-1.70	7.576E-36
<i>Resf1</i>	-1.95	7.576E-36
<i>L1td1</i>	-1.60	2.524E-35
<i>Smc3</i>	-1.83	2.263E-34
<i>Ktn1</i>	-1.86	2.45E-34
<i>Snhg14</i>	-1.93	5.158E-34
<i>Kif5b</i>	-1.72	1.795E-33
<i>Smc6</i>	-1.79	2.694E-33
<i>Hsp90aa1</i>	-1.64	3.85E-33
<i>Pnn</i>	-1.62	1.103E-32
<i>Tug1</i>	-1.72	1.43E-32
<i>Mphosph8</i>	-1.79	1.659E-32
<i>Zfp445</i>	-1.89	1.969E-32
<i>Rif1</i>	-1.99	3.111E-32
<i>Esf1</i>	-1.94	6.142E-32
<i>Nipbl</i>	-1.83	7.972E-32
<i>Naa15</i>	-1.69	8.884E-32
<i>Nemf</i>	-2.00	1.752E-31
<i>Yme1l1</i>	-1.62	2.551E-31
<i>Hells</i>	-1.62	2.74434E-31
<i>Smc5</i>	-1.75	3.38335E-31
<i>Bclaf1</i>	-1.55	5.55136E-31
<i>Prex2</i>	-1.54	9.5394E-31
<i>Ppip5k2</i>	-1.71	3.25398E-30
<i>Pcm1</i>	-1.75	3.30098E-30
<i>Nol8</i>	-1.81	7.44379E-30
<i>Fmr1</i>	-1.76	8.47379E-30
<i>Ccar1</i>	-1.60	2.11125E-29
<i>Smc1a</i>	-1.41	8.35131E-29

Gene Name	log2FC	padj
<i>Zfp62</i>	-2.00	1.297E-28
<i>Phip</i>	-1.86	1.783E-28
<i>Kif18a</i>	-2.29	2.063E-28
<i>Pnizr</i>	-1.65	4.147E-28
<i>Casp8ap2</i>	-1.82	4.147E-28
<i>Upf2</i>	-1.85	5.314E-28
<i>Ppp4r3b</i>	-1.73	6.84E-28
<i>Suz12</i>	-1.48	7.195E-28
<i>Rock1</i>	-2.41	1.467E-27
<i>Cops2</i>	-1.60	2.013E-27
<i>Sept7</i>	-1.87	3.067E-27
<i>Ckap5</i>	-1.43	4.013E-27
<i>Mis18bp1</i>	-1.89	4.522E-27
<i>Cwc22</i>	-1.49	6.518E-27
<i>Nasp</i>	-1.41	9.35E-27
<i>Akap9</i>	-1.78	1.138E-26
<i>Smc2</i>	-1.65	1.215E-26
<i>Setd2</i>	-1.63	1.5E-26
<i>Heg1</i>	-1.47	1.861E-26
<i>Hltf</i>	-1.58	2.072E-26
<i>Rsrc2</i>	-1.61	2.104E-26
<i>Ipo7</i>	-1.48	2.206E-26
<i>Aspm</i>	-1.54	2.774E-26
<i>Top1</i>	-1.49	3.537E-26
<i>Senp6</i>	-1.36	4.416E-26
<i>Tax1bp1</i>	-1.45	1.033E-25
<i>Sltm</i>	-1.52	1.114E-25
<i>Usp15</i>	-1.53	1.955E-25
<i>Rabep1</i>	-1.44	3.51E-25
<i>Rbm39</i>	-1.34	3.555E-25
<i>Dock11</i>	-1.68	5.822E-25
<i>Ift74</i>	-1.99	7.2E-25
<i>Ppil4</i>	-1.64	9.301E-25
<i>Rad50</i>	-1.45	1.282E-24
<i>Golga4</i>	-1.44	1.96E-24
<i>Xpo1</i>	-1.36	2.15E-24
<i>Smarca5</i>	-1.37	3.204E-24
<i>Sgo2a</i>	-1.73	5.573E-24
<i>Dst</i>	-1.61	6.135E-24

Gene Name	log2FC	padj
<i>Cd2ap</i>	-1.76	7.555E-24
<i>Cenpe</i>	-2.37	8.279E-24
<i>Dnm1l</i>	-1.49	8.863E-24
<i>Trpm7</i>	-1.72	9.319E-24
<i>Yes1</i>	-1.63	1.363E-23
<i>Eif5b</i>	-1.52	1.402E-23
<i>Evi5</i>	-1.84	1.418E-23
<i>Ncl</i>	-1.29	1.594E-23
<i>Taok1</i>	-1.41	2.117E-23
<i>U2surp</i>	-1.46	2.117E-23
<i>Cip2a</i>	-1.54	2.284E-23
<i>Rasa1</i>	-1.66	2.409E-23
<i>Pds5b</i>	-1.43	3.638E-23
<i>Dmxl1</i>	-1.65	3.921E-23
<i>Ankrd44</i>	-1.57	4.17E-23
<i>Ccdc66</i>	-2.00	4.468E-23
<i>Cwf19l2</i>	-1.84	5.802E-23
<i>Supt16</i>	-1.37	5.981E-23
<i>Armcx4</i>	-1.40	7.834E-23
<i>Qser1</i>	-1.51	1.153E-22
<i>Rbm25</i>	-1.53	1.189E-22
<i>Arid4b</i>	-1.82	1.28E-22
<i>Nsrp1</i>	-1.48	1.304E-22
<i>Ncapg</i>	-1.58	1.351E-22
<i>Cntrl</i>	-1.65	2.157E-22
<i>Abce1</i>	-1.33	2.521E-22
<i>Bub1</i>	-1.35	2.57E-22
<i>Apc</i>	-1.54	2.671E-22
<i>Zfp644</i>	-1.66	3.125E-22
<i>Uba6</i>	-1.61	3.394E-22
<i>Upf3b</i>	-1.55	3.394E-22
<i>Psme4</i>	-1.28	3.798E-22
<i>Map1b</i>	-1.50	4.123E-22
<i>Dnajc13</i>	-1.56	4.239E-22
<i>Sh3bgrl</i>	-1.40	4.803E-22
<i>Mphosph10</i>	-1.39	5.076E-22
<i>Ssb</i>	-1.37	5.076E-22
<i>Itsn2</i>	-1.64	5.288E-22
<i>Cep83</i>	-1.56	5.44E-22

Gene Name	log2FC	padj
<i>Zfp322a</i>	-1.53	7.345E-22
<i>Prpf39</i>	-1.81	1.042E-21
<i>Dnrtip2</i>	-1.28	3.272E-21
<i>Ddx10</i>	-1.33	3.282E-21
<i>Cdc27</i>	-1.42	3.305E-21
<i>Zfp292</i>	-1.65	3.376E-21
<i>Kif23</i>	-1.23	3.509E-21
<i>Slk</i>	-1.34	3.65E-21
<i>Jmjd1c</i>	-1.66	4.288E-21
<i>Prpf4b</i>	-1.36	5.456E-21
<i>Larp4</i>	-1.34	5.995E-21
<i>March7</i>	-1.53	5.995E-21
<i>Luc7l3</i>	-1.38	6.066E-21
<i>Macf1</i>	-1.32	7.345E-21
<i>Ttc3</i>	-1.33	7.991E-21
<i>Rbbp6</i>	-1.45	8.005E-21
<i>Myef2</i>	-1.29	8.529E-21
<i>Rev3l</i>	-1.90	1.055E-20
<i>Hsp90b1</i>	-1.16	1.055E-20
<i>Psip1</i>	-1.19	1.235E-20
<i>1700020I14Rik</i>	-1.29	1.335E-20
<i>Hmmr</i>	-1.52	1.383E-20
<i>Esco2</i>	-1.65	1.43E-20
<i>Elovl6</i>	-1.23	1.433E-20
<i>Rsf1</i>	-1.40	1.519E-20
<i>Mtf2</i>	-1.35	1.546E-20
<i>Cul4b</i>	-1.40	1.861E-20
<i>Bdp1</i>	-1.67	2.029E-20
<i>Mpdz</i>	-1.43	2.893E-20
<i>Ccdc47</i>	-1.21	2.893E-20
<i>Dhx36</i>	-1.30	3.036E-20
<i>Scaf11</i>	-1.19	3.295E-20
<i>Rlim</i>	-1.29	4.116E-20
<i>Gbbp1</i>	-1.25	4.723E-20
<i>Zfp930</i>	-1.79	5.75E-20
<i>Wapl</i>	-1.30	7.511E-20
<i>Nop58</i>	-1.22	7.683E-20
<i>Ddx46</i>	-1.23	8.852E-20
<i>Tmem184c</i>	-1.53	9.976E-20

Gene Name	log2FC	padj
<i>Washc4</i>	-1.84	1.136E-19
<i>Cebpz</i>	-1.16	1.142E-19
<i>Ireb2</i>	-1.28	1.165E-19
<i>Top2a</i>	-1.14	1.279E-19
<i>Cenpf</i>	-1.87	1.35E-19
<i>Shprh</i>	-1.48	1.36E-19
<i>Med13</i>	-1.48	1.397E-19
<i>Bclaf3</i>	-1.64	1.402E-19
<i>Arhgap12</i>	-1.45	1.428E-19
<i>Zfp518a</i>	-1.81	1.496E-19
<i>Nusap1</i>	-1.17	1.989E-19
<i>Fkbp3</i>	-1.20	2.246E-19
<i>Matr3</i>	-1.35	2.312E-19
<i>Ttk</i>	-1.33	2.312E-19
<i>Far1</i>	-1.36	2.344E-19
<i>Trip11</i>	-1.83	2.639E-19
<i>Rb1cc1</i>	-1.73	2.905E-19
<i>Zfp397</i>	-1.71	3.093E-19
<i>Pnpt1</i>	-1.38	3.229E-19
<i>Eprs</i>	-1.16	3.242E-19
<i>Pten</i>	-1.20	3.328E-19
<i>Zfp146</i>	-1.45	3.41E-19
<i>G2e3</i>	-1.40	3.525E-19
<i>Plaa</i>	-1.20	3.721E-19
<i>Jakmip2</i>	-1.94	4.06E-19
<i>Peg3</i>	-1.25	4.086E-19
<i>Pds5a</i>	-1.31	5.735E-19
<i>Vps35</i>	-1.17	6.596E-19
<i>Acsl4</i>	-1.21	6.665E-19
<i>Thoc2</i>	-1.64	7.29E-19
<i>Zranb2</i>	-1.28	7.902E-19
<i>Fcho2</i>	-1.74	8.717E-19
<i>Topbp1</i>	-1.22	9.742E-19
<i>Chd9</i>	-1.42	1.022E-18
<i>Uba3</i>	-1.24	1.056E-18
<i>Prpf40a</i>	-1.30	1.059E-18
<i>Haus6</i>	-1.39	1.123E-18
<i>Cul3</i>	-1.35	1.129E-18
<i>Shcbp1</i>	-1.36	1.16E-18

Gene Name	log2FC	padj
<i>Arfgef1</i>	-1.74	1.207E-18
<i>Bbx</i>	-1.37	1.281E-18
<i>Cul1</i>	-1.16	1.283E-18
<i>Haus3</i>	-1.68	1.322E-18
<i>Srek1</i>	-1.30	1.592E-18
<i>Dmtf1</i>	-1.43	2.043E-18
<i>Pola1</i>	-1.49	2.153E-18
<i>Dzip3</i>	-1.83	2.153E-18
<i>Rfc1</i>	-1.15	2.165E-18
<i>Pkn2</i>	-1.30	2.221E-18
<i>Creb1</i>	-1.30	2.221E-18
<i>Sp3</i>	-1.36	2.779E-18
<i>Zmym2</i>	-1.33	3.056E-18
<i>Lin7c</i>	-1.22	3.275E-18
<i>Ddx3x</i>	-1.22	3.666E-18
<i>Cenpc1</i>	-1.38	3.807E-18
<i>Eif5</i>	-1.18	4.06E-18
<i>Pcmt1</i>	-1.55	4.076E-18
<i>Oxr1</i>	-1.32	4.972E-18
<i>Ccdc77</i>	-1.34	5.001E-18
<i>Phf3</i>	-1.45	5.194E-18
<i>Usp32</i>	-1.42	5.248E-18
<i>2610307P16Rik</i>	-1.61	5.316E-18
<i>Nek1</i>	-1.50	6.265E-18
<i>Tmem30a</i>	-1.28	6.591E-18
<i>Rnf6</i>	-1.28	7.147E-18
<i>Gnai3</i>	-1.17	7.581E-18
<i>Bptf</i>	-1.20	8.061E-18
<i>Ccp110</i>	-1.34	8.157E-18
<i>Mbtd1</i>	-1.20	8.64E-18
<i>Chd1</i>	-1.34	8.658E-18
<i>Etaa1</i>	-1.28	9.25E-18
<i>Hook3</i>	-1.58	9.909E-18
<i>Alkbh8</i>	-1.46	9.988E-18
<i>Csde1</i>	-1.16	9.988E-18
<i>Rc3h2</i>	-1.48	1.07E-17
<i>Zfp141</i>	-1.52	1.129E-17
<i>Braf</i>	-1.53	1.252E-17
<i>Zfc3h1</i>	-1.44	1.57E-17

Table 25: Histone H3 abundance in fractions upon Zc3h14 depletion.

Zc3h14 KD	Input		Nucleus		Cytoplasm	
	Ctrl	KD	Ctrl	KD	Ctrl	KD
<i>Histone H3</i> abundance	9.15E-07	9.57E-07	1.17E-06	1.02E-06	7.25E-07	8.54E-07
	2.68E-06	2.45E-06	1.11E-06	1.09E-06	2.79E-06	2.71E-06
	6.04E-07	6.31E-07	1.36E-06	1.04E-06	5.85E-07	6.14E-07
normalized abundance	1.000	1.046	1.000	0.868	1.000	1.177
	1.000	0.914	1.000	0.979	1.000	0.969
	1.000	1.046	1.000	0.766	1.000	1.050
log2 fold change	0	0.065	0	-0.205	0	0.235
	0	-0.13	0	-0.03	0	-0.045
	0	0.065	0	-0.385	0	0.07
Average	2.438E-15		-2.067E-01		8.667E-02	
Stdv	1.126E-01		1.775E-01		1.407E-01	
T.test (pvalue)	1.000E+00		1.139E-01		3.463E-01	

Table 26: Histone H3 abundance in fractions upon Zc3h14 overexpression.

Zc3h14 Oex	Input		Nucleus		Cytoplasm	
	Ctrl	KD	Ctrl	KD	Ctrl	KD
<i>Histone H3</i> abundance	4.61E-07	3.78E-07	1.06E-06	1.28E-06	1.24E-06	1.21E-06
	2.25E-06	2.21E-06	2.46E-06	2.44E-06	4.06E-06	5.57E-06
	2.69E-06	2.86E-06	9.57E-07	1.14E-06	3.61E-06	2.83E-06
normalized abundance	1.000	0.821	1.000	1.214	1.000	0.976
	1.000	0.979	1.000	0.993	1.000	1.371
	1.000	1.064	1.000	1.189	1.000	0.785
log2 fold change	0.0	-0.3	0.0	0.3	0.0	0.0
	0.0	0.0	0.0	0.0	0.0	0.5
	0.0	0.1	0.0	0.2	0.0	-0.4
Average	-0.0750		0.1733		0.0233	
Stdv	0.1915		0.1595		0.4057	
T.test (pvalue)	0.5348		0.1329		0.9254	

I. Eidesstattliche Versicherung

Erklärung

Ich erkläre hiermit, dass ich mich bisher keiner Doktorprüfung im mathematisch- naturwissenschaftlichem Bereich unterzogen habe.

Frankfurt am Main, den _____

Marius Wegener _____

Versicherung

Ich versichere hiermit, dass die vorgelegte Doktorarbeit über „The roles of SRSF3 in nuclear splicing surveillance“ selbständig und ohne unzulässige fremde Hilfe verfasst, andere als die in ihr angegebene Literatur nicht benutzt und, dass ich alle ganz oder annähernd übernommenen Textstellen, sowie verwendete Grafiken, Tabellen und Auswertungsprogramme gekennzeichnet habe.

Außerdem versichere ich, dass die vorgelegte elektronische mit der schriftlichen Version der Doktorarbeit übereinstimmt.

Frankfurt am Main, den _____ Marius Wegener

II. Curriculum Vitae

MARIUS WEGENER

date of birth: 12.04.1986
 place of birth: Mainz, Germany
 Citizenship: German

EDUCATION

09/2015 - today **PhD candidate** in the department of RNA regulation in higher Eukaryotes
 • **Topic:** The role of SRSF3 in nuclear splicing surveillance

09/2012 – 11/2014 **Master of Science in Molecular Biosciences** at the **Goethe University Frankfurt**
 • **Grade: 1.3**

09/2012 – 11/2014 **Master thesis** at the **Goethe University Frankfurt,**
 • **Topic:** Mechanisms of translation initiation in *Escherichia coli*

09/2009 – 09/2012 **Bachelor of Engineering in Bioprocess Engineering,** Fach-Hochschule Frankfurt – University of Applied Science
 • **Grade: 1.7**

02/2009 – 09/2009 **Bachelor thesis at the Institute for Microtechnology, Mainz**
 • **Topic:** Immunological fluorescence-based detection of Mycotoxins in a lab-on-a-chip system

08/1996 – 06/2007 **Abitur, Dilthey Schule Wiesbaden**
 • **Grade: 2.5**

CONFERENCES AND PUBLICATIONS

10/2018 **Short talk:** RMU-RNA Salon “Genomics approaches in RNA biology”, Giessen Germany

07/2018 **Publication:** Wegener, Marius; Müller-McNicoll, Michaela (2018): **Nuclear retention of mRNAs - quality control, gene regulation and human disease.**

In: Seminars in cell & developmental biology 79, S. 131–142. DOI: 10.1016/j.semcdb.2017.11.001.

- 07/2018 **Poster presentation:** Splicing 2018, Caparica Portugal
- 04/2018 **Publication:** Ludwig, Petra; Huber, Madeleine; Lehr, Matthias; Wegener, Marius; Zerulla, Karolin; Lange, Christian; Soppa, Joerg (2018): **Non-canonical Escherichia coli transcripts lacking a Shine-Dalgarno motif have very different translational efficiencies and do not form a coherent group.** In: Microbiology (Reading, England) 164 (4), S. 646–658. DOI: 10.1099/mic.0.000619.
- 07/2017 **Publication:** Botti, Valentina; McNicoll, Francois; Steiner, Michaela C.; Richter, Florian M.; Solovyeva, Anfisa; Wegener, Marius et al. (2017): **Cellular differentiation state modulates the mRNA export activity of SR proteins.** In: The Journal of cell biology 216 (7), S. 1993–2009. DOI: 10.1083/jcb.201610051.
- 06/2017 **Poster presentation:** RNA 2017 meeting, Prague Czech Republic
- 12/2016 **Publication:** Wegener, Marius; Vogtmann, Kristina; Huber, Madeleine; Laass, Sebastian; Soppa, Jörg (2016): **The glpD gene is a novel reporter gene for E. coli that is superior to established reporter genes like lacZ and gusA.** In: Journal of microbiological methods 131, S. 181–187. DOI: 10.1016/j.mimet.2016.10.015.
- 09/2013 **invention disclosure:** Immobilization of Aflatoxine/Sterigmatocytine for the development of Mycotoxine assays, Institute of Microtechnology, Mainz.
- 08/2012 **invention disclosure:** honeycomb collimator, Institute of Microtechnology, Mainz.

FURTHER TRAINING

- 11/2017 **Processing and Analysis of Scientific images**
- Dr Jan Brocher, Grade, Frankfurt
- 11/2017 **Scientific paper writing:** Producing a first draft of your paper
- Prof Dr Volker Grimm, Grade, Frankfurt
- 10/2016 Method course: **Analysis of Next generation RNA-seq data** for expression profiling and protein binding RNAs
- University of Regensburg
- 04/2016 **GMP and Quality management in pharmaceutical industries**
- Dr Heinrich Prinz/Christoph Prinz, SFB902 Frankfurtl

III. Acknowledgements

I would like to express my deepest gratitude to Jun. Prof. Michaela Müller-McNicoll for providing me with the opportunity to work on this wonderful project. Thank you for always being open to my input, and supporting my ideas by creating ways to investigate my hypothesis, sharing your knowledge about scientific techniques and data analysis, and introducing me to my collaboration partners when I needed them. Thank you for great conversations and one-on-one meetings, which encouraged me in proceeding with my studies and helped me to identify many new aspects I did not consider. Thank you for providing us with workshops, which helped me to think outside the box, and taking our personal development into consideration. I learned so much in those years.

I am very grateful to Dr. Kathi Zarnack for her contribution and supervision of my project, and for her excellent feedback during numerous meetings, due to her superb skills in bioinformatic and statistical data analysis. Thank you for your guidance and support.

I would also like to thank PhD Francois McNicoll, for constantly being open to my questions and providing me with insights into a perfectly prepared and well-designed experiment. Your perfectionism had a substantial impact on my way of working, and encouraged me to see scientific data with a more critical eye. Your input during lab meetings and journal clubs prepared us for difficult situations, and turned regular presentations into good exercise for the defense of my doctor's thesis. Your passion for science is contagious, and I appreciate our scientific discussions during which I always learned something new. Thank you for your participation in my project by experimentally designing and performing RNA-binding and heterokaryon assays, and helping me when I was running out of time.

The greatest contribution to this work has surely come from Camila Freitas Stahl. You put me up when I was down during those past years, and forced me to continue when I was giving up. Together, we discussed my results and challenges, thought about conclusions and created solutions. You always put my project over yours and helped me perform experiments when I was feeling overwhelmed. I will always be grateful for your support during the writing process. Without your energy, I would never have come so far and this thesis would have been impossible to finish. I want to deeply thank you and dedicate this thesis to you.

Furthermore, I would like to thank all the members of Ak Müller-McNicoll. Special thanks go to Benjamin Arnold and Oliver Schwich for their great suggestions, helpful input, the interest in my results, and solving my IT problems. I enjoyed working with every single person in the group and appreciated the respectful and fun atmosphere. I express my deepest gratitude to all the students who were part of this project. A special thank you to Samoil Sekulovski, Maria Salamanca, Andrea Bosáková and Tanja Roth. Discussing their projects helped me to understand mine.

I want to express my gratitude to You Zhou, who performed an excellent bioinformatic analysis of my data when I was running out of time.

I would like to thank Dr. Christian Münch for performing the mass spectrometric analysis, and for his excellent collaboration.

I also would like to thank Prof. Dr. Klaus Stelzer from the Buchmann Institute for Molecular Life Sciences who provided me with a facility to perform confocal microscopy studies.

I would like to acknowledge Prof. Dr. Katja Sträßer who provided me with an excellent Zc3H14 antibody.

Furthermore, I would like to thank Deutsche Forschungsgemeinschaft for funding this project via the SFB 902 “Molekulare Mechanismen der RNA-basierten Regulation”. A special thanks to everybody involved in the organization of the SFB 902. The summer schools, conferences and workshops you provided, gave me great insights into other topics and techniques and were a wonderful platform for meeting all the great scientists that I got to know over the years.

I want to acknowledge all my friends who gave me mental support and listened to my boring lab stories. Special thanks to Emil Eze and Roman Rauer for their genuine interest in this project, their valuable input, and seeing things from a different perspective. Many thanks also to Stephanie Schweininger for proofreading this thesis under time pressure.

Lastly, I would like to thank my whole family for their continuous support and encouragement. Meeting you on the weekends gave me so much energy. Your unconditional love, sense of humor, patience, optimism and advice were essential to make me forget my frustrations in the lab, and was more valuable than you could ever imagine.